UNIVERSITY OF SIENA

Department of Biotechnology, Chemistry, and Pharmacy

Doctorate in Chemical and Pharmaceutical Sciences

Coordinator: Prof. Stefano Mangani

XXXII Cycle

MARIE SKŁODOWSKA-CURIE ACTIONS

TRAining in Cancer mechanisms & Therapeutics (TRACT)

Innovative Training Networks (ITN): H2020-MSCA-ITN-2016

Project Coordinator: Prof. Daniela Zisterer, Trinity College Dublin, Ireland

Early Stage researcher (ESR) 8

Development of Novel Autophagy Modulators to Improve the Sensitivity of Oral Squamous Cell Carcinoma to Chemotherapy

Doctorate Supervisors:

Prof. Giuseppe Campiani

Prof. Stefania Butini

Doctorate Fellow:

Tuhina Khan

TUHINA KHAN Signed
09/06/2021

Academic Year: 2019/2020

PREFACE

Project 1: "Development of autophagic modulators to improve the sensitivity of oral squamous cell carcinoma".

Oral squamous cell carcinoma (OSCC) is the sixth most common cancer with 500,000 people affected annually worldwide. It is the predominant malignant neoplasm in the oral cavity and affects the floor of the mouth, tongue, buccal mucosa, alveolus, retromolar trigone, gingival, hard palate, and lip. Known etiological factors in OSCC are alcohol and tobacco consumption, genetic predispositions, chronic inflammations and viral infections. Depending on the stage of the tumor, chemotherapy (e.g., cisplatin and 5-fluorouracil), radiation therapy, chemoradiotherapy, surgical removal of the tumor and combination therapy are recommended. Unfortunately, late-stage diagnosis, the scarcity of effective therapeutic strategies, and drug resistance during chemotherapy are the main challenges in OSCC. Autophagy is a catabolic process to maintain the turnover of organelles and intracellular proteins for the conservation of cellular homeostasis. It is often stimulated in the presence of stress-mediated circumstances. It can play a dual role in tumorigenesis depending on the type and stage of the tumor. Generally, in the early stage of cancer, induction of autophagy can help to resist tumor progression by maintaining genetic integrity, mediating stress and hypoxia etc. On the other hand, in the advanced stage, the induction of autophagy can serve as a survival mechanism by overcoming the deprivation of nutrients and providing resistance to drugs for anticancer therapy etc. Over the past decade, stress-induced autophagy has been demonstrated to contribute in the drug resistance and malignant progression in preclinical and clinical studies. In addition, genetic knockdown or pharmacological impairment of autophagy has produced therapeutic benefits. Therefore, autophagy inhibitors (e.g., chloroquine and hydroxychloroquine) are being studied in different types of tumors despite their toxicity and high dose requirements in clinical trials. Interestingly, several studies have confirmed autophagy as one of the main drug resistance mechanisms in OSCC. Therefore, new autophagy inhibitors with improved potency and safety profiles are the need of the hour to evaluate the true therapeutic benefits of inhibiting autophagy in tumors, including OSCC Pyrrolobenzoxazepines (**PBOXs**) and Pyrrolonaphthoxazepines (**PNOXs**) are microtubule targeting anticancer agents that bind to the colchicine site. This has been confirmed by accurate X-ray crystallographic studies. They exert their anticancer activity on a wide range of tumor cell lines, including multidrug-resistant cells. The therapeutic potential of **PBOX** compounds in a group of *in vivo* and *ex vivo* cancer models and normal counterparts was also assessed. **PBOXs** show minimal toxicity to normal blood and bone marrow. Interestingly, **PBOX-6** had autophagy inducing effects in human colon cancer cells. Treatment of **PBOX-6** against pharmacological inhibition of late-stage autophagy with Bafilomycin A1 improved **PBOX-6**-induced apoptosis in cancer cells. Further characterizations have shown that **PBOX-6**-induced autophagy plays a cytoprotective role with respect to autophagic cell death. Motivated by this observation, we wanted to perform selective and rational structural modifications in the core structure of both **PBOX**/**PNOX** compounds to modify and subsequently produce an inverse (inhibiting) effect on the autophagic process. We focused on developing autophagy inhibitors in OSCC while maintaining the key profile as potent pro-apoptotic agents. Being a highly dynamic process, autophagy machines offer numerous numbers of drug targets. Unfortunately, these targets are often multifunctional and involved in many other cellular processes. Therefore, targeting one of them is not related only to autophagy and inhibition of autophagy always directs the path towards targeting the late stage, i.e. lysosomal fusion with the autophagosomes of the machinery. In this attempt, we converted two activity profiles, namely the autophagy inhibitory effect of chloroquine and the pro-apoptotic effect of **PBOX**/**PNOX**.

Appropriate molecular modeling docking was performed to design a new series of **PBOX/PNOX** compounds. Regarding the inhibitory effect of autophagy, we focused on the mechanism of action of chloroquine. This is well known and supported by the fact that the underlying mechanism of action for chloroquine is the presence of the basic moiety and the subsequent changes of the lysosomal pH to compromise the lysosomal function. We explored the **PBOX/PNOX** class of compounds and described the development of a series of pro-apoptotic molecules. Structural adaptation to the binding pockets of the central structure was implemented using the mechanistic perception of the known inhibitor of autophagy and the molecular modeling approach. The compounds have been carefully characterized by biological and medicinal chemistry approaches. We evaluated their ability to inhibit the cell growth and induce apoptosis on several cancer cell lines. The selected compounds were tested for their effect on the resistance cells and the corresponding parent cells. The mutagenic safety profile was also inspected for the compounds. In addition, the pharmacokinetic properties and metabolic stability were calculated *in vitro* with the human liver microsome. Finally, the selected compounds were inspected for their effect on the autophagic process against SCC4 and HL-60 cell lines. The quantification of the LC3-II/LC3-I and p62 proteins both under basal and starvation mediation conditions was assessed using chloroquine as a positive control. These studies revealed the chloroquine-like mode of action for **PNOX** compounds on the autophagic process. The obtained data proposed a relevant therapeutic potential for the developed compounds as autophagy inhibitors with innate pro-apoptotic activity.

Project 2: "Development of new β-lactam based HDAC6 inhibitors as anticancer agents".

Several diseases including cancer have a fundamental epigenetic etiology. In eukaryotic cells, histone proteins play an essential role in organizing DNA structures. Histone acetylation and deacetylation include a key example of post-translational modifications that work in epigenetic regulation. Histone deacetylases (HDAC) belongs to the family of hydrolases that remove acetyl groups from lysine residues and therefore regulate the key processes like gene expression. They are classified into four different classes based on their yeast homology. Class I HDACs are made up of isoforms 1, 2, 3, and 8; while class II enzymes include isoforms 4, 5, 6, 7, 9, and 10. Class III HDACs are NAD^+ dependent enzymes called sirtuins (SIRT 1-7). Class IV contains only isoform 11. Classes I, II and IV are zinc dependent enzymes. A common structural feature of HDAC inhibitors (HDACi) is the presence of a zinc binding group (ZBG), a portion of linker and a group of caps. Many HDACi have been identified as therapeutic tools in the treatment of various ailments including cancer. Unfortunately, all the FDA-approved HDACis have proven to be non-selective or partially selective with several side effects. Significant research efforts are currently focused on the development of selective HDACi with less side effects. The β-lactam family has been used for many years to treat bacterial infections. Interestingly, β-lactams have also been explored for selective HDAC inhibition by several research papers. We focused on the development of selective HDAC6 inhibitors, with a β-lactam core structure. After performing a molecular modeling approach, we designed a series of compounds with different caps groups and linkers, keeping hydroxamic acid as a common ZBG. The newly developed structures were inspired by the scaffold of a previously developed inhibitor identified by our research group. All the compounds have been tested for the inhibitory effect on both the HDAC1 and HDAC6 isoforms. The best compound showed an IC_{50} value of 3.4 nM on HDAC6 with 1265-fold selectivity compared to the HDAC1 isoform.

PREFAZIONE

Progetto 1: "Sviluppo di nuovi modulatori autofagici per migliorare la sensibilità del carcinoma orale a cellule squamose".

Il carcinoma orale a cellule squamose (OSCC) è il sesto tumore più comune al mondo con 500.000 persone colpite ogni anno al mondo. Fattori eziologici noti nell'OSCC sono il consumo di alcol e tabacco, predisposizioni genetiche, infiammazioni croniche e infezioni virali. A seconda dello stadio del tumore, si raccomanda la chemioterapia (Cisplatino e 5-fluorouracile), la radioterapia, la chemioradioterapia, la rimozione chirurgica del tumore e la terapia combinata. L'impossibilità di fare diagnosi in fase precoce, la scarsità di strategie terapeutiche efficaci e la resistenza ai farmaci durante la chemioterapia sono le principali sfide che si pongono per l'OSCC. L'autofagia è un processo catabolico per mantenere il turnover degli organelli e delle proteine intracellulari per la conservazione dell'omeostasi cellulare. Può svolgere un duplice ruolo nella tumorigenesi a seconda del tipo e dello stadio del tumore. Generalmente, nella fase iniziale del cancro, l'induzione dell'autofagia può aiutare a resistere alla progressione del tumore mantenendo l'integrità genetica, mediando lo stress e l'ipossia ecc. D'altra parte, nella fase avanzata, l'induzione dell'autofagia può servire come meccanismo di sopravvivenza superando la privazione dei nutrienti e fornendo resistenza ai farmaci per la terapia antitumorale ecc. Nell'ultimo decennio, è stato dimostrato che l'autofagia indotta dallo stress contribuisce alla resistenza ai farmaci e alla progressione maligna negli studi preclinici e clinici. Inoltre, il knockdown genetico o la compromissione farmacologica dell'autofagia ha prodotto benefici terapeutici. Pertanto, gli inibitori dell'autofagia (clorochina e idrossiclorochina) sono allo studio in diversi tipi di tumori nonostante la loro tossicità e le elevate esigenze di dose negli studi clinici. È interessante notare che diversi studi hanno confermato l'autofagia come uno dei principali meccanismi di resistenza ai farmaci nell'OSCC. D'ora in poi, nuovi inibitori con una migliore potenza e profili di sicurezza sono una necessità utile per valutare i veri benefici terapeutici dell'inibizione dell'autofagia nei tumori, incluso l'OSCC. Le pirrolobenzossazepine (**PBOX**) e le pirrolonaftossazazine (**PNOX**) sono molecole che agiscono come agenti pro-apototici legando la tubulina sul sito della colchicina e agiscono sui composti anticancro. Ciò è stato confermato da accurati studi cristallografici a raggi X. Tali composti la loro attività antitumorale su una vasta gamma di linee cellulari tumorali, comprese le cellule multiresistenti. È stato anche verificato il potenziale terapeutico dei composti della **PBOX** in un gruppo di modelli di cancro in vivo ed ex vivo e su linee cellulari normali. I **PBOX** mostrano una tossicità minima nei confronti di cellule enatiche normali e sul midollo osseo. È interessante notare che **PBOX-6**, una delle molecole prototipiche imnsieme a **PBOX-15**, ha mostrato effetti pro-autofagici in cellule umane di tumore al colon. Ulteriori caratterizzazioni hanno mostrato che l'autofagia indotta da **PBOX-6** svolge un ruolo citoprotettivo. Motivati da questa osservazione, volevamo effettuare modifiche strutturali selettive e razionali nella struttura centrale di entrambi i composti **PBOX**/**PNOX** per modificare e successivamente produrre un effetto inverso (inibendo) il processo autofagico. Ci siamo concentrati sullo sviluppo di inibitori dell'autofagia nell'OSCC mantenendo il profilo chiave di potenti agenti pro-apoptotici. Essendo un processo altamente dinamico, i meccanismi dell'autofagia offrono numerosi numeri di target farmacologici. Tali bersagli molacolari sono spesso polifunzionali essendo coinvolti in molti altri processi cellulari. Pertanto, il targeting di uno di essi può non essere correlato solo all'autofagia. Pertanto, abbiamo pensato di inibizione l'autofagia focalizzandoci allo stadio tardivo, cioè al porcesso di fusione lisosomiale con gli autofagosomi. per sviluppate tale obiettivo abbiamo pensato di unire i due profili di attività, ovvero l'effetto inibitorio dell'autofagia del **CQ** e l'effetto pro-apoptotico dei

PBOX/PNOX sviluppando nuove molecole che possedessero le catatteristiche chimiche apporporiate tranedno spunto dalle strutture molecolari di riferimento.

A tal fine sono stati eseguiti stidi compurazionali di docking di modellistica molecolare per progettare una nuova serie di composti a struttura **PBOX/PNOX**. Per quanto riguarda l'effetto inibitorio dell'autofagia, ci siamo concentrati sul meccanismo d'azione della **CQ** dove la presenza di strutture basiche compromette la funzione lisosomiale. Abbiamo pertando supportato sulla struttura **PBOX/PNOX** vari elementi farmacoforici chiave ottenedo nuove entità chimiche. Tali composti sono stati accuratamente caratterizzati da approcci di chimica biologica e medicinale. Abbiamo valutato la loro capacità di inibire la crescita cellulare e di indurre l'apoptosi su diverse linee cellulari tumorali. I composti selezionati sono stati testati per il loro effetto sulle cellule resisti e sulle cellule sane corrispondenti. Anche il profilo di mutagenicità è stato ispezionato. Inoltre, sono state calcolate le proprietà farmacocinetiche e la stabilità metabolica in vitro dopo incubazione con microsomi epatici umani. Infine, i composti selezionati sono stati studiati per valuatere il loro effetto sul processo autofagico contro le linee cellulari SCC4 e HL-60. La quantificazione delle proteine LC3-II / LC3-I e p62 sia in condizioni basali che in "Starvation" (deprivazione di nutrienti) è stata valutata usando la **CQ** come controllo positivo. Questi studi hanno svelato una modalità di azione simile alla **CQ** per i nuovi composti **PNOX** sul processo autofagico. Complessivamente i dati ottenuti hanno hanno permesso di iopotizzare epr i nuovi analoghi sviluppati un potenziale terapeutico rilevante come inibitori dell'autofagia dotati anche di attività pro-apoptotica.

Progetto 2: "Sviluppo di nuovi inibitori dell'enzima HDAC6 a struttura di beta-lattica come agenti antitumorali".

Diverse malattie tra cui il cancro hanno un'eziologia epigenetica. Nelle cellule eucariotiche, le proteine dell'istone svolgono un ruolo essenziale per organizzare le strutture del DNA. L'acetilazione e la deacetilazione dell'istone includono un esempio chiave di modificazioni post-traduzionali che funzionano nella regolazione epigenetica. Gli enzimi della classe istone deacetilasi (HDAC) appartengono alla famiglia delle idrolasi che rimuovono i gruppi acetilici dai residui di lisina e regolano quindi i processi chiave come l'espressione genica. Sono raggruppati in 4 diverse classi (I-IV) in base alla loro omologia del lievito. Gli HDAC di classe I sono costituiti dalle isoforme 1, 2, 3 e 8; mentre gli enzimi di classe II includono le isoforme 4, 5, 6, 7, 9 e 10. Gli HDAC di classe III sono enzimi NAD + dipendenti chiamati sirtuine (isoforme SIRT 1-7). La classe IV contiene solo l'isoforma 11. Le classi I, II e IV sono enzimi zinco dipendenti. Una caratteristica strutturale comune degli inibitori dell'HDAC (HDACi) è la presenza di un gruppo legante lo zinco (ZBG), una porzione linker e una testa stericamente ingombrante. Molti HDACi sono stati identificati come strumenti terapeutici per il trattamento di vari disturbi tra cui il cancro. Sfortunatamente, tutti gli HDACi approvati dalla FDA hanno dimostrato di essere non selettivi o parzialmente selettivi indicendo diversi effetti collaterali. Significativi sforzi di ricerca sono attualmente focalizzati sullo sviluppo di HDACi selettivi che producano minori effetti collaterali. Ci siamo concentrati sullo sviluppo di inibitori selettivi dell'HDAC6 a struttura β-lattamica. Dopo aver eseguito un approccio di modellistica molecolare, abbiamo progettato una serie di composti con diverse teste stericamente ingombranti e linker, mantenendo l'acido idrossamico come ZBG comune. Le strutture di nuova concezione sono state ispirate alla struttura molecolare di un inibitore precedentemente sviluppato dal nostro gruppo di ricerca. Tutti i composti sintetizzati sono stati testati per l'effetto inibitorio su entrambe le isoforme di HDAC1 e HDAC6. Il miglior composto ha mostrato un valore IC_{50} di 3,4 nM su HDAC6 con selettività 1265 volte rispetto all'isoforma HDAC1.

PREFACE ABBREVIATIONS

DNA	Deoxyribonucleic acid
FDA	US food and drug administration
HDAC	Histone deacetylases
HDACi	Histone deacetylases inhibitors
HL	Human leukemia
IC_{50}	Half maximal inhibitory concentration
LC3	Light chain 3
NAD	Nicotinamide adenine dinucleotide
OSCC	Oral squamous cell carcinoma
PBOX	Pyrrolobenzoxazepines
PNOX	Pyrrolonaphthoxazepines
SIRT	Sirtuins
ZBG	Zinc binding group

INDEX

Part 1

Development of pyrrolobenzoxazepines/pyrrolonaphthoxazepines as autophagy modulators

PART 1 CHAPTER I

BACKGROUND

1.1.1 Introduction

1.1.1.1 Epidemiology of OSCC

Oral squamous cell carcinoma (OSCC) is the major malignant neoplasm in the oral cavity after verrucous carcinoma, identical carcinoma, and the small salivary adenocarcinoma. OSCC represents more than 90% of all oral malignant lesions.[1] It has been reported as the sixth most common cancers by the International Union Against Cancer, with an annual incidence of 275,000 cases worldwide.[2,3] Early-stage OSCC detection displays an 80% survival rate at five years while advanced-stage detection leads to survival rates range of 20% to 40%.[4] The poor survival rate largely depends on the late development of the symptoms, the consequent late diagnosis, and the scarcity of effective treatments. Epidemiology of oral cancer, as well as OSCC, is not well documented since it is often included in the broader subgroup of oropharyngeal carcinomas.[5] However, oral cancers are highly frequent in Southern Asia (e.g., India and Sri Lanka) and Pacific Islands (e.g., Papua New Guinea having the highest incidence rate worldwide for both male and female). It accounts for the leading cause of cancer death among men in India and Sri Lanka.[6] The Indian subcontinent holds the one-third oral cancer burden worldwide, and it ranks among the top three forms of cancer in India. Annually 130,000 people succumb to oral cancer in this country, which translates into approximately 14 deaths per hour.[7]

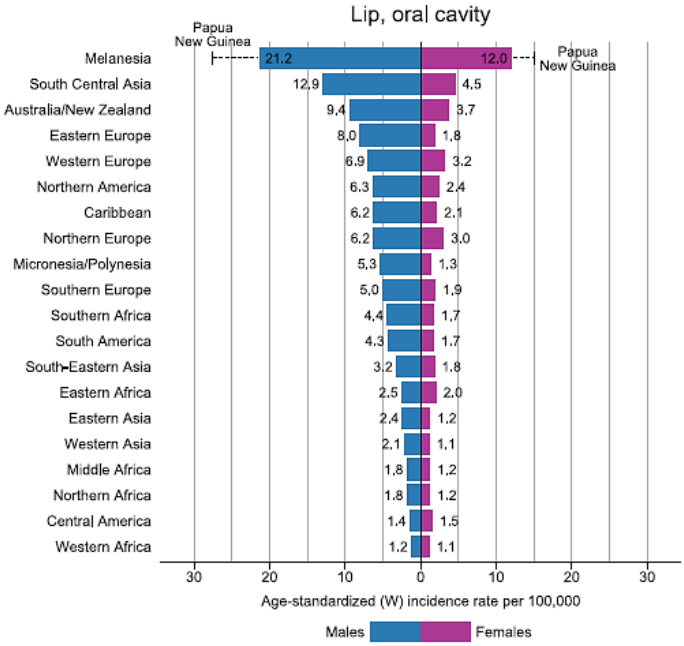

FIGURE 1. Bar chart of region-specific incidence and age-standardized rates by sex for lip and oral cavity cancer in 2018. Source: GLOBOCAN 2018.[6]

1.1.1.2 Genetic and molecular alternations in OSCC

The most frequent chromosomal aberrations involved in OSCC are 3p, 4q, 5q21-22, 8p21-23, 9p21-22, 11q13, 11q23, 13q, 14q, 17p, 18q, and 22q. These alternations are able to affect the expression and function of tumor regulating genes, p16 (9p21), APC (5q21-22), and p53 (17p13). Further genetic changes involved in OSCC are the polymorphisms in glutathione S-transferase M1, cytochrome P450 family 1 member A1, and aldehyde dehydrogenase.[8] Epigenetic modifications, e.g., methylation of DNA and acetylation/methylation of histones can silence the tumor suppressor genes in OSCC.[9] OSCC metastasis has been reported as a complex process involving cell detachments from the tumor tissue and lymphatic system or blood vessels to facilitate their motility, invasion, and proliferation. Loss of E-cadherin reduces the intercellular adhesion, which results in the epithelial-mesenchymal transition process and molecular alterations in tumor cells.[10] The molecular-level understanding of OSCC has been developed extensively over a period of years. In general, chronic carcinogenic exposure induces a modification in the key genetic and epigenetic regulatory molecules to modify cell signaling pathways. Therefore, the identification of these modifying mechanisms *via* target-specific regulatory molecules is vital. In addition, cell adhesion molecules, interleukins, cytokines, vascular endothelial growth factor, and epidermal growth factor receptor are also correlated with OSCC. It has

been described that the p53 pathway is down-regulated in 80% of OSCC and accounts for almost 75% of DNA binding domain mutations. However, the alternative ways which lead to the inactivation of p53 include the overexpression of Human Papilloma Virus (HPV) E6, amplification of MDM2, and inhibition of cyclin-dependent kinase inhibitor 2A (CDKN2A) (**Figure 2**). Interestingly, mutated p53 bearing tumors are stated as more resistant to chemotherapy and radiotherapy than the wild type p53 bearing ones.[8] So, the investigation of mutations and alternations in p53 requires a more detailed exploration.[11] The inactivation of CDKN2A also disturbs the retinoblastoma (Rb) pathway in more than 70% of the cases of OSCC either by deletion or epigenetic modification.[12] Overexpressed cyclin D1 (CCND1) provides the mechanistic evidence by the loss of CDKN2A and upregulation of CCND1 is strongly associated with its activation and ultimately to the cell cycle progression.[8]

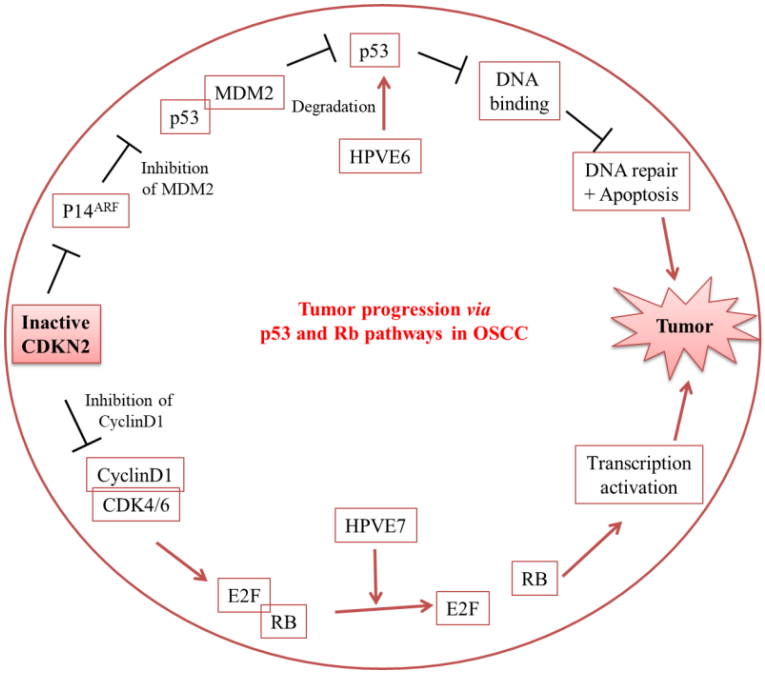

FIGURE 2. General schematic representation of tumor progression in OSCC due to CDKN2 suppression

1.1.1.3 Aetiology in OSCC

- **Tobacco products**

Several systematic reviews have strongly supported the association between exposure to smoked/smokeless tobacco with the insurgence of OSCC.[13,14] Ten years of smoking cessation-period could diminish the risk of oral cancer to levels similar to that of a never-

smoker.[15,16] The continuous exposure to heat resulting from the tobacco combustion stimulates the aggression to the oral mucosa.[17] Tobacco-related lesions are at risk of oral epithelial dysplasia [18] and potentially premalignant oral epithelial lesions (PPOELs, the most common being represented by leukoplakia).[19,20] Chewing or smoking tobacco leads to the release of almost 300 carcinogenic molecules that are converted into reactive metabolites to interact with DNA by the oxidative enzymes. Polycyclic aromatic hydrocarbons, e.g., benzo[*a*]pyrene diol epoxide and *N*-nitrosamines, are considered as the most important toxic substances in tobacco smoke. In addition to these substances, radioactive elements (e.g., carbon-14 and polonium-210), and pesticide residues from tobacco cultivation have also been detected.[21] Also, smokeless tobacco products contain several carcinogens, such as nitrosamines, that are abundantly found in the oral fluids of smokers as well as non-smokers.[22]

- **Alcohol Consumption**

Several epidemiologic studies, as well as reports from the International Agency for Research on Cancer and the World Cancer Research Fund, have confirmed alcohol ingestion as a variable risk factor for OSCC. In OSCC, the risk seems to be synergistically related to tobacco consumption, and it appears to be linked with overall alcohol consumption rather than to the number of drinks per day.[23] Ingested ethanol is absorbed from the upper gastrointestinal tract, followed by its transportation to the liver to be metabolized into acetaldehyde by alcohol dehydrogenase 1B and the successive detoxification into acetic acid by aldehyde dehydrogenase 2. Acetaldehyde can also be produced in the human oral cavity by the interaction of microorganisms such as yeasts and bacteria with ethanol.

- **Viral Infections**

In the 1980s, the possible correlation of HPVs with oral cancer was evaluated for the first time. HPVs, a group of host-specific DNA viruses with remarkable epithelial cell specificity (keratinocytes), is the most common type of viruses in OSCC.[24] The ability to insert the specific DNA fragments into the host cellular genome has provided HPV with oncogenic potential.[25,26] In OSCC, the prevalence of HPV virus varies from 20% to 25% primarily because of the differences in demography and ethnicity.[27,21] Moreover, the level of Herpes Simplex Virus (HSV) I antibodies is high in smokers and even higher in smokers with head and neck cancers, suggesting that prolonged exposure to HSV may

sensitize the mucosa to tobacco carcinogens.

- **Genetic Predispositions**

Understanding of the genetic origin of oral cancer has grown significantly as it is accepted that solid tumors are genetically not stable. It is mostly known that the accumulation of genetic variations in proto-oncogenes can lead to OSCC through a multi-step process.[28] Genetically determined diseases that interfere in DNA metabolism can give rise to PPOELs and/or OSCC. Inherited genetic polymorphisms in the p53 pathway affect tumor formation, progression, and/or response to therapy. Frequent CDKN2A gene mutations or the recurrent loss of gene expression in oral lesions have been suggested as an early step in OSCC.[5]

- **Other Factors**

Oral cancers have also been associated with a low intake of fruits, vegetables, and a protective role may be afforded by diets high in fruits, vegetables, and fiber.[5] Consumption of yellow vegetables, cruciferous vegetables, and citrus fruits more than once a week showed a protective effect, whereas red meat intake more than once a week conferred an increased risk.[29] In highly rare instances, it may be possible for *Candida* species to cause OSCC by the generation of carcinogenic agents from specific stains or perhaps from altered immune surveillance, independent of tobacco and/or alcohol exposure. Syphilis, caused by *Treponema pallidum*, has long been proposed as a risk factor of OSCC. Oral lichen planus, a chronic inflammatory condition, is considered a potential cause for inducing OSCC though the exact mechanism is not known yet. Hematinic deficiency can cause histopathologic and/or clinically detectable PPOELs, presumably by interfering with epithelial proliferation. There is some evidence that patients with scleroderma (systemic sclerosis) are at risk of a variety of malignancies, including OSCC.[30]

FIGURE 3. Predominant etiologic factors in OSCC progression

1.1.1.4 Current Therapies

The mode of OSCC treatment depends on various factors such as the stage of the disease, overall patient health status, and the site of the disease. Stages of OSCC are classified by the size of the tumor, its tissue invasion, and spread to the lymph nodes (**Table 1**).[31]

Table 1. A general classification of OSCC stages

Stages	Tumor thickness	Lymph node spread	Lymph node bearing tumor	Affected body parts
0	Isolated	none	none	none
I	< 2 cm	none	none	none
II	2-4 cm	none	none	none
III	> 4 cm/any size	One lymph node, same side of head and neck	≥ 3 cm	none
IV	any size	> one lymph node, both sides of neck	> 6 cm	lips or oral cavity, penetrated deep inside facial tissues, muscles, jaws and other parts

- **Radiation therapy (RT)**

In OSCC, primary radiotherapy (RT) with/without chemotherapy (CT) may be deployed for: i) early-stage cases to avoid anticipated failure of surgery, ii) high operative risk patients due to comorbidity and/or poor health status, iii) cases of technically unconvincing surgery due to previous multiple surgeries. Postoperative radiotherapy, though desirable, requires careful planning and multidisciplinary collaboration and may not always be

attainable in the event of complicated surgeries. Considerable experience has been accumulated with effective low-dose-rate, high-dose-rate, and pulsed-dose rate brachytherapy in a large clinical series of OSCC. However, these techniques require expertise and resources, primarily to supply the operating room resources and radiotherapy protection requirements. In particular, the high sensitivity of OSCC to (chemo) radiotherapy leads to complete and durable pathological responses in a high proportion of patients following CRT, which may render surgery unnecessary in a subgroup of complete responders, and this is an area ripe for research. [32]

- **Chemotherapy**

The first-line treatment of both very large and unresectable OSCC involves the use of drugs, such as cisplatin (**1 Figure 1**), carboplatin (**2**), 5-fluorouracil (**3**), methotrexate (**4**) and taxanes (paclitaxel, **5**, docetaxel, **6**).[33–37] These therapies, however, did not show any significant increase in the level of overall survival (OS) over the past two decades. Association of CT and RT resulted in a synergistic benefit with a high level of response in inoperable stages of OSCC. It utilizes the potential delivery and the tumor radiosensitizing property of the drug along with the damage in genetic material (DNA) by the ionization energy of the radiation.[38] However, both therapies face a significant drawback of nonspecific cell death resulting in mucositis, myelosuppression, and alopecia.[31] A broad sample of patients with Union for International Cancer Control (UICC) stage IV OSCC of 1-year OS for 69% of the oral cavity subgroup (n = 20) with single Cisplatin IaCh and multimodal treatment but 80% OS after Cis/5-FU IaCh treatment was described.[39] In 2018, it was reported for the first time that the combined Cis/5-FU therapy had significantly better OS, with less adverse effects than the MTX/bleomycin treatment in both the uni- and multi-variable analyses.[40] In patients with recurrent oral cancer, cisplatin IaCh can be considered for consecutive treatment after standard therapy, in order to deliver a higher dose to the tumor.[39] The principal disadvantages of this approach are the feasibility of the protocol at only a few institutes with the infrastructure, resources for this specialized procedure, and its elevated costs.[41] It was hypothesized that induction chemotherapy (ICT) would increase OS, disease-free survival, and progression-free survival by improving distant control.[42] Shrinkage in the tumor volume before definitive treatment with ICT could enhance RT feasibility and tolerability whilst reducing the disfiguring effects of surgery and radiation.[43] However, most OSCCs exhibit limited response to chemotherapy

involving cytotoxic drugs due to mechanisms that either block the intracellular transport of these agents or interfere with their intracellular molecular targets, e.g., autophagy.[5]

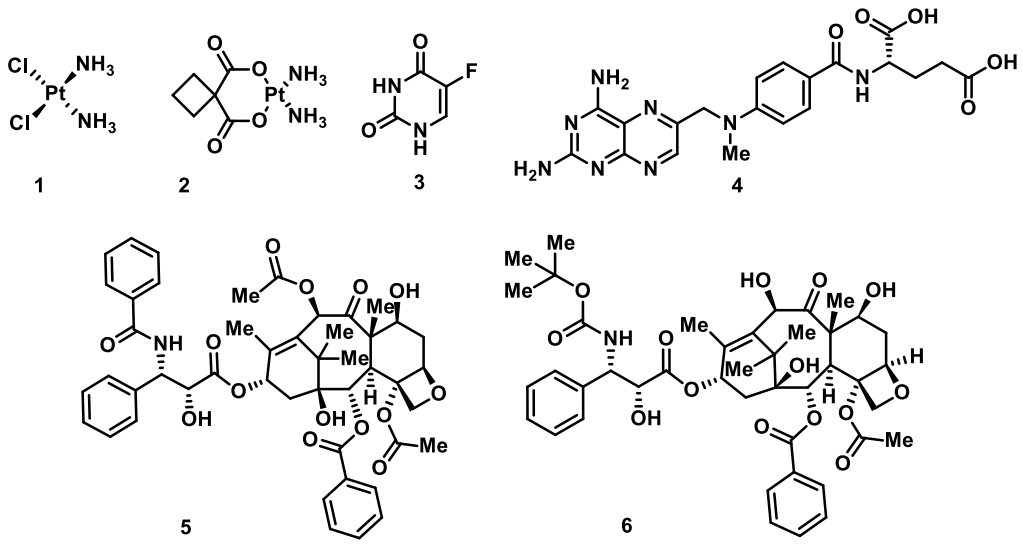

FIGURE 4 Available chemotherapeutic drugs (**1-6**) for the treatment of OSCC

- **Surgical therapy**

Surgical resection is still the main therapy in most patients treated with curative intention. In OSCC, surgical removal of the tumor is performed alone on small size tumors with satisfactory outcomes except in the case of the inoperable tumor; CRT is often used with surgery for this. After the surgery, most patients depend on a feeding tube for their nutrition. Many patients suffer from disfiguration and long-term effects, including fatigue, speech problems, swallowing difficulties, weakness, dizziness, hearing loss, and sinus damage. Surgeries types include maxillectomy, mandibulectomies, glossectomies, radical neck-dissection Mohs surgery, and a combination of glossectomy and laryngectomy.[44–47] Additional reconstructive surgery such as bone grafting and surgical flaps from the forearm may be required to rebuild the structures removed during the excision of cancer.[31]

1.1.2 Autophagy

Eukaryote cells conceive two critical mechanisms to maintain the cellular homeostasis via protein degradation, namely the ubiquitin-proteasome system and autophagy.[48] In 2016, Professor Yoshinori Ohsumi was awarded the Nobel Prize in Physiology or Medicine for his contribution to the discovery of autophagy regulatory mechanisms. Autophagy is involved in the recycling of nutrients such as amino acids and lipids in damaged or

superfluous macromolecules and organelles (e.g., mitochondria), in order to protect the cell from toxins and to maintain metabolism and energy homeostasis. It may occur in three different forms, macroautophagy (hereafter referred to as autophagy) or mitophagy if the digested organelle is a mitochondria, microautophagy, and chaperone-mediated autophagy. During autophagy, double-membraned autophagosomes engulf cytoplasm and proteins, which need to be degraded. Moreover, this mechanism can be used by the cell to digest damaged organelles, pathogens, and protein aggregates.[49] In microautophagy, the degradation of the molecules takes place inside the lysosomes upon the invagination of their membrane. In chaperone-mediated autophagy heat shock proteins, such as Hsp70 are employed by the cell as markers for the proteins to be digested.[50] Different stimulations, e.g., oxidative stress, hypoxia, organelle damage, and protein aggregation, can induce autophagy. A dysregulation in the autophagic process has been related to many human pathologies, such as cancer, cardiovascular disorders, neurodegeneration, infection, pulmonary and metabolic diseases.[51]

- **Regulatory mechanisms of the autophagy machinery**

Understanding the autophagy machinery is a prerequisite for identifying new diagnostic and therapeutic targets. The study of autophagy has accelerated in the past decade because of the discovery of more than 36 autophagy-related genes (ATGs), which are responsible for the core machinery as well as required for selective modes of autophagy. Autophagy can be divided into canonical and noncanonical pathways depending on the corresponding intervention of the proteins deriving from ATGs. The canonical pathway requires the hierarchical intervention of all ATG proteins, while the noncanonical autophagy requires only a subset of them. Schematically, autophagy involves several major steps: induction, nucleation, elongation and completion, autophagolysosome formation, degradation, and recycling (**Figure 5**).

(I) Induction: It initiates with the deactivation of the mechanistic target of rapamycin complex 1 (mTORC1), an autophagy suppresser, by the inhibition of the autophagy activating kinase 1 complex (ULK1). mTORC1 gets deactivated by reduced upstream signaling from the phosphoinositide 3-kinase/Akt and the mitogen-activated protein kinase (PI3K/MAPK) pathway. 5'-adenosine monophosphate-activated protein kinase (AMPK), a key kinase regulating cellular energy homeostasis, can trigger ULK1 and inhibit mTORC1.[52,53] Bcl-2 protein bind to the BH3 domain of Beclin-1 autophagy is inhibited, in

contrary when non-Bcl-2 protein bind with the BH3 domain the autophagy is induced.[54–58] The activation of ULK1 and beclin-1 can lead to the formation of the two-membraned phagophore.

(II) Autophagosome maturation: Several ATGs and proteins take part in the phagophore nucleation and successive maturation to generate the autophagosome. ATG7 and ATG10 facilitate the covalent binding of ATG12 to ATG5. Successively, ATG12-ATG5 conjugate gets non covalently linked to ATG16.[59] The conversion of the protein light chain 3 (LC3) to LC3-I by the proteolytic action of ATG4 and the successive link to ATG7, allows the association of LC3-I with ATG-3. LC3-I becomes LC3-II after the conjugation with the lipid phosphatidylethanolamine (PE) mediated by the catalytic action of ATG-3 and the ATG5-ATG12-ATG16 complex. LC3-II gets incorporated into the membrane of the autophagosome. During the maturation of the vesicle, the organelles and proteins to be degraded are sequestered by p62/sequestosome 1 (p62).[60]

(III) Autophagolysosome formation: The matured autophagosome is transported to the lysosome to get fused with and form the autophagolysosome. The formation of the autophagolysosome is determined by the action of two lysosome-associated proteins (LAMP-1 and LAMP-2), necessary also to keep the integrity of the membrane of the lysosome.[61]

(IV) Degradation and Recycling: After the fusion, lipases, proteases, nucleases, and sulfatases are responsible for the digestion of the autolysosome content. It is relevant to evidence that during the digestion step, also, the p62 is degraded.[62]

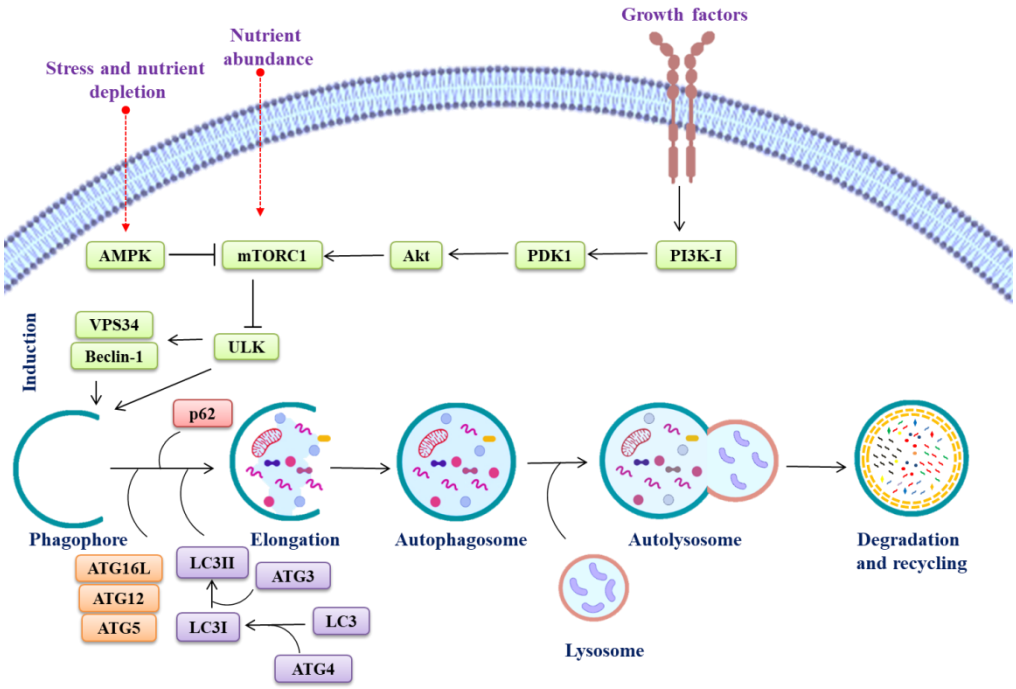

Figure 5. Schematic representation of autophagic machinery

- **Autophagy in cancer**

The proportional relationship between autophagy and apoptosis triggers a significant cross-talk in the tumor suppression.[63] Interestingly, autophagy can play a dual and contradictory role in cancer formation and progression. In healthy cells, it acts as a tumor suppressor through the digestion of mutated proteins and genes (oncogenes) that may lead to cell mutation and cancer. On the other side, the activity of autophagy is usually upregulated in cancer cells. It is usually triggered by the lack of nutrients and oxygen in the microenvironment and it provides the amino acids, free fatty acids, and glucose necessary for the survival and the proliferation of the tumor. Treatment of several solid tumors with 5-FU or cisplatin can lead to an increased autophagic flux, thus resulting in chemoresistance of the cancer cells against these drugs.[64] Henceforth, based on the stage of the tumor progression, both the inhibition and induction of autophagy may represent promising therapeutic strategies in the fight against cancer.[65, 62, 66] Abnormal expressions of key autophagic proteins have been found in various human cancers. In fact, it has been reported that beclin1 is monoallelically deleted in 40% to 75% of cases of breast, ovarian, and prostate cancer. Inhibition or downregulation of autophagy in these cancers suggests that basal levels of autophagy are crucial to suppress tumor development.[64] Moreover,

knockdown of beclin1 has been associated with an increase in spontaneous malignancy in mice, whereas the restoration of its expression has been associated with inhibition of tumor growth.[67] In contrast, it has been reported that some cancer cells may become dependent on autophagy.[68] Given that, the role of autophagy in cancer seems to be context-dependent and it may vary depending on the class and stage of the malignancy.[69] Moreover, it may be crucial to evaluate the signaling pathways controlling autophagy regulation and their activation/mutation in cancer. Both tumor suppressor and oncogenes regulate autophagy during cancer development, and their activation or mutation may result in the induction of specific cellular pathways that may determine the role of autophagy as pro-death or pro-survival mechanism.[70] Tumor-suppressor genes act as pro-autophagic factors, whereas oncogenes act as anti-autophagic factors.[71] Autophagy regulation is controlled by several signalling pathways, also involved in tumor progression.

In conclusion, the strong implication of autophagy in cancer has been widely demonstrated. Several signalling pathways have been reported to regulate autophagy. These pathways are complex and interact on multiple levels. A further mechanistic understanding of the role of autophagy in different cellular contexts is necessary and it may provide a valuable approach to develop novel therapeutic treatments. In this context, the development of new molecules targeting specific stages of the autophagy machinery as well as the characterization of molecules endowed with different effect on autophagy is highly desirable.

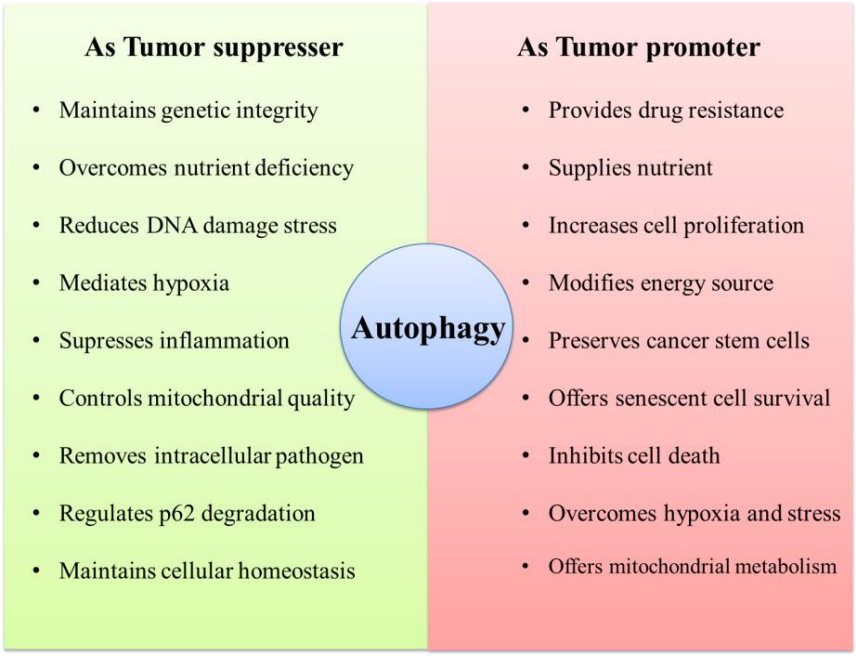

Figure 6. Autophagy as a double-sword mechanism in tumorigenesis including OSCC

- **Detection methods and biological assays in autophagy**

Substantial efforts have been engazed to develop new methods for autophagy detection. It involves the direct observation of autophagy-related vesicles and/or the quantification of autophagic/lysosomal signature biomarkers. For the accurate autophagic activity estimation, it is essential to determine the autophagic flux, which defines the amount of autophagic degradation. The presence of double-membrane vesicles provides one of the most critical evidence in the formation of autophagosomes. These structures can be detected by transmission electron microscopy. LC3-II is one of the most common biomarkers used in the detection of the number of autophagosomes and autophagy-related structures. The western blot (WB) analysis is usually able to detect the levels of LC3-II compared to LC3-I, and higher concentrations of LC3-II usually means a higher number of autophagosomes. Often, LC3-II is degraded by the action of the lysosomal enzymes and a method to detect the autophagic flux is to calculate the difference in the amount of LC3-II between samples with and without a lysosome inhibitor (e.g., bafilomycin A1) higher the ratio, higher is the autophagic flux. However, LC3-II can be found in other non-autophagic structures, so it is better to perform additional analysis, e.g., determination of p62, to determine the effective autophagic flux. p62 directly binds to LC3 and is selectively degraded during the autophagic process. Measuring the amount of p62 and checking the ratio between its concentrations in cells previously treated with an autophagy inhibitor allows quantification of the autophagic flux. Green fluorescent protein-LC3 (GFP-LC3) is a plasmid, used as a marker that replaces the native LC3. It leads to the formation of green punctate structures (detected by fluorescence staining for confocal imaging, indicated as green dots) when the GFP-LC3 is recruited by the autophagosome. Usually, the number of puncta detected is proportional to the intensity of the higher autophagic flux. The mRFP-GFP-LC3 tandem fluorescent protein assay takes advantage of the different sensibility of the tandem marker, mRFP-GFP. This protein bound to the LC3 emits both green and red fluorescence (more often shown as yellow signals in merged pictures). The green fluorescence is quenched when the pH is acidic because of the lower stability of the GFP-LC3 bond. Instead, the red fluorescence depending on the bond between mRFP and LC3 is stable until pH 4-5 or even lower. The autophagic flux can be visualized using a single probe: the induction of autophagy will be observed as an increase in the puncta of both colors, but the inhibition in autophagosome maturation will result in a decreased amount of

the red puncta. The increase in the red puncta can be determined by an enhanced autophagic flux or by reduced activity of the lysosomal enzymes. Immune electron microscopy with GFP can be used in tissues to check the amount of LC3 of autophagic structures *in vivo.*[72, 73]

- **Autophagy inhibitors in OSCC**

In recent years, many compounds have been described as autophagy modulators in cancer cells. Most of the autophagy modulators discovered so far are represented by natural products or compounds active on other biological targets.[65] Best to our knowledge, only five compounds have been characterized as autophagy inhibitors in OSCC (**Figure 7**). Four of them are able to block the autophagic flux by impairing the lysosomal activity. Lysosomes play a crucial role in the growth and metabolism of the cells. An acidic pH range of 4.5 to 5 is needed in order to facilitate the catalytic functions of the lysosomal hydrolytic enzymes during the degradation of the lysosomal content. Lysosomal damage was observed in animal models treated with chloroquine (CQ, **7a**, **Figure 7**) and subsequent studies revealed that it was able to penetrate the lysosomal membrane to accumulate inside this organelle as a protonated form in the acidic environment. The increased concentration of protonated **CQ** inside the lysosome blocks the activity of the lysosomal enzymes and leading to the block in the autophagic machinery. Nowadays, **CQ** is commonly used in biological assays to block the autophagic flux and assess the role of autophagy when employing newly discovered anti-cancer agents. **CQ** and its analogue hydroxychloroquine (HCQ, **7b**), are reported as the lysosomotropic inhibitors in OSCC. **HCQ** resulted in induction of apoptosis and inhibition of cancer cell growth in a safer and more tolerable mode than **CQ** in both *in vitro* and clinical trials.[74] Also, the lysosomotropic agent Lys05 (**8**) showed tenfold improved potency compared to **HCQ** in both *in vitro* and *in vivo* models. However, high doses of **CQ** and **HCQ** are required to obtain sufficient autophagy inhibition in patients. Bafilomycin A1 (**9**), a lysosomotropic agent, blocks the fusion of the autophagosome with lysosome by a specific inhibition of V-ATPase activity. Three new chromone based compounds were tested for their anti-cancer activity against OSCC cells. The best compound, namely derivative **10**, displayed an IC_{50} value of 1.0 µM against HSC2 (oral cavity squamous cell carcinoma) cells in a cell viability assay. By WB analysis, a total loss of the autophagy marker LC3-II (usually expressed in high levels in HSC2 cells) was observed. This suggested that **10** was able to suppress autophagy, thus

activating the apoptotic cascade. However, the mechanistic target of **10** in OSCC is still not specified.[75]

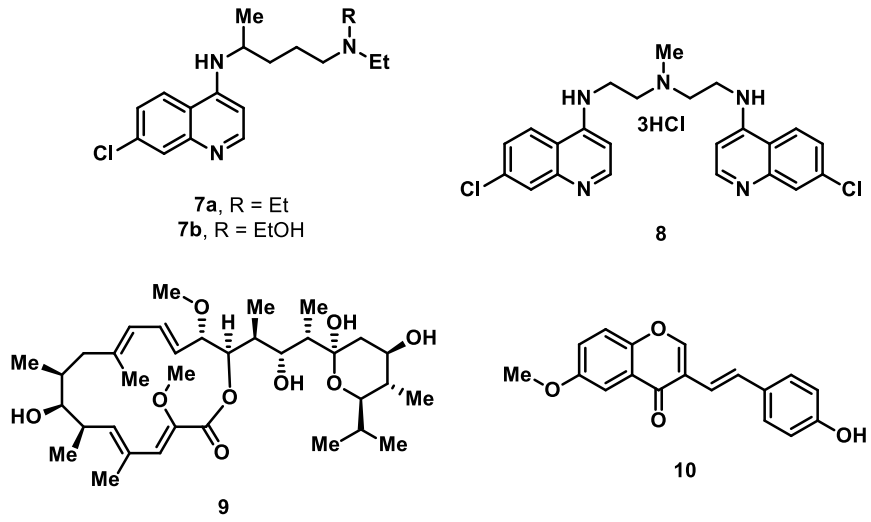

Figure 7. Available autophagy inhibitors (**7**-**10**) in OSCC

1.1.3 Microtubules

- **Microtubule dynamics**

Microtubules (MTs) are fundamental constituents of the cellular cytoskeleton and play essential roles in proliferation, intracellular trafficking, migration, and mitosis. MTs are hollow cylindrical tubes consisting of 13 aligned protofilaments, constructed from head-to-tail fashion bound α- and β-tubulin heterodimers (**Figure 8A**).[76,77] MTs go through a cyclic dynamic instability between polymerization and depolymerization state (**Figure 8B**). These complex dynamics has been considered as an intrinsic property of MT due to the association of polymerizing and depolymerizing MTs within a cell population. Although the precise biomechanics of the MT dynamic is not completely unveiled, it is definitely linked to the hydrolysis of guanosine- 5′- triphosphate (GTP). Both the α- and β-tubulin subunit can bind one GTP molecule. The GTP at the α-end remains unaffected, but the β-end can get hydrolyzed.[78] The cycle gets initiated through the addition of GTP- tubulin dimers to the growing end of MT protofilaments. After that, the hydrolysis of GTP to guanosine diphosphate (GDP) takes place with a following dissociation of the GDP-tubulin dimer from MT.[79] It is generally accepted that a GTP rich "cap" on the end of the MT allows it to stabilize and grow with a straight conformation; whereas, when the cap is lost

through hydrolysis, the core of the protofilament becomes unstable and shortens rapidly as the GDP- tubulin subunits are released from the MT ends.[80–82]

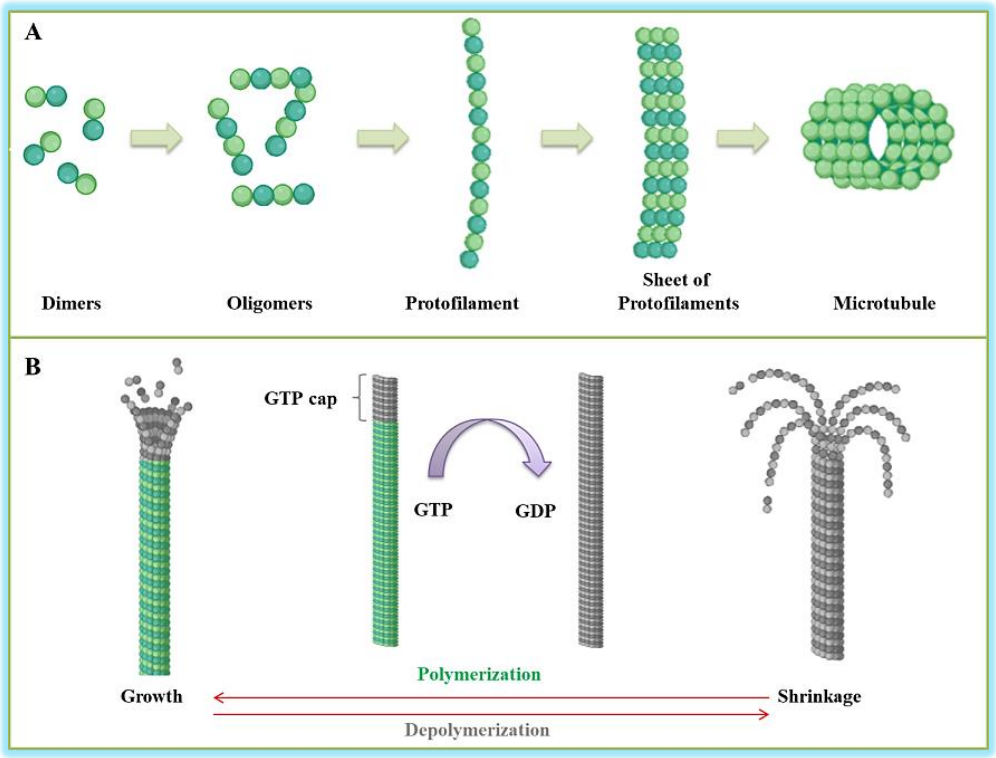

Figure 8. (A) Formation of microtubules after constructing the sheet of protofilaments by the α- and β-tubulin heterodimers; (B) Microtubule dynamics. During polymerization, a GTP rich cap gets bound to the microtubule and acts as a primer for GTP-tubulin addition to the elongated end of the microtubule. In depolymerization, GTP is hydrolyzed into GDP and GDP protofilaments are released from the microtubule.

- **Microtubules in cancer**

Cancer cell connote an uncontrolled and unscheduled proliferation along with genomic instability. Several anti-cancer strategies have focused on targeting the rapid multiplication of cancer cells to arrest the cell cycle and promote cell death.[83] In the framework of anti-cancer small-molecule drug development, MTs are responsible for the separation of chromosomes during mitosis.[84] Mitosis is the fifth phase of a typical cell cycle in which DNA is divided into two daughter cells. In mitosis, the cytoskeleton transforms from a steady interphase array to an active bipolar spindle. Spindle mid zones are formed during the later stages of mitosis from antiparallel MTs and the irregular mid-zone formation leads to failure of cytokinesis, yielding unequal chromosome segregation.[85] In cell

division, chromosome segregation is promoted by spindle formation and co- assembly of actin filaments with MTs.[86] During M phase, an essential bipolar MT array (mitotic spindle) segregates chromosomes to prevent chromosome loss and aneuploidy. The mitotic spindles radiate outward from centrioles and attach to the centromeres of sister chromatids in dividing cells.[87] This is followed by the simultaneous addition of tubulin at the kinetochore and is accompanied by a comparable rate of tubulin loss at the opposite poles.[88,89] If a chromosome is unable to achieve bipolar attachment to the spindle, the cell is unable to continue through the cell cycle and is blocked in the metaphase, eventually to succumb to apoptosis.[90] MT dynamics are also governed by a variety of regulator proteins and mechanisms, and they function both spatially and temporally. Interfering with MT dynamics is an attractive anti-cancer strategy, and many drugs employing this tactic are therapeutically effective in a wide range of malignancies. Mitotic arrest in the G2/M phase, a hallmark of MT- targeting agents, is thought to occur through the perturbation of mitotic spindle machinery and failure to pass mitotic checkpoints.[91]

- **Microtubule targeting agents (MTAs)**

Compounds that can bind to MTs called microtubule targeting agents (MTAs) have long been one of the most important drug classes for cancer chemotherapy due to the importance of MTs in cells, particularly in uncontrolled cell division.[76,92] In addition, MTAs are also approved to treat fungal, bacterial infections, non-neoplastic conditions such as gout, and non-familial Mediterranean fever.[93–96] MTAs are currently under investigation for the treatment of many neurological disorders.[97,98] There are several sites on the tubulin heterodimer to which MTAs can bind, the most common are the vinca alkaloid, taxane, colchicine, and laulimalide binding sites. These drugs are generally divided into one of two classes; stabilizing agents, which enhance polymerization, or destabilizing agents, which inhibit tubulin polymerization.[99]

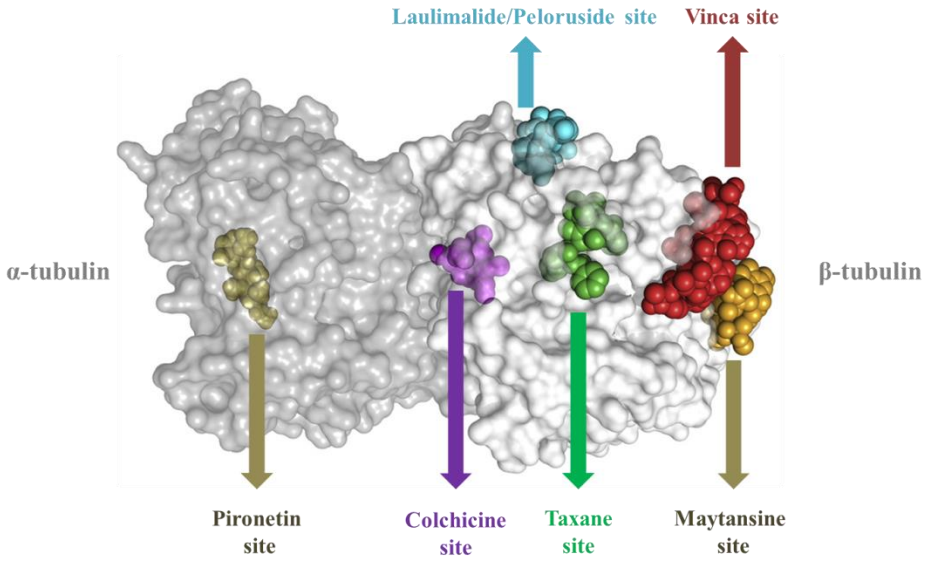

Figure 9. Binding sites of the microtubule-targeting agent on tubulin dimer with α- and β-tubulin in dark and light grey, respectively. The structures of the representative ligands in sphere representation for each site were superimposed on the respective binding sites. The distinct binding sites were highlighted in cyan (laulimalide/ peloruside site), slate (vinca site), orange (maytansine site), green (taxanes site), magenta (colchicine site), and yellow (pironetin site).

(I) Microtubule stabilizing agents (MSAs)

- **Taxane site**

The taxane site, located in the β-tubulin, contributes to a significant class of microtubule-stabilizing agents (MSAs). Some MSAs, targeting the taxanes sites are paclitaxel (**5**), docetaxel (**6**), epothilone A and B (**11a**,**b**), zampanolide (**12**), taccalonolide (**13**), and discodermolide (**14**).[100–105] All taxane-site ligands establish both hydrophobic and polar contacts with several secondary structural elements. Collective observations suggest that different taxane-site ligands, although binding to the same pocket on β-tubulin, may achieve their microtubule-stabilizing effect through different molecular mechanisms.[100,106] The site for taxanes could thus be considered as an ensemble of functionally diverse subsites whose differential occupation by a ligand elicits different conformational effects in tubulin within the microtubule lattice.[99] Paclitaxel and docetaxel are used in chemotherapeutics to treat patients with various solid tumors, including ovarian, breast, head and neck, lung, and prostate cancers. However, severe adverse effects and development of multi-drug resistance (MDR) have largely compromised the use of

paclitaxel and docetaxel. In addition to transporter- mediated resistance, overexpression of class III β tubulin isoform also limits the efficacy of many taxanes.[91]

- **Laulimalide/Peloruside site**

Another MSAs laulimalide (**15**) and peloruside A (**16**) exhibit significant cytotoxic activity against a broad range of cancer cells and have unique features compared to taxane-site ligands used in the clinics.[107] Both laulimalide and peloruside A synergistically enhanced MT assembly, induced by stabilizing agents, including paclitaxel, epothilones A and B.[108] Furthermore, laulimalide and peloruside A stabilize the M loop at the taxoid binding site, which contributes to cross-talk and explains the observed synergism between these agents and taxane site ligands.[109] Recently, high-resolution X-ray crystallography and cryo-EM studies allowed the description of the laulimalide/peloruside site on β-tubulin, which is distinct from the taxanes site and is located at the luminal side of the microtubule.[101,109]

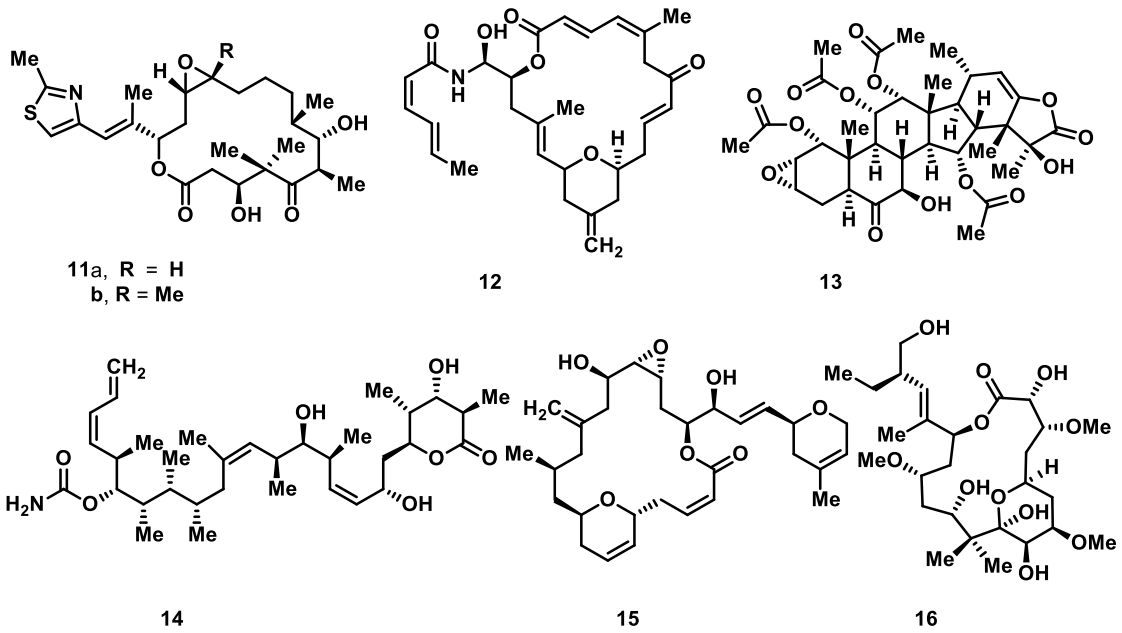

FIGURE 10. Available microtubule-stabilizing agents (**11**-**16**)

(II) Microtubule destabilizing agents (MDAs)

- **Colchicine site**

Colchicine-site ligands, targeted by microtubule destabilizing agents (MDAs), are probably the most extensively studied MTAs. A large number of structurally diverse colchicine-

binding ligands of natural or synthetic origin, e.g., colchicine (**17**) itself, combretastatin A4 (**18**), 2-methoxyestradiol (**19**), and nocodazole (**20**) have been characterized by X-ray crystallography of medium and high resolution. The colchicine site is a deep pocket, that is mostly buried in the intermediate domain of β-tubulin and located near the intra-dimer interface between the α- and β-tubulin subunits.[110,111] The site can be subdivided into the main zone in the center of the domain and two additional accessory pockets that either face the α-tubulin subunit or are buried deeper in the β-tubulin subunit. To date, none of the structurally characterized colchicine-site ligands occupies all three zones simultaneously.[112] In the bound state, all the core secondary structural elements of the colchicine site interact with the ligand through mainly hydrophobic and very few polar contacts. During microtubule assembly, tubulin dimers undergo conformational changes from a curved conformation in their free state to a straight structure in microtubules.[113,114] This conformational transition is characterized by the movement of the intermediate domain of both α- and β-tubulin subunits, in which strands S8 and S9, among others, move closer to helix H8. These changes are accompanied by a translation of helix H7 and lead to an overall contraction of the colchicine site. Thus, binding of a ligand to the colchicine site inhibits microtubule formation mainly by preventing the curved-to-straight conformational change in tubulin.[99] To overcome the conventional MDR, there have been numerous efforts to develop colchicine binding site inhibitors because of their therapeutic advantages over taxanes and vinca alkaloids.[115,116] One of the main mechanisms of MDR is due to the overexpression of class III β-tubulin that alters the conformation of the taxane binding site but does not confer resistance to colchicine binding site agents. Also, the efficacy of the vinca drug, vinorelbine, is reduced when class III β-tubulin is overexpressed, suggesting that that the resistance from β-III-tubulin isoforms are binding site-specific.[117,118] This offers an advantage for chemotherapeutic drugs targeting the colchicine binding site. These contributions offer new strategies to alleviate the problem of MDR and they provide practical implications for the further investigation of colchicine binding site agents.[119–128]

- **Vinca site**

The vinca alkaloids represent the oldest family of compounds that target the vinca site of tubulin. Vinblastine (**21**) and vincristine (**22**) have received extensive effective clinical evaluation against a variety of malignancies.[129] The vinca site-targeting agents known to date comprise several chemical classes of compounds, such as the highly potent cytotoxic peptides dolastatins, auristatins, and tubulysins, as well as eribulin, diazonamides, and

triazolopyrimidines.[130–133] Ligands targeting the vinca site bind at the inter-dimer interface between two longitudinally aligned tubulin dimers. The vinca site consists of a core zone, which has been defined based on interactions established by vinca alkaloids, and a pocket that extends towards the exchangeable guanosine nucleotide site on β-tubulin.[134,135] MT destabilization by vinca-site ligands is achieved either by introducing a molecular wedge at the tip of MTs, which prevents the curved-to-straight transition of tubulin necessary for proper incorporation into MTs or by sequestering tubulin dimers into ring-like oligomers that are incompatible with the straight protofilament structure in MTs. Ligand binding further inhibits proper positioning of the catalytic α-tubulin residues that promote GTP-hydrolysis on β-tubulin.[136,137] However, the degree of curvature of longitudinally aligned tubulin dimers can be modulated by the different types of vinca-site ligands.[138] Though, vincas are among the most commonly used MTAs, they also are susceptible to the development of drug- resistant mechanisms and toxic side effects.[91]

- **Maytansine site**

The maytansine site is distinct from the vinca site and is located on an exposed pocket of β-tubulin, adjacent to the guanosine nucleotide and is shaped by hydrophobic and polar residues of this subunit.[139] It was clarified by X-ray crystallography of the unrelated MDAs maytansine (**23**), PM60184 (**24**), etc. in complex with tubulin.[139–141] The maytansine derivative DM1 (**25**) is currently in clinical use for the treatment of metastatic breast cancer.[140] This observation implies that maytansine-site ligands directly block the formation of longitudinal tubulin contacts in microtubules either by inhibiting the addition of further tubulin dimers to the plus ends of growing microtubules or by forming incompetent assembly tubulin–ligand complexes at high ligand concentrations.[133] The overall shape of this pocket is invariant, suggesting that the ligands bind independently of the conformational state of tubulin.[139]

- **Pironetin site**

Pironetin (**26**) was reported to show antimitotic and antitumor activity by inhibiting microtubule formation.[142] A covalent-binding mechanism of action of pironetin was proposed based on structure-activity relationship studies and Lys352 of α-tubulin was identified as the pironetin-binding site by systematic alanine-scanning mutagenesis.[143,144] Using this information in combination with molecular dynamics simulations, it has been further speculated that pironetin destabilizes microtubules by perturbing the formation of

lateral tubulin contacts in microtubules.[145] Two recent independent X-ray crystallography studies reported the covalent binding of pironetin to Cys316 of α-tubulin.[146,147] The ligand binds to an extended hydrophobic pocket on α-tubulin and establishes two secondary structural key longitudinal tubulin contacts along protofilaments in MTs. It was proposed that their perturbation can prevent MT formation either at high ligand concentrations by forming incompetent assembly tubulin–pironetin complexes, or at substoichiometric compound concentrations by inhibiting the addition of further tubulin dimers at the minus ends of MTs that expose α-tubulin subunits.[147] Notably, pironetin site is the only known cavity to date that exclusively resides in the α-tubulin subunit.

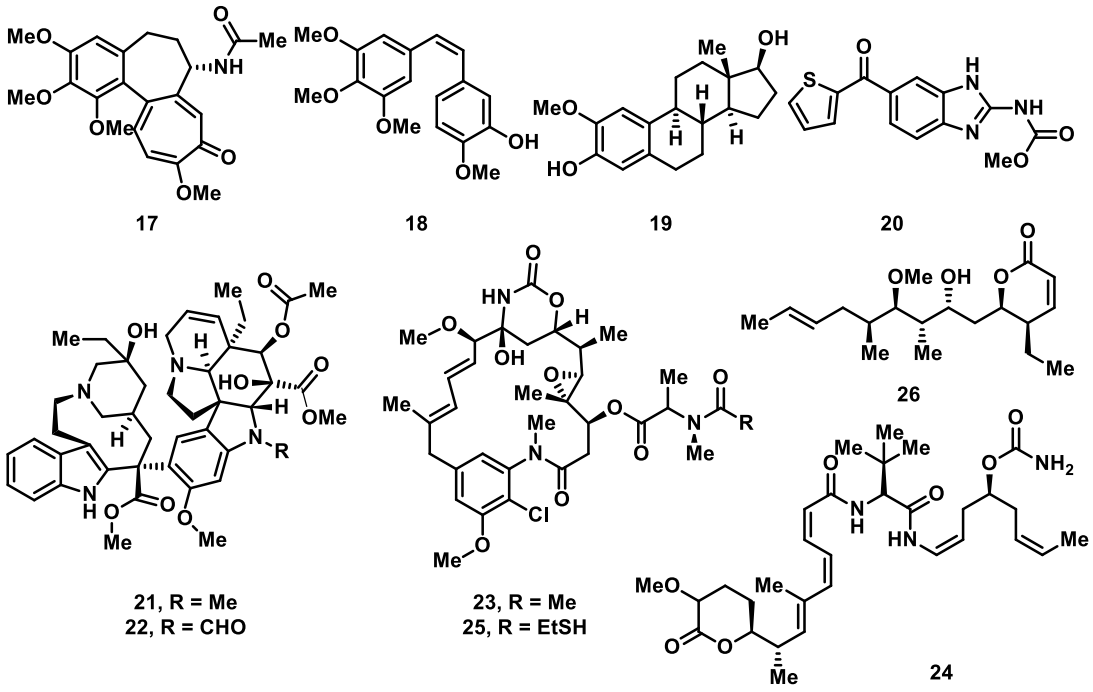

FIGURE 11. Available microtubule-destabilizing agents (**17**-**26**)

PART 1 CHAPTER II

PYRROLOBENZOXAZEPINES (PBOXs) and PYRROLONAPHTHOXAZEPINES (PNOXs)

1.2.1 General features of PBOXs/PNOXs

The general chemical structure of pyrrolobenzoxazepines (**PBOXs**) and pyrrolonaphthoxazepines (**PNOXs**) are depicted in **Figure 12**.[148] It contains a seven-membered heterocyclic ring (namely the ozazepine, as it contains O and N) with a fused benzene (**PBOXs**) or naphthalene (**PNOXs**) system (in pocket 1) as the fundamental core. In general, pocket 2 could be occupied by an ester (e.g., methyl ester) or carbamate (e.g., dimethylcarbamate, diethylcarbamate, etc.) lateral chain; whereas pocket 3 comprises of an aromatic system (e.g., 1-naphthyl, 3-benzofuran, 4-benzofuran, etc.).[149]

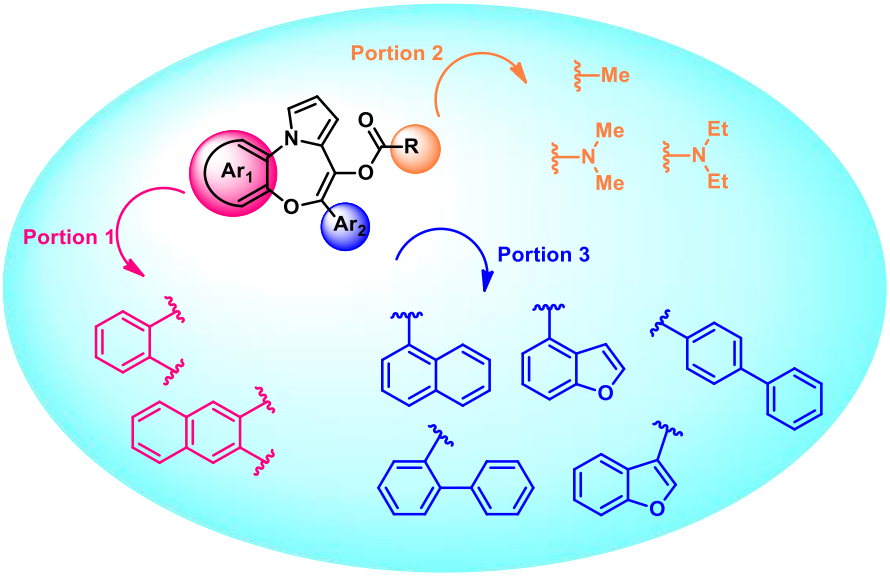

FIGURE 12. Core chemical structures of pyrrolobenzoxazepines (PBOXs) and pyrrolonaphthoxazepines (PNOXs)

PBOX/PNOX compounds are able inhibit the growth of a wide range of cancer cell lines including breast cancer, prostate cancer, ovarian carcinoma, human colon cancer, oral squamous carcinoma, neuroblastoma, acute malignant hematopoietic, lymphoblastic leukemia, embryo and other myeloma and leukemia. Based on the effect of **PBOX/PNOX** compounds on apoptosis and other cellular processes, they have been categorized into pro-apoptotic and non-apoptotic family (**Figure 13**).[150] It was conclusively established that **28**

and **29**, also denoted as **PBOX-6** and **PBOX-15**, respectively, induced a major loss in mitochondrial membrane potential and subsequent release of cytochrome c.[151] Cytosolic cytochrome c is a critical element of the apoptosome complex to sequentially signal the caspase activation. These two compounds are also able to activate the initiator caspase, caspase-9 and its effector caspases (caspase-3 and -7). The mitochondrial/intrinsic pathway is regulated by the interaction of Bcl-2 family members with mitochondria to increase the mitochondrial permeability and agree to the release of cytochrome c. Accordingly, The **PBOXs**/**PNOXs** also extensively modulate several members of the Bcl-2 family. The Bcl-2 pathway is central for a cell to undergo apoptosis as it proceeds to irreversible commitment to cell death. **28** and **29** target the anti-apoptotic subset of the Bcl-2 family in several ways, specifically by phosphorylation/inactivation and downregulation and/or cleavage.[150,152]

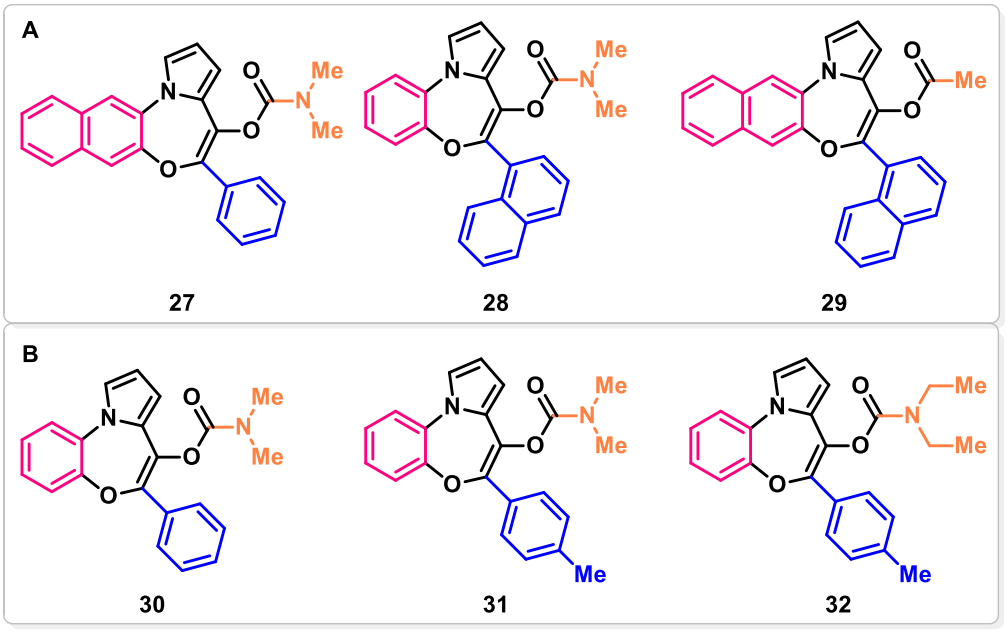

FIGURE 13. Representative examples of (A) pro-apoptotic (**27**-**29**) and (B) non-apoptotic (**30**-**32**) **PBOX**/**PNOX** compounds

1.2.2 PBOXs/PNOXs are microtubule-destabilizing agents

MTAs can induced G_2/M arrest and apoptosis in many human tumor cells. A detailed time course distribution study of cell cycle phases of MCF-7 cells in response to **28** treatment demonstrated that the apoptosis was temporally preceded by arrest in the G_2/M phase of the cell cycle.[153] This fact was verified by an increase in cyclin B1 and activation of CDK1 complex. Triggered by this fact, the effect of **28** and other pro-apoptotic member **29** on the

microtubule network of MCF-7 cell lines was investigated. An indirect immunofluorescence study demonstrated that both **27** and **28** successfully depolymerize the microtubule network in a dose-dependent manner (**Figure 14**). They were able to inhibit the assembly of purified tubulin *in vitro* (in cell culture), whereas the non-apoptotic member **32** had no effect on both the microtubule network and the purified tubulin assembly.

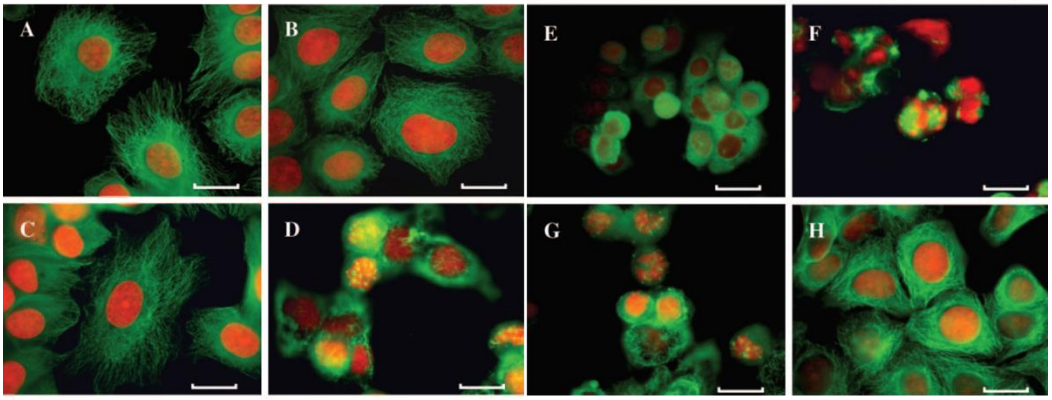

FIGURE 14. Effect of **28**, **29**, **32**, paclitaxel, and nocodazole upon the microtubule network of MCF-7 cellular organization. MCF-7 cells were treated with either vehicle [0.5% (v/v) ethanol] (**A**), 100 nM, 1 μM, or 10 μM of **28** (**B**, **C**, and **D**, respectively), 1 μM of nocodazole (**E**), 1 μM of paclitaxel (**F**), 1 μM of **29** (**G**), or 25 μM of **32** (**H**) for 16 h. The microtubule network (indicated in green) and the cellular DNA (indicated in red) were visualized by Nikon PS200 fluorescence microscopy. The results are mean of three independent experiments.

The same observation was replicated in TR-146, and Ca9.22 cell lines.[154]

To further confirm the mechanism and the biological target, binding studies with isolated tubulin were performed *in vitro* which confirmed the tubulin destabilizing properties to be factual for a number of **PBOX**/**PNOX** analogues (see **Figure 15**).[155]

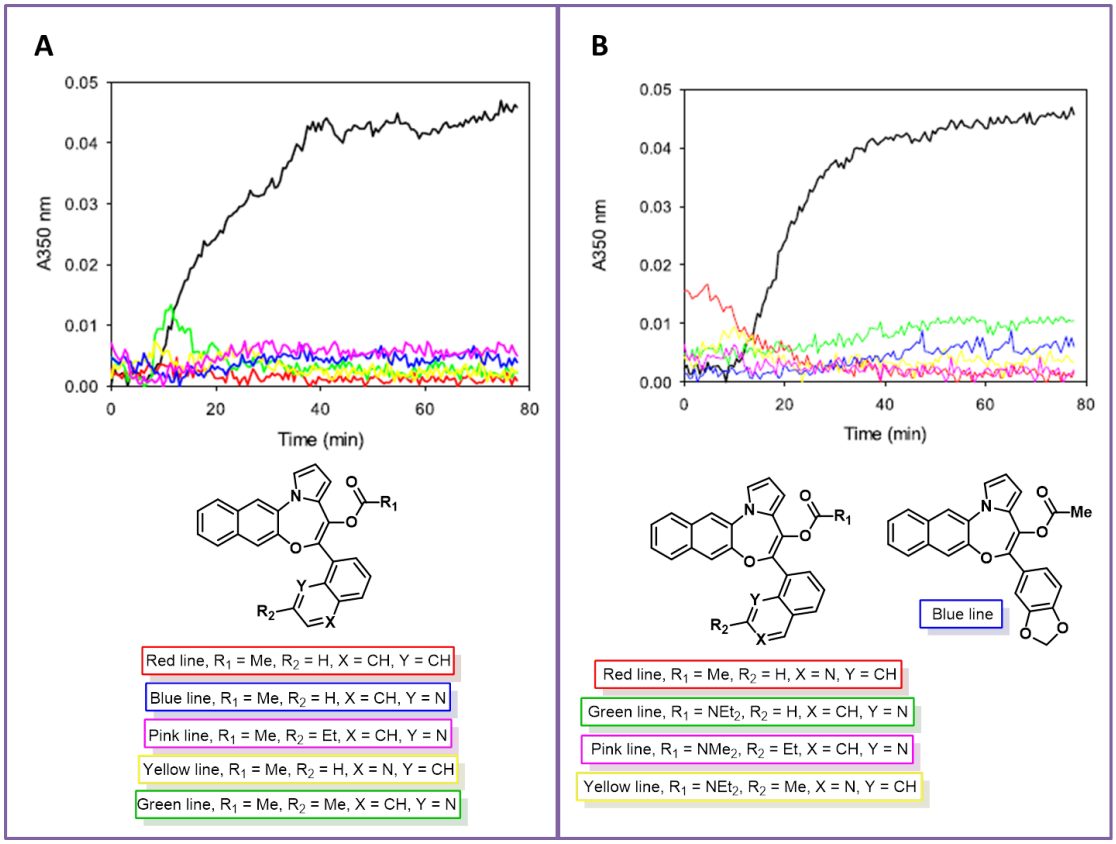

FIGURE 15. Turbidity time course for the assembly of 25 mM tubulin at 37 °C with 27.5 mM of two different sets of PNOX compounds (**A** and **B**) at 350 nm. Black line (DMSO, vehicle), coloured line (PNOX, as mentioned). Polymerization of tubulin with different compounds was monitored by absorbance at 355 nm (Filter A00019x) in 96 well plates (Falcon, transparent, flat bottom) with an Appliskan (Thermo Scientific). 25 mM of Tubulin in GAB buffer was prepared by mixing 10mM Sodium Phosphate, 30% Glycerol, 1mM EGTA, 6mM $MgCl_2$, and 1mM GTP of pH = 6.7. The buffer was supplemented with 27.5 mM of either the tested compounds or DMSO as vehicle. The turbidity was measured at 37 °C for 70 min. Data was transferred by using the Thermo Scientific SKanIt Software for Appliskan (version 2.3). The charts were plotted by SigmaPlot 13.0. To obtain the precise absorbance value of the compounds at 350nm, all the data were normalized to the value of absorbance of the initial stable plateau.

1.2.3 PBOXs/PNOXs: a colchicine site-binding ligand

Since tubulin possesses a complex molecular structure and dynamic unstable nature, X-ray crystallography is considered as the gold standard to accurately define the binding site of a particular agent in the microtubule network. Unfortunately, the attempts of co-crystallization/soaking of **PBOX/PNOX** compounds remained unsuccessful due to the high lipophilicity of the early developed analogues. Therefore, huge efforts have been implemented to develop new analogues to attenuate the lipophilicity by incorporating

precise structural modifications e.g., polar groups and/or heteroatoms. The most successful analogue in this quest was compound **33**, a quinolone-based derivative of the lead compound **29**, **PBOX-15** (**Figure 16**).

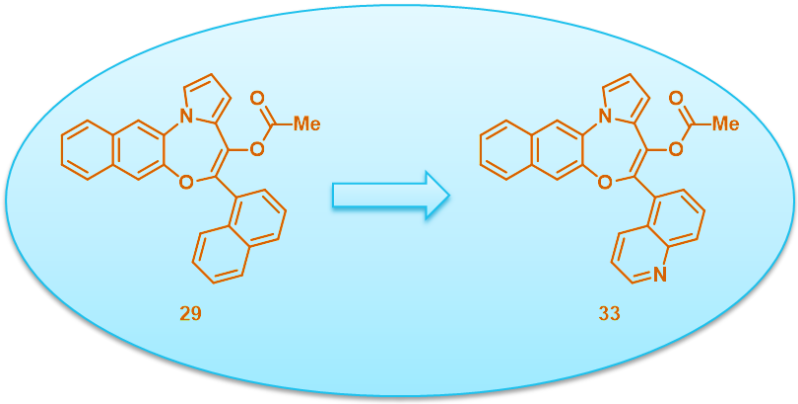

FIGURE 16. Development of compound **33** by introducing a quinoline moiety in compound **29** to overcome the lipophilicity of **PNOXs**.

The **33**-tubulin complex structure was investigated by X-ray crystallography (**Figure 16A**) to define the mode of interaction of **33** at the molecular level. Compound **33** was soaked into a crystal of a protein complex composed of two α- and β-tubulin heterodimers, the stathmin-like protein RB3, and tubulin tyrosine ligase. Using this approach, **33**-tubulin structure was determined to 2.4 Å resolutions and it was found that the compound gets bound to the colchicine site of tubulin.[155]

The superimposition of the β-tubulin chains of the free (PDB ID 4I55) and **33**-bound tubulin structures revealed a flip of the T7 loop of β-tubulin and a conformational change of the T5 loop of α-tubulin on ligand binding. These structural adaptations are necessary to accommodate the ligand in its binding site and are observed for other colchicine-site ligands. The fused system, acetoxyl and quinolyl moieties of **33** are buried into the colchicine site, generating most of the hydrophobic interactions with the β-tubulin. The interaction is further alleviated by a hydrogen-bond between the carbonyl of the acetoxyl group of **33** and βQ247 of the T7 loop of β-tubulin and a water-mediated contact between the nitrogen of the quinolyl moiety with the main chain carbonyl of βG237, amine groups of βT240, and βC241 from the H7 helix of β-tubulin. Moreover, the **PNOX** moiety is stacked between the sidechains of both K254 and K352 residues of β-tubulin. The NZ nitrogen of K352 is 5.7 Å distant from the center of the pyrrole ring of **33**, proposing that a cation-π stacking contact can be established. To compare the tubulin-binding mode of **33** with colchicine, the β-tubulin chains from the colchicine-tubulin (PDB ID 4O2B) and **33**-tubulin structures (**Figure 16B**) were superimposed. No functional common group in the

respective binding pockets of colchicine and **33** was found. The main differences are observed for the conformations of αT5 and βT7 loops. Compared to colchicine, bulky **PNOXs** moiety of **33** induces a flip of αT179 by establishing more hydrophobic contacts with αT5-loop. The conformational flip of the βT7 loop is induced by the acetoxyl moiety of **33** by displacing the side chain of L248. Together with L255 this residue is involved in the stabilization of the trimethoxy-substituted ring of colchicine. The 7-membered ring moiety of colchicine superimposes with the naphthyl group of the naphthoxazepine moiety of **33**, thereby forming similar hydrophobic contacts to tubulin. The common feature is a water-mediated contact between the 2-methoxy group of colchicine and the main chain carbonyl group of βV238 and the main chain amine group of βC241 of β-tubulin; in the vicinity, a water-mediated contact is also formed with the nitrogen of the quinolyl moiety of **33**. βA250 appears to be largely involved in hydrophobic contacts with both compounds (with pyrrole moiety of **33** and with the hepta-membered ring and the trimethoxyphenyl moiety of colchicine) (**Figure 16B**). These results define **33** as a colchicine binder. It is known that colchicine-site ligands inhibit microtubule polymerization by preventing the curved-to-straight conformational switch in tubulin assembly. Inspection of the **33** binding mode in the "curved" (T2R-TTL) and "straight" (PDB ID 1JFF) tubulin states stated that the ligand destabilizes microtubules by a similar mechanism.[155]

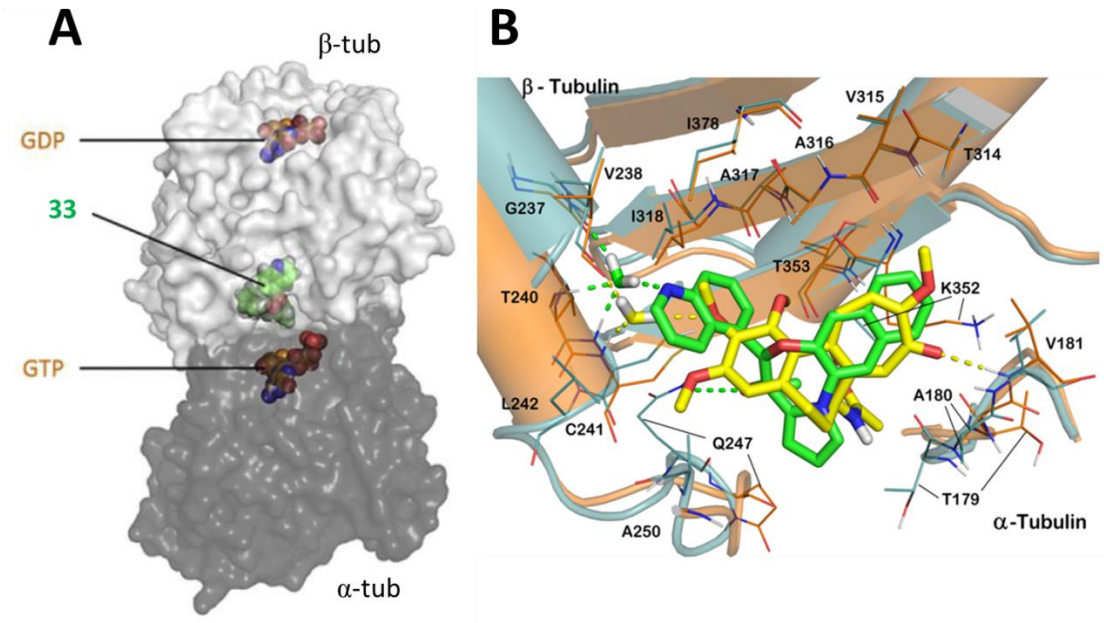

FIGURE 16. (**A**) Overall view of the X-ray crystal structure of the **33**-tubulin complex. The α- and β-tubulin subunits are represented in dark and light grey surface representation, respectively. **33** and the guanosine nucleotide molecules are shown in green and orange spheres representation, respectively. (**B**) Superposition between the crystal structures of colchicine-tubulin (orange cartoon

and yellow sticks) and **33**-tubulin (dark green cartoon and green sticks) complexes. Water molecules and H-bonds are coloured in the same colour as the ligands in the same complex.

PART 1 CHAPTER III

AIM OF WORK

As already described, autophagy is a cellular process of degradation and recycling triggered in response to normal physiological processes and adverse stress. As a result, it emerges as a supplier of drug resistance during chemotherapy in various cancers, including OSCC. Though depending on the stage of the tumor, it may serve as a double-sword mechanism to suppress tumorigenesis, in major cases inhibition of autophagy has been described as a favourable approach in cancer, as well as OSCC treatment. This might be due to the late stage diagnosis of OSCC malignancies. Driven by this influential fact, as a Medicinal Chemistry research group, we have focused on the development of autophagy inhibitors in OSCC while maintaining the key profile as potent pro-apoptotic agents.[150,154–157]

Being a highly dynamic process, autophagy machinery offers several numbers of pharmacological targets. Unfortunately, these targets (e.g., VPS34, ULK1, ATG5-ATG12-ATG16L complex) are often multifunctional and involved in several other cellular processes. Therefore, targeting one of them is not related with autophagy only. In addition, these proteins and their isomers are able to functionally compensate each other. As a result, targeting one component does not necessarily inhibit the autophagic machinery. Thus, the inhibition of autophagy always directs the path towards targeting the late-stage of the machinery. Since the formation of autolysosomes belong to the late-stage autophagy, targeting the lysosome fusion with autophagosomes are targeted. In this quest, **CQ** and **HCQ** along with other **CQ** analogues have engaged the attention despite of the associated toxicity and high-dose requirement in clinical trials. Noteworthy, the development of autophagy inhibitor should be designed to overcome these limitations.

Interestingly, **PBOX** compound **28** was reported to have autophagy inducing effect in human colon cancer cells. Treatment of **28** against the pharmacological inhibition of late stage autophagy with **9** enhanced **28**-induced apoptosis in the cancer cells. Further characterizations showed that **28**-induced autophagy plays a cytoprotective role as opposed to autophagic cell death.[157] Motivated by this observation, we wanted to perform selective and rational structural modifications in the core structure of both **PBOX** compound **28** and **PNOX** compound **29** to modify and subsequently producing a reverse effect on the

autophagic machinery. A further step onward, we have focused on the development of autophagy inhibitors with inherent pro-apoptotic activity.

In an attempt, we have converged two activity profiles i.e. the autophagy inhibitory effect of **CQ** and the pro-apoptotic effect of the **PBOXs**/**PNOXs**. An appropriate molecular modelling docking has been performed in order to design a new series of **PBOX**/**PNOX** compounds. Regarding the autophagy inhibitory effect, we have focused on the mechanism of action of **CQ**. This is well known and supported that the underlying mechanism behind **CQ** action is the presence of the basic moiety and successive lysosomal pH change to impair the lysosomal function.

Henceforth, the aim of this project was to successfully synthesize and characterize novel autophagy inhibitors in OSCC with inherited pro-apoptotic potential.

For both the compounds, all the three portions of the molecules have been explored with the introduction of polar groups/hetero atoms (**Table 2**). To mimic the **CQ** functionality, a large number of quinoline-ring bearing compounds have been under focus to be synthesized. Initially, in my PhD work the reference compound **29** was been resynthesized in large amount for the extensive cellular tests, as it was always used as a reference compound in the needed biological studies. The fused aromatic ring in portion 1 was modified by either the aromatic quinoline or methyl/acetyl protected piperazine system. The portion 2 was largely explored by the phenyl, 2-biphenyl, 1-naphthyl, 5-quinoline, 8-quinoline, and 5-isoquinoline rings. Portion 3, possessing the lateral chain was explored by means of most diverse modifications. Apart from the conventional methyl ester and diethyl amine carbamate system, the first remarkable attempt was to incorporate the lateral chain of **CQ** itself. Foreseeing the fact of long chain length and some plausible steric hindrance in the binding pocket, efforts have been focused more to insert a tertiary amine containing methyl piperazine system. A free piperazine ring has also been inserted to quantify the effect of the presence of a secondary amine group. In addition the lateral chain was reformed with the 3-pyridineand 4-pyridine ring to compare the effect of aliphatic and aromatic basic moiety in the same core structures.

Table 2. Synthesized analogues (**32**-**51**) of compound **28** and **29**

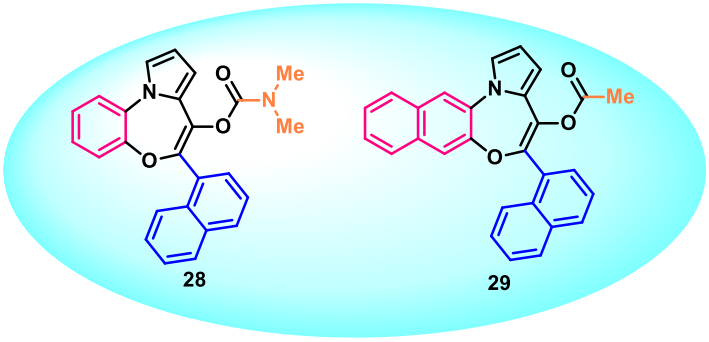

Cpd	Ar_1	Ar_2	R	Cpd	Ar_1	Ar_2	R
32	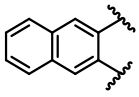			42		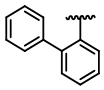	
33	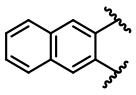	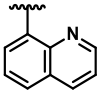		43	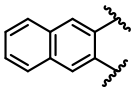	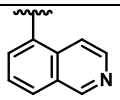	
34	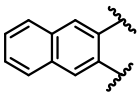	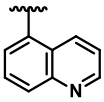	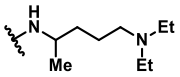	44	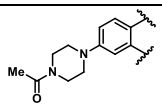		
35	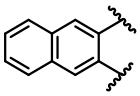	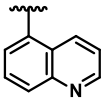	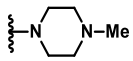	45	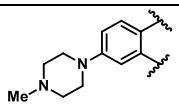	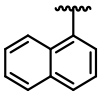	
36	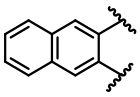	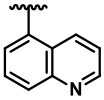	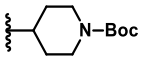	46	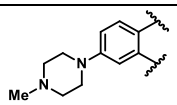	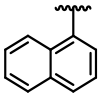	
37	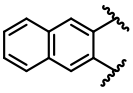	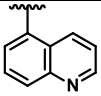	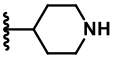	47	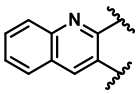	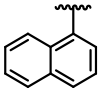	
38	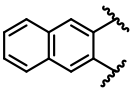	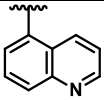		48			
39				49			
40				50			
41							

PART 1 CHAPTER IV

CHEMISTRY

1.4.1 Retrosynthetic pathway to synthesize PBOXs/PNOXs

The general retrosynthetic scheme for the synthesis of the novel compounds **32-51** is described in **Figure 17**. The synthesis of the key ketone templates (**52**) could be derived from the carboxylic acids **53** by applying an intramolecular Friedel-Craft acylation. Compounds **53** could be synthesized by either applying a Jocic-Reeve reaction with a pyrrolylephenols **54** and suitable aldehydes **55** or from a direct saponification on the corresponding esters **56**. Compounds **56** can be achieved by either an alkylation reaction between **54** and the suitable α-bromoesters **58** or a Mitsunobu reaction between **54** and α-hydroxyester derivatives **57**.

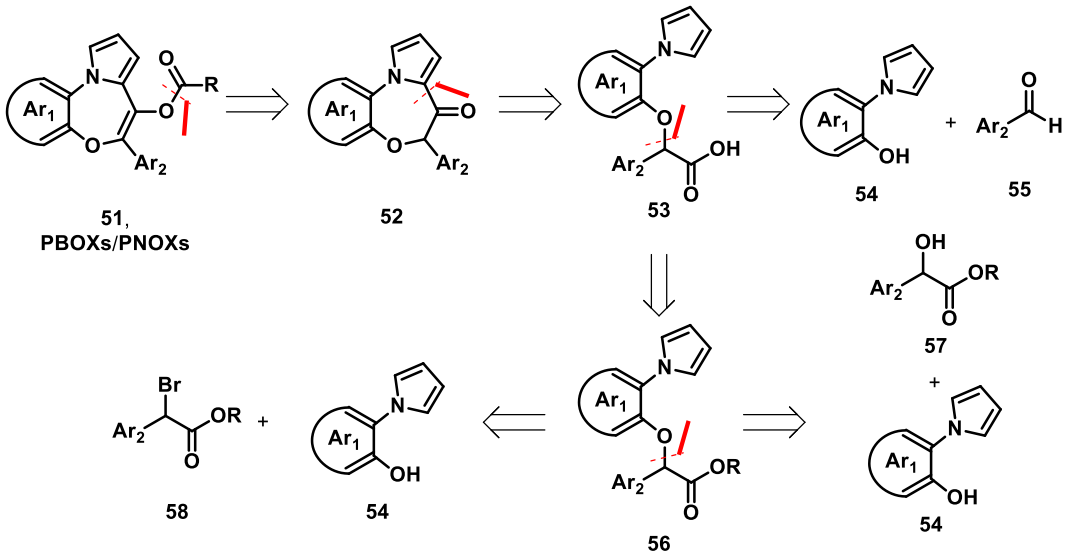

FIGURE 17. Schematic representation of the retrosynthetic pathway for the construction of **PBOX** and **PNOX** compounds.

1.4.2 Development of Jocic-Reeve pathway to synthesize PBOXs/PNOXs

As denoted in **Figure 18**, the esters (**56**) could be derived from the reaction between pyrrolylephenol derivatives (**54**) and suitable α-bromoester **58a** (**Figure 18A**) or α-hydroxyester **57a** (**Figure 18B**). These approaches have been followed to synthesize the **PBOX**/**PNOX** templates for several years.

Both the routes involved the treatment of an aryl bromide (**59a**) with *n*-butyllithium to insert the α-carbon atom to serve as the key for adding the α-bromo or α-hydroxy functionalities for aryl-alkyl ether construction (**Figure 18**). Otherwise with the alkylation route, the synthesis started from the suitable aldehydes (**55a**) easily accessible by treatment with dry *N*,*N*-dimethylformamide and **59a** in the presence of *n*-butyllithium. The additional carbon atom could then be introduced by a Wittig homologation protocol to synthesize the corresponding enol-ether which, upon treatment in acidic condition, afforded the homologated aldehyde (**60a**). The following oxidation to afford the corresponding methylester derivative was performed with *N*-iodosuccinimide and methyl iodide in presence of potassium carbonate. The oxidation step, as well as the subsequent radical bromination finally delivered the desired α-bromo derivatives in five steps with the overall yield of 15% (**Figure. 18A**).

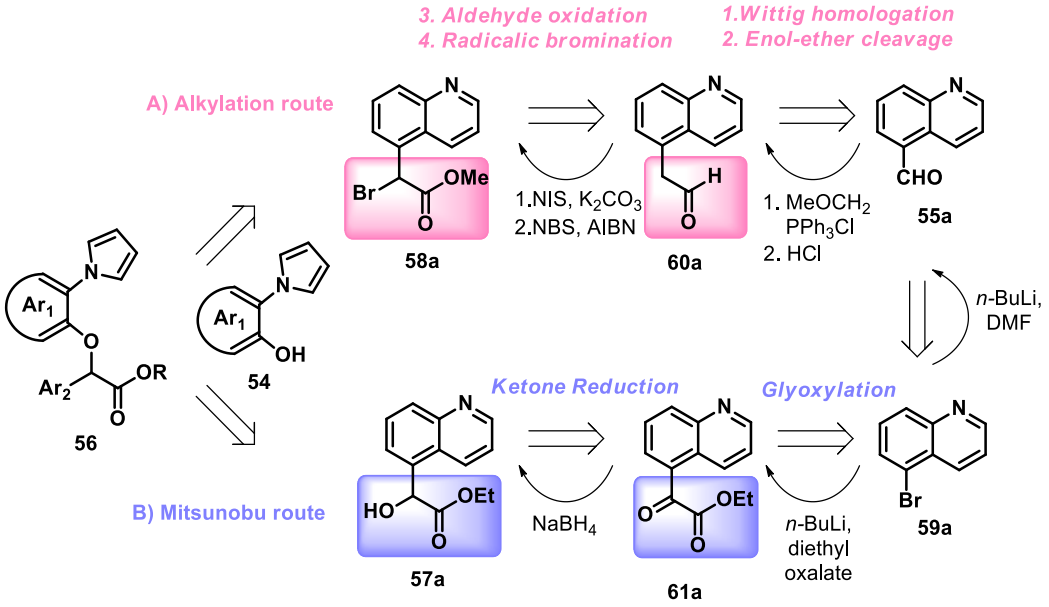

Figure 18. Outline of the synthesis of the α-bromoderivatives **58a** and α-hydroxyderivatives **57a**, to obtain the key ester **56**, according to the previously employed alkylation and Mitsunobu routes, respectively.

Due to the time-consuming and often tricky synthesis of α-bromopheylacetic derivatives of quinolines and other heterocycles, we afterward projected a Mitsunobu-based route to construct the key aryl-alkyl ether template. Consequently, a glyoxylate intermediate could represent a new and convenient access to the required α-hydroxyester derivatives (**57a**) to undergo Mitsunobu reaction with the pyrrolylphenols (**54**). This revised path shortened by three steps the original route to the ester intermediates **56**. The Mitsunobu route, although

shorter and more straightforward, demonstrated several pitfalls. The insertion of the glyoxalyl moiety by reaction with ethyl chlorooxoacetate in presence of *n*-butyllithium produced a series of side products with following tiresome purifications and poor yields. In addition, the simultaneous presence of keto and ester functionalities led to the simultaneous over-reduction to the corresponding diol (overall yield 6%, **Figure 18B**). Further, the over-reduction occurred to different extents depending on the substrate, temperature, time, and reaction scale, often, in a quite unpredictable fashion. Also, the Mitsunobu reaction itself displayed moderate yields and is not suitable for large scale-up applications and led to the formation of a significant number of side products.

Since, both of these options exhibited a number of drawbacks, leading to inadequate overall yields to synthesize the **PBOXs**/**PNOXs**, we proposed a Jocic-type protocol for the construction of the target core. After a preliminary investigation focusing on the isolation of a trichloromethyl carbinol derivative, we moved towards a multicomponent single-step approach. Screening of a variety of solvents and bases identified the optimum conditions for the preparation of the crucial α-aryloxy carboxylic acids to undergo an intramolecular ring-closure. The novel chemical route considerably improved the overall yields in comparison to the previously employed rotes for the preparation of **PBOX**/**PNOX**-based compounds (**Figure 19**).[158]

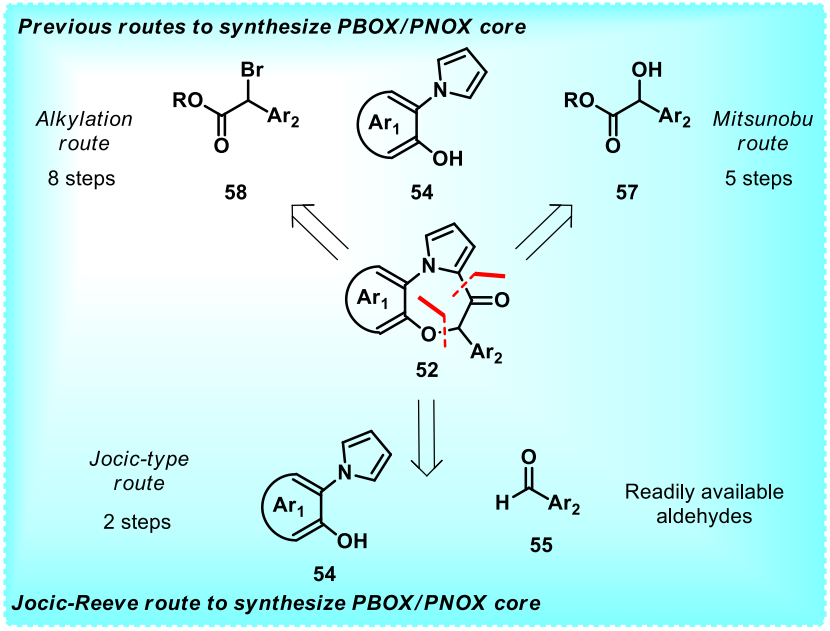

Figure 19. Representative **PNOX** derivatives, previous retrosynthetic analysis, and newly proposed Jocic-type approach.

In our context, the designed Jocic-Reeve process employed the aldehyde to be converted into the corresponding trihalomethyl carbinol and a phenol derivative to function as the nucleophile. As shown in **Figure 20**, the carbinol (**62**) underwent a conversion into the corresponding *gem*-dihaloepoxide (**64**) which, upon attack of the phenoxide nucleophile, provided the corresponding acyl halide, promptly converted into the desired carboxylic acid.

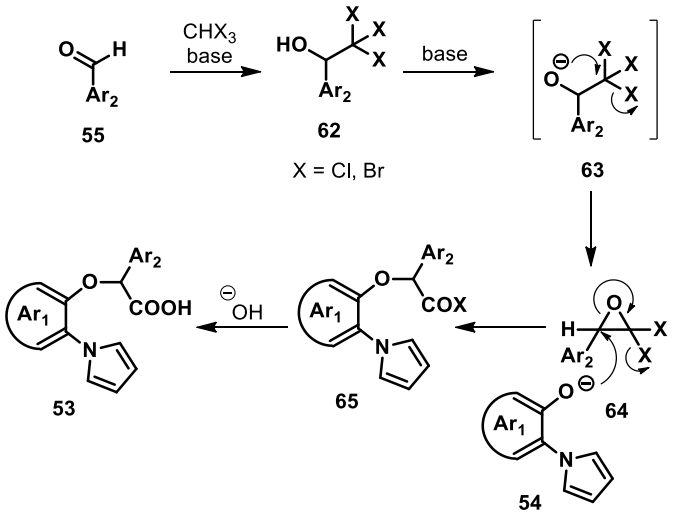

Figure 20. Designed Jocic-Reeve pathway to synthesize the carboxylic acid derivative **53**, key intermediate for the synthesis of the **PBOX**/**PNOX** cores.

Consequently, we identified a series of focused attempts based on both literature data and our longstanding experience in α-aryloxycarboxylic acid synthesis (**Table 3**). Initially, we investigated the result of a single-pot system (entries 1–8, **Table 3**) on 1-naphthyl, 5-quinolyl and 8-quinolyl aldehydes by using sodium hydroxide as base and bromoform as halogen source. Interestingly, this attempt offered the desired acids for 1-naphthyl (entry 2, **Table 3**) and 5-quinolyl (entry 5, **Table 3**) systems with good yields but remained unproductive for the 8-quinolyl aldehyde (entry 6, **Table 3**). An extended reaction time along with a modified equivalency (entry 7 and 8, **Table 3**) of the starting materials appeared to be unsatisfactory for this, resulting in poor yield (entry 7, **Table 3**) or in a complex by-products mixture (entry 8, **Table 3**). Moreover, starting materials were recovered in good extent for almost every reactions of the 8-quinolyl system. Relying on the mechanistic understanding of the Jocic-Reeve reaction pathway, we tried to explore this procedure in a two-pot system (entry 9 to 14, **Table 3**). However, it could not offer us a better outcome, which was also complicated by the lack of reproducibility (entry 11, **Table 3**). For both the attempts, 1-naphthyl and 5-quinolyl systems produced a

considerable amount of side products obtained through a Cannizzaro side ractrion. Application of a milder alkaline system (entry 13, **Table 3**) to reduce this particular disadvantage was not helpful as it could not offer the desired α-aryloxycarboxylic acid.

Table 3. Reaction conditions explored for the Jocic-type synthesis of aryloxy carboxylic acids **15**.

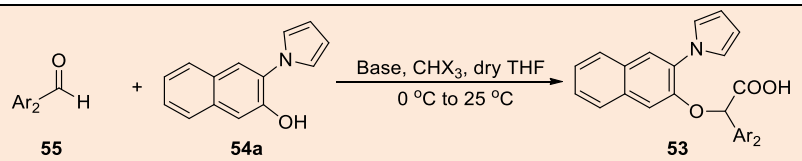

55 **54a** **53**

Entry[a]	Method[b,c]	Ar_2	54a (eq.)	X (eq.)	Base (eq.)	Temp (°C)[d]	Time (h)[e]	Yield (%)[f]
1	A[b]	1-naphthyl	0.3	Br (1.7)	NaOH (1.7)	rt	6	4
2			0.3	Br (1.7)	NaOH (1.7)	rt	12	48
3			1.0	Br (1.7)	NaOH (1.7)	rt	12	3
4			1.0	Br (5.0)	NaOH (5.0)	rt	12	-
5		5-quinolyl	0.3	Br (1.7)	NaOH (1.7)	rt	12	28
6		8-quinolyl	0.3	Br (1.7)	NaOH (1.7)	rt	12	-
7			0.3	Br (1.7)	NaOH (1.7)	rt	48	5
8			0.5	Br (1.7)	NaOH (1.7)	rt	36	-
9	B[c]	1-naphthyl	0.3	Br (1.7)	NaOH (1.7)	rt	6	11
10			0.3	Br (1.7)	NaOH (1.7)	rt	12	20
11			0.5	Br (1.7)	NaOH (1.7)	rt	12	37[g]
12			1.0	Br (5.0)	NaOH (5.0)	rt	12	-
13			0.5	Br (1.7)	Cs_2CO_3 (1.7)	rt[h]	72	-
14			0.3	Cl (1.7)	NaOH (1.7)	50[i]	14	-

[a] Reactions were conducted with 1 eq of aldehyde in dry THF except for entry 11 (2 drops of DMF added to THF) [b] Phenol was treated with base and aldehyde followed by the haloform in a single pot system [c] Phenol and aldehyde, along with haloform were treated in two separate flasks followed by the transferring of phenoxide system to the aldehyde and haloform [d] Temp was maintained at 0 °C for 1 h and then was allowed to reach room temp for method A; whereas, for method B temp was maintained at 0 °C for 1 h before and after the transferring of the phenoxide system except for entry 9-11 [e] Reaction time after reaching at room temp [f] Isolated yield of purified product. [g] Not reproducible and not scalable. [h] Tempe was maintained at 0 °C for 3 h before and 1 h after transferring the phenoxide system [i] Temp was maintained at 0 °C for 1 h before and after the transferring of phenoxide system and was increased to 50 °C for 2 h.

1.4.3 Synthesis of reference compound 29

The synthesis of the reference compound **29** is described in **Scheme 1** by following both the alkylation route and Jocic-Reeve route. Both the routes used the pyrrolylphenol compound, **54a**, which was synthesized from the corresponding amino compound **68a**, by following a Clauson-Kass protocol in presence of a 6 N hydrochloric solution in dioxane medium at 120 °C. The alkylation route started with commercially available 2-(naphthalen-1-yl)acetic acid, **66** with a subsequent esterification and α-bromination to the ester group headed for **58b**. Afterward, in a convergent approach, the nucleophilic substitution was performed between **54a** and **58b** to obtain the aryl-alkyl ester **56a** in presence of potassium carbonate in *N*,*N*-dimethylformamide solution at 85 °C. The ester was then treated under a basic saponification condition to produce **53a**. On the other hand, for the Jocic-Reeve pathway, the acidic compound **53a** was directly obtained from **54a** and the commercially available naphthaldehyde **55b**. The aryl-alkyl ether containing acid (**53a**) was then subjected to an intramolecular Friedel-Craft reaction for the ring closure at the α-carbon of the pyrrole ring to obtain the precursor ketone, **52a**. In the final step a sodium enolate of compound **52a** was generated in presence of sodium *bis*(trimethylsilyl)amide in dry THF medium at -78 °C and a successive treatment with acetyl chloride to produce the target compound **29**.

Scheme 1. Synthesis of compound **29**

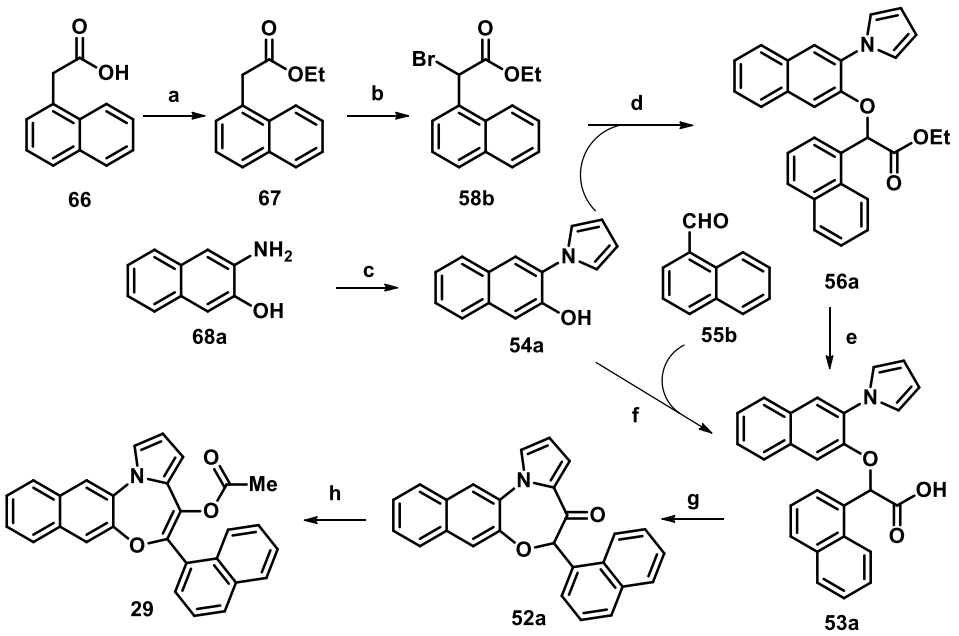

Reagents and conditions: (a) $SOCl_2$, EtOH, 70 °C, 12 h, quantitative; (b) NBS, AIBN, CCl_4, 80 °C, 12 h, quantitative; (c) 2,5-dimethoxytetrahydrofuran, 1,4-dioxane, HCl (6 N), 120 °C, 1 h, 80%; (d) K_2CO_3, DMF dry, 85 °C, 12 h, 90%; (e) NaOH (5% aqueous solution), THF, EtOH, 25

°C, 12 h, quantitative; (f) NaOH, $CHBr_3$, THF dry, 0 °C (1 h) to 25 °C (12 h), 48%; (g) PCl_5, DCM dry, 40 °C, 12 h, 50%; (h) NaHMDS, CH_3COCl, -78 °C (3h) to 25 °C, (12 h), 60%.

1.4.4 Synthesis of compounds 32 and 33

Synthesis of final compounds **32** and **33** is described in **Scheme 2** by comparing both the Mitsunobu-based and the Jocic-Reeve-based pathways. The synthesis started from the bromoaniline **69**, which was converted into the 8-bromoquinoline **59b** by a Skraup reaction. In Mitsunobu route 5-bromoquinoline (**59a**) and 8-bromoquinoline (**59b**) were used for the synthesis of **32** and **33**, respectively. **59a**,**b** were converted into their corresponding ethyl glyoxylates derivatives **61a**,**b** by using diethyl oxalate in presence of *n*-butyllithium. Selective reduction of the ketone group was completed by reaction with sodium borohydride in dry THF to provide the α-hydroxyester derivatives **57a**,**b**. Arylpyrroles **54a** was submitted to a Mitsunobu reaction with **57a**,**b** derivatives providing aryl-alkyl ethers **56b**,**c**. These esters were then used to synthesize the final compounds **32** and **33**, as already described in **Scheme 1**. For the Jocic-Reeve pathway the key aldehydes **55a**,**c** were prepared from the corresponding bromo derivatives by a formylation reaction. The syntheses, up to the final compounds **32** and **33**, were achieved by following the same conditions and pathways as already described before for the synthesis of **29**.

Scheme 2. Synthesis of compound **32** and **33**

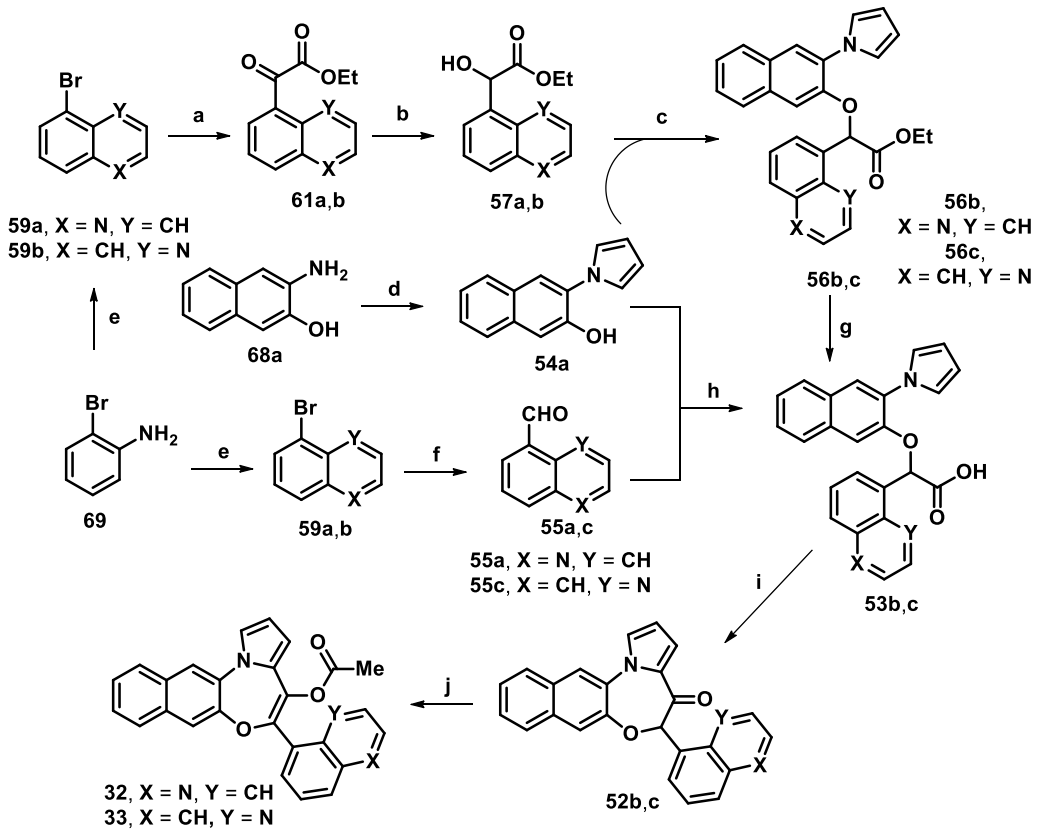

Reagents and conditions: (a) *n*-BuLi, (2.5 M solution in hexane), diethyl oxalate, dry THF, -78 °C, 10 min, 20%; (b) $NaBH_4$, dry THF, 25 °C, 2 h, 21%; (c) PPh_3, DIAD, dry DCM, from 0 °C to 25 °C, 24 h, 49% for **56b** and 68% for **56c**; (d) 2,5-dimethoxytetrahydrofuran, 1,4-dioxane, HCl (6 N), 120 °C, 1 h, 80%; (e) glycerol, $PhNO_2$, $FeSO_4 \cdot 7H_2O$, conc. H_2SO_4, 150 °C, 7 h, 60%; (f) *n*-BuLi (2.5 M solution in hexane), dry DMF, dry THF, -78 °C, 15 min, 69% for **55a** and 53% for **55c**; (g) NaOH (5% aqueous solution), THF, EtOH, 25 °C, 12 h, 88% for **53b** and 85% for **53c**; (h) NaOH, $CHBr_3$, THF dry, 0 °C (1 h) to 25 °C (12 h), 37% for **53b** and 30% for **53c**; (i) PCl_5, DCM dry, 40 °C, 12 h, 75% for **52b** and 52% for **52c**; (j) NaHMDS, CH_3COCl, -78 °C (3 h) to 25 °C, (12 h), 75% for **32** and 18% for **33**.

1.4.5 Synthesis of compound 34-41

- **Synthesis of compounds 34-39**

Synthesis of the final compounds **34-39** is reported in **Scheme 3** from the prefinal ketone **52b** and is reported in. For, **34** and **35**, the synthesis was accomplished by activating *in situ* the sodium enolate of **52b** into a carbonate system in the presence of 4-nitrophenyl chloroformate, which were successively reacted with *N*,*N*-diethylpentane-1,4-diamine and *N*-methylpiperazine to produce **34** and **35**, respectively.[159] Compound **36** was synthesized by treating the sodium enolate of **52b** with *tert*-butyl 4-(chlorocarbonyl)piperidine-1-

carboxylate, prepared *in situ* from the corresponding acid in the presence of thionyl chloride. Deprotection of **36** with trifluoroacetic acid generated the final compound **37**. Though, the formation of compound **38** by treating the isonicotinoyl chloride and the sodim enolate like others was confirmed by the accurate mass spectrometry and crude NMR analysis, unfortunately, we could not isolate this compound possibly due to its stability issues encountered in both the silica and alumina gel chromatographic purification techniques. We tried to overcome this drawback by exchanging the lateral chain of isonicotinoyl ester with a nicotinoyl ester and compound **39** was successfully synthesized (and isolated) from the sodium enolate of **52b** and nicotinoyl chloride.

Scheme 3. Synthesis of compound **34-39**

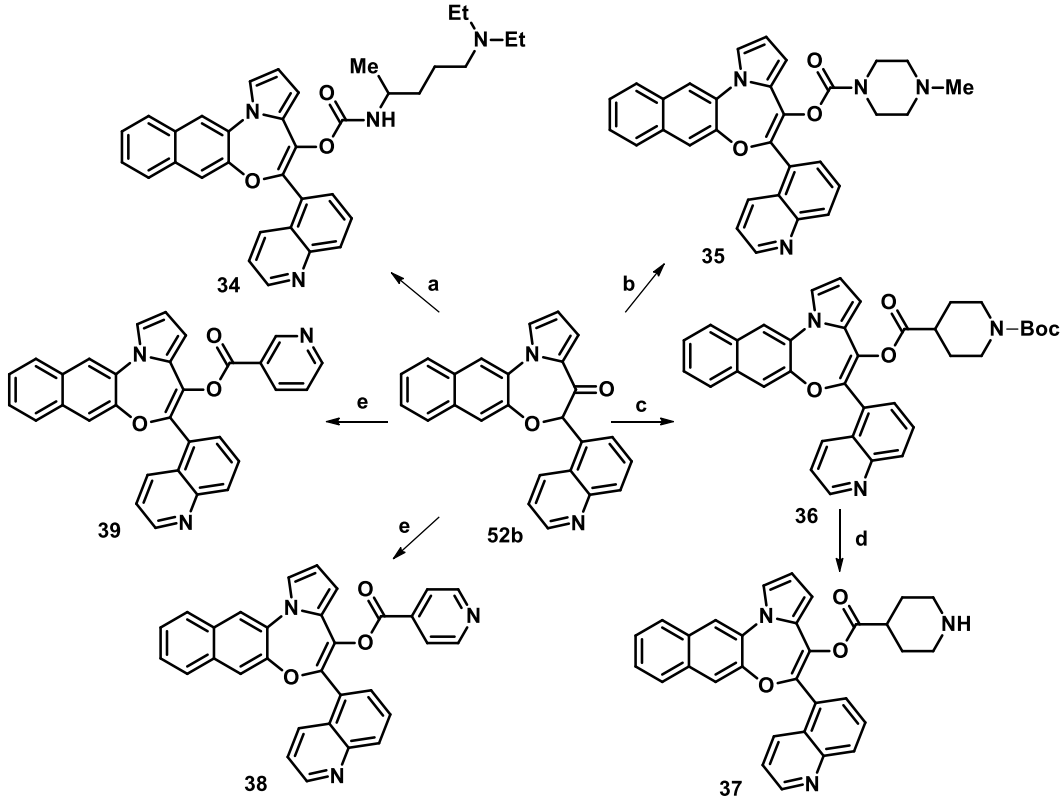

Reagents and conditions: (a) NaHMDS, 4-nitrophenyl chloroformate, *N*,*N*-diethylpentane-1,4-diamine, -78 °C (1 h) to 25 °C (4 h), 30%; (b) NaHMDS, 4-nitrophenyl chloroformate, *N*-methylpiperazine, -78 °C (1 h) to 25 °C (4 h), 56%; (c) NaHMDS, *tert*-butyl 4-(chlorocarbonyl)piperidine-1-carboxylate, -78 °C (3 h) to 25°C (12 h), 64%; (d) NaHMDS, nicotinoyl chloride, -78 °C (3 h) to 25°C, (12 h), 31%; (e) TFA, DCM dry, 0 °C to 25 °C 15 min, 96%.

- **Synthesis of compounds 40 and 41**

The synthesis of the final compounds **40** and **41** was completed by using the ketone compound **52c** (**Scheme 4**). For this task, we followed the same synthetic conditions and reagents as already discussed in **Scheme 3** for the synthesis of compounds **35** and **37**.

Scheme 4. Synthesis of compound **40** and **41**

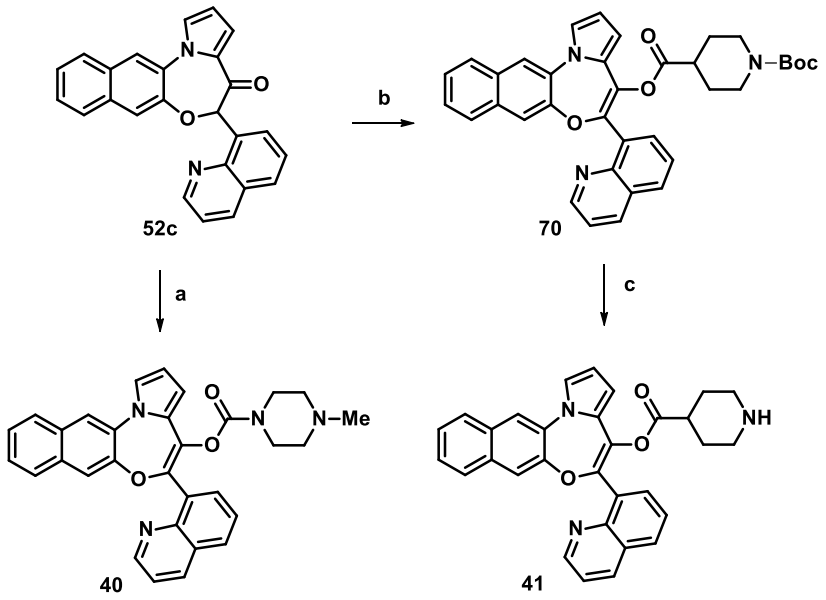

Reagents and conditions: (a) NaHMDS, 4-nitrophenyl chloroformate, *N*-methylpiperazine, -78 °C (1 h) to 25 °C (4 h), 20%; (b) NaHMDS, *tert*-butyl 4-(chlorocarbonyl)piperidine-1-carboxylate, -78 °C (3 h) to 25°C (12 h), 65%; (c) TFA, DCM dry, 0 °C to 25 °C 15 min, 48%.

- **Exploration to develop carbamate and ester lateral chains**

A number of different reaction conditions have been applied for the construction of particular carbamates (CQ lateral chain, piperazine moiety) and ester (piperidine moiety) functionality incorporation (e.g., in compound **34**, **35**, and **37**) in the lateral chain of portion 3 of the **PNOX** compounds. Like several reported research works in the field of carbamate bond formation, we conceived the reaction pathways to either activate our parent ketone system or the lateral chain itself. In order to accomplish that, we used several conditions for the enolate formation and different activated system like phosgene, triphosgene, 4-nitrochloroformate, and *N*,*N*-disuccinimidyl carbonate (**Table 4**). We used the pre-final ketone of our reference compound **28** and the *N*,*N*-diethylpentane-1,4-diamine as the amine foundation of the carbamate functionality. As reported in **Table 4**, none of our attempts (entry 1-4, **Table 4**) was successful until we applied NaHMDS to form the enolate and successive carbonate activation by using 4-nitrochloroformate and then treat

the reaction mixture with the amine in presence of a basic source like trimethylamine (entry 5, **Table 4**).

Table 4. Reaction conditions applied for the construction of carbamate functionality

Entry	Reaction condition	Outcome
1	KH (30% in mineral oil), DSC, THF dry, DMF dry, TEA, 25 °C, 1.5 h	X
2	KH (30% in mineral oil), triphosgene, THF dry, DIPEA, 25 °C, 2 h	X
3	KH (30% in mineral oil), 4-nitrochloroformate, THF dry, 25 °C, 3 h	X
4	NaHMDS (1 M in THF), phosgene, THF dry, -78 °C, 1 h	X
5	NaHMDS (1 M in THF), 4-nitrochloroformate, THF dry, TEA -78 °C, 3 h	60%

As regards the ester functionality insertion, we employed a two-pot approach of activating the amine source in advance and subsequent addition to the enolate mixture. We used the ketone **52b** and different piperidine-4-carboxylic acid system with the activating agents like thionyl chloride and carbonyldiimidazole in a number of reaction conditions (**Table 5**). For all the attempts, with the exception of entry 6, though the activation was successful as confirmed by the precise mass spectroscopy, NMR analysis, and the TLC the final ester bond was never detected. In fact, each time we recovered up to 90-98% of the starting material. However, to our delight employment of the Boc-protected piperidine carboxylic acid produced the ester bond, as well as the desired compound, when by treatment with thionyl chloride.

Table 5. Reaction conditions applied for the construction of ester functionality

Entry	Amine source	Reaction condition	Outcome
1	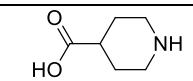	CDI, TEA, DCM dry, 25 °C, 12h	Starting material recovered
2	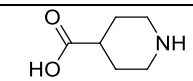	$SOCl_2$, DCM dry, 0 °C, 12h	Starting material recovered
3	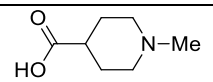	CDI, TEA, DCM dry, 25 °C, 12h	Starting material recovered
4	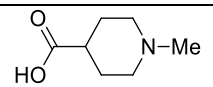	$SOCl_2$, DCM dry, 0 °C, 12h	Starting material recovered
5	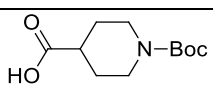	CDI, TEA, DCM dry, 25 °C, 12h	Starting material recovered
6	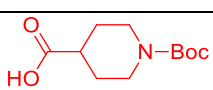	$SOCl_2$, DCM dry, 0 °C, 12h	quantitative

1.4.6 Synthesis of compounds 42 and 43

The synthesis of the compounds **42** and **43** was attained by following the Mitsunobu reaction route as reported in **Scheme 5**. The synthesis started from the commercially available 2-bromobiphenyl **59c** and 5-bromoisoquinoline **59d** (synthesized by a selective bromination on isoquinoline **71**) to produce the α-hydroxyesters **57c** and **57d**, respectively. These were then used for the key Mitsunobu step with the pyrrolylphenols **54a**,**b** for the preparation of the esters **56d**,**e**. The corresponding acids **53d**,**e** were then cyclised into **52d**,**e** and finally converted into the final compounds **42** and **43**.

Scheme 5. Synthesis of compound **42** and **43**

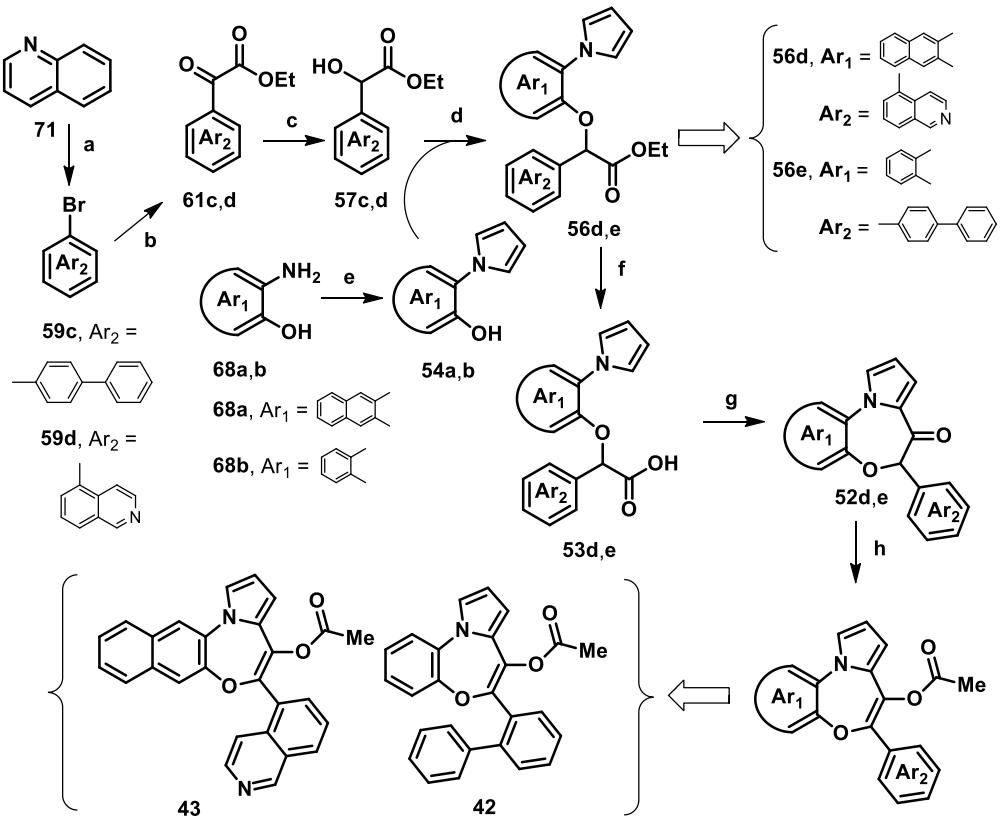

Reagents and conditions: (a) NBS, H_2SO_4, from -25 °C to 25 °C, 24 h, 70%; (b) *n*-BuLi, (2.5 M solution in hexane), diethyl oxalate, dry THF, -78 °C, 10 min, 18% for **61c** and 40% for **61d**; (c) $NaBH_4$, dry THF, 25 °C, 2h, 56% for **57c** and 50% for **57d**; (d) PPh_3, DIAD, dry DCM, from 0 °C to 25 °C, 24 h, 35% for **56d** and 56% for **56e**; (e) 2,5-dimethoxytetrahydrofuran, 1,4-dioxane, HCl (6 N), 120 °C, 1 h, 80% for **54a** and 60% for **54b**; (f) NaOH (5% aqueous solution), THF, EtOH, 25 °C, 12 h, 80% **53d** and 90% for **53e**; (g) PCl_5, DCM dry, 40 °C, 12 h, 60% for **52d** and 37% for **52e**; (h) NaHMDS, CH_3COCl, -78 °C (3h) to 25 °C, (12 h), 84% for **42** and 30% for **43**.

1.4.7 Synthesis of compounds 44-46

In **Scheme 6**, the synthesis of the piperazine moiety containing compound **44** is reported. The synthesis was initiated with 4-bromo-2-nitrophenol (**72**). In the first instance, the benzyl-protected phenol (**73**) was produced by using benzyl bromide in the presence of potassium carbonate. After that, **73** was submitted to a palladium-catalyzed Buchwald-Hartwig cross-coupling reaction in the presence of piperazine to synthesize the intermediate **74.**[160] Compound **74** underwent to an acetylation on the free piperazine moiety with of acetic anhydride and triethylamine to produce the intermediate **75.**[161] Subsequently, **75** was treated with trifluoroacetic acid and thioanisole to perform a benzyl deprotection and yielding the nitrophenol intermediate (**76**).[162] The nitrophenol was then reduced to the resultant aminophenol (**77**) with iron and calcium chloride.[163] After that, the amine **77** was exposed to a Clauson-Kaas reaction protocol with acetic acid and 2,5-dimethoxytetrahydrofuran to synthesize the pyrrole derivative **54c**.[164]. This was submitted to an alkylation reaction with the ester **58b** with sodium hydride to generate the aryl-alkyl ether skeleton containing ester derivative **56f**. The ester was hydrolyzed into the corresponding acids **53f**, which was treated with the Lewis acid phosphorus pentachloride towards an intramolecular Friedel-Crafts cyclization to synthesize the key ketone **52f** in dichloromethane medium. The final ester compound **44** was synthesized by reacting acetyl chloride with the potassium enolate of **52f**.[159]

Scheme 6. Synthesis of compound **44**

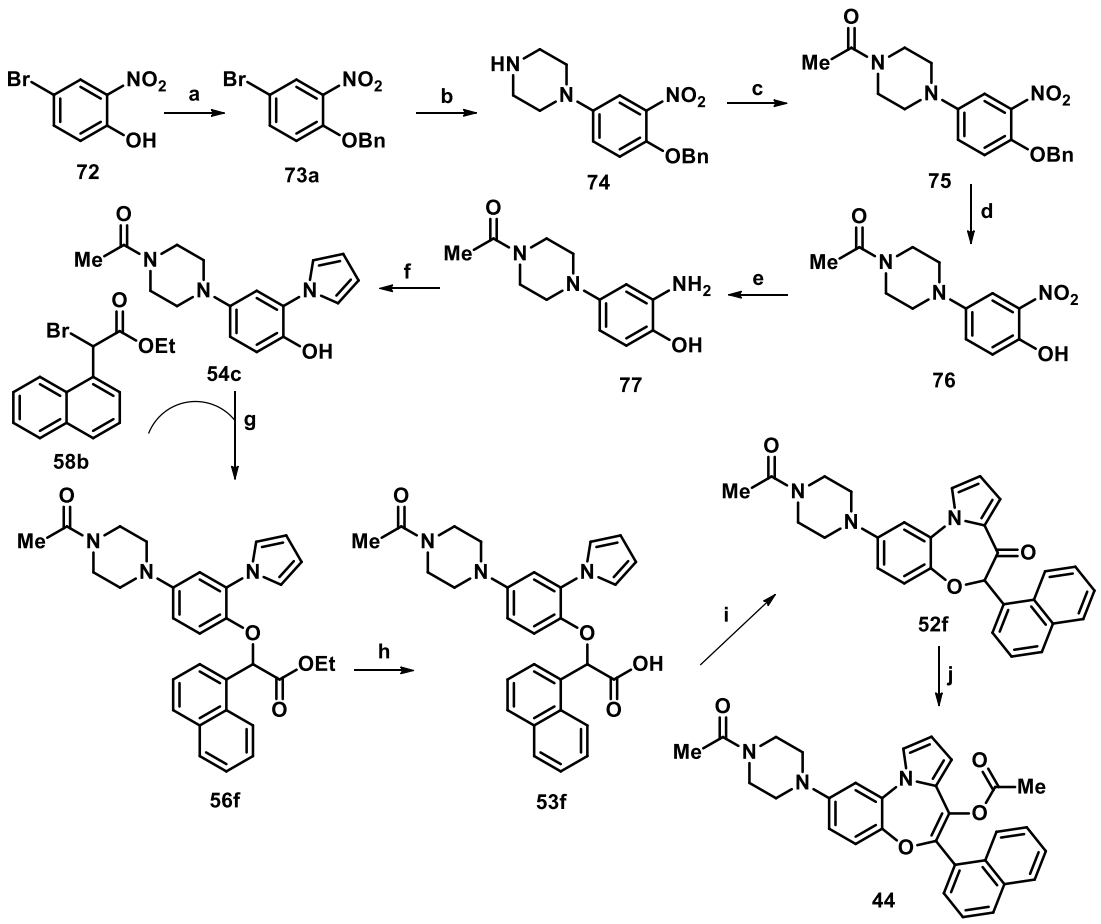

Reagents and conditions: (a) $PhCH_2Br$, K_2CO_3, DMF dry, 85 °C, 12 h, quantitative; (b) piperazine, $Pd(OAc)_2$, ±BINAP, Cs_2CO_3, 1,4-dioxane, sealed tube, 120 °C, 12 h, 71%; (c) TEA, Ac_2O, 25 °C, 12 h, quantitative; (d) TFA, toluene, thioanisole, 25 °C, 12 h, 85%; (e) Fe, $CaCl_2$, 75% EtOH (aq), 90 °C, 30 min, 54%; (f) 2,5-dimethoxytetrahydrofuran, AcOH, H_2O, 120 °C, 5 h, 50%; (g) NaH, THF dry, 25 °C, 12 h, quantitative; (h) NaOH (5% aqueous solution), THF, MeOH, 25°C, 2 h, quantitative; (i) PCl_5, DCM dry, 45 °C, 12 h, 20%; (j) TEA, DMAP, Ac_2O, DCM dry, 0 °C to 25 °C, (12 h), 30%.

The synthesis of the piperazine moiety containing compounds **45** and **46** is reported in **Scheme 7**. The synthesis was initiated as the synthesis of **44** to have the compound **73**. The nitro compound was reduced to the corresponding aminophenol (**78a**) in the presence of iron and calcium chloride.[163] Afterward, the amine was used in a Clauson-Kaas reaction protocol in the presence of 2,5-dimethoxytetrahydrofuran in hydrochloric acid and water medium to generate the pyrrolyl compound **79a**.[163,165] After that, **79a** underwent a palladium-catalyzed Buchwald-Hartwig cross-coupling reaction in the presence of N-methylpiperazine to obtain the intermediate **80a**.[160] The methylpiperazine intermediate, **80a** was successively treated with palladium over carbon in methanol under hydrogen

atmosphere to go through a benzyl-deprotection and synthesize compound **54d**. This latter was submitted to the Jocic-Reeve reaction conditions using the aldehydes **55a**,**b** to directly synthesize the aryl-alkyl ether skeleton containing acid intermediates (**53g**,**h**). The acid **53g** was treated with phosphorus pentachloride as the Lewis acid to give an intramolecular Friedel-Crafts cyclization to afford the key ketone (**52g**) in dichloroethane medium. Despite several efforts (reported later in details) we could not cyclize the acid **53h**. The final ester compound **45** was synthesized by reacting acetyl chloride with the sodium enolate of the ketone. On the other hand, **s**ynthesis of the carbamate-bades compound **46** was accomplished by activating the *in situ* generated sodium enolate of **52g** into a carbonate system with 4-nitrophenyl chloroformate, which was successively reacted with diethylamine.[159]

Scheme 7. Synthesis of compound **45** and **46**

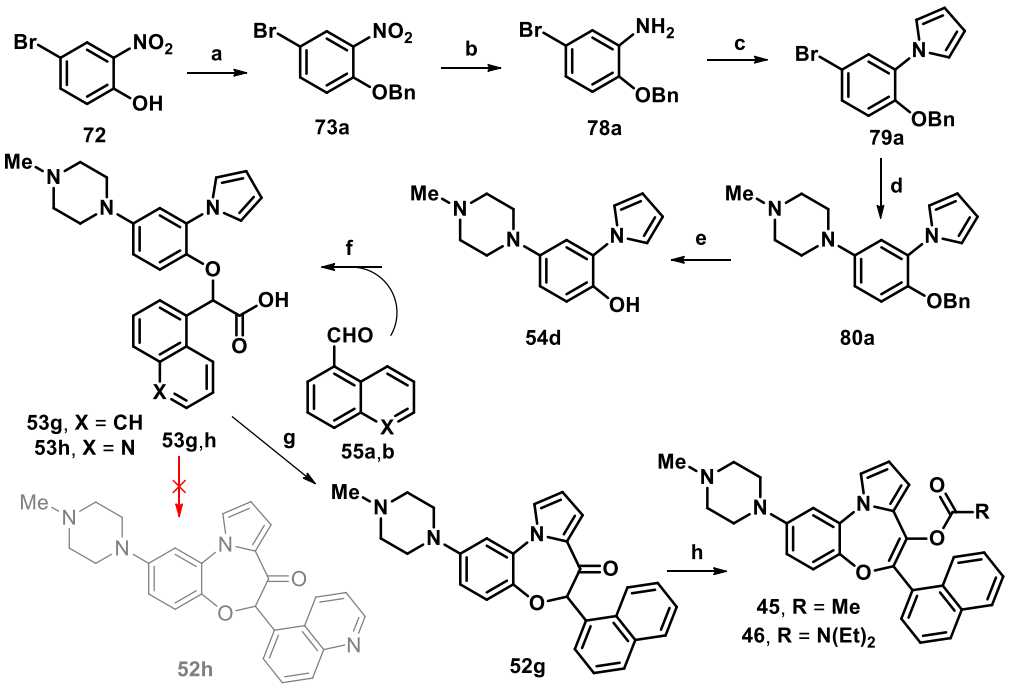

Reagents and Conditions: (a) $PhCH_2Br$, K_2CO_3, DMF dry, 85 °C, 12 h, quantitative; (b) *N*-methylpiperazine, $Pd(OAc)_2$, ±BINAP, Cs_2CO_3, 1,4-dioxane, sealed tube, 120 °C, 12 h, 71%; (c) Pd/C, H_2, MeOH, 25 °C, 2 h quantitative; (d) Fe, $CaCl_2$, 75% EtOH (aq), 90 °C, 30 min, 54%; (e) 2,5-dimethoxytetrahydrofuran, 1,4-dioxane, aq. HCl (6 N), 120 °C, 1 h, 88%; (f) NaOH, $CHBr_3$, THF dry, 0 °C (1 h) to 25°C (12 h), 39% for **53g** and 10% for **53h**; (g) PCl_5, DCE dry, 85 °C, 12 h, 42%; (h) NaHMDS, CH_3COCl, -78 °C (3h) to 25 °C, (12 h), 23% for **45** or NaHMDS, 4-nitrophenyl chloroformate, diethylamine, -78 °C (1 h) to 25 °C (4 h), 33% for **46.**

- **Alternative synthetic approaches to obtain the building block 54d**

An alternative synthetic pathway is described in the **Scheme 8** where the O-atom was protected by a MOM group. The overall yield of this new pathway is 30% in comparison to 52% yield of the followed benzyl protection route.

Scheme 8. Alternative synthetic pathway for the development of **54d**

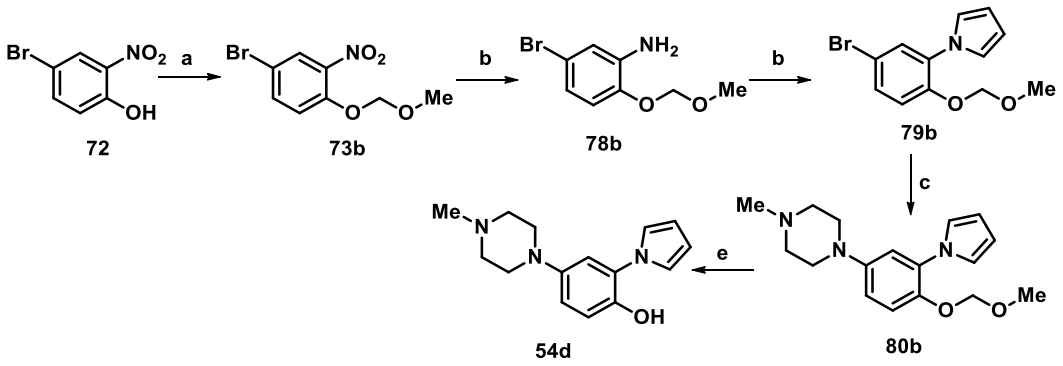

Reagents and conditions: (a) MOMCl, *N*,*N*-Diisopropylethylamine, $CHCl_3$, 45 °C, 16 h, 71%; (b) Fe, $CaCl_2$, EtOH (75% in H_2O), 90 °C, 30 min, 74%; (c) 2,5-dimethoxytetrahydrofuran, CH_3COOH, H_2O, 110 °C, 12 h, 67%; (d) *N*-methylpiperazine, $Pd(OAc)_2$, BINAP, Cs_2CO_3, 1,4-dioxane, sealed tube, 120 °C, 12 h, 67%; (e) HCl (6N), MeOH, DCM, 25 °C, 1 h, 90%.

- **Proposed synthetic approaches for the synthesis of 45**

In **Scheme 9** three of our proposed synthetic approaches to finalise compound **45** are indicated. In the Route 1, we attempted to perform a Buchwald-Hartwig amination directly on compound **72**. However, the very first reaction remained unsuccessful and we had to drop this idea. In Route 2, **72** was benzyl protected with the as usual procedure to produce **73b**. This compound was then was submitted to a Buchwald-Hartwing amination to produce compound **81**. However, the successive selective reduction of the nitro group to amine in presence of iron powder and calcium chloride did not produce any result; whereas the reduction under hydrogen pressure and in presence of palladium on carbon generated a mixture of several side products. Therefore, we had to conceive another route, Route 3. In this pathway, **72** was first subjected to a nitro to amine reduction to synthesize **82** which was then trated in a Clauson-Kass reaction protocol to synthesize the pyrrole compound **83**. This pyrrole was used for the alkylation reaction with the α-bromoester **58b** to synthesizze the key ester compound **56g**. Regrettably, the next step of the Buchwald-amination did not produce any result again. The attempt to perform the amination on **83** also remain unsuccessful.

Scheme 9. Designed and proposed synthetic pathway for the development of **45**

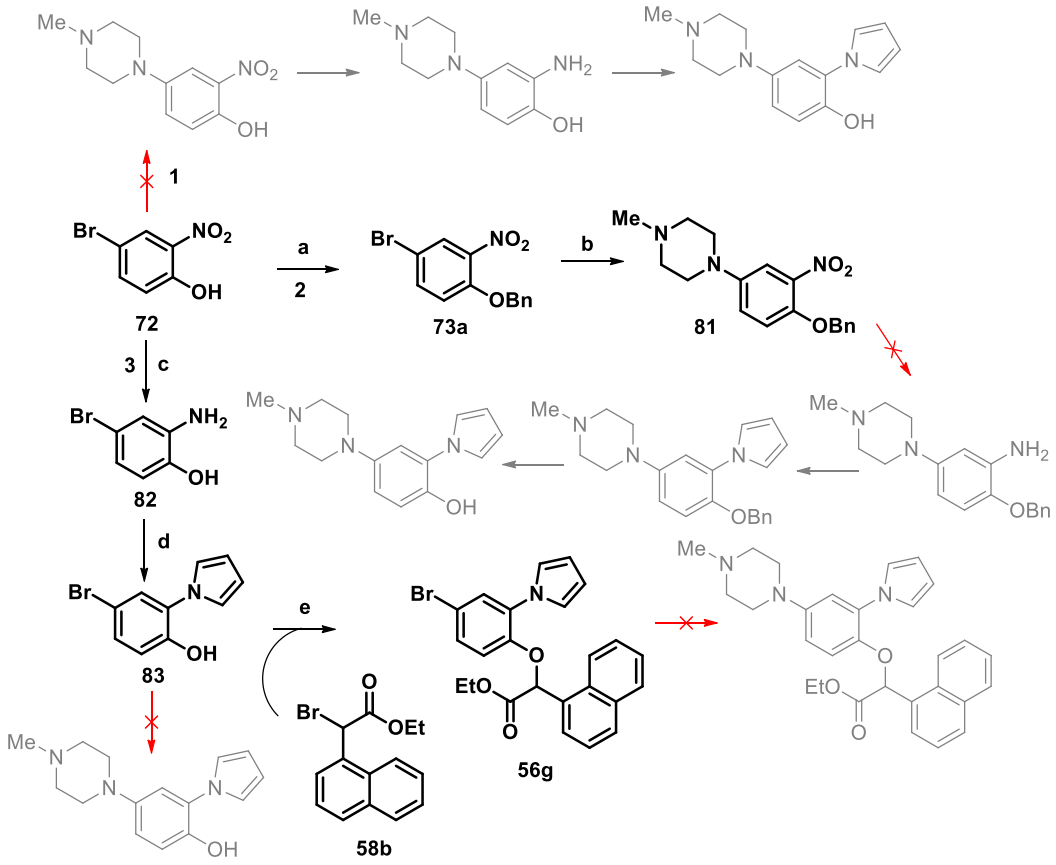

Reagents and Conditions: (a) $PhCH_2Br$, K_2CO_3, DMF dry, 85 °C, 12 h, quantitative; (b) *N*-methylpiperazine, $Pd(OAc)_2$, BINAP, Cs_2CO_3, 1,4-dioxane, sealed tube, 120 °C, 12 h, 71%; (c) Fe, $CaCl_2$, EtOH (75% in H_2O), 90 °C, 30 min, 70%; (d) Pd/C, H_2, MeOH, 25 °C, 2 h, quantitative. (e) K_2CO_3, DMF dry, 85 °C, 12 h, 60%.

- **Applied Buchwald-Hartwig amination reaction conditions**

We have performed an exhaustive literature search and applied those synthetic approaches for the development of the Buchwald-Hartwig amination reaction (**Table 6**).[166] The more widely and successfully used metal-complex are based on palladium (entry 1-6 and 10, **Table 6**), copper (entry 8, **Table 6**), and iron (entry 7, **Table 6**) metals. A variety of ligands like BINAP (entry 1-3 and 6, and 10, **Table 6**), Xantphos (entry 5, **Table 6**), and *L*-proline (entry 8, **Table 6**) to form the metal-ligand complex are used. About the basic source, potassium and cesium carbonates are considered for most of the methods while toluene and dioxane efficiently serve as the reaction medium either in a sealed tube or under reflux conditions at high temperature (**Table 6**).

After a number of investigations we found the best performing reaction condition and reagents as described in entry 10, **Table 6** for our compounds.

Table 6. Applied Buchwald-Hartwig amination conditions

Entry	Metal complex	Ligand	Base	Solvent	Temp (° C)	Time (h)	Condition
1	$Pd(OAc)_2$	BINAP	Cs_2CO_3	dioxane	120	12	Reflux
2	$Pd(OAc)_2$	BINAP	Cs_2CO_3	toluene	110	12	Reflux
3	$Pd(OAc)_2$	BINAP	$NaOBu^t$	toluene	110	12	Reflux
4	$Pd(OAc)_2$	Triisobutyl-phosphatrane	$LiN(SiMe_3)_2$	Toluene	80	20	Reflux
5	$Pd_2(dba)_3$	Xantphos	Cs_2CO_3	dioxane	120	12	Sealed tube
6	$Pd_2(dba)_3$	BINAP	Cs_2CO_3	dioxane	120	12	Reflux
7	DPPF	$(DPPF)PdCl_2$	Cs_2CO_3	THF	25	1	normal
8	CuI	L-proline	K_2CO_3	DMSO	110	48	Reflux
9	-	-	-	neat	100	12	Sealed tube
10	$Pd(OAc)_2$	BINAP	Cs_2CO_3	dioxane	120	12	Sealed tube

- **Modifications of the synthetic approach towards ketones 52g,h**

The already reported Friedel-Crafts cyclization in the presence of PCl_5 in DCM medium often suffered from a poor and unpredictable yield due to the formation of the corresponding methyl ester analogue as a side product. This observation has been verified by Mass spectrometry and NMR analyses for differently substituted **PBOX/PNOX** compounds. Though we could re-use this ester in future attempts, the ester formation was consuming almost half of the starting acidic compounds. This fact prompted us to investigate this step in more details and from our mechanistic understanding we predicted that the distillation of the used solvent (DCM) in the presence of $CaCl_2$ could serve as an *in situ* methanol source. So we changed the solvent system from DCM to DCE. Interestingly, and as a confirm of our hypothesis, this modification solved the limitation in this method. Later, we executed the cyclization step with altered molar equivalents of PCl_5 for further reaction yield improvements and identified the use of 1.1 equivalent of PCl_5 as the best choice (entry 2 and 11, Method A, **Table 7**). Furthermore, we attempted the cyclization of our already produced ketone **52b**, **52g**, and **52h** with hexafluoro-2-propanol (Method B), zinc chloride (Method C), and boron trifluoride diethyl etherate (Method D) as the Lewis acidic source (**Table 7**).[167] [168] [169] Method B and C appeared as a substantial alternate strategy to produce **52b** (entry 3 and 4, **Table 7**) but remained unsuccessful for the generation of **52g** (entry 12 and 13, **Table 7**) as well as **52h** (entry 18 and 19, **Table 7**). Unfortunately, none of the methods could produce the cyclized ketone **52h**.

Table 7. Optimization in the Friedel-Craft cyclization

Entry	Methods	Ar_1	Ar_2	Lewis acid (eq.)	Solvent	Temp. (°C)	Time (h)	Yield (%)
1	A[a]	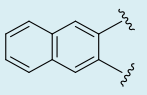		PCl_5 (3)[b]	DCM	45	12	66
2				**PCl_5 (1.1)**	**DCE**	**45**	**12**	**85**
3	B[c]			HFIP	DCM	25	6	70
4	C[d]			$ZnCl_2$	DCM	0→45	4	75
5	A	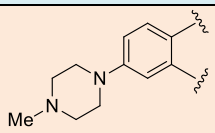	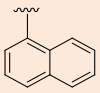	PCl_5 (1.1)	DCM	45	12	28
6				PCl_5 (1.1)[b]	DCM	45	12	X
7				PCl_5 (1.3)	DCM	45	12	X
8				PCl_5 (1.3)[b]	DCM	45	12	X
9				PCl_5 (3)	DCM	45	12	X
10				PCl_5 (3)[b]	DCM	45	12	X
11				**PCl_5 (1.1)**	**DCE**	**85**	**12**	**42**
12	B			HFIP	DCM	25	6	X
13	C			$ZnCl_2$ (2)	DCM	0→ 45	4	X
14	D[e]			$BF_3{\cdot}Et_2O$	DCM	25	7	X
15	A	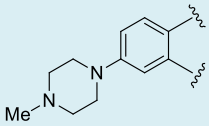		PCl_5 (1.1)	DCM	45	12	X
16				PCl_5 (3)[b]	DCM	45	12	X
17				PCl_5 (1.1)	DCE	85	12	X
18	B			HFIP	DCM	25	6	X
19	C			$ZnCl_2$ (2)	DCM	0→ 45	4	X
20	D			$BF_3{\cdot}Et_2O$	DCM	25	7	X

[a]PCl_5 was added one single time to the reaction mixture. [b]PCl_5 was divided and added in five small portions to the reaction mixture. [c]A solution of HFIP in DCM (2:3) was added. [d]Trifluoroacetic anhydride (1.4 eq) was added to the reaction mixture with a subsequent addition of zinc chloride. [e]Ethyl chloroformate (1.1 eq) and TEA (1.1 eq) was added to the reaction mixture followed by borontrifluoride diethyletherate

- **Proposed synthetic approaches for the synthesis of 52h**

In the next attempt, we tried to modify the synthetic pathway to achieve the ketone **52h** starting from the intermediate **83** (**Scheme 10**). We wanted to cyclize the system before the insertion of the piperazine moiety in order to avoid the basic nature of the substrate of the

Friedel-Craft cyclization that has to be performed in and acidic medium. To this effort, we performed a Jocic-Reeve reaction with the pyrrolylephenol intermediate **83** and the aldehyde **55a** to produce the corresponding acid **53i**. After that, the cyclization as reported in Method A, **Table 10** was successfully executed for the formation of the **52i** ketone. However, the Buchwald amination reaction protocol applied to **52i** remained unsuccessful. We also wanted to perform the reaction in a protected keto functionality containing system, but the protection trial did not produce the desired product.

Scheme 10. Proposed synthetic pathway for the development of **52h**

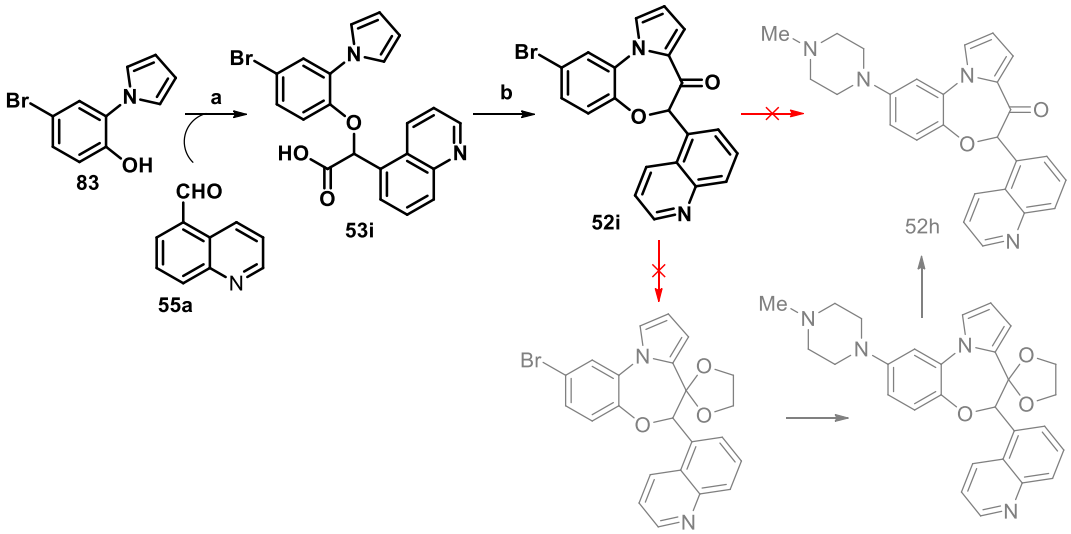

Reagents and Conditions: (a) NaOH, $CHBr_3$, THF dry, 0 °C (1 h) to 25°C (12 h), 60%; (g) PCl_5, DCE dry, 85 °C, 12 h, 65%.

1.4.8 Synthesis of compounds 47-50.

Synthesis of the compounds **47-50** is described in **Scheme 11**. It started with the commercially available 2-chloroquinoline **84** that was selectively boronated at C-3 following a C-2-chloro orientation in presence of LDA and trimethylborate at -78 °C in THF medium. The boronic acid **85** was then successfully hydrolyzed into **86**, the corresponding chloroquinolinol with ammonium chloride and hydrogen peroxide in ethanol. The hydroxy group was protected by means of a benzyl group before performing a Buchwald-Hartwig amination employing the conditions usually followed by us, and we generated the pyrrolyl compound **80c**. Afterwards, **80c** was treated with Pd/C under hydrogen atmosphere for synthesizing **54e**, the Jocic-Reeve substrate with naphthaldehyde to yield the aryl-alkyl ether containing carboxylic acid **53j**. Then, it was cyclized with PCl_5

in dry DCE under reflux for generating the ketone **52j**, which was used for the synthesis of the four target compounds. Synthesis of **47**, **88**, and **50** was achieved by following the protocol as already described for the synthesis of **32**, **36**, and **37**, respectively. For the synthesis of **48** and **49**, the attempts with 4-nitrophenylchloroformate to generate the activated carbonate system and then treat it with the corresponding amines were unsuccessful. Therefore, we used the very reactive phosgene to generate the activated chloroformate system to react with the amine and produce the carbamate bond. Notably, we had to use the phosgene in excess (12 equivalents) amount to increase the reaction yield.

Scheme 11. Synthesis of compound **47-51**

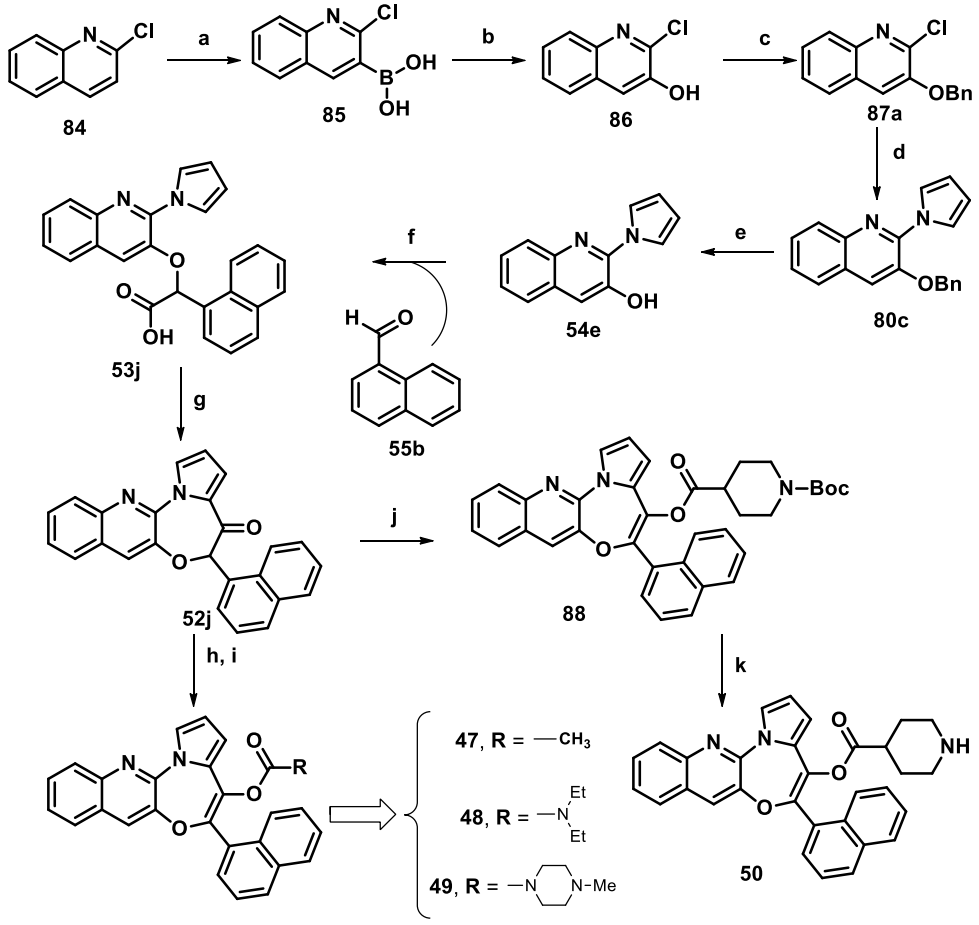

Scheme 5: (a) *n*-BuLi, DIPA, $B(OMe)_3$, THF dry, -78 °C, 5 h, 79%; (b) NH_4Cl, H_2O, H_2O_2, EtOH, 25 °C, 18 h, 90%; (c) K_2CO_3, $PhCH_2Br$, DMF dry, 85 °C, quantitative; (d) pyrrole, $Pd(OAc)_2$, ±BINAP, Cs_2CO_3, 1,4-dioxane, sealed tube, 120 °C, 12 h, 58%; (e) Pd/C, H_2, MeOH, 25 °C, 2 h quantitative; (f) NaOH, $CHBr_3$, THF dry, 0 °C (1 h) to 25°C (12 h), 56%; (g) PCl_5, DCE dry, 85 °C, 12 h, 75%; (h) NaHMDS, CH_3COCl, -78 °C (1 h) to 25 °C (2 h), 72% for **47**; (i) NaHMDS,

$COCl_2$ (20% in toluene), diethylamine, -78 °C (1 h) to 25 °C (2 h), 42% for **48** or NaHMDS, $COCl_2$ (20% in toluene), N-methylpiperazine, -78 °C (1 h) to 25 °C (2 h), 65% for **49** (j) NaHMDS, *tert*-butyl 4-(chlorocarbonyl)piperidine-1-carboxylate, -78 °C (1 h) to 25°C (2 h), quantitative; (k) TFA, DCM dry, 0 °C to 25 °C 1 h, 79%.

- **Alternative synthetic approaches to obtain the building block 54e**

The target intermediate **54e** was also synthesized from an alternative approach as described in **Scheme 12**. In this approach, compound **86** was protected with a methyl group to produce **87b**, which served as the Buchwald-Hartwig amination substrate to afford the pyrrolyl compound **80d**. Finally, the methyl group was removed by treating **80d** in presence of boron tribromide in DCM solution.

Scheme 12. Synthetic approaches for the building block **54e**

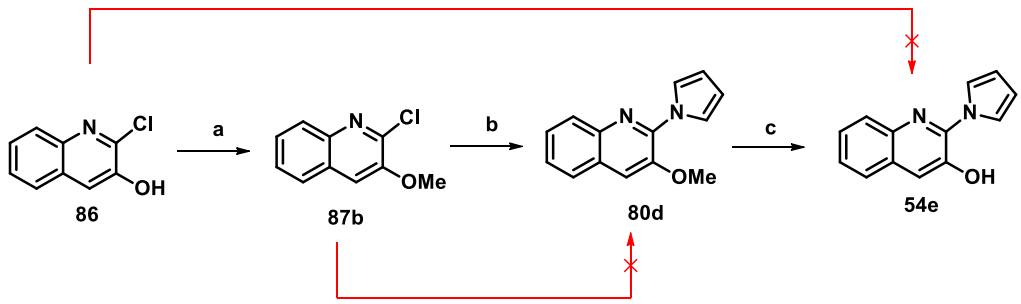

Reagents and Conditions: (a) CH_3I, K_2CO_3, DMF dry, 85 °C, 12 h, quantitative; (b) $Pd(OAc)_2$, ± BINAP, Pyrrole, Cs_2CO_3, 1,4-dioxane, sealed tube, 100 °C, 12 h, 74%; (c) BBr_3, DCM dry, 0 °C (30 min) to 25 °C (12 h), 55%.

We have also tried to apply the direct Buchwald amination on the compound **86**, but the attempt remained unsuccessful. In addition the effort to insert the pyrrole in the quinoline ring of **87b** by applying a direct metal-free aromatic substitution was unsuccessful.

- **Proposed synthetic approaches for the building block 54f and 54g**

A huge effort was engaged for the development of the quinoline ring containing building block **54f** and **54g** as reported in **Scheme 13** and **Scheme 14**. For **54f**, we initially started from compound **89** and applied a Clauson-Kaas protocol for the pyrrole ring formation. The nitro group of the pyrrolic compound **90** was reduced to the corresponding amino compound in presence of iron powder and calcium chloride reflux condition in ethanol.

After the unsuccessful Skraup reaction on **91**, the free hydroxyl group was protected by both the benzyl and methyl groups. However, the Skraup reaction performed on the protected system **92** also failed.

Scheme 13. Synthetic approaches for the building block **54f**

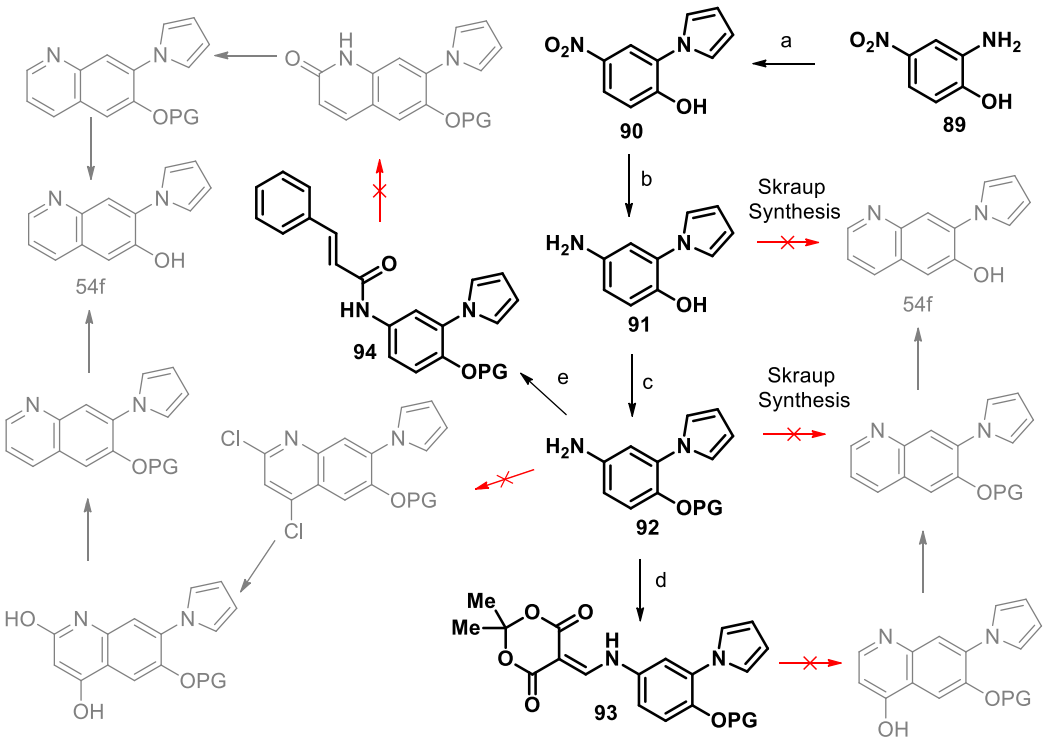

Reagents and Conditions: (a) 2,5-dimethoxytetrahydrofuran, 1,4-dioxane, aq. HCl (6 N), 120 °C, 1 h, quantitative; (b) Fe, $CaCl_2$, 75% EtOH (aq), 90 °C, 30 min, 70%; (c) $PhCH_2Br$/MeI, K_2CO_3, DMF dry, 85 °C, 12 h, quantitative; (d) meldrum acid, $CH(OMe)_3$, DMF dry, 105 °C, 80%; (e) cinnamoyl chloride, DCM dry, TEA, 25 °C, 2 h, 90%.

Afterwards, three different approaches on **92** were applied as described in **Scheme 13**. Each of these attempts failed at the ring closure step.

The synthesis of **54f** was also performed with methoxybenzaldehyde **95** under a Friedlander quinoline ring synthesis condition. Compound **95** was treated with concentrated sulfuric acid and nitric acid to synthesize the di-nitro compoun **96**, which was then reduced to the *bis*-amino compound **97**. The next step of the quinoline ring synthesis in presence of acetaldehyde and potassium hydroxide did not produce any result.

The synthesis of the building block **54g** was investigated in a Pomeranz-Fritsch quinoline synthesis protocol by starting from the **98** in the presence of 2,2-dimethoxyethylamine in

toluene medium under reflux condition for 12 h. This step was a quantitative yielding method for synthesizing **99**. Regrettably, we faced again the undesirable failure in the ring closure step.

Scheme 14. Synthetic approaches for the building block **54f** and **54g**

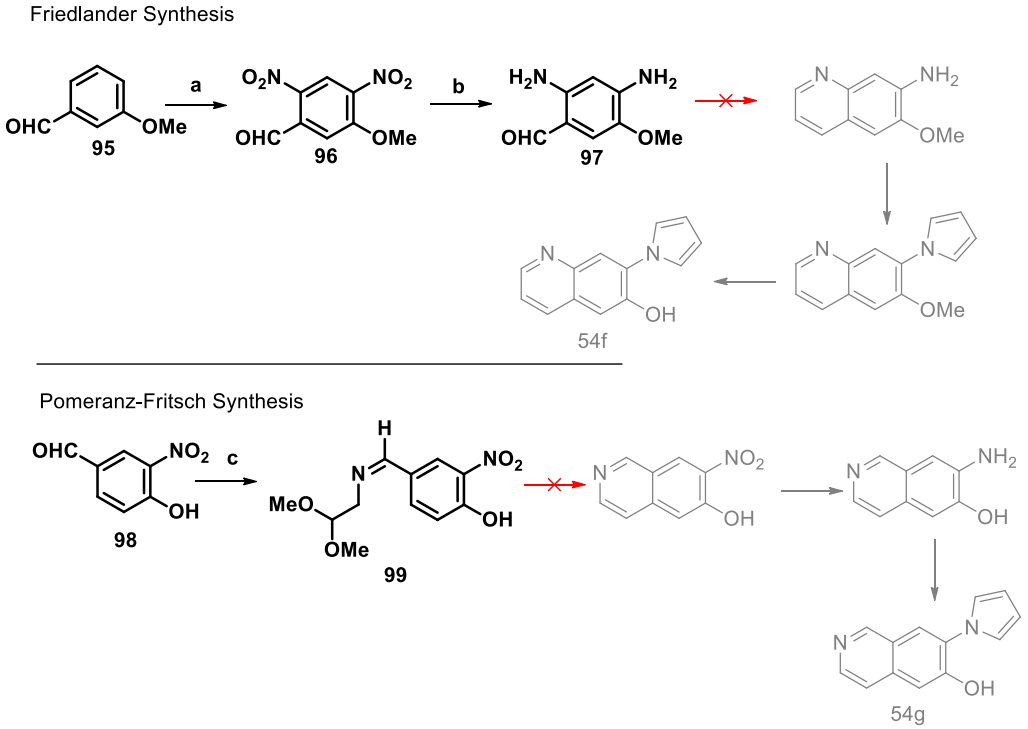

Reagents and Conditions: (a) H_2SO_4, HNO_3, -10 °C 1 h, 20%; (b) Fe, $CaCl_2$, 75% EtOH (aq), 90 °C, 30 min, 48%; (c) 2,2-dimethoxyethylamine, toluene, 110 °C, 12h, quantitative.

PART 1 CHAPTER V

RESULTS AND CONCLUSIONS

1.5.1 Results

1.5.1.1 Biological Results

All the synthesized compounds (**32**-**39** and **42**-**46**) were subjected to several biological tests on a wide range of tumor cell lines. Their cytotoxicity, pro-apoptotic and anti-autophagy profiles were assessed. The results available to date are reported and briefly discussed below.

- **Apoptosis test on HL-60 cell lines**

We measured the dissipation of the mitochondrial membrane potential in TMRM loaded HL-60 cells following the treatment with the compounds (**Figure 21**). All the compounds with the exception of **45** and **46** promote apoptosis in HL-60 cell line.
Interestingly, **29**, **32**, **35**, **37**, **39**, and **46** were able to induce apoptosis *ex vivo* in splenocytes obtained from the Eμ-TCL1 mouse model of chronic lymphocytic leukemia described by an increase of leukemic B cells dependent in part of defective apoptosis.

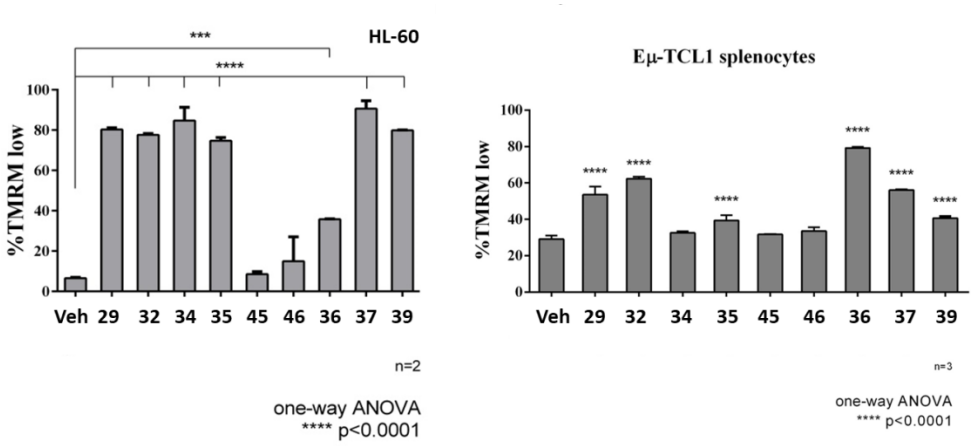

Figure 21. TMRM assay of compounds on HL-60 cell line and Eμ-TCL1 splenocytes to determine the percentage of apoptosis for 48 h at a concentration of 10 μM.

- **Preliminary cytotoxicity assessment**

The effects of the compounds (**34-37**, **39**, **45**, and **46**) on mouse fibroblast NIH3T3 have been inspected by evaluating the percentage of viable cells with the concentration range of 0.1 to 120 μM (**Table 8**). This test, being performed on a "normal" murine cell line is used

for predicting liability of toxic effects versus normal cells and could be used for calculating safety windows and/or therapeutic indexes. Literature data reported that the IC_{50} of taxol, colchicine, **29**, and **32** against mouse fibroblast NIH 3T3 are in the range of 25 ± 3, 25 ± 4, 126 ± 4, and 42 ± 9, respectively.[170] Compound **28** and its analogues required a relatively higher concentration range (~ 5 μM, **46**; ~ 45 μM, **45**) for attaining the 50% cell inhibitory effect. On the other hand, all the **29** analogues displayed a higher IC_{50} value than compound **29** and **32** in cancer cell lines.

Table 8. Cytotoxicity assessment of the compounds on the growth of mouse fibroblast NIH 3T3.

Cpds	Concentrations (μM)[a]									
	0.1	**0.15**	**0.3**	**0.45**	**0.6**	**5**	**6**	**45**	**90**	**120**
	% of viable cells[b]									
34	90±5[c]	91±6[c]	85±7[c]	78±7[c]	63±6[c]	32±5[c]	**47±4[c]**	9±4[c]	5±2[c]	0[c]
35	78±5[c]	71±5[c]	69±7[c]	**55±6[c]**	20±7[c]	0[c]	7±3[c]	0[c]	0[c]	0[c]
36	93±7[c]	91±5[c]	88±9[c]	76±7[c]	66±6[c]	23±5[c]	**53±6[c]**	8±4[c]	5±2[c]	0[c]
37	81±7[c]	72±7[c]	66±8[c]	59±5[c]	**48±3[c]**	12±6[c]	33±5[c]	5±4[c]	6±3[c]	0[c]
39	94±6[c]	86±6[c]	81±4[c]	75±6[c]	73±5[c]	52±4[c]	**65±6[c]**	39±5[c]	31±4[c]	15±5[c]
45	100±3	104±7	99±5	97±7	97±4	69±5[c]	83±6[c]	**49±4[c]**	17±4[c]	0[c]
46	104±7	97±7	98±7	95±6	96±4	**55±6[c]**	87±5[c]	18±3	12±3	10±5

[a]% of cell viability was quantified by Neutral Red Uptake (NRU) test and the data normalized as percentage of control. All Data are stated as mean ± s.d. of three experiments repeated in six replicate; [b]All compounds were tested at an increasing concentration range from 0.1 to 120 μM.; [c]Values are statistically different versus negative control, $p \leq 0.05$.

We also worked in a panel of ovarian and HeLa cell lines, carrying general (i.e. Pgp overexpression) or specific (i.e. βIII-tubulin isotype overexpression) mechanisms of resistance against their wild-type counterparts for some of the compounds (**Table 9**). As observed from the IC_{50} values, **35** is the most active from this series. Also, **37** as well as **34** is able to avoid the specific βIII-tubulin resistance. Moreover, **35** is not a substrate of Pgp as it appears from the IC_{50} outcome obtained in A2780AD cell line which overexpresses this pump. We henceforth postulate that **35** is not affected by this mechanism of resistance in cancer cells. Compound **29**, **32**, **33**, and **37** were also tested in HL-60 and a multiple myeloma cell line, NCI-H929.

Table 9. Cytotoxicity assessment of the compounds on the growth of different cell lines and the evaluation of the IC_{50} (nM) value

Cells	29	32	33	34	35	37	42	43
A549				138 ± 47	774 ± 25	614 ± 31		
A2780	249 ± 17	80 ± 12	76 ± 13	1031 ± 71	600 ± 115			300 ± 12
A2780AD	240 ± 33	92 ± 16	79 ± 15	1213 ± 81	399 ± 50			810 ± 48

R/S	0.96	1.15	1.03	1.18	0.67		2.69
HeLa				921 ± 265	469 ± 64		
HeLaβ3				661 ± 54	331 ± 104		
R/S				0.72	0.71		
HL-60		295	263				
NCI-H929	376	363				>50	

- **Cytotoxicity assessment on different cell lines**

Subsequently, we characterized the selected compounds on the panels of three OSCC cell lines, tongue squamous cell carcinoma (SCC4), gingival squamous cell carcinoma (Ca9.22), and buccal mucosa squamous cell carcinoma (TR146) (**Table 10**). The AlamarBlue assay was performed to investigate the effect of six compounds (**32-35**, **37**, and **45**) along with the reference compound **29** on cell viability in SCC4 cells for 48 h. IC_{50} values were calculated using Graphpad Prism to estimate the variation in cell sensitivity with the compounds (**Table 10**). All the compounds (**29**, **32-35**, and **37**) were able to decrease the cell viability in a dose-dependent manner and having the IC_{50} value (160 nM, 222 nM, 130 nM, 908 nM, 539 nM, and 849 nM, respectively) in the nanomolar range but no effect was shown for the treatment with **45**. The three selected compounds were successively tested on Ca9.22 gingival squamous carcinoma cells (p53 mutated) and TR146 keratinizing squamous cell carcinoma of buccal mucosal origin. Compound **35** showed an impressive cell viability results for both the cell lines (Ca9.22, IC_{50} ~ 130 nm; TR146, IC_{50} ~ 880 nm), while the other two compounds were active in a micromolar concentration range (**34**: IC_{50}: Ca9.22 ~ 2 μM, TR146 ~ 1.5 μM; **37**: IC_{50}: Ca9.22 ~ 2 μM, TR146 ~ 4.5 μM).

Table 10. Cytotoxicity assessment of the compounds on the growth of OSCC cell lines and the evaluation of the IC_{50} (μM) value at 48 h

Cells	29	32	33	34	35	37	45
SCC4	0.16	0.22	0.13	0.91	0.54	0.85	X
CA9.22	0.17	13.4		2 ± 0.5	0.13 ± 0.01	2 ± 0.2	
TR146				1.5 ± 0.25	0.88 ± 0.06	4.5 ± 1.2	

The four selected compounds (**32**, **34**, **35**, and **37**) have been further characterized on a multidrug resistance esophageal squamous cell carcinoma cell line (ESCC), KYSE-520. It has been described that KYSE 520 cells have elevated the expression levels of cyclooxygenase-2 (COX-2),[171] which might be accountable for a role in carcinogenesis, cancer progression, and MDR.[172–174] COX-2 has been revealed to induce the expression of the MDR 1 gene encoding Pgp, *via* phosphorylation of c-Jun at Ser63/73, resulting in the efflux of chemotherapeutics in colorectal cancer.[175,176] An AlamarBlue assay was performed to investigate the cell viability of KYSE-520 (**Table 11**). All the compounds exhibited the cytotoxic effects in a time-dependent manner. **32** and **34** were not able to affect the cell viability at 48 h even at 500 μM but displayed the effect at 72 h with the IC_{50} of 138.3 and 41.94 μM. Excitingly, both the newly developed compounds **35** and **37** were able to prevent the cell growth at both the two time settings (IC_{50} of 3.6 μM at 48 h, 1.68 μM at 72 h and 1.68 μM at 48 h, 0.89 μM at 72 h, respectively) and **37** was the most active compound on KYSE-5220 cell lines by producing a high nanomolar range of IC_{50} value at 72 h.

Table 11. Cytotoxicity assessment of the compounds on the growth of ESCC and EAC cell lines and the evaluation of the IC_{50} (μM) value at 72 h.

Cells	32	33	34	35	37
KYSE-520		41.94	1.68	0.89	
OE-33	0.32		1.40	0.57	2.32
OE-19	0.73			0.73	
FLO-1	0.28			0.40	
MFD-1	1.10			1.20	
SKGT4	0.51			0.55	

Additionally, the compounds have been then tested on a panel of human caucasian esophageal adenocarcinoma (EAC) (**Table 11**).[177–179] In the first attempt, an MTT assay was performed to explore the effects of the compounds on the cell viability at 72 h of OE-33. **32** and **35** were able to affect the cell growth with an IC_{50} value of 296 nM and 391 nM, respectively. **34** and **37** exhibited the IC_{50} of 1.40 μM and 1.32 μM, respectively. The

best performing **35** along with the reference **32** were then tested on OE-19, FLO-, MFD-1, and SKGT4 cell lines. Both the compounds displayed an inhibitory effect on the cell growth in for OE-19 (**32** and **35**, IC_{50} = 730 nM), FLO-1 (**32**, IC_{50} = 280 nM; **35**, IC_{50} = 400 nM), SKGT4 (**32**, IC_{50} = 510 nM; **35**, IC_{50} = 550 nM), MFD-1 ((**32**, IC_{50} = 1.10 μM; **35**, IC_{50} = 1.20 μM).

- **Apoptosis test on different cell lines**

As shown, compounds **29** and **32** demonstrated comparable efficacy in SCC4 (**Figure 22**, panel B) and NCI-H929 (**Figure 22**, panel A) cells, while compound **42** demonstrated negligible efficacy in both the cell lines. Regarding the Ca9.22 cells (**Figure22**, panel C), compound **42** does not seem to be effective at 500 nM when compared to the other cell lines, while compound **32** displays only modest efficacy. However, the activity assessment of these **PBOX** compounds on the OSCC cell lines supports further studies for the development of the new analogues.

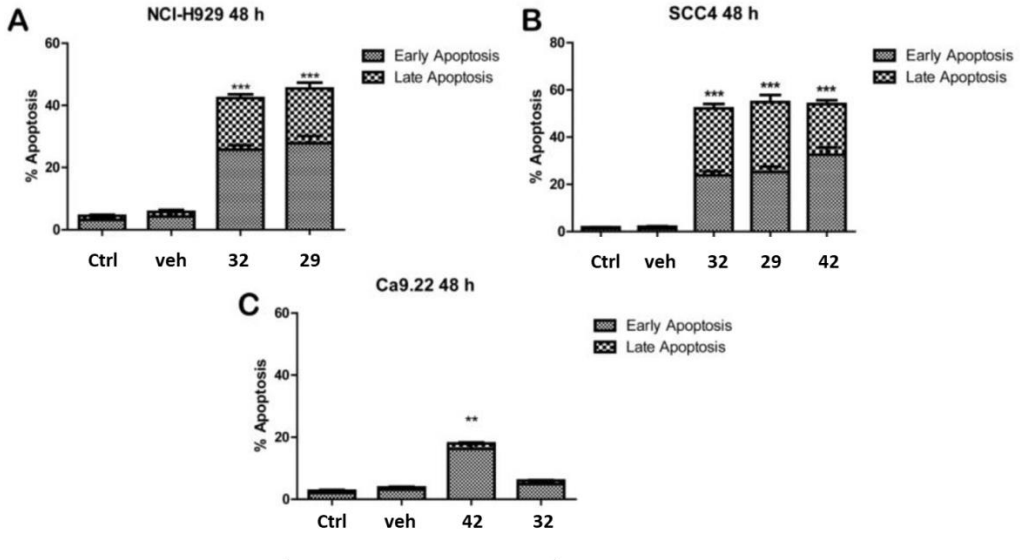

Figure. 22. (**A**) NCI-H929 cells were seeded at a density of 30 × 10^4 cells/mL and were left untreated (control) or treated with either vehicle (1% EtOH (v/v)) or 500 nM of **29** and **32** for 48 h (**B**) SCC4 cells were seeded at a density of 15 × 10^4 cells/mL and were treated with either vehicle control (1% EtOH (v/v)) or 500 nM of **29** or **32** or 50 mM of **42** for 48 h (**C**) Ca9.22 cells were seeded at a density of 30 × 10^4 cells/mL and were treated with either vehicle control (1% EtOH (v/v)) or 500 nM **32**, or 500 nM of **42** for 48 h.

Apoptosis induction for the other compounds was also evaluated in SCC4, Ca9.22, and TR146 cells using the Annexin V/Propidium iodide dual staining assay (**Figure 23**). The

cells were treated with the compounds at both 0.5 and 2 μM of concentrations for 48 h. **33**, **34**, and **35** induced apoptosis in SCC4 cells at both the concentrations, while no apoptosis was observed following the treatment with **45** at that concentration. Compound **37** was not able to induce apoptosis at 0.5 μM concentration but produced a positive result when treated with 2 μM. In addition, the compounds have been evaluated for their apoptosis efficacy on Ca9.22 and TR146 cell lines at a concentration of 500 nM for 48 h. As expected, **35** produced the best result. These results are in line with the results obtained from the AlamarBlue viability assay.

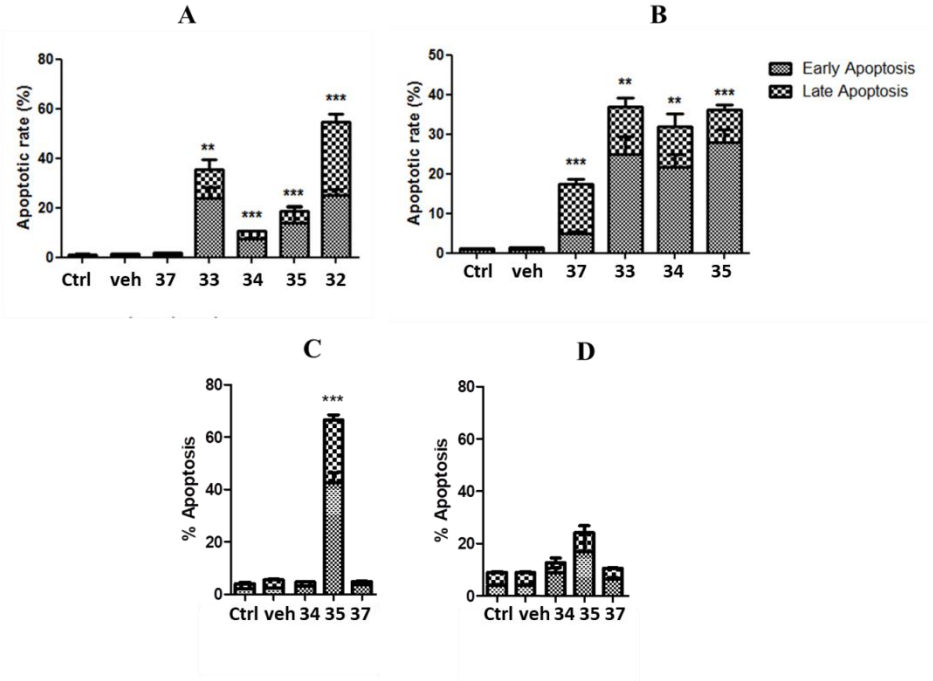

Figure 23. AnnexinV/Propidium iodide assay of all the compounds on OSCC cells. (**A**) compound concentration of 0.5 μM and (**B**) compound concentration of 2 μM. Values represent the mean ± S.E.M of three independent experiments (N = 3). Statistical analysis was performed using an unpaired one-tailed student t-test to compare mean values between vehicle and treated cells ***p < 0.001, **p < 0.01. (**C**) Ca9.22 cells were seeded at a density of 30 X 10^4 cells/mL and were left untreated (control) or treated with either vehicle (1% EtOH (v/v)) or 500 nM of compound for 48 h. (**D**) TR146 cells were seeded at the density of 30 X 10^4 cells/mL and were treated with either vehicle control (1% EtOH (v/v)) or 500 nM of compound for 48 h. Values represent the mean ± S.E.M of three independent experiments (N = 3). Statistical analysis was performed using a T-test. **p = 0.001".

Guided by the cell viability outcomes, the apoptosis induction effect of the compounds has been analyzed at 3 and 10 μM of concentrations for 72 h incubation time by an Annexin

V/Propidium iodide dual staining assay (**Figure 24**). All the compounds were able to induce apoptosis (from > 20% to < 60%) at both concentrations. **32**, **35**, and **37** showed a concentration-dependent apoptosis induction and these results further supports the results found from the AlamarBlue viability assay.

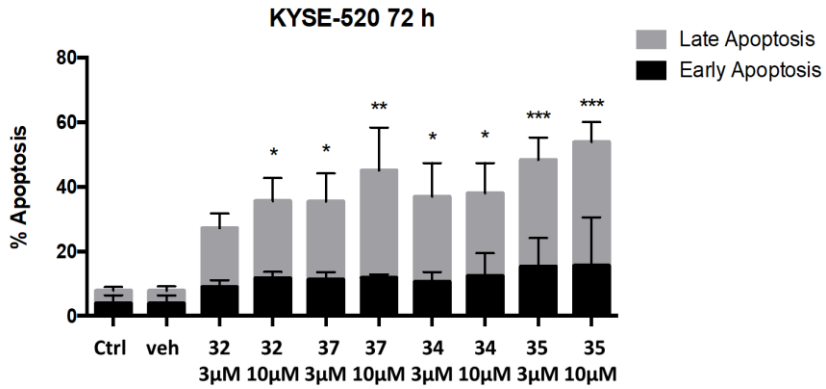

Figure 24. Annexin V/Propidium iodide assay of the compounds against KYSE-520 cells at 3 μM and 10 μM of concentrations.

- **Mutagenicity test of the selected compounds**

We determined the mutagenic effects of two of the best performing compounds (**35** and **37**) in the *Salmonella typhimurium* strains, TA98 and TA100. The Ames test is performed to detect potential mutagenicity risks at the early-stage drug development (**Figure 25**). Though, the assay can be executed with/without the rat liver fraction, S9, the latter condition is a more in-depth analysis to assess the potential mutagenicity risks resulting from the metabolites of the compounds. Interestingly, after applying both the experimental conditions, no mutagenic effects were determined for both the compounds for the concentration range, tested (0.3-60 μM)

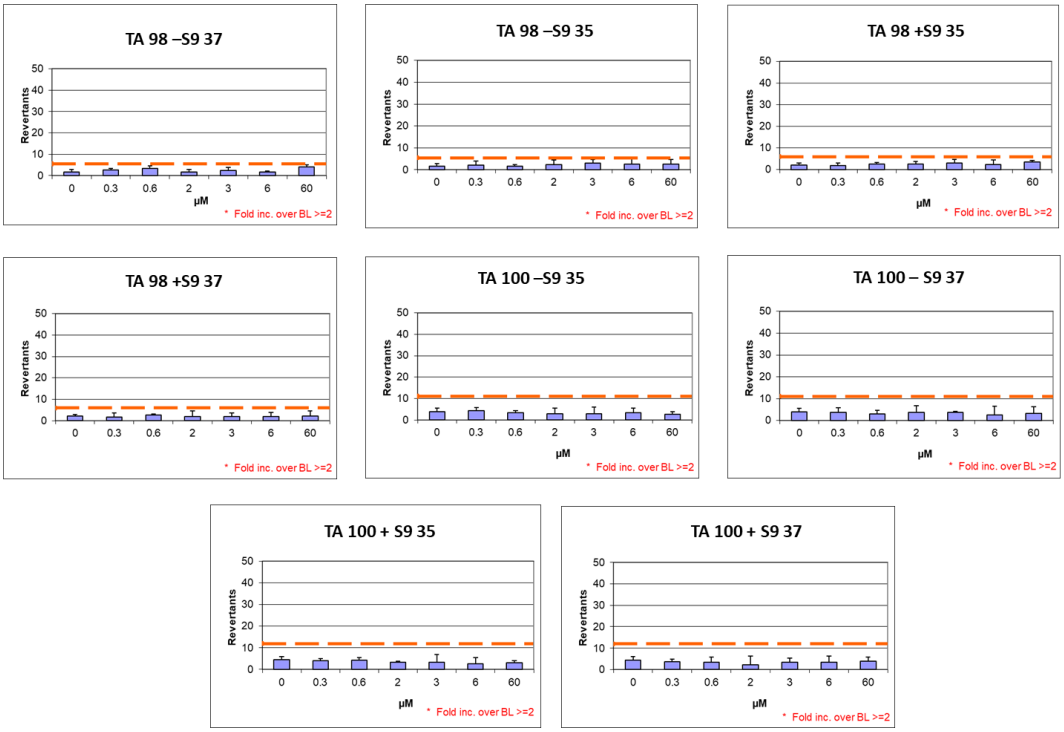

Figure 25. Ames tests performed on *S. typhimurium* TA98 and TA100 strains for compounds **35** and **37**.

- **Autophagy tests of the compounds on OSCC and HL-60 cell lines**

To address the influence of **PNOX** compounds (**Table 12**) on both basal and stimulated autophagy, we quantified the accumulation of the LC3B-II protein by immunoblot assays with the reference compound **29** and its three analogues **32**, **100**, and **101**.

Table 12. Compounds for the preliminary investigation on autophagic flux in HL-60 cell lines

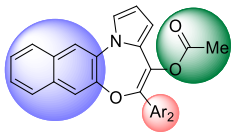

Cmpds	29	32	100	101
Ar_2	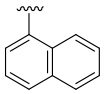	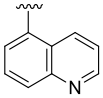	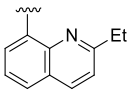	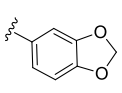

Since autophagy is a dynamic process, accumulation of LC3B-II within the cells does not necessarily correspond to an increase of autophagy but could reflect a reduction in autophagosome turnover too. Hence we compared the amount of LC3B-II in compound-treated samples both in presence or absence of **CQ** (**Figure 26**). HL-60 cells were treated with the tested compounds for 1 h 45 min and accumulation of LC3B-II was quantified by

immunoblot (**Figure 26A**). Significant higher levels of LC3B-II, which were further increased in presence of **CQ**, were found in samples treated with **29**, **32**, and **100** compared with cells in full medium showing that these compounds are able to induce the accumulation of autophagosomes in HL-60 cells in basal condition (**Figure 26A**). Furthermore, **32** and **100** appeared to be more active compared to **29** (**Figure 26A**). To investigate the effect of these compounds on autophagy stimulated by serum deprivation, cells were starved for 15 min before the addition of the compounds and LC3B-II were measured in presence/absence of **CQ** after 1 h 45 min. Accumulation of LC3B-II was considerably higher in serum starved samples co-treated with **32**, **100**, and **101** compared with untreated and **29**-treated samples indicative of **29** and **100** being the most effective derivatives on the autophagic process in both the conditions. Moreover, a reduction of the LC3B-II protein was found in treated samples, but not in the same samples co-treated with **CQ** after a longer treatment of 16 h in serum supplemented medium compared with untreated cells. The enhancement of LC3B-II accumulation in samples treated with **CQ**, compared with **CQ**-untreated samples may be indicative of a pro-autophagic effect of compounds rather than of an inhibitory effect on the autophagic process. In support of a pro-autophagic effect of the analogues in HL-60 cells, short treatment of 1 h 45 min with compounds in serum supplemented samples resulted in the increase of LC3B-II levels which is further enhanced in samples co-treated with **CQ** (**Figure 26A**). Despite this analysis of the autophagic flux which reflects the net amount of LC3B-II delivered to lysosomes, suggests a pro-autophagic effect, additional assays are required to better characterize the pro-autophagic effect of novel compounds. Our preliminary data demonstrated that our novel analogues are able to target the autophagic process and that **1** and **35** are the best performing analogues so far identified when tested at 10 mM.

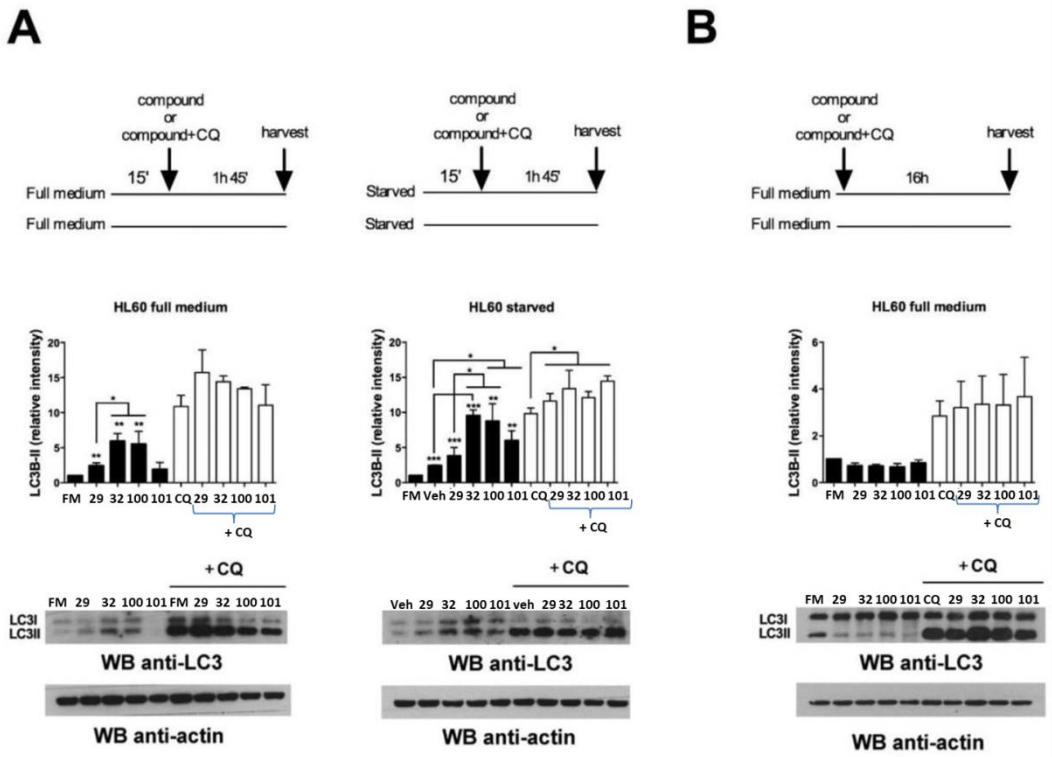

Figure 26. Immunoblot analysis of LC3B-II levels in HL-60 cells cultured in serum supplemented RPMI 1640 or in Earle's Balanced Salts (EBSS) medium and treated with 10 mM of compounds in presence or absence of 40 mM **CQ** for (**A**) 1 h 45 min or (**B**) 16 h. Control immunoblot with anti-actin antibodies of the same filters are shown. Densitometric analysis of LC3B-II amount from three independent experiments and normalization with actin level. Bar graphs represent the relative intensity of LC3B-II. *, $p < 0.05$ **, $p < 0.01$ versus full medium as calculated by Student's t-test.

There is not always a straightforward predecessor/successor relationship between LC3-I and LC3-II, because the conversion of LC3-I to LC3-II depends on the cell type as well as the autophagy induction type. Therefore, p62 levels are often used for the quantification of autophagic flux. However, there is not always a clear correlation between increases in LC3-II and decreases in p62.[180,181]

Five compounds (**32-35**, and **37**) were tested on SCC4 cells to evaluate their autophagy modulating effects (**Figure 27**). Autophagy was stimulated by pre-incubating the cells with EBSS medium for 30 minutes before treating the cells with 10 μM of concentration for each compound.[182] **CQ** at 10 μM concentration was used as positive control for autophagy inhibition. Cells were harvested for 3 h and the expression levels of LC3-II/-I and p62 were evaluated by WB analysis. Densitometric analysis of p62, LC3-I and LC3-II bands were performed using ImageLab software and values represent the mean ± S.E.M. of four independent experiments. Statistical analysis was performed by unpaired one-tailed t-test.

p ≤ 0.01, *p ≤ 0.05. As expected, a significant increase in the LC3-II/LC3-I ratio was observed in cells treated with **CQ in presence/absence of EBSS due to the inhibition of autophagic flux at the very late stage, thereby resulting in the block of LC3-II turnover.[181] Interestingly, a substantial and significant increase in the LC3-II/LC3-I ratio was also observed in cells treated with the compounds **35** and **37** in basal condition and a further increase was found in the starved condition. This comparable profile of **CQ** with **35** and **37** suggests the potent autophagy flux inhibitory nature of the two compounds. However, compounds **32**-**34** also elicited an increase in the levels of LC3-II/LC3-I in both basal and starved conditions but in a minor extent. A slight increase in p62 levels in cells treated with the compound **37** in presence/absence of EBSS was observed, an effect also elicited by **CQ**, confirming the autophagy inhibitory nature of this novel compound.

Taken together these results suggest that the compounds enhance the expression of LC3-II protein in SCC4 cells, indicating that they exhibit autophagy modulatory properties. Besides, a similar profile of autophagic protein expression in cells treated with the compounds **35** and **37** compared to **CQ** indicate that these two novel compounds are potent autophagic flux inhibitors.

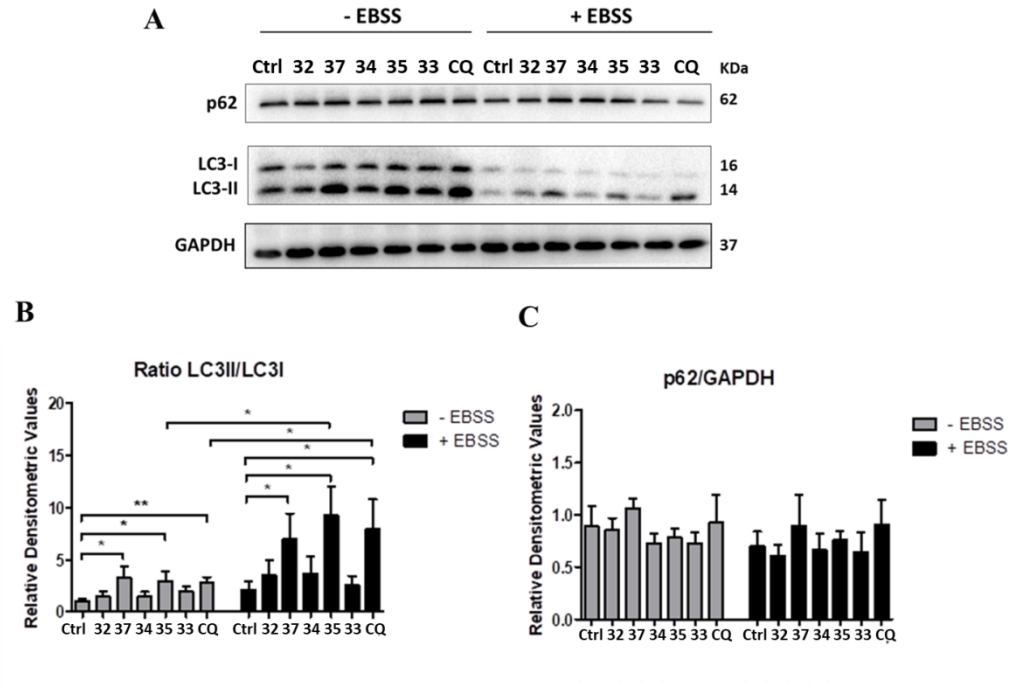

Figure 27. Autophagy study of the compounds on SCC4 cell lines by quantifying LC3-II/LC3-I and p62 densitometric values in basal and starved condition

We have further characterized the compounds on a panel of HL-60 cell lines by comparing the amount of LC3-II both in presence/absence of **CQ** (**Figure 28**).[183] HL-60 cells were treated in full medium with the tested compounds and accumulation of LC3-II was measured by immunoblot. The treatment with the compounds resulted in an increase in LC3-II compared to basal condition, with higher levels observed when the compounds were used in combination **CQ**. These data suggest that the tested compounds induce the accumulation of autophagosomes in HL-60 cells. Accordingly, levels of p62 were significantly increased in HL-60 cells treated with the compounds compared with vehicle treated cells confirming that these compounds are responsible for autophagosome accumulation. Since both the accumulation of p62 and LC3-II occur when autophagy is inhibited,[181] these results further support that **35** and **37** likely act as autophagy inhibitors.

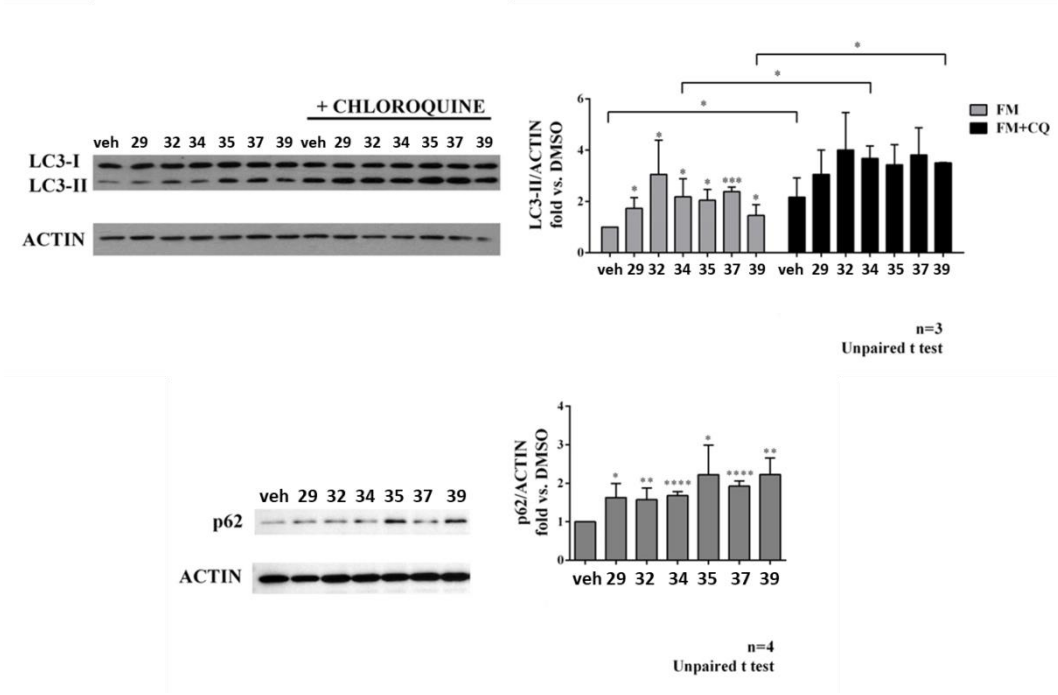

Figure 28. Autophagy study of the compounds on HL-60 cell lines by quantifying LC3-II/LC3-I and p62 densitometric values

1.5.1.2 Characterization of the selected compounds on tubulin dynamics

Our previous studies have confirmed the **PBOX**/**PNOX** compounds as a microtubule disrupting agents. The turbidity of a solution can reveal the microtubule formation due to its large structures and hence can help in observing the tubulin assembly reaction. Therefore, we followed to assess the microtubule depolymerizing effects of the selected compounds (**34**, **35**, and **37**). A turbidity time-course experiment in the presence of 25 μM

of the compounds on 25 μM of tubulin at 37 °C was performed to monitor the absorbance at 350 nm (**Figure 29**). Podophyllotoxin, a well-known colchicine site binding compound, was used as a positive control. As evidenced, all the compounds depolymerized the microtubule network in a similar way as podophyllotoxin. Though compound **37** did not produce as good results as the other two compounds, it still showcased a negative effect on the microtubule network. However, this particular behaviour could also be attributed to the formation of tubulin aggregates.

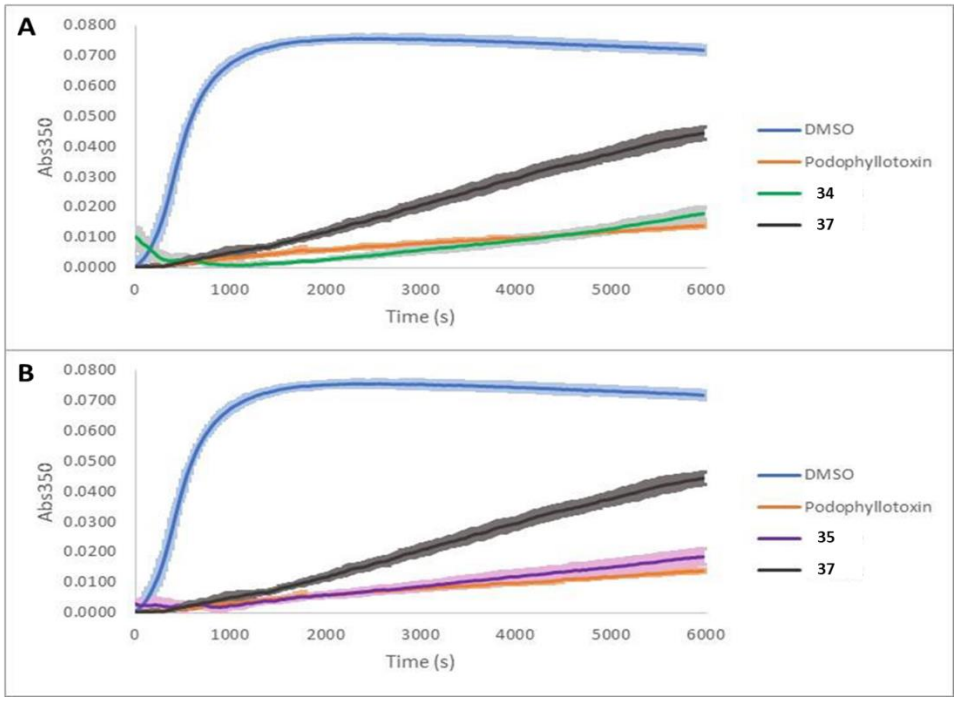

Figure 29. Microtubule polymerization curves of **34** combined with **37** (A) and **35** combined with **37** (B) in GAB buffer, both with the Podophyllotoxin curve added as a destabilizing control.

1.5.1.3 Pharmacokinetics of the selected compounds

We also sought to assess the drug-like property of the selected analogues (**34**, **35**, and **37**). The aqueous solubility at pH = 3 and pH = 7.4 and the chemical stability (at pH = 3) of the compounds were measured by HPLC methods (**Table 13**). As predicted, the presence of the basic amine system amended the solubility profile of the compounds in the acidic pH = 3, but unfortunately none of them was soluble at pH = 7.4. The solubility of **34** at T = 0 was 99 μM but it was not stable in the pH = 3 after 24 h which might be attributed to the presence of the inherited carbamate moiety of the compound. Interestingly, despite bearing a carbamate moiety, **35** displayed the solubility of 204 μM at pH = 3 after 24 h and the chemical stability of 91% at 36 h. **37** demonstrated the highest solubility among these

compounds of 271 μM at pH = 3 after 24 h and the chemical stability of almost quantitative value with 97% at 36 h. However, these facts might be accredited to the innate secondary amine and ester moiety instead of a tertiary amine and a carbamate moiety.

Table 13. Solubility and chemical stability of the selected analogues.

Cpds	Solubility[a] (μM)		Chemical stability[b] (%)
	pH = 3	pH = 7.4	
34	n.d[c]	n.d	n.d
35	204	n.d	91
37	271	n.d	97

[a]Solubility at 24 h; [b]Chemical stability at 36 h; [c]n.d, not determined, not quantifiable.

1.5.1.4 Metabolic profile of the selected compounds

We have performed the *in vitro* studies to assess the metabolic stability of **35** and **37** in human liver microsomal (HLM) preparations. The plot of non-metabolized compound [natural logarithm of % of recovered compound (100% at time 0 min)] as a function of incubation time exhibited a monoexponential decay relationship for both the compounds (**Figure 30**). The apparent decay constant (k), half-life time t½), and intrinsic clearance (CLint) are reported in **Table 14**.

Table 14. Apparent decay constant (k), half-life time t½), and intrinsic clearance (CLint) value of **55** and **57**.

Cpds	k (min^{-1})	t½ (min)	CLint
55	0.022	30.8	55
57	0.0076	91.2	19

The Clint values indicate that **35** is a preferred substrate for the xenobiotic metabolized system present in the HLM. On the contrary, **37** with a lower Clintr value indicate a higher metabolic stability than **35**. However, both the drugs can be categorized into the medium clearance compounds.[184] Moreover, both compounds were not metabolized when incubated at 37 °C for 60 min with boiled microsomes or in presence of HLM but without the NADPH-GS. Taken together these results clearly indicate that CYP(s) are responsible of the **35** and **37** metabolism. From in silico analysis with MetaSite ® the hydroxylation of naphthalene ring and the demethylation of N-methylpyperazine moiety appears the of two

major CYP-dependent reactions towards **35** with a similar probability score. On the contrary, **37** seem to be metabolized only by the introduction of an OH moiety in the naphthalene ring.

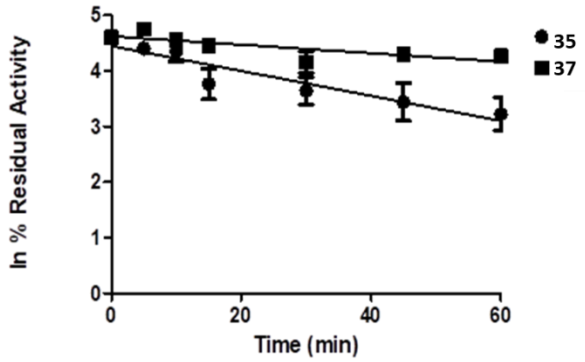

Figure 30. The plot of non-metabolized compound [natural logarithm of % of recovered compound (100% at time 0 min)] as a function of incubation time expressing a monoexponential decay relationship for both the compounds

1.5.1.5 Molecular docking of the compounds

In order to gain more evidence about the binding mode of the developed compounds, a comprehensive SAR study was performed to examine the behavior of the novel series of molecules within the colchicine binding site of tubulin.

A molecular docking calculation was performed by our co-workers in our computational laboratories by means of Glide software implemented in Maestro suite (Schrödinger Release 2015-4: Glide, Schrödinger, LLC, New York, NY, 2015) as previously reported by us and described in the experimental section.[99] Starting from the PDB structure 6GJ4, a crystal structure of α/β tubulin in complex with our previously developed compound **32**, and to assess the validity of our computational protocol the crystallized compound was re-docked into the protein binding site, showing slight difference in its binding mode as confirmed by the very low value of RMSD: 0.2744.

For the newly developed compounds we found that they were able to accommodate within the active site as compound **32** (**Figure 30** and **31**) except for compound **46** due to its bulky substituents in Ar_2 and R position, it was not possible to retrieve a proper accommodation within the binding site. For the other analogues a similar pattern of interaction was found. The main contacts established by this series of molecules are represented by: a cation-π stacking established between K352 and the pyrrole ring of the

scaffold, along with some hydrophobic interactions within the binding cavity with residues T179, A180 and V181 (α subunit), C241, L248, A250, L255, A316, I318 and K352 (β subunit) (**Figure 30** and **31**). While the compounds that hold a 5-quinoline substituent in Ar_1, were also able to interact, through water-mediated contacts, with the backbone of G237 and C241 as well as with the sidechain of C241 (**Figure 30**). For compounds **5e**,**f** containing a acetylpiperazine and a methylpiperazine, respectively in Ar_2 a different accommodation in the binding site has been observed. As represented in **Figure 31A**, for **44** the core turns to project the OCOMe toward the hydrophobic cavity and the acetylpiperazine toward the opening of the binding site. This allows **44** to reach the residue R221 belonging to the α-subunit by establishing double H-bonds. For compound **45** (**Figure 31B**) the substitution of the acetyl with a methyl group, exposes the piperazine moiety to the solvent without establishing any relevant polar contact with the cavity residues.

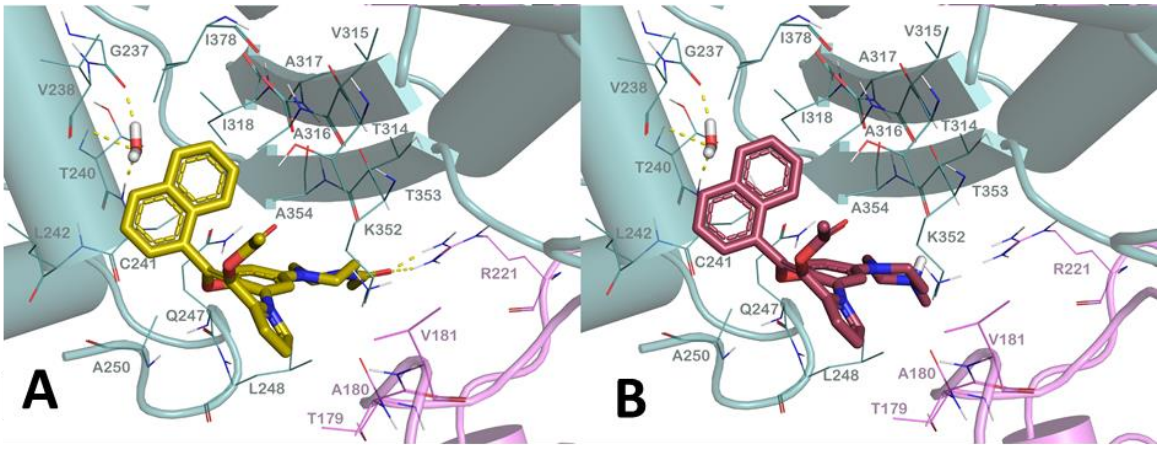

Figure 31. Complexes of compounds **44** and **45** (represented as sticks in different colours, panels A and B, respectively) with tubulin (α-tubulin is represented in pink cartoon, β-tubulin is represented in teal, PDB ID: 6GJ4) as found by molecular docking calculation.

The introduction of a 5-quinolyl in Ar_1 permits the formation of water mediated H-bonds with G237, V238, and T240 for compounds **34-37** and **39** (**Figure 32**). The changes in the R lateral chain determined a different pattern of interaction with the residues located at the entry of the binding site. In particular, compound **34** (**Figure 32B**), with its *N*,*N*-diethylaminopentan-2-yl carbamate lateral chain is able to interact through two H-bonds with the backbone of Q247 and the side chain of K352. **35** (**Figure 32C**), substituted with the *N*-methylpiperazine, cannot establish H-bonds, results less solvent-exposed and better accommodated within the binding cavity by targeting the hydrophobic residues L248 and

A354. Moreover the central region of the molecule is involved in a double π-π stacking with K352. The bulky lateral chain of compound **36** (**Figure 32D**) establishes an additional H-bond through the carbonyl oxygen with K352 along with the discussed hydrophobic contacts. Deprotection of the lateral chain gave in the free piperidine of compound **37** (**Figure 32E**). It mainly targets the residues T179, A180 and V181 (α subunit), C241, L248, A250, L255, A316, I318, K352 and A354. The substitution of the piperidine with a pyridine-3-yl system, (**39**, **Figure 32F**), allowed an H-bond with Q247 through the nitrogen atom of the pyridine, while maintaining the other contacts.

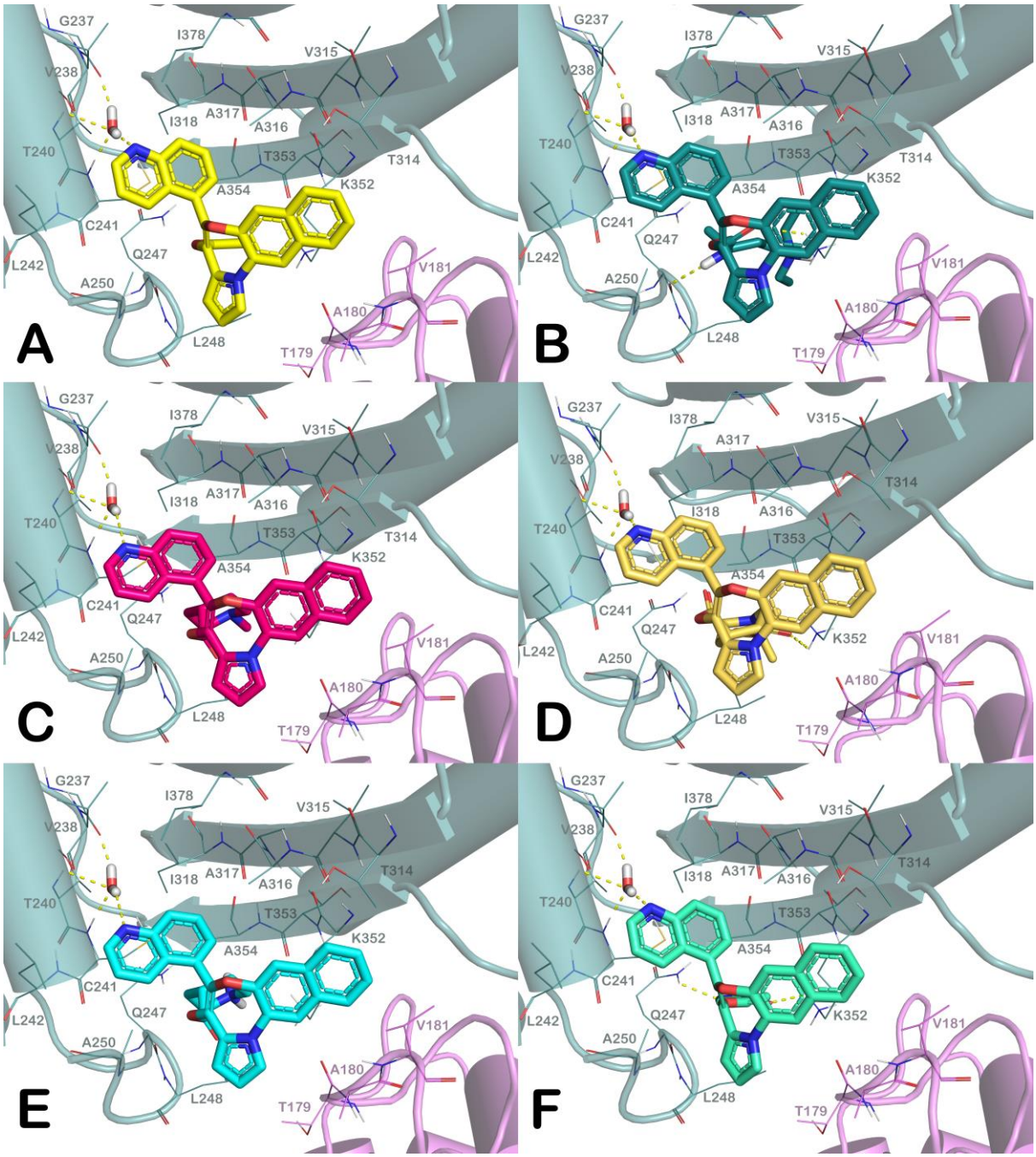

Figure 32. Complexes of compounds **32** panel A, **34-39** (represented as sticks in different colours, panels B-F respectively) with tubulin (α-tubulin is represented in pink cartoon, β-tubulin is represented in teal, PDB ID: 6GJ4) as found by molecular docking calculation.

1.5.2 Conclusions

In conclusions, we explored the **PBOX** and **PNOX** class of MTAs and described the development of a series of potent pro-apoptotic molecules. The structural adaptation at the binding pockets of the core structure has been implemented by utilizing the mechanistic perception of known autophagy inhibitor, **CQ** and the molecular modelling approach. We tried to mimic the **CQ** functional moieties in our compounds while holding on to their inherited pro-apoptotic activity. Compounds were accurately characterized by biological, biochemical and medicinal chemistry approaches. We evaluated their ability to inhibit the cell proliferation and to induce apoptosis on a wide variation of tumor cells, including multidrug-resistant cell lines. Selected compounds were tested for their effect on the resistance cells and the corresponding parental cells. The mutagenic safety profile has also been inspected for the compounds. Additionally, pharmacokinetic properties and the *in vitro* metabolic stability with HLM have been calculated. Finally, the selected compounds were inspected for their effect on the autophagic process against SCC4 and HL-60 cell lines. Quantification of LC3-II/LC3-I and p62 protein at both the basal and starvation-mediated conditions was evaluated by considering **CQ** as a positive control. These studies unveiled the **CQ**-like mode of action of **PNOXs** compounds on the autophagic process. The obtained data proposed for a relevant therapeutic potential for the developed compounds **35** and **37** as autophagy inhibitors with innate pro-apoptotic activity.

PART 1 CHAPTER V

EXPERIMENTAL SECTION

General Remarks

All chemicals and reagents were purchased from the commercial suppliers and used without further purification, unless and otherwise specified. Reaction progress was observed by thin-layer chromatography (TLC), carried out on silica (60 F254) or alumina (60 F254, basic) gel plates with detection by UV and the products were purified by means of either silica (60M, 0.040-0.063 μm) or alumina (90, standarized) column chromatography. ^{1}H and ^{13}C NMR spectra were documented in the indicated deuteriated solvent on a Varian 300 MHz or a Bruker 400 MHz spectrometer by using the residual signal of the deuterated solvent as internal standard. Splitting patterns are indicated by s (singlet), d (doublet), dd (doublet of doublets), t (triplet), q (quartet), m (multiplet), and br (broad); chemical shifts (δ) are defined in parts per million (ppm) and coupling constants (J) in Hertz (Hz). ESI-MS spectra were performed by an Agilent 1100 Series LC/MSD spectrometer. HRESI-MS were carried out by a Thermo Finningan LCQ Deca XP Max ion-trap mass spectrometer equipped with Xcalibur software, operated in positive ion mode and conducted at the University of Naples, Italy. Yields denote to purified products. HPLC analysis were performed with a Shimadzu Prominence apparatus equipped with a scanning absorbance UV-VIS detector (Diode Array SPD-M20A) also equipped with a thermostatic chamber and Purospher®STAR, RP-18ε (5 μM) HPLC column. All moisture-sensitive reactions were executed under nitrogen atmosphere using oven-dried glassware and freshly distilled dry solvents.

Ethyl 2-(naphthalen-1-yl)acetate ***(67)***

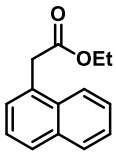

67

Thionyl chloride (16 mL, 214.8 mmol) was added to a solution of commercially available **66** (10 g, 53.70 mmol) in ethanol (37 mL) at 0 °C and then the mixture was refluxed 80 °C for 12 h. The solvent was evaporated completely under reduced pressure at 20 °C. The crude was dissolved in DCM and the organic solution was washed with $NaHCO_3$ (s.s). The

organic layer was dried with anhydrous sodium sulfate, filtered, and concentrated. The title compound **67** was obtained in quantitative yield and used for the next step without any further purification. ^{1}H NMR (300 MHz, CDCl3) δ: 8.01 (d, *J* = 8.1 Hz, 1H), 7.86 (d, *J* = 1.8 Hz, 1H), 7.80 (dd, J_1 = 6.6 Hz, J_2 = 2.7, 1H), 7.41-7.56 (m, 4H), 4.12-4.19 (m, 2H), 4.07 (s, 2H), 1.23 (t, *J* = 6.9 Hz, 3H). ESI-MS *m/z* 215.0 $[M+H]^+$.

*Ethyl 2-bromo-2-(naphthalen-1-yl)acetate (**58b**)*

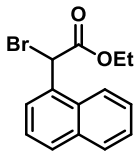

58b

NBS (3984 mg, 22.4 mmol) and catalytic amount of AIBN was added to a solution of **67** (4g, 18.7 mmol) in CCl_4 (90 mL) at room temperature and then the mixture was refluxed at 90 °C for 12 h in presence of a lamp. The solvent was removed completely under reduced pressure. The crude was dissolved with DCM and was washed with water. The organic layer was dried with anhydrous sodium sulfate, filtered, and concentrated. The residue was purified on a silica gel column chromatography (PE/EtOAc 15:1) to obtain the title compound **58b** in quantitative yield. ^{1}H NMR (300 MHz, $CDCl_3$) δ: 8.13 (d, *J* = 8.7 Hz, 1H), 7.81 (d, *J* = 7.2 Hz, 1H), 7.45-7.62 (m, 3H), 6.16 (s, 1H), 4.26-4.30 (m, 2H), 1.26 (t, *J* = 6.9 Hz, 3H). ESI-MS *m/z* 293.8 $[M+H]^+$, 315.9 $[M+Na]^+$

*3-(1H-Pyrrol-1-yl)naphthalen-2-ol (**54a**)*

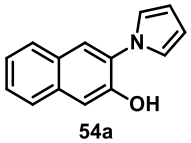

54a

2,5-Dimethoxytetrahydrofuran was added to the suspension of commercially available 68a in acetic acid and water at room temperature. The mixture was refluxed at 100 °C for 5h. After cooling down the mixture to room temperature, acetic acid was removed under reduced pressure. The residue was dissolved in EtOAc and washed with a saturated solution of NaCl and water. The residue was purified on a silica gel column chromatography (*n*-hexane/EtOAc 10:1) to obtain the title compound in 80% yield. ^{1}H

NMR (300 MHz, $CDCl_3$) δ: 7.75 (s, 3H), 7.49-7.37 (m, 3H), 6.98 (s, 2H), 6.45 (s, 2H), 5.34 (s, 1H); ESI-MS *m/z* 210.0 $[M+H]^+$.

*Ethyl 2-((3-(1H-pyrrol-1-yl)naphthalen-2-yl)oxy)-2-(naphthalen-1-yl)acetate (**56a**)*

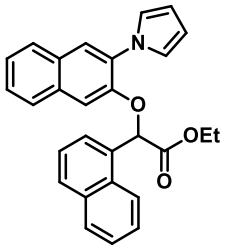

56a

K_2CO_3 (315 mg, 2.28 mmol) was added to a solution of **54a** (318 mg, 1.52 mmol) in dry DMF (8 mL) at room temperature and stirred for 2 h at room temperature. A solution of **56a** (532 mg, 1.83 mmol) in dry DMF (8 mL) was added to the reaction mixture and refluxed at 90 °C for 12 h. Reaction mixture was cooled down and DMF was evaporated under reduced pressure. Resulting crude was dissolved in EtOAc and washed with the saturated solution of NaCl. The organic layer was dried over anhydrous sodium sulfate, filtered, and concentrated. The residue was purified by a silica gel column chromatography (PE/EtOAc 15:1) to obtain the title compound in 90% yield. ^{1}H NMR (300 MHz, $CDCl_3$) δ: 8.36 (d, *J* = 8.3 Hz, 1H), 7.88 (t, *J* = 8.1 Hz, 2H), 7.82-7.76 (m, 2H), 7.71 (d, *J* = 7.7 Hz, 1H), 7.63-7.36 (m, 7H), 7.27 (s, 2H), 6.48 (s, 1H), 6.39 (s, 2H), 4.27-4.06 (m, 2H), 1.16 (t, *J* = 7.1 Hz, 3H). ESI-MS *m/z* 422. $[M+H]^+$.

*2-((3-(1H-Pyrrol-1-yl)naphthalen-2-yl)oxy)-2-(naphthalen-1-yl)acetic acid (**53a**)*

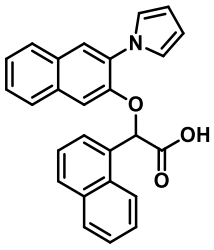

53a

Method A: A solution of 2.3 mL of NaOH (5% aqueous solution) was added to the solution of 56a (340 mg, 0.81 mmol) in THF/ethanol (10 mL) of 1:1 mixture at room temperature and stirred for 12h. All the solvent was removed completely under reduced pressure and the crude was dilute with water. The pH of the aqueous layer was adjusted to

3 by using 1(N) HCl solution and was extracted with EtOAc (3 x10 mL). The organic layer was washed with a saturated solution of brine, dried with anhydrous sodium sulfate, filtered, and concentrated to obtain the title compound in quantitative yield without any purification.

Method B: Compound **54a** (100 mg, 0.39 mmol) was dissolved in dry THF (1 mL) and cooled to 0 °C. A finely ground sodium hydroxide powder (242 mg, 6.05 mmol) was added to the solution and the mixture was stirred at 0 °C for 10 min. 1-Naphthaldehyde (**55b**, 570 mg, 3.65 mmol) and bromoform (1528 mg, 6.046 mmol) were added dropwise, sequentially, to the reaction mixture at 0 °C. The reaction mixture was stirred at 0 °C for 1 h and then at 25 °C for 12 h. The solvent was evaporated under reduced pressure and the residue was diluted with water. A solution of 1 (N) HCl was added to adjust the pH at 2 and was extracted with EtOAc (3 x 5 mL). The combined organic layers were dried over anhydrous sodium sulfate, filtered and concentrated under reduced pressure. The residue was purified on a silica gel column chromatography (DCM/MeOH/NH_4OH 10:1:0.1) to afford the title compound in 48% yield ^{1}H NMR (300 MHz, $CDCl_3$) δ: 8.25 (d, *J* = 8.4 Hz, 1H), 7.84 (t, *J* = 7.7 Hz, 2H), 7.75 (s, 1H), 7.71 (d, *J* = 6.5 Hz, 1H), 7.63 (dd, *J* = 11.2, 4.3 Hz, 1H), 7.57-7.47 (m, 3H), 7.42-7.36 (m, 3H), 7.30 (s, 1H), 7.16 (t, *J* = 2.1 Hz, 2H), 6.40 (s, 1H), 6.35 (t, *J* = 2.1 Hz, 2H); ^{13}C NMR (75 MHz, $CDCl_3$) δ: 173.9, 148.8, 133.8, 132.2, 131.5, 130.5, 130.0 (2C), 129.2, 128.9, 127.3, 126.9, 126.7, 126.6, 126.5, 126.0, 125.3, 125.2, 124.5, 123.6, 122.6 (2C), 110.4, 109.4 (2C), 82.4. MS-ESI *m/z*: 391.7 $[M-H]^-$

*5-(Naphthalen-1-yl)naphtho[2,3-b]pyrrolo[1,2-d][1,4]oxazepin-4(5H)-one (**52a**)*

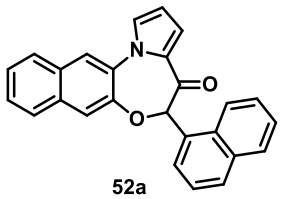

52a

To a stirred solution of acid **53a** (311 mg, 0.79 mmol) in dry DCE (40 mL) phosphorus pentachloride (198 mg, 0.95 mmol) was added and the reaction mixture was refluxed at 85 °C for 12 h. Then saturated aqueous $NaHCO_3$ was added dropwise and the aqueous layer was extracted with DCM (3 x 20 mL). The combined organic layers were dried over anhydrous sodium sulfate, filtered, and concentrated. The residue was purified by flash chromatography on silica gel (*n*-hexane/EtOAc 3:1) to afford the title compound as a

yellow amorphous solid in 50% yield. ^{1}H NMR (300 MHz, $CDCl_3$) δ: 8.24 (d, *J* = 8.4 Hz, 1H), 7.84 (t, *J* = 8.3 Hz, 3H), 7.78 (s, 1H), 7.62-7.36 (m, 8H), 7.27 (s, 2H), 6.63-6.58 (m, 1H), 6.26 (s, 1H). ^{13}C NMR (75 MHz, $CDCl_3$) δ: 189.9, 133.9, 133.8, 133.6, 133.2, 132.0, 131.5, 130.9, 130.0, 129.9, 129.6, 128.7, 127.4, 127.3, 127.1, 127.0, 126.7, 126.4, 126.2, 125.9, 124.8, 124.5, 121.3, 120.6, 120.2, 112.3. MS-ESI *m/z*: 375.9 $[M+H]^+$.

*5-(Naphthalen-1-yl)naphtho[2,3-b]pyrrolo[1,2-d][1,4]oxazepin-4-yl acetate (**29**)*

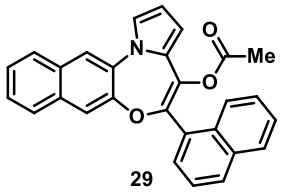

29

To a solution of **52a** (20 mg, 0.053 mmol) in dry THF (1 mL) sodium *bis*(trimethylsilyl)amide (1 M solution in THF, 133 mL, 0.13 mmol) was added dropwise at -78 °C. After 45 min acetyl chloride (8 mL, 0.11 mmol) was added. The mixture was stirred for further 4 h at -78 °C. Subsequently, 1 mL of aqueous saturated NH_4Cl was added. The aqueous phase was extracted with EtOAc (3 x 5 mL). The organic layer was dried over anhydrous sodium sulfate, filtered, and concentrated. The residue was purified on a silica gel column chromatography (*n*-hexane/EtOAc 15:1) to obtain the title compound in 60% yield. ^{1}H NMR (300 MHz, $CDCl_3$) δ: 8.15 (d, *J* = 7.3 Hz, 1H), 7.94-7.79 (m, 4H), 7.63 (d, *J* = 7.9 Hz, 1H), 7.54-7.31 (m, 8H), 6.49 (s, 2H), 1.87 (s, 3H). ESI-MS *m/z* 418.0 $[M+H]^+$.

*8-Bromoquinoline (**59b**)*

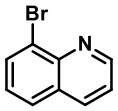

59b

$FeSO_4 \cdot 7H_2O$ (121 mg, 0.44 mmol) and nitrobenzene (1.78 g, 14.53 mmol) were heated at 110 °C. In a separate flask, 2-bromoaniline **69** (2.50 g, 14.53 mmol) and glycerol were sequentially added to conc. H_2SO_4 and the resulting mixture heated at 70 °C. This solution was then added to the $PhNO_2$ $FeSO_4 \cdot 7H_2O$ at 110 °C and the mixture was heated at 150 °C for 7 h. After cooling to room temperature, the mixture was poured into ice and neutralized to pH = 8 with 4N NaOH. The aqueous phase was extracted 10 times with EtOAc. The

combined organic layers were dried over anhydrous sodium sulfate, filtered, and concentrated. The residue was purified by flash chromatography on silica gel (PE/DCM 1:1) to afford the title compound as a brown oil in 60% yield. ^{1}H NMR (300 MHz, $CDCl_3$) δ: 9.05 (dd, 1H, J_1 = 1.5 Hz, J_2 = 4.2 Hz), 8.18 (dd, 1H, J_1 = 1.5 Hz, J_2 = 8.4 Hz), 8.05 (dd, 1H, J_1 = 1.2 Hz, J_2 = 7.2 Hz), 7.78 (d, 1H, J = 7.8 Hz), 7.50-7.38 (m, 2H); ESI-MS *m/z* 209.9 $[M+H]^+$, 231.9 $[M+Na]^+$.

*Ethyl 2-oxo-2-(quinolin-5-yl)acetate (**61a**)*

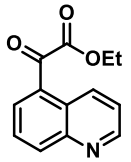

61a

To a solution of compound **59a** (250 mg, 1.22 mmol) in dry THF (2.5 mL), *n*-BuLi (2.5 M solution in *n*-hexane, 1.50 mmol) was added dropwise at -78 °C. After 10 min, diethyl oxalate (165 mL, 1.22 mmol) was added at -78 °C. The reaction mixture was stirred at -78 °C for 10 min (TLC monitoring) and then quenched with 3mL of a saturated solution of $NaHCO_3$. The aqueous layer was extracted with EtOAc (3 x 5 mL). The combined organic layers were dried over anhydrous sodium sulfate, filtered, and concentrated. The residue was purified by flash chromatography on silica gel (*n*-hexane/EtOAc 4:1) to afford the title compound as a yellow amorphous solid in 20% yield. ^{1}H NMR (300 MHz, $CDCl_3$) δ: 9.39 (d, J = 8.7 Hz, 1H), 9.01 (d, J = 4.1 Hz, 1H), 8.40 (d, J = 8.4 Hz, 1H), 8.08 (d, J = 7.2 Hz, 1H), 7.81 (t, J = 7.9 Hz, 1H), 7.60 (dd, J_1 = 8.7, J_2 = 4.1 Hz, 1H), 4.50 (q, J = 7.1 Hz, 2H), 1.46 (t, J = 8 Hz, 3H); ESI-MS *m/z* 230.1 $[M+H]^+$.

*Ethyl 2-oxo-2-(quinolin-8-yl)acetate (**61b**)*

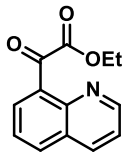

61b

Compound **61b** was prepared from **59b** following the procedure described for the preparation of **61a**. The residue was purified by flash chromatography on silica gel (PE/EtOAc 9:1) to afford the title compound as a yellow amorphous solid in 20% yield. ^{1}H NMR (300 MHz, $CDCl_3$) δ: 8.89 (dd, 1H, J_1 = 1.5 Hz, J_2 = 3.9 Hz), 8.34 (dd, 1H, J_1 = 1.5

Hz, J_2 = 7.2 Hz), 8.23 (dd, 1H, J_1 = 1.5 Hz, J_2 = 8.4 Hz), 8.10 (dd, 1H, J_1 = 1.2 Hz, J_2 = 8.1 Hz), 7.69 (t, 1H, J = 7.8 Hz), 7.50-7.46 (m, 1H), 4.44 (m, 2H), 1.42 (t, 3H, J = 6.9 Hz); ESI-MS *m/z* 230.0 $[M+H]^+$, 252.0 $[M+Na]^+$, 481.0 $[2M+Na]^+$.

*Ethyl 2-hydroxy-2-(quinolin-5-yl)acetate (**57a**)*

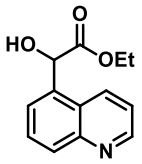

57a

To a solution of compound **61a** (130 mg, 0.57 mmol) in dry THF (5 mL), $NaBH_4$ (13 mg, 0.34 mmol) was added at 25 °C. The reaction mixture was stirred at 25 °C for 30 min (TLC monitoring), and then quenched with saturated aqueous NH_4Cl (1 mL). THF was evaporated under reduced pressure and the aqueous residue extracted with EtOAc (3 x 10 mL). The combined organic layers were dried over anhydrous sodium sulfate, filtered, and concentrated. The residue was purified by flash chromatography on silica gel (DCM/acetone 1:1) to afford the title compound as a yellow amorphous solid in 21% yield. ^{1}H NMR (300 MHz, $CDCl_3$) δ: 8.83 (d, J = 4.2 Hz, 1H), 8.56 (d, J = 8.7 Hz, 1H), 8.05 (d, J = 8.4 Hz, 1H), 7.67-7.52 (m, 2H), 7.39 (dd, J = 8.6, 4.2 Hz, 1H), 5.76 (s, 1H), 4.27-4.03 (m, 2H), 1.10 (t, J = 7.2 Hz, 3H); ESI-MS *m/z* 231.9 $[M+H]^+$.

*Ethyl 2-hydroxy-2-(quinolin-8-yl)acetate (**57b**)*

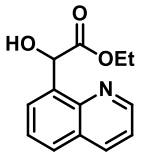

57b

Compound **57b** was prepared from **61b** following the procedure described for the preparation of **57a**. The residue was purified by flash chromatography on silica gel (*n*-hexane/EtOAc 4:1) to afford the title compound as a pale yellow amorphous solid in 21% yield. ^{1}H NMR (300 MHz, $CDCl_3$,) δ: 8.87 (dd, 1H, J_1 = 1.8 Hz, J_2 = 4.5 Hz), 8.20 (dd, 1H, J_1 = 1.8 Hz, J_2 = 8.4 Hz), 7.80 (dd, 1H, J_1 = 1.5 Hz, J_2 = 8.1 Hz), 7.71 (d, 1H, J = 6.9 Hz), 7.57-7.52 (m, 1H), 7.44 (q, 1H, J = 3.9 Hz), 5.66 (s, 1H), 4.26-4.05 (m, 2H), 1.12 (t, 3H, J = 4.2 Hz); ESI-MS *m/z* 232.0 $[M+H]^+$, 254.0 $[M+Na]^+$, 485.0 [2M+Na]+.

*Methyl 2-[(3-(1H-pyrrol-1-yl)naphthalen-2-yl)oxy]-2-(quinolin-5-yl)acetate (**56b**)*

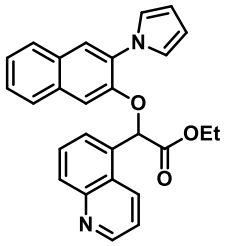

56b

Triphenylphosphine (393 mg, 1.5 mmol) and DIAD (196 μL, 1.0 mmol) were added to the solution of **57a** (230 mg, 1.0 mmol) in dry THF (10 mL) at 0 °C and stirred for 10 min. A solution of pyrrolylphenol compounds **54a** (209 mg, 1.0 mmol) in dry THF (8 mL) was added to the reaction mixture and was stirred at 25 °C for 24 h. THF was evaporated under reduced pressure. The residue was diluted with DCM and washed with water and a saturated solution of brine. The organic layer was dried over anhydrous sodium sulfate, filtered, and concentrated. The residue was purified by silica gel column chromatography (*n*-hexane/EtOAc 3:1) to afford the title compound as a yellow solid in 49% yield. ^{1}H NMR (300 MHz, $CDCl_3$) δ: 8.93 (d, 1H, *J* = 3.9 Hz), 8.62 (d, 1H, *J* = 8.7 Hz), 8.12 (d, 1H, *J* = 8.1 Hz), 7.77-7.66 (m, 5H), 7.48-7.36 (m, 4H), 7.12 (t, 2H, *J* = 2.1 Hz), 6.32 (t, 2H, *J* = 2.1 Hz), 6.27 (s, 1H), 3.67 (s, 3H); ESI-MS *m/z* 409 $[M+H]^+$, 431 $[M+Na]^+$, 447 $[M+K]^+$.

*Methyl 2-[(3-(1H-pyrrol-1-yl)naphthalen-2-yl)oxy]-2-(quinolin-8-yl)acetate (**56c**)*

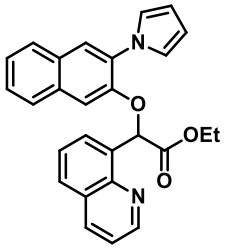

56c

The title compound **56c** was prepared from **54a** and **57b** by following the described procedure as **56b**. The residue was purified by flash chromatography on silica gel (*n*-hexane/EtOAc 7:3) to afford the title compound as a white solid in 68% yield. ^{1}H NMR (300 MHz, $CDCl_3$) δ: 9.05 (t, *J* = 2.4 Hz, 1H), 8.20 (dd, J_1 = 1.5 Hz, J_2 = 8.1 Hz, 1H), 7.94 (d, 1H, *J* = 7.5 Hz), 7.83 (d, 1H, *J* = 8.1 Hz), 7.73 (m, 2H), 7.65 (d, 1H, *J* = 8.1 Hz), 7.60-7.37 (m, 6H), 7.27 (t, 2H, *J* = 2.4 Hz), 6.35 (t, 2H, *J* = 1.5 Hz), 3.70 (s, 3H); ^{13}C NMR (75 MHz, $CDCl_3$) δ: 170.3, 150.1, 149.2, 145.3, 136.4, 133.3, 132.3, 131.5, 128.9, 128.9,

128.5, 128.1, 127.2, 126.6, 126.5, 126.2, 124.8, 123.7, 122.6 (2C), 121.4, 109.9, 109.0 (2C), 73.3, 52.6. ESI-MS *m/z* 409 $[M+H]^+$.

*Quinoline-5-carbaldehyde (**55a**)*

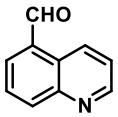

55a

To a solution of **59a** (100 mg, 0.48 mmol) in dry THF (1.5 mL) at -78 °C, *n*-BuLi (2.5M in *n*-hexane, 300 mL, 0.72 mmol) was added dropwise. The resulting solution turned to red and dry DMF (192 mL, 2.49 mmol) was added. After 10 min at -78 °C, the mixture was quenched with water. The reaction was poured into a saturated aqueous solution of $NaHCO_3$ (10 mL) and extracted with EtOAc (3 x 10 mL). The combined organic layers were dried over anhydrous sodium sulfate, filtered, and concentrated. The residue was purified by flash chromatography on silica gel (*n*-hexane/EtOAc 4:1) to afford the title compound as a yellow solid in 69% yield. ^{1}H NMR (300 MHz, $CDCl_3$) δ: 10.37 (s, 1H), 9.62 (d, 1H, J = 8.7 Hz), 9.02 (t, 1H, J = 2.1 Hz), 8.38 (d, 1H, J = 8.7 Hz), 8.07 (dd, 1H, J_1 = 5.4 Hz, J_2 = 7.2 Hz), 7.92-7.88 (m, 1H), 7.58 (dd, 1H, J_1 = 4.5 Hz, J_2 = 8.7 Hz); ESI-MS *m/z* 158 $[M+H]^+$.

*Quinoline-8-carbaldehyde (**55c**)*

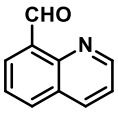

55c

Compound **55c** was obtained from **59b** (500 mg, 2.4 mmol) following the procedure described for the preparation of **55a**. The residue was purified by flash chromatography on silica gel (*n*-hexane/EtOAc 10:1) to afford the title compound as a yellow solid in 53% yield. ^{1}H NMR (300 MHz, $CDCl_3$) δ: 11.44 (s, 1H), 9.03 (dd, J_1 = 1.8 Hz, J_2 = 4.2 Hz, 1H), 8.31 (dd, J_1 = 1.2 Hz, J_2 = 7.2 Hz, 1H), 8.23 (dd, J_1 = 1.8 Hz, J_2 = 8.1 Hz, 1H), 8.08 (dd, J_1 = 1.5 Hz, J_2 = 8.4 Hz, 1H), 7.66 (t, J = 7.8 Hz, 1H), 7.50 (dd, J_1 = 4.5 Hz, J_2 = 8.4 Hz, 1H); ESI-MS *m/z* 158 $[M+H]^+$; 180 $[M+Na]^+$.

*2-[(3-(1H-Pyrrol-1-yl)naphthalen-2-yl)oxy]-2-(quinolin-5-yl)acetic acid (**53b**)*

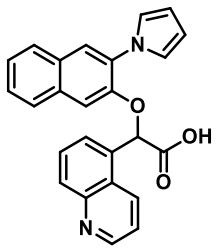

53b

Compound **53b** was obtained by following the two procedures from **56b** (Method A) or **54a** and **55a** (Method B) described for **53a**. The title compound was obtained as a yellow amorphous solid and submitted to the next step without further purification for Method A in 88% yield or by purifying the residue in silica column chromatography in Method B (DCM/MeOH 10:1) in 37% yield. ^{1}H NMR (300 MHz, CD_3OD) δ: 8.88 (dd, J_1 = 11.5 Hz, J_2 = 6.5 Hz, 1H), 8.04 (d, J = 8.5 Hz, 1H), 7.90 (d, J = 6.6 Hz, 1H), 7.84-7.74 (m, 4H), 7.65 (s, 1H), 7.55-7.35 (m, 4H), 7.14-7.09 (m, 2H), 6.61 (s, 1H), 6.25-6.21 (m, 2H); ^{13}C NMR (75 MHz, DMSO) δ: 171.1, 150.5, 149.7, 148.3, 135.1,134.4, 132.5, 131.2, 129.7, 129.1, 128.6, 127.7, 127.1, 126.7 (2C), 126.5, 124.8, 123.4, 122.7 (2C), 121.4, 109.8, 109.1 (2C), 78.2. ESI-MS *m/z* 395 $[M+H]^+$, 417 $[M+Na]^+$.

*2-[(3-(1H-Pyrrol-1-yl)naphthalen-2-yl)oxy]-2-(quinolin-8-yl)acetic acid (**53c**)*

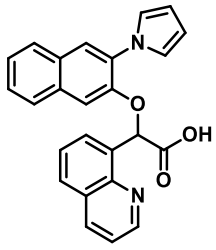

53c

Compound **53c** was obtained by following the two procedures from **56c** (Method A) or from **54a** and **55c** (Method B) in 30% yield as described for **53a**. However, for the work-up in Method B the aqueous layer was not acidified and the extraction was performed at a pH of 8. The title compound was obtained as a yellow amorphous solid and submitted to the next step without further purification for Method A in 85% yield or by purifying the residue in silica column chromatography in Method B (DCM/MeOH 10:1) in 30% yield. ^{1}H NMR (300 MHz, $CDCl_3$) δ: 8.93 (d, 1H, J = 4.5 Hz), 8.35 (d, 1H, J = 8.4 Hz), 8.00 (d, 1H, J = 7.2 Hz), 7.86 (d, 1H, J = 8.4 Hz), 7.78-7.74 (m, 3H), 7.62-7.56 (m, 2H), 7.45-7.39

(m, 3H), 7.26-7.23 (m, 2H), 6.72 (s, 1H), 6.36 (s, 2H); ESI-MS *m/z* 395 $[M+H]^+$, 417 $[M+Na]^+$.

*5-(Quinolin-5-yl)naphtho[2,3-b]pyrrolo[1,2-d][1,4] oxazepin-4(5H)-one (**52b**)*

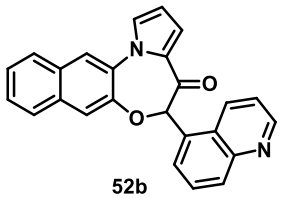

52b

Compound **52b** was obtained following the procedure described for **52a**. The residue was purified by chromatography on alumina (*n*-hexane/EtOAc 10:1) to afford the title compound as a white amorphous solid in 75% yield. ^{1}H NMR (300 MHz, $CDCl_3$) δ: 8.97 (d, 1H, *J* = 3.9 Hz), 8.53 (d, 1H, *J* = 8.1 Hz), 8.09 (d, 1H, *J* = 8.7 Hz), 7.88-7.82 (m, 2H), 7.60-7.36 (m, 9H), 6.64-6.61 (m, 1H), 6.13 (s, 1H); ^{13}C NMR (75 MHz, $CDCl_3$) δ: 189.2, 150.4, 148.6, 147.3, 133.2, 132.9, 132.8, 132.1, 131.2, 131.1, 131.0, 128.5, 127.9, 127.4 (2C), 127.1, 126.7, 126.5, 121.6, 121.4, 120.6, 120.4, 112.5, 89.0. ESI-MS *m/z* 377 $[M+H]^+$.

*5-(Quinolin-8-yl)naphtho[2,3-b]pyrrolo[1,2-d][1,4]oxazepin-4(5H)-one (**52c**)*

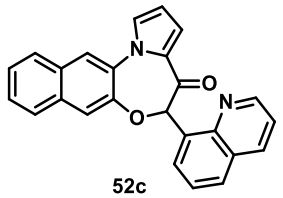

52c

The compound **52c** was synthesized from **53c** by following the same procedure as described for **52a** in 52% yield. ^{1}H NMR (300 MHz, $CDCl_3$) δ: 8.81(s, 1H), 8.14 (dd, 1H, J_1 =1.2 Hz, J_2 = 8.1 Hz), 7.87-7.78 (m, 4H), 7.62-7.26 (m, 8H), 6.86 (br s, 1H), 6.58 (q, 1H, J_1 = 2.4 Hz, J_2 = 4.2 Hz); ESI-MS *m/z* 377 $[M+H]^+$, 399 $[M+Na]^+$.

*5-(Quinolin-5-yl)naphtho[2,3-b]pyrrolo[1,2-d][1,4]oxazepin-4-yl acetate (**32**)*

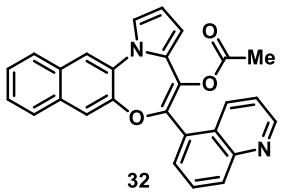

32

Following the procedure described for **29** a crude was obtained that was purified by chromatography on alumina (DCM/PE 7:3) to afford the title compound as a white solid (75% yield). ^{1}H NMR (300 MHz, $CDCl_3$) δ: 8.97 (dd, 1H, J_1 = 1.5 Hz, J_2 = 3.9 Hz), 8.52 (d, 1H, J = 8.4 Hz), 8.21 (d, 1H, J = 8.4 Hz), 7.85-7.87 (m, 2H), 7.38-7.72 (m, 7H), 7.31 (s, 1H), 6.50 (t, 2H, J = 1.2 Hz), 1.88 (s, 3H); ^{13}C NMR (75 MHz, $CDCl_3$) δ: 168.8, 150.9, 150.2, 135.0, 132.7, 132.4, 131.6, 131.3, 130.8, 129.3, 128.0, 127.7 (2), 127.4, 127.3, 126.9, 126.6 (2), 122.8, 121.6, 121.7, 121.1, 119.3, 111.5, 111.1, 104.4, 20.7; FT-IR (neat) ν_{max} = 1756 cm^{-1}. ESI-MS *m/z* 419 $[M+H]^+$, 441 $[M+Na]^+$, 457 $[M+K]^+$. HRMS-ESI (*m/z*): $[M+H]^+$ calcd for $C_{27}H_{19}N_2O_3$ 419.13957; found 419.13815. Anal. ($C_{27}H_{18}N_2O_3$).

*5-(Quinolin-8-yl)naphtho[2,3-b]pyrrolo[1,2-d][1,4]oxazepin-4-yl acetate (**33**)*

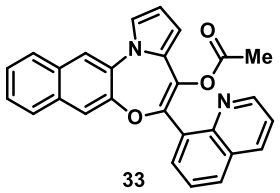

33

To a suspension of potassium *tert*-butoxide (30 mg, 0.26 mmol) in dry THF (1.0 mL), a solution of compound **52c** (40 mg, 0.11 mmol) in dry THF (1.0 mL) was added, and the solution immediately turned orange. After 1 h acetyl chloride (15 mL, 0.21mmol) was added dropwise. The mixture was stirred at 25 °C for 8 h, then NH_4Cl (s.s) was added and the resulting mixture was extracted with EtOAc (3 x 5 mL). The combined organic layers were dried over anhydrous sodium sulfate, filtered, and concentrated. The residue was purified by flash chromatography on silica gel (*n*-hexane/EtOAc 4:1) to afford the title compound as a pale yellow solid (18% yield). ^{1}H NMR (300 MHz, $CDCl_3$) δ: 9.02-9.04 (m, 1H), 8.22 (dd, 1H, J_1 = 1.5 Hz, J_2 = 8.4 Hz), 7.90-7.83 (m, 4H), 7.69 (dt, 1H, J_1 =1.5 Hz, J_2 = 7.2 Hz), 7.62 (d, 1H, 7.8 Hz), 7.54-7.38(m, 7H), 6.50-6.43 (m, 2H), 1.92 (s, 3H); ^{13}C NMR (75 MHz, $CDCl_3$) δ: 169.3, 151.3, 151.0, 146.7, 145.4, 136.5, 134.6, 133.2, 132.6, 132.4, 131.5, 130.5, 130.4, 129.8, 128.9, 127.8, 127.7, 127.3, 126.3, 126.2, 122.3, 121.7, 120.9, 119.6, 111.2, 110.7, 20.9; FT-IR (neat) ν_{max} = 1751 cm^{-1}. ESI-MS *m/z* 419 $[M+H]^+$, 441 $[M+Na]^+$, 457 $[M+K]^+$.

*5-(Quinolin-5-yl)naphtho[2,3-b]pyrrolo[1,2-d][1,4]oxazepin-4-yl(5-(diethylamino)pentan-2-yl) carbamate (**34**).*

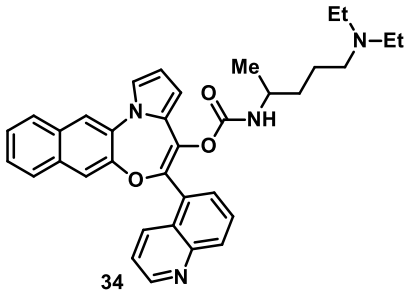

34

To a solution of **52b** (20 mg, 0.053 mmol) in dry THF (1 mL), sodium *bis*(trimethylsilyl)amide (1 M solution in THF, 133 mL, 0.13 mmol) was added at -78 °C and stirred for 30 min. A solution of 4-nitrophenyl chloroformate (48 mg, 0.24 mmol) in dry THF (1 mL) was prepared at 0 °C in a separate flask and transferred slowly to the reaction mixture at -78 °C. The reaction mixture was allowed to reach 25 °C and stirred for further 3 h. Formation of the activated carbonate intermediate was confirmed by TLC on silica gel and ESI-MS *m/z* analysis (542.5 $[M + H]^+$). After that, *N*,*N*-diethylpentane-1,4-diamine (7 µL, 0.14 mmol) and TEA (16 µL, 0.10 mmol) were added together into the reaction mixture at 25 °C and stirred for another 1 h. Water was slowly added to the reaction mixture at 0 °C and the solution was extracted rapidly with EtOAc (3 x 5 mL). The combined organic layers were dried over anhydrous sodium sulfate, filtered, and concentrated under reduced pressure at 20 °C. The crude was purified by using a silica gel column chromatography (EtOAc/MeOH/TEA 20:1:0.1) to obtain the title compound in 30% yield as a light green oil. ^{1}H NMR (300 MHz, $CDCl_3$) δ: 8.93 (s, 1H), 8.53 (d, *J* = 8.4 Hz, 1H), 8.14 (d, *J* = 8.1 Hz, 1H), 7.83 (s, 2H), 7.71-7.55 (m, 3H), 7.49-7.33 (m, 4H), 7.26 (d, *J* = 8.1 Hz, 1H), 6.50 (d, *J* = 11.3 Hz, 2H), 6.07 (s, 1H), 3.46 (s, 1H), 2.34 (dd, *J* = 21.5, 15.4 Hz, 6H), 1.28 (d, *J* = 25.5 Hz, 4H), 0.97-0.75 (m, 9H); ^{13}C NMR (75 MHz, $CDCl_3$) δ: 153.2, 150.7, 150.4, 148.3, 144.1, 135.0, 132.6, 132.0, 131.2, 130.6, 128.7, 127.9, 127.7, 127.4, 127.1, 126.7, 126.2, 122.2, 121.3, 120.8, 118.9, 111.1, 110.4, 52.4, 46.7, 46.2, 34.5, 22.4, 20.5, 10.7. ESI-MS *m/z* 561.6 $[M+H]^+$. HRMS-ESI (*m/z*): $[M+H]^+$ calculated for $[C_{35}H_{37}N_4O_3]^+$ 561.2845, found 561.2845.

*5-(Quinolin-5-yl)naphtho[2,3-b]pyrrolo[1,2-d][1,4]oxazepin-4-yl 4-methylpiperazine-1-carboxylate (**35**).*

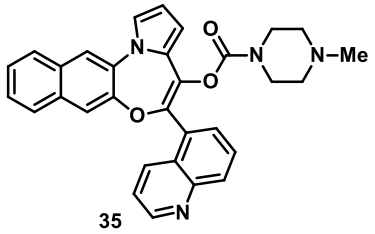

35

The title compound **35** was obtained from **52b** by following the same procedure as described in the synthesis of **34** in presence of *N*-methylpiperazine. The crude was purified by using a silica gel column chromatography (DCM/MeOH 10:1) to obtain compound **35** in 56% yield as a light green oil compound. ^{1}H NMR (300 MHz, $CDCl_3$) δ: 8.95 (d, *J* = 3.8 Hz, 1H), 8.51 (d, *J* = 8.4 Hz, 1H), 8.17 (d, *J* = 8.3 Hz, 1H), 7.83 (d, *J* = 4.9 Hz, 2H), 7.75-7.57 (m, 3H), 7.52-7.22 (m, 5H), 6.49 (t, *J* = 8.1 Hz, 2H), 3.24 (s, 4H), 2.15 (d, *J* = 5.9 Hz, 4H), 1.87 (s, 3H); ^{13}C NMR (75 MHz, $CDCl_3$) δ: 152.5, 150.7, 150.5, 148.3, 143.9, 135.2, 135.0, 132.5, 132.1, 131.3, 131.1, 130.8, 128.8, 127.8, 127.6, 127.4, 127.1, 126.7, 126.3, 126.2, 122.4, 121.3, 120.8, 118.9, 111.2, 110.6, 54.3, 45.9, 44.3, 43.8. ESI-MS *m/z* 503.3 $[M+H]^+$. HRMS-ESI (*m/z*): $[M+H]^+$ calculated for $[C_{31}H_{27}N_4O_3]^+$ 503.2071, found 503.2070.

*1-tert-Butyl 4-(5-(quinolin-5-yl)naphtho[2,3-b]pyrrolo[1,2-d][1,4]oxazepin-4-yl)piperidine-1,4-dicarboxylate (**36**).*

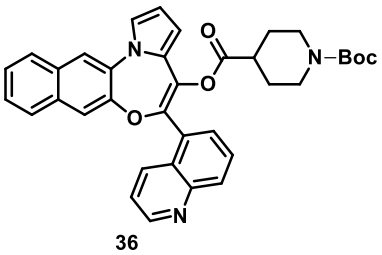

36

To a solution of **52b** (20 mg, 0.05 mmol) in dry THF (1 mL), sodium *bis*(trimethylsilyl)amide (1 M solution in THF, 160 µL, 0.16 mmol) was added dropwise at -78 °C and stirred for 45 min. In a separate flask, thionyl chloride (58 µL, 0.78 mmol) was added dropwise to a solution of 4-(*tert*-butoxycarbonyl)piperazine-1-carboxylic acid (40 mg, 0.39 mmol) in dry DCM (1 ml) at 0 °C and stirred at 25 °C for 10 min; the formation of *tert*-butyl 4-(chlorocarbonyl)piperidine-1-carboxylate was confirmed by ESI-MS analysis. The solvent from the later flask was removed completely under reduced pressure at 20 °C, the residue was solubilized in dry THF at 25 °C, and the solution was cooled to 0

°C. This cold solution was transferred dropwise to the former flask at -78 °C. The reaction mixture was stirred at 25 °C for 12 h. Subsequently a saturated solution of $NaHCO_3$ was added dropwise and the aqueous layer was extracted with EtOAc (3 x 5 mL). The combined organic layers were dried over anhydrous sodium sulfate, filtered, and concentrated under reduced pressure at 25 °C. The residue was purified by alumina column chromatography (Hex/EtOAc/DCM/MeOH 20:2:0.1:0.2) to afford the title compound in 64% yield as a white solid. ^{1}H NMR (300 MHz, $CDCl_3$) δ: 8.97 (dd, *J* = 4.2, 1.7 Hz, 1H), 8.53-8.39 (m, 1H), 8.22-8.09 (m, 1H), 7.86 (d, *J* = 5.8 Hz, 2H), 7.72-7.60 (m, 2H), 7.53-7.32 (m, 6H), 6.51-6.35 (m, 2H), 3.72 (d, *J* = 23.0 Hz, 2H), 2.64 (t, *J* = 12.4 Hz, 2H), 2.35-2.17 (m, 1H), 1.59 (s, 4H), 1.40 (s, 9H). ^{13}C NMR (75 MHz, $CDCl_3$) δ: 172.3, 154.5, 150.8, 148.4, 134.8, 134.5, 132.5, 132.2, 131.31, 131.2, 130.8, 128.6, 127.7, 127.5, 127.2, 126.9, 126.7, 126.4, 122.6, 121.5, 121.0, 119.1, 111.2, 110.6, 79.7, 42.8, 40.7, 29.7, 28.4, 27.4. ESI-MS *m/z* 588.0 $[M+H]^+$. HRMS-ESI (*m/z*): $[M+H]^+$ calculated for $[C_{36}H_{34}N_3O_5]^+$ 588.2482, found 588.2481.

*5-(Quinolin-5-yl)naphtho[2,3-b]pyrrolo[1,2-d][1,4]oxazepin-4-ylpiperidine-4-carboxylate (**37**).*

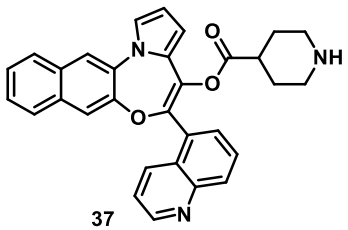

37

To a cold solution of compound **36** (20 mg, 0.003 mmol) in dry DCM (4 mL) at 0 °C, TFA (340 µL, 4.44 mmol) was added dropwise. The reaction mixture was stirred at 25 °C for 30 min. Subsequently a saturated solution of $NaHCO_3$ was added dropwise at 0 °C and the aqueous layer was extracted with DCM (3 x 5 mL). The combined organic layers were dried over anhydrous sodium sulfate, filtered, and concentrated under reduced pressure at 25 °C. The residue was purified by silica gel column chromatography (DCM/MeOH 10:1) to afford the compound **37** in 96% yield as a light brown solid. ^{1}H NMR (300 MHz, CD_3OD) δ: 8.89 (dd, *J* = 4.3, 1.7 Hz, 1H), 8.48 (dt, *J* = 8.3, 1.3 Hz, 1H), 8.12 (dt, *J* = 8.5, 1.1 Hz, 1H), 8.01 (s, 1H), 7.92 (d, *J* = 8.1 Hz, 1H), 7.77 (dd, *J* = 8.6, 7.1 Hz, 1H), 7.65 (d, *J* = 8.0 Hz, 1H), 7.59-7.36 (m, 5H), 7.32 (s, 1H), 6.51-6.43 (m, 2H), 2.76 (dt, *J* = 13.1, 3.9 Hz, 2H), 2.50-2.32 (m, 3H), 1.51 (dd, *J* = 13.4, 3.6 Hz, 2H), 1.30-1.18 (m, 2H). ^{13}C NMR

(75 MHz, $CDCl_3$) δ: 172.4, 150.8, 148.3, 144.0, 134.9, 134.5, 132.5, 132.2, 131.3, 131.1, 130.9, 128.7, 127.7, 127.5, 127.2, 126.9, 126.7, 126.4 (2C), 122.6, 121.5, 121.0, 119.1, 111.2, 110.7, 44.8, 40.5, 29.7, 27.9. ESI-MS *m/z* 488.0 $[M+H]^+$. HRMS-ESI (*m/z*): $[M+H]^+$ calculated for $[C_{31}H_{26}N_3O_3]^+$ 488.1964, found 488.1963.

*5-(Quinolin-5-yl)naphtho[2,3-b]pyrrolo[1,2-d][1,4]oxazepin-4-yl nicotinate (**39**).*

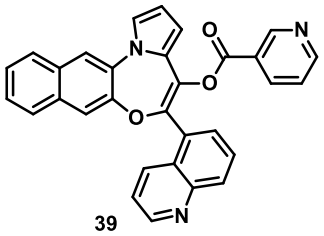

39

The compound **39** was synthesized from **52b** by following the same procedure as described for **32** in presence of nicotinoyl chloride. The residue was purified by an alumina column chromatography (*n*-hexane/EtOAc/DCM/MeOH 20:2:0.1:0.2) to afford the title compound in 31% yield as a white solid. ^{1}H NMR (300 MHz, $CDCl_3$) δ: 9.02 (s, 1H), 8.96 (dd, *J* = 4.2, 1.7 Hz, 1H), 8.71 (dd, *J* = 4.9, 1.8 Hz, 1H), 8.59 (d, *J* = 8.6 Hz, 1H), 8.13-8.04 (m, 2H), 7.88 (d, *J* = 7.9 Hz, 2H), 7.68-7.55 (m, 3H), 7.55-7.39 (m, 4H), 7.36-7.27 (m, 2H), 6.50 (d, *J* = 2.4 Hz, 2H). ^{13}C NMR (75 MHz, $CDCl_3$) δ: 163.3, 154.1, 151.1, 150.7, 148.3, 144.6, 137.4, 134.9, 134.7, 132.4, 132.2, 131.4, 131.2, 130.6, 129.7, 128.8, 127.6, 127.5, 127.2, 126.7, 126.6, 126.5 (2C), 124.6, 123.4, 122.8, 121.5, 121.0, 119.2, 111.3, 111.0; ESI-MS *m/z* 482.1 $[M+H]^+$. HRMS-ESI (*m/z*): $[M+H]^+$ calculated for $[C_{31}H_{20}N_3O_3]^+$ 482.1487, found 482.1487.

*5-(Quinolin-8-yl)naphtho[2,3-b]pyrrolo[1,2-d][1,4]oxazepin-4-yl 4-methylpiperazine-1-carboxylate (**40**)*

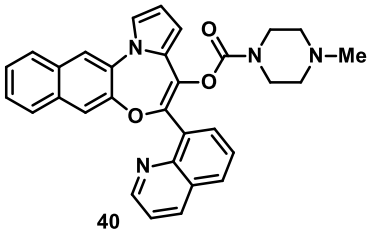

40

The compound **40** was synthesized from **52c** by following the same procedure as the synthesis of **34** in presence of *N*-methylpiperazine. The residue was purified by a silica gel column chromatography (DCM/MeOH 60:1) affording the title compound in 20% yield.

^{1}H NMR (300 MHz, CD_3OD) δ: 8.84 (d, *J* = 3.3 Hz, 1H), 8.43 (d, *J* = 8.3 Hz, 1H), 8.10-8.00 (m, 2H), 7.93 (d, *J* = 7.8 Hz, 1H), 7.84 (d, *J* = 6.8 Hz, 1H), 7.73-7.35 (m, 7H), 6.50 (d, *J* = 6.0 Hz, 2H), 3.52-3.31 (m, 4H), 2.72 (d, *J* = 15.5 Hz, 3H), 2.55 (s, 5H). ^{13}C NMR (75 MHz, CD_3OD) δ: 152.8, 150.8, 150.2, 145.6, 144.4, 136.9, 134.7, 132.6, 132.3, 132.0, 131.5, 130.6, 129.6, 128.8, 127.4, 127.2, 126.8, 126.1, 125.9, 122.2, 121.6, 120.4, 118.6, 110.6, 110.1, 53.1, 43.2, 41.9; ESI-MS *m/z* 503.1 $[M+H]^+$, 525.1 $[M+Na]^+$, 1027.4 $[2M+Na]^+$.

*1-tert-Butyl 4-(5-(quinolin-8-yl)naphtho[2,3-b]pyrrolo[1,2-d][1,4]oxazepin-4-yl) piperidine-1,4-dicarboxylate (**70**)*

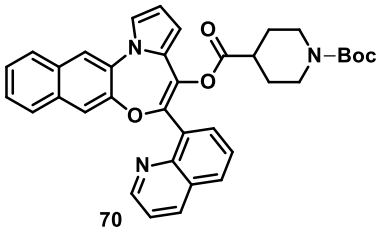

70

The compound **70** was synthesized from **52c** by following the same procedure as described for the synthesis of **36** and the title compound was purified by a silica gel column chromatography (PE/EtOAc 5:1) in 65% yield. ^{1}H NMR (300 MHz, $CDCl_3$) δ: 9.05 (s, 1H), 8.24 (d, *J* = 8.5 Hz, 1H), 7.97-7.78 (m, 3H), 7.64 (d, *J* = 7.0 Hz, 2H), 7.42 (dd, *J* = 24.7, 16.3 Hz, 6H), 6.43 (s, 2H), 3.76 (d, *J* = 12.9 Hz, 2H), 2.67 (s, 2H), 2.32 (s, 2H), 1.49 (d, *J* = 21.7 Hz, 2H), 1.37 (d, *J* = 23.3 Hz, 9H); 589.7 $[M+H]^+$.

*5-(Quinolin-8-yl)naphtho[2,3-b]pyrrolo[1,2-d][1,4]oxazepin-4-yl piperidine-4-carboxylate (**41**)*

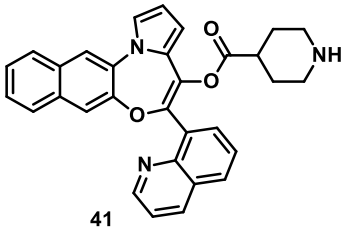

41

The compound **41** is synthesized from **70** by following the same protocol as **37** and the title compound was purified by a silica gel column chromatography (DCM/MeOH 10:1) in 48% yield. ^{1}H NMR (300 MHz, $CDCl_3$) δ: 9.03 (s, 1H), 8.23 (d, *J* = 7.8 Hz, 1H), 8.01-7.77 (m, 3H), 7.64 (d, *J* = 6.3 Hz, 2H), 7.58-7.31 (m, 6H), 6.41 (d, *J* = 12.7 Hz, 2H), 2.66 (t, *J* = 52.6 Hz, 4H), 2.43 (s, 1H), 1.72 (d, *J* = 38.6 Hz, 4H). ^{13}C NMR (75 MHz, $CDCl_3$) δ: 170.8,

151.1, 146.4, 145.2, 136.4, 133.9, 132.6, 132.2, 132.1, 131.3, 130.2, 128.6, 127.5, 127.1, 126.8, 126.2, 125.9, 122.3, 121.8, 120.8, 119.4, 111.1, 110.3, 41.9, 37.3, 29.7, 23.9; 489.1 $[M+H]^+$.

*5-Bromoisoquinoline (**59d**)*

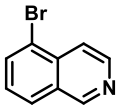

59d

Isoquinoline **71** (1156 mg, 8.95 mmol) was suspended in conc. H_2SO_4 (9.7 mL) at 0 °C. After cooling to -25 °C, NBS (1912 mg, 10.74 mmol) was added. The reaction mixture was stirred at -25 °C for 2 h and then at 25 °C for additional 24 h. Subsequently, ice was added and the mixture was treated with conc. NH_4OH (10 mL) to pH = 8-10. The resulting solution was extracted with EtOAc (3 x 10 mL). The combined organic layers were dried over anhydrous sodium sulfate, filtered, and concentrated. The residue was purified by flash chromatography on silica gel (PE/EtOAc 4:1) to afford the title compound as a pale pink solid in 70% yield. ^{1}H NMR (300 MHz, $CDCl_3$) δ: 9.24 (s, 1H), 8.65 (d, *J* = 5.9 Hz, 1H), 8.00-7.95 (m, 3H), 7.48 (t, *J* = 7.8 Hz, 1H); ESI-MS *m/z* 209.1 $[M+H]^+$.

*Ethyl 2-([1,1'-biphenyl]-2-yl)-2-oxoacetate (**61c**)*

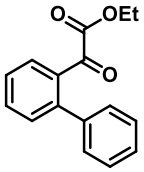

61c

Compound **61c** was prepared from **59c** following the procedure described for the preparation of **59a**. The residue was purified by flash chromatography on silica gel (PE/EtOAc 50:1) to afford the title compound as yellow oil in 18%. ^{1}H NMR (300 MHz, $CDCl_3$) δ: 7.82 (d, *J* = 7.5 Hz, 1H), 7.63 (t, *J* = 7.4 Hz, 1H), 7.52-7.25 (m, 7H), 3.75 (t, *J* = 6.9 Hz, 2H), 1.25 (q, *J* = 7.2 Hz, 3H); ESI-MS *m/z* 276.9 $[M+Na]^+$.

*Ethyl 2-hydroxy-2-(isoquinolin-5-yl)acetate (**61d**)*

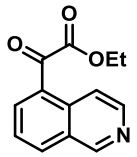

61d

The compound **61d** was prepared from **59d** following the procedure described for the preparation of **61a**. The residue was purified by flash chromatography on silica gel (PE/EtOAc 3:1) to afford the title compound as a pale orange amorphous solid in 40% yield. ^{1}H NMR (400 MHz, $CDCl_3$) δ: 9.32 (s, 1H), 8.79 (d, *J* = 6.0 Hz, 1H), 8.70 (d, *J* = 6.1 Hz, 1H), 8.27-8.17 (m, 2H), 7.69 (t, *J* = 7.6 Hz, 1H), 4.47 (q, *J* = 7.2 Hz, 2H),1.43 (t, *J* = 6.8 Hz, 3H); ESI-MS m/z 230.1 $[M+H]^+$.

*Ethyl 2-([1,1'-biphenyl]-2-yl)-2-hydroxyacetate (**57c**)*

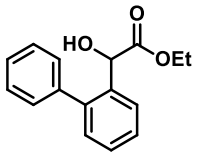

57c

Compound **57c** was obtained from **61c** following the procedure described for **57a**. The residue was purified by column chromatography on silica gel (PE/EtOAc 10:1) to afford the title compound as a yellow oil in 56% yield. ^{1}H NMR (300 MHz, $CDCl_3$) δ: 7.55-7.28 (m, 9H), 5.35 (d, *J* = 5.1 Hz, 1H), 4.19-4.02 (m, 2H), 1.12 (t, *J* = 7.2 Hz, 3H); ESI-MS *m/z* 279.9 $[M+Na]^+$.

*Ethyl 2-hydroxy-2-(isoquinolin-5-yl)acetate (**57d**)*

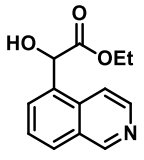

57d

Compound **57d** was obtained from **61d** following the procedure described for **57a**. The residue was purified by flash chromatography on silica gel (PE/EtOAc 1:1) to afford title compound as a pale yellow amorphous solid in 50% yield. ^{1}H NMR (400 MHz, $CDCl_3$) δ: 9.24 (s, 1H), 8.54 (d, *J* = 6.0 Hz, 1H), 7.95-7.91(m, 2H), 7.75 (d, *J* = 7.2 Hz, 1H), 7.58 (t, *J*

= 7.6 Hz, 1H), 5.73 (s, 1H), 4.31-4.06 (m, 2H), 3.76 (s, 1H), 1.11 (t, *J* = 7.2 Hz, 3H); ESI-MS *m/z* 232.1 $[M+H]^+$.

*2-(1H-Pyrrol-1-yl)phenol (**54b**)*

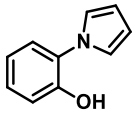

54b

Compound **54b** was synthesized from **68b** by following the same procedure as described for **68a**. The residue was purified on a silica gel column chromatography (PE/EtOAc 10:1) in 60% yield. ^{1}H NMR (300 MHz, $CDCl_3$) δ: 7.26 (t, *J* = 8.7 Hz, 3H), 7.11-6.93 (m, 2H), 6.86 (s, 2H), 6.40 (s, 2H), 5.22 (s, 1H); 157.8 $[M-H]^-$.

*Ethyl 2-((3-(1H-pyrrol-1-yl)naphthalen-2-yl)oxy)-2-(isoquinolin-5-yl)acetate (**56d**)*

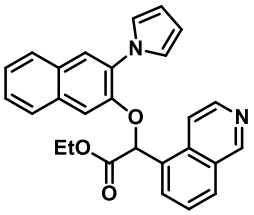

56d

The title compound **56d** was synthesized from **57d** and **54a** by following the same protocol as described for **56b**. The residue was purified by flash chromatography on silica gel (DCM/MeOH 100:1) to afford the title compound as colorless oil in 35% yield. ^{1}H NMR (400 MHz, $CDCl_3$) δ: 9.25 (s, 1H), 8.56 (d, *J* = 6.0 Hz, 1H), 8.06 (d, *J* = 6.0 Hz, 1H), 7.94 (dd, J_1 = 11.2, J_2 = 7.8 Hz, 2H), 7.77 (s, 1H), 7.74 (s, 1H), 7.70 (d, *J* = 8.0 Hz, 1H), 7.58 (t, *J* = 8 Hz, 1H), 7.46-7.36 (m, 2H), 7.34 (s, 1H), 7.16 (s, 2H), 6.34 (s, 2H), 6.30 (s, 1H), 4.21-4.05 (m, 2H), 1.11 (t, *J* = 7.1 Hz, 3H); ESI-MS *m/z* 423.0 $[M+H]^+$, 445.0 $[M+Na]^+$.

*Ethyl 2-(2-(1H-pyrrol-1-yl)phenoxy)-2-([1,1'-biphenyl]-2-yl)acetate (**56e**)*

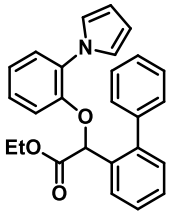

56e

The title compound **56e** was prepared from **57c** and **54b** by following the same procedure as **56b**. The residue was purified by column chromatography on alumina (PE/EtOAc 25:1) to provide the title compound as colourless oil in 56%. ^{1}H NMR (300 MHz, $CDCl_3$) δ: 7.81-7.76 (m, 1H), 7.47-7.30 (m, 8H), 7.19-7.01 (m, 4H), 6.72 (t, J = 7.8 Hz, 1H), 6.39 (dd, J_1 = 1.8 Hz, J_2 = 2.7 Hz, 2H), 5.81 (d, J = 11.4 Hz, 1H), 4.31-4.16 (m, 2H), 1.31-1.21 (m, 3H); ESI-MS *m/z* 398.0 $[M+H]^+$, 420.9 $[M+Na]^+$.

*2-((3-(1H-Pyrrol-1-yl)naphthalen-2-yl)oxy)-2-(isoquinolin-5-yl)acetic acid (**53d**)*

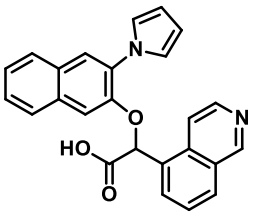

53d

Compound **53d** was obtained from **56d** by following the procedure described for **53a** Method A. The title compound was obtained in 80% yield as an orange amorphous solid and submitted to the next step without further purification. ^{1}H NMR (400 MHz, CD_3OD) δ: 9.24 (s, 1H), 8.36 (d, J = 6.4 Hz, 1H), 8.28 (d, J = 6.4 Hz, 1H), 8.10 (d, J = 8.4 Hz, 1H), 8.04 (d, J = 7.2 Hz, 1H), 7.80-7.74 (m, 3H), 7.66 (t, J = 7.6 Hz, 1H), 7.62 (s, 1H), 7.40 (dt, J_1 = 15.2 Hz, J_2 = 7.2 Hz, 2H), 7.12 (s, 2H), 6.50 (s, 1H), 6.20 (s, 2H); ^{13}C NMR (75 MHz, CD_3OD) δ: 175.6, 148.7, 136.3, 136.1, 135.9, 132.6, 131.6, 131.0, 130.9, 130.1, 129.4, 129.3, 127.0 (2C), 126.5, 126.3, 124.9, 124.3, 122.4 (2C), 122.0, 110.6, 108.6 (2C), 77.1. ESI-MS *m/z* 395.0 $[M+H]^+$.

*2-(2-(1H-Pyrrol-1-yl)phenoxy)-2-([1,1'-biphenyl]-2-yl)acetic acid (**53e**)*

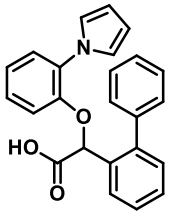

53e

Compound **53e** was obtained from **56e** by following the procedure described for **53a** in Method A. The title compound was obtained in 90% yield as a brown amorphous solid and submitted to the next step without further purification. ^{1}H NMR (300 MHz, $CDCl_3$) δ: 9.83 (s, 1H), 7.70-7.67 (m, 9H), 7.45-7.27 (m, 9H), 7.11-7.02 (m, 4H), 6.63 (d, 1H, *J* = 7.5 Hz), 6.35-6.33 (m, 2H), 5.74 (s, 1H); ^{13}C NMR (75 MHz, $CDCl_3$) δ: 174.7,149.3,142.6, 139.6, 132.2, 131.6, 130.2, 129.6 (2C),129.1, 128.3 (2C), 128.2, 127.7, 127.6, 127.0, 125.8, 122.9, 121.9 (2C), 116.2, 109.1 (2C), 75.2. ESI-MS *m/z* 369.9 $[M+H]^+$.

*5-(Isoquinolin-5-yl)naphtho[2,3-b]pyrrolo[1,2-d][1,4]oxazepin-4(5H)-one (**52d**)*

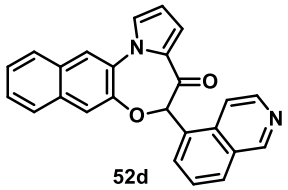

52d

Compound **52d** was obtained from **53d** following the procedure described for **52a** in dry DCM solution. The residue was purified by flash chromatography on silica gel (*n*-hexane/EtOAc 10:1) to afford the title compound as a white amorphous solid in 60% yield. ^{1}H NMR (400 MHz, $CDCl_3$) δ: 9.26 (s, 1H), 8.60 (d, *J* = 5.6 Hz, 1H), 7.96-7.91 (m, 2H), 7.85-7.80 (m, 3H), 7.59-7.35 (m, 7H), 6.61 (dd, J_1 = 4 Hz, J_2 = 2.8 Hz, 1H), 6.13 (s, 1H); ESI-MS *m/z* 377.0 $[M+H]^+$.

*6-([1,1'-Biphenyl]-2-yl)benzo[b]pyrrolo[1,2-d][1,4]oxazepin-7(6H)-one (**52e**)*

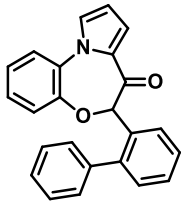

52e

Compound **52e** was obtained from **53e** following the procedure described for **52d**. The residue was purified by column chromatography on alumina (PE/EtOAc 20:1) to afford the

title compound as a yellow oil (37%). ^{1}H NMR (300 MHz, CDCl^{3}) δ: 7.59-7.52 (m, 2H), 7.45-7.27 (m, 12H), 7.08-7.02 (m, 1H), 6.49 (dd, J_1 = 3.0 Hz, J_2 = 0.9 Hz, 1H), 5.61 (s, 1H); ^{13}C NMR (75 MHz, $CDCl_3$) δ: 190.8, 149.0, 142.7, 140.4, 139.8, 135.0, 133.6, 130.1, 129.5 (2), 128.6, 128.4, 128.2 (2), 127.7, 127.6, 127.4, 126.1, 125.8, 123.6, 122.2, 120.5, 111.8, 88.0. ESI-MS *m/z* 352.0 $[M+H]^+$, 374.9 $[M+Na]^+$.

*6-([1,1'-Biphenyl]-2-yl)benzo[b]pyrrolo[1,2-d][1,4]oxazepin-7-yl acetate (**42**)*

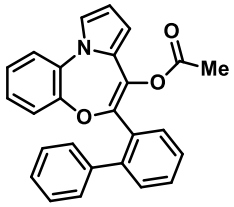

42

Compound **42** was obtained following the procedure described for **29** from **52e**. The residue was purified by flash chromatography on silica gel (PE/EtOAc 20:1) to afford the title compound as a yellow oil in 84% yield.^{1}H NMR (300 MHz, $CDCl_3$) δ: 7.49-7.41 (m, 5H), 7.37-7.30 (m, 1H), 7.28-7.18 (m, 4H), 7.12-7.05 (m, 2H), 6.95 (td, J_1 = 6.6 Hz, J_2 = 1.2 Hz, 1H), 6.58 (d, J = 7.2 Hz, 1H), 6.33 (m, 1H), 6.26 (dd, J_1 = 1.5 Hz, J_2 = 2.1 Hz, 1H), 1.99 (s, 3H); ^{13}C NMR (300 MHz, $CDCl_3$) δ: 168.6, 152.1, 146.4, 141.7, 141.2, 132.8, 132.5, 131.6, 130.6, 130.4, 129.4, 128.6, 128.2, 127.2, 127.1, 126.8, 126.7, 125.2, 122.3, 122.2, 121.3, 110.6, 109.9, 20.6; ESI-MS *m/z* 416.1 $[M+Na]^+$.

*5-(Isoquinolin-5-yl)naphtho[2,3-b]pyrrolo[1,2-d][1,4]oxazepin-4-yl acetate (**43**)*

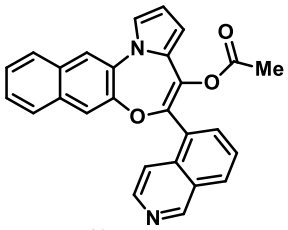

43

Compound **43** was obtained following the procedure described for **29** from **52d**. The residue was purified by flash chromatography on silica gel (DCM/Acetone 100:1) to afford the title compound as a colourless oil in 30% yield. ^{1}H NMR (300 MHz, $CDCl_3$) δ: 9.34 (s, 1H), 8.54 (d, J = 6.4 Hz, 1H), 8.06 (d, J = 8.2 Hz, 1H), 7.98 (d, J = 6.4 Hz, 1H), 7.87-7.85 (m, 2H), 7.74 (d, J = 6.7 Hz, 1H), 7.65-7.61 (m, 3H), 7.49-7.35 (m, 4H), 7.31 (s, 1H), 6.50 (d, J = 3.2 Hz, 2H), 1.87 (s, 3H); ^{13}C NMR (75 MHz, $CDCl_3$) δ: 168.6, 152.4, 150.7,

143.7, 142.9, 134.7, 134.2, 132.5, 132.1, 131.5, 131.3, 130.0, 129.3, 128.87, 127.4, 127.1, 127.0, 126.8, 126.4 (2), 122.6, 120.9, 119.4, 119.0, 111.2, 110.9, 20.5; ESI-MS *m/z* 419.1 $[M+H]^+$.

*2-(Benzyloxy)-4-bromo-1-nitrobenzene (**73a**).*

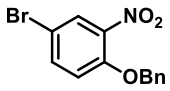

73a

To a solution of **72** (2000 mg, 9.22 mmol) in dry DMF (10 mL), potassium carbonate (1911 mg, 11.06 mmol) was added at 25 °C and the reaction mixture was stirred for 2 h. Then a solution of benzyl bromide (1892 mg, 11.06 mmol) in dry DMF (10 ml) was added and the reaction mixture was refluxed at 85 °C for 12 h. Water (20 mL) was added to dilute the reaction mixture, followed by the extraction with EtOAc (3 x 15 mL). The combined organic layers were washed with a saturated solution of NH_4Cl, $NaHCO_3$, and brine. The washed organic phase was dried over anhydrous sodium sulfate, filtered, and concentrated under reduced pressure. The product was obtained in quantitative yield as a yellow solid and it was used in the next step without any further purification. ^{1}H NMR (300 MHz, $CDCl_3$) δ: 7.95 (s, 1H), 7.56 (d, *J* = 8.8 Hz, 1H), 7.48-7.27 (m, 5H), 7.00 (d, *J* = 8.9 Hz, 1H), 5.19 (s, 2H); ESI-MS *m/z* 385.6 $[M+Br]^-$.

*1-(4-(Benzyloxy)-3-nitrophenyl)piperazine (**74**).*

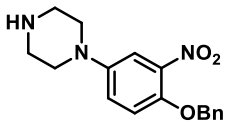

74

Palladium(II) acetate (14 mg, 0.06 mmol) was added to a suspension of (±) BINAP (61 mg, 0.09 mmol) in 1,4-dioxane (3 mL) in a sealed tube at 25 °C and the mixture was heated at 50 °C for 30 min. After that compound **73a** (49 mg, 0.61 mmol), piperazine (152 mg, 1.83 mmol) and cesium carbonate (323 mg, 0.92 mmol) were added, sequentially, and heated at 100 °C for 12 h in the sealed tube. Reaction mixture was filtered over a pad of celite. Solvent was removed completely under reduced pressure; the residue was dissolved in water, and extracted with EtOAc. The combined organic layers were dried over anhydrous sodium sulfate, filtered, and concentrated under reduced pressure. The residue

was purified by an alumina gel column chromatography (petroleum ether/EtOAc 5:1) to afford the title compound **74** in 71% yield as an orange solid. ^{1}H NMR (400 MHz, $CDCl_3$) δ: 7.43-7.24 (m, 6H), 7.05-6.99 (m, 2H), 5.14 (s, 2H), 3.07-2.98 (m, 8H), 1.66 (s, 1H); ESI-MS *m/z* 314.0 $[M+H]^+$.

*1-(4-(4-(Benzyloxy)-3-nitrophenyl)piperazin-1-yl)ethanone (**75**).*

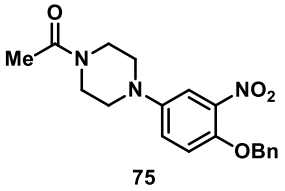

75

TEA (45 μL, 0.320 mmol) was added to a solution of **74** (100 mg, 0.32 mmol) in acetic anhydride (2 mL) at 25 °C and stirred for 12 h. The solvent was removed completely under reduced pressure. The residue was diluted with a saturated solution of $NaHCO_3$ and extracted with DCM. The combined organic layers were dried over anhydrous sodium sulfate, filtered, and concentrated under reduced pressure to obtain the title compound **75** in quantitative yield as orange oil. ^{1}H NMR (400 MHz, $CDCl_3$) δ: 7.39-7.34 (m, 6H), 7.09-6.95 (m, 2H), 5.14 (s, 2H), 3.79-3.67 (m, 2H), 3.65-3.52 (m, 2H), 3.14-2.97 (m, 4H), 2.11 (s, 3H); ESI-MS *m/z* 356.0 $[M+H]^+$, 377.9 $[M+Na]^+$.

*1-(4-(4-Hydroxy-3-nitrophenyl)piperazin-1-yl)ethanone (**76**).*

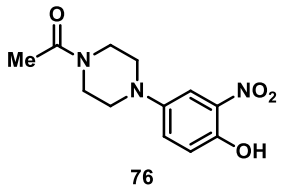

76

Thioanisole (2.3 ml, 19.99 mmol) was added dropwise to a solution of **75** (142 mg, 0.40 mmol) in TFA (3 mL) and toluene (3 mL) at 25 °C and the reaction mixture was refluxed at 70 °C for 12 h. The solvent was removed completely under reduced pressure and the residue was purified by silica gel column chromatography (petroleum ether/EtOAc 20:1) to afford the title compound **76** in 85% yield as a red solid. ^{1}H NMR (400 MHz, $CDCl_3$) δ: 10.27 (s, 1H), 7.48 (d, *J* = 2.9 Hz, 1H), 7.28 (dd, *J* = 9.2, 2.9 Hz, 1H), 7.07 (d, *J* = 9.2 Hz, 1H), 3.80-3.72 (m, 2H), 3.65-3.56 (m, 2H), 3.13-3.01 (m, 4H), 2.12 (s, 3H).

*1-(4-(3-Amino-4-hydroxyphenyl)piperazin-1-yl)ethanone (**77**)*

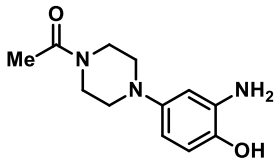

77

Iron powder (429 mg, 7.68 mmol) and calcium chloride (360 mg, 3.24 mmol) was added into a solution of **76** (320 mg, 1.206 mmol) in ethanol:water (3:1, 18 mL) at 25 °C. The reaction mixture was refluxed at 90 °C for 30 min. After that, the solvent was removed completely under reduced pressure. Residue was dissolved in a saturated solution of $NaHCO_3$ and was extracted with EtOAc (3 X 10 mL). The combined organic layers were filtered over a pad of celite, dried over anhydrous sodium sulfate, filtered and concentrated under reduced pressure. The residue was purified by silica gel column chromatography ($CHCl_3$/MeOH 20:1) to afford the title compound **77** in 50% yield as a red solid. ^{1}H NMR (400 MHz, DMSO) δ: 8.39 (s, 1H), 6.47 (d, *J* = 8.4 Hz, 1H), 6.24 (d, *J* = 2.6 Hz, 1H), 5.98 (dd, *J* = 8.4, 2.6 Hz, 1H), 4.39 (s, 2H), 3.55-3.43 (m, 4H), 2.90-2.72 (m, 4H), 1.98 (s, 3H); ESI-MS *m/z* 236.0 $[M+H]^+$, 258.0 $[M+Na]^+$.

*1-(4-(4-Hydroxy-3-(1H-pyrrol-1-yl)phenyl)piperazin-1-yl)ethanone (**54c**).*

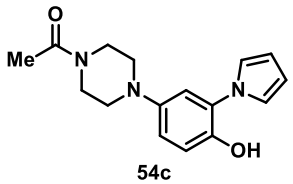

54c

The compound **54c** was synthesized from **77** following the same synthetic procedure as described for **54a** in 50% yield as a purple solid by an alumina gel column chromatography ($CHCl_3$/MeOH 50:1). ^{1}H NMR (400 MHz, $CDCl_3$) δ: 7.24 (s, 1H), 6.96 (t, *J* = 10.0 Hz, 1H), 6.88 (d, *J* = 17.4 Hz, 3H), 6.37 (s, 2H), 5.18 (s, 1H), 3.77 (s, 2H), 3.62 (s, 2H), 3.18-2.95 (m, 4H), 2.12 (s, 3H); ESI-MS *m/z* 286.0 $[M+H]^+$, 308.0 $[M+Na]^+$.

*Ethyl 2-(4-(4-acetylpiperazin-1-yl)-2-(1H-pyrrol-1-yl)phenoxy)-2-(naphthalen-1-yl)acetate (**56f**).*

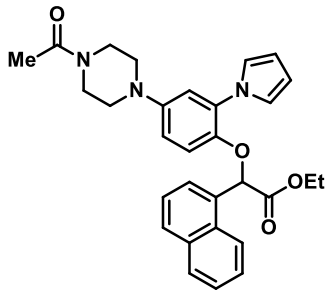

56f

Sodium hydride (18 mg, 0.77 mmol) was added to a solution of **54c** (200 mg, 0.70 mmol) in dry THF (5 ml) at 25 °C and stirred for 1 h. A solution of **58b** (226 mg, 0.77 mmol) in dry THF (5 ml) was added dropwise to the reaction mixture and stirred for another 12 h. The solvent was removed completely under reduced pressure. The residue was dissolved in DCM and washed with brine, dried over anhydrous sodium sulfate, filtered, and concentrated under reduced pressure. The residue was purified by a silica gel column chromatography ($CHCl_3$/MeOH 30:1) to afford the title compound **56f** in quantitative yield as yellow oil. ^{1}H NMR (400 MHz, $CDCl_3$) δ: 8.19 (d, *J* = 8.1 Hz, 1H), 7.85-7.77 (m, 2H), 7.57 (d, *J* = 7.0 Hz, 1H), 7.52-7.43 (m, 2H), 7.39 (t, *J* = 7.7 Hz, 1H), 7.09 (t, *J* = 2.0 Hz, 2H), 6.92 (t, *J* = 8.3 Hz, 1H), 6.87 (d, *J* = 2.7 Hz, 1H), 6.65 (dd, *J* = 8.9, 2.7 Hz, 1H), 6.29 (t, *J* = 2.0 Hz, 2H), 5.91 (s, 1H), 4.08 (qq, *J* = 10.8, 7.1 Hz, 2H), 3.76-3.67 (m, 2H), 3.58-3.50 (m, 2H), 3.03 (dd, *J* = 10.1, 5.3 Hz, 4H), 2.09 (s, 3H), 1.08 (t, *J* = 7.1 Hz, 3H).

*2-(4-(4-Acetylpiperazin-1-yl)-2-(1H-pyrrol-1-yl)phenoxy)-2-(naphthalen-1-yl)acetic acid (**53f**).*

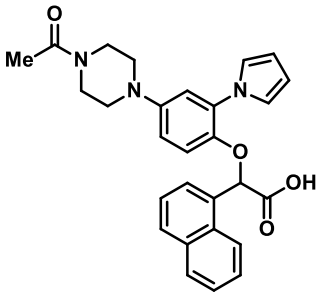

53f

The title compound **53f** was synthesized in quantitative yield as a yellow solid from **56f** by following the same procedure as **56a** Method A without performing any purification. ^{1}H NMR (400 MHz, Me_3OD) δ: 8.24-8.17 (m, 1H), 7.82 (dd, *J* = 15.1, 6.0 Hz, 2H), 7.52-7.41 (m, 3H), 7.36 (t, *J* = 7.6 Hz, 1H), 7.08-6.97 (m, 3H), 6.89 (d, *J* = 2.4 Hz, 1H), 6.74 (d, *J* =

9.0 Hz, 1H), 6.18 (s, 2H), 5.92 (s, 1H), 3.65 (dd, *J* = 15.6, 10.8 Hz, 4H), 3.11-2.98 (m, 4H), 2.09 (s, 3H).

*2-(4-Acetylpiperazin-1-yl)-6-(naphthalen-1-yl)benzo[b]pyrrolo[1,2-d][1,4]oxazepin-7(6H)-one (**52f**).*

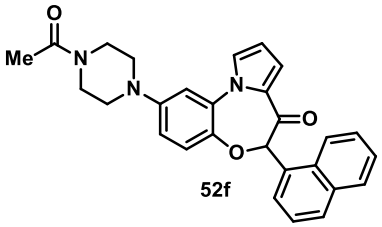

The title compound **52f** was synthesized from **53f** by following the same procedure as **52d** The residue was purified by silica gel column chromatography ($CHCl_3$/MeOH 80:1) in 20% yield as a yellow solid. ^{1}H NMR (400 MHz, $CDCl_3$) δ: 8.19 (d, *J* = 8.1 Hz, 1H), 7.83 (t, *J* = 9.5 Hz, 1H), 7.78 (d, *J* = 8.0 Hz, 1H), 7.52 (dt, *J* = 14.6, 6.9 Hz, 2H), 7.41 (s, 1H), 7.35-7.14 (m, 3H), 6.87 (s, 1H), 6.66 (s, 1H), 6.57-6.45 (m, 2H), 6.17 (s, 1H), 3.72 (s, 2H), 3.56 (s, 2H), 3.07 (s, 4H), 2.10 (s, 3H).

*2-(4-Acetylpiperazin-1-yl)-6-(naphthalen-1-yl)benzo[b]pyrrolo[1,2-d][1,4]oxazepin-7-yl acetate (**44**).*

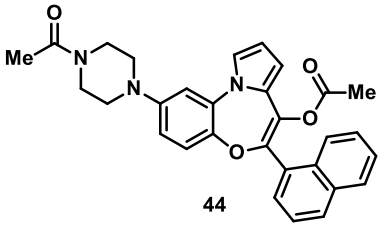

TEA (17 μL, 0.12 mmol), DMAP (4 mg, 0.03 mmol), and acetic anhydride (11 μL, 0.12 mmol) were added sequentially to a solution of **52f** (27 mg, 0.06 mmol) in dry DCM (2 mL) at 0 °C and stirred at 25 °C for 12 h. A solution of NH_4Cl (s.s) was added to the reaction mixture and was extracted with DCM (3 x 5 mL). The combined organic layers were dried over anhydrous sodium sulfate, filtered, and concentrated under reduced pressure. The residue was purified by a silica gel column chromatograpghy (100% $CHCl_3$) to afford the title compound in 30% yield as a yellow solid. ^{1}H NMR (400 MHz, $CDCl_3$) δ: 8.06 (d, *J* = 8.5 Hz, 1H), 7.87 (d, *J* = 7.7 Hz, 2H), 7.53-7.38 (m, 4H), 7.19 (s, 1H), 6.92 (s,

1H), 6.80 (d, *J* = 8.8 Hz, 1H), 6.66 (dd, *J* = 8.8, 2.4 Hz, 1H), 6.41 (s, 2H), 3.83-3.74 (m, 2H), 3.67-3.58 (m, 2H), 3.23-3.11 (m, 4H), 2.13 (s, 3H), 1.83 (s, 3H). ESI-MS *m/z* 494.4 $[M+H]^+$.

*2-(Benzyloxy)-5-bromoaniline (**78a**).*

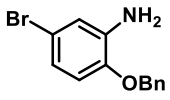

78a

The compound **78a** was synthesized from **73a** following the same synthetic procedure as described for **77** in 71% yield as a yellow solid by a silica gel column chromatography (petroleum ether/EtOAc 5:1). ^{1}H NMR (300 MHz, $CDCl_3$) δ: 7.98 (d, *J* = 2.5 Hz, 1H), 7.58 (dd, *J* = 8.9, 2.5 Hz, 1H), 7.46-7.29 (m, 5H), 7.00 (d, *J* = 9.0 Hz, 1H), 5.22 (s, 2H); ESI-MS *m/z* 278.0 $[M+H]^+$.

*1-(2-(Benzyloxy)-5-bromophenyl)-1H-pyrrole (**79a**).*

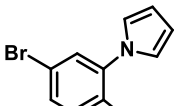

79a

A solution of **78a** (2750 mg, 9.89 mmol) was prepared in 1,4-dioxane (45 mL). 2,5-Dimethoxytetrahydrofuran (1 mL, 9.887 mmol) and HCl (6 N, 3 mL) were added to the solution at 25 °C and was refluxed at 100 °C for 10 min. The reaction mixture was quenched with a saturated solution of $NaHCO_3$ and the aqueous layer was extracted with EtOAc (3 x 20 mL). The combined organic layers were dried over anhydrous sodium sulfate, filtered, and concentrated under reduced pressure. The residue was purified by silica gel column chromatography (PE/EtOAc 10:1) to afford the compound **79a** in quantitative yield as an yellow solid. ^{1}H NMR (300 MHz, $CDCl_3$) δ: 7.45 (d, *J* = 2.4 Hz, 1H), 7.39-7.28 (m, 6H), 7.02 (t, *J* = 2.2 Hz, 2H), 6.93 (d, *J* = 8.8 Hz, 1H), 6.31 (t, *J* = 2.1 Hz, 2H), 5.06 (s, 2H); ESI-MS *m/z* 329.0 $[M+H]^+$.

*1-(4-(Benzyloxy)-3-(1H-pyrrol-1-yl)phenyl)-4-methylpiperazine (**80a**).*

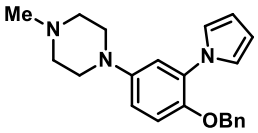

80a

The compound **80a** was synthesized from compound **79a** by following the same synthetic procedure as described for **74** in presence of *N*-methylpiperazine in 88% yield as an orange oil by an alumina column chromatography (PE/EtOAc 5:1). ^{1}H NMR (300 MHz, $CDCl_3$) δ: 7.39-7.26 (m, 5H), 7.11 (t, *J* = 2.2 Hz, 2H), 7.00 (s, 1H), 6.97 (d, *J* = 2.9 Hz, 1H), 6.81 (dd, *J* = 8.9, 3.0 Hz, 1H), 6.38 (t, *J* = 2.2 Hz, 2H), 4.95 (s, 2H), 3.24-3.12 (m, 4H), 2.67-2.54 (m, 4H), 2.39 (s, 3H); ESI-MS *m/z* 348.0 $[M+H]^+$.

*4-(4-Methylpiperazin-1-yl)-2-(1H-pyrrol-1-yl)phenol (**54d**).*

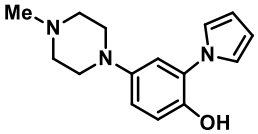

54d

To a solution of **80a** (500 mg, 1.44 mmol) in MeOH (41 mL), a catalytic amount of 10% Pd-C was added under nitrogen atmosphere, followed by a careful replacement by hydrogen atmosphere and the reaction mixture was stirred at 25 °C for 2 h. The solvent was removed completely and the residue was diluted with EtOAc. Palladium was filtered over a pad of celite. The desired product **54d** was obtained without any purification in quantitative yield as a red solid.

This compound was also obtained from intermediate **80b**. Compound **80b** (40mg, 0.13 mmol) dissolved in DCM (700 µL) then a solution of 6N HCl (50 µL) in MeOH (700 µL) was added. The reaction mixture was stirred at room temperature and controlled by TLC. Solvent was removed completely and the residue was diluted with a solution of $NaHCO_3$ (s.s) and the was extracted with DCM. The organic layer was dried with anhydrous sodium sulfate, filtered, and concentrated at room temperature. The product **54d** was obtained without any purification as a rose solid in 90% yield. ^{1}H NMR (300 MHz, MeOD) δ: 7.00 (td, *J* = 2.2, 0.7 Hz, 2H), 6.96-6.75 (m, 3H), 6.19 (td, *J* = 2.2, 0.7 Hz, 2H), 3.24-3.11 (m, 4H), 2.90 (t, *J* = 5.0 Hz, 4H), 2.59-2.52 (m, 3H); ESI-MS *m/z* 258.0 $[M+H]^+$.

*2-(4-(4-Methylpiperazin-1-yl)-2-(1H-pyrrol-1-yl)phenoxy)-2-(naphthalen-1-yl)acetic acid (**53g**).*

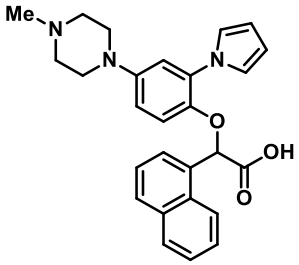

53g

The title compound **53g** was synthesized from **54d** and **55b** as described for **53a**, Method B. However, the pH of the aqueous solution was adjusted to 5-6 instead of 2. The residue was purified by silica gel column chromatography (DCM/MeOH/NH_4OH 10:1:0.1) to afford the acid **53g** in 39% yield as a yellow solid. ^{1}H NMR (300 MHz, DMSO) δ: 8.34 (d, *J* = 9.0 Hz, 1H), 7.93-7.88 (m, 1H), 7.86 (d, *J* = 8.2 Hz, 1H), 7.62 (d, *J* = 7.2 Hz, 1H), 7.51-7.46 (m, 2H), 7.42 (d, *J* = 8.0 Hz, 2H), 7.21 (d, *J* = 2.1 Hz, 2H), 6.82 (d, *J* = 2.8 Hz, 1H), 6.77 (d, *J* = 9.1 Hz, 1H), 6.28 (s, 1H), 6.14-6.08 (m, 2H), 3.05 (s, 4H), 2.54 (s, 4H), 2.26 (s, 3H); ESI-MS *m/z* 441.9 $[M+H]^+$, 439.8 $[M-H]^-$.

*2-(4-Methylpiperazin-1-yl)-6-(naphthalen-1-yl)benzo[b]pyrrolo[1,2-d][1,4]oxazepin-7(6H)-one (**52g**).*

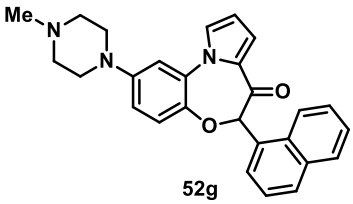

52g

Compound **52g** was synthesized from **53g** by following the same procedure as described for **52a**. The residue was purified by alumina column chromatography (PE/EtOAc 3:1) to afford the title compound in 42% yield as a yellow solid. ^{1}H NMR (300 MHz, $CDCl_3$) δ: 8.20 (d, *J* = 8.2 Hz, 1H), 8.06 (d, *J* = 13.9 Hz, 1H), 7.91-7.69 (m, 2H), 7.57-7.16 (m, 6H), 6.88 (d, *J* = 2.8 Hz, 1H), 6.53 (dtt, *J* = 6.5, 3.2, 1.9 Hz, 2H), 6.16 (s, 1H), 3.16 (q, *J* = 6.6, 5.0 Hz, 4H), 2.57 (t, *J* = 5.0 Hz, 4H), 2.35 (d, *J* = 1.2 Hz, 3H). ^{13}C NMR (75 MHz, $CDCl_3$) δ: 190.4, 149.2, 133.9, 133.8, 132.3, 131.6, 129.8, 129.7, 128.7, 128.2, 127.5, 126.6, 126.3, 126.2, 125.9, 124.9, 124.6, 124.0, 121.0, 114.9, 111.8, 109.5, 54.9, 49.2, 46.0; ESI-MS *m/z* 424.1 $[M+H]^+$.

*2-(4-Methylpiperazin-1-yl)-6-(naphthalen-1-yl)benzo[b]pyrrolo[1,2-d][1,4]oxazepin-7-yl acetate (**45**).*

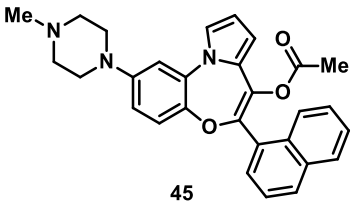

45

The compound **45** was synthesized from **52g** by following the same procedure as described for the synthesis of **29**. The residue was purified by alumina column chromatography (*n*-hexane/EtOAc/DCM/MeOH 20:2:0.1:0.2) to afford the title compound in 23% yield as a brown solid. ^{1}H NMR (300 MHz, $CDCl_3$) δ: 8.13-8.01 (m, 1H), 7.88 (d, *J* = 7.9 Hz, 2H), 7.56-7.35 (m, 4H), 7.22 (t, *J* = 2.3 Hz, 1H), 6.91 (d, *J* = 2.8 Hz, 1H), 6.79 (d, *J* = 8.9 Hz, 1H), 6.67 (dd, *J* = 8.9, 2.8 Hz, 1H), 6.45-6.35 (m, 2H), 3.22 (t, *J* = 5.1 Hz, 4H), 2.59 (t, *J* = 5.0 Hz, 4H), 2.36 (s, 3H), 1.84 (s, 3H); ^{13}C NMR (75 MHz, $CDCl_3$) δ: 168.9, 146.3, 133.8, 133.7, 133.6, 131.2, 130.8, 129.8, 129.7, 129.6, 128.2, 127.5, 127.0, 126.4 (2C), 126.1, 125.0, 123.2, 123.1, 121.4, 111.6, 110.9, 110.2, 54.0, 48.0, 29.7, 20.5. ESI-MS *m/z* 466.1 $[M+H]^+$. HRMS-ESI (*m/z*): $[M+H]^+$ calculated for $[C_{29}H_{28}N_3O_3]^+$ 466.2122, found 466.2121.

*2-(4-Methylpiperazin-1-yl)-6-(naphthalen-1-yl)benzo[b]pyrrolo[1,2-d][1,4]oxazepin-7-yl diethylcarbamate (**46**).*

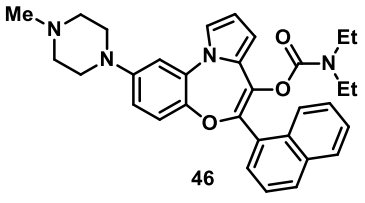

46

The title compound was synthesized from **52g** by following the same protocol as described for **34** in presence of diethylamine. The residue was purified by alumina column chromatography (petroleum ether/EtOAc 1:1) to afford **46** in 33% yield as a yellow oil. ^{1}H NMR (300 MHz, $CDCl_3$) δ: 8.17-8.05 (m, 1H), 7.91-7.80 (m, 2H), 7.60-7.35 (m, 4H), 7.20 (t, *J* = 2.3 Hz, 1H), 6.92 (d, *J* = 2.8 Hz, 1H), 6.81 (d, *J* = 8.9 Hz, 1H), 6.66 (dd, *J* = 8.9, 2.9 Hz, 1H), 6.42 (d, *J* = 2.4 Hz, 2H), 3.21 (t, *J* = 5.0 Hz, 4H), 3.08 (d, *J* = 7.2 Hz, 2H), 2.93 (d, *J* = 7.4 Hz, 2H), 2.60 (t, *J* = 5.0 Hz, 4H), 2.37 (s, 3H), 0.88 (t, *J* = 7.4 Hz, 3H), 0.64 (t, *J*

= 6.9 Hz, 3H); ^{13}C NMR (75 MHz, $CDCl_3$) δ: 153.4, 149.2, 146.2, 145.4, 134.3, 133.6, 133.5, 131.5, 131.4, 129.7, 129.2, 128.4, 128.0, 127.3, 126.7, 126.2, 125.9, 125.0, 122.6, 121.1, 114.5, 110.6, 109.6, 55.0, 49.4, 46.0, 42.0, 41.5, 14.1, 13.6, 13.1; ESI-MS *m/z* 523.2 [M+H]+. HRMS-ESI (*m/z*): [M+H]+ calculated for $[C_{32}H_{35}N_4O_3]^+$ 523.2692, found 523.2691.

*4-Bromo-1-(methoxymethoxy)-2-nitrobenzene (**73b**)*

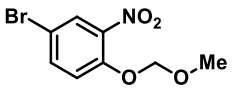

73b

To a stirred solution of 4-bromo-2-nitrophenol **72** (500 mg, 2.31 mmol) in dry DCM. *N*,*N*-diisopropylethylamine (589 µL, 3.46 mmol) and chloromethyl methyl ether (228 µL, 3.00 mmol) was added. The reaction mixture was stirred for 16 h at 45 °C. Water was added and extracted (3 x 10 mL) with DCM. The organic layer was dried over anhydrous Na_2SO_4, filtered, and concentrated. The residue was purified by flash chromatography on silica gel (PE/EtOAc 30:1) to afford the compound **43** as yellow solid in 71% yield. ^{1}H NMR (300 MHz, $CDCl_3$) δ: 7.93 (d, *J* = 2.4 Hz, 1H), 7.60 (dd, *J* = 9.0, 2.4 Hz, 1H), 7.22 (d, *J* = 9.0 Hz, 1H), 5.27 (s, 2H), 3.51 (s, 3H).

*5-Bromo-2-(methoxymethoxy)aniline (**78b**)*

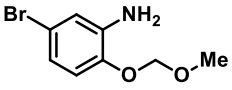

78b

Starting from **73b**, the compound **78b** was obtained following the procedure described for the preparation of compound **78a**. The residue was purified by flash chromatography on silica gel (PE/EtOAc 5:1) to afford the title compound as a yellow solid in 74% yield. ^{1}H NMR (300 MHz, $CDCl_3$) δ: 6.91-6.63 (m, 3H), 5.15 (d, *J* = 1.8 Hz, 2H), 3.79 (br, 2H), 3.47 (d, *J* = 1.9 Hz, 3H).

*1-(5-Bromo-2-(methoxymethoxy)phenyl)-1H-pyrrole (**79b**)*

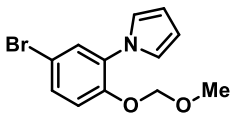

79b

The compound **79b** is synthesized from **78b** by following the same procedure as described for **54a**. The residue was purified by flash chromatography on silica gel chromatography (PE/EtOAc, 5:1) to afford the title compound as a yellow solid in 67% yield. ^{1}H NMR (300 MHz, $CDCl_3$) δ: 7.44 (d, *J* = 2.5 Hz, 1H), 7.34 (ddd, *J* = 8.8, 2.5, 0.5 Hz, 1H), 7.15 (d, *J* = 8.8 Hz, 1H), 6.99-6.94 (m, 2H), 6.33-6.28 (m, 2H), 5.11 (s, 2H), 3.40 (d, *J* = 0.5 Hz, 3H).

*1-(4-(Methoxymethoxy)-3-(1H-pyrrol-1-yl)phenyl)-N-methylpiperazine (**80b**)*

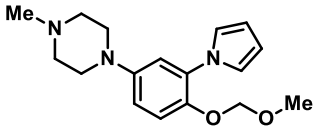

80b

Starting from **79b**, compound **80b** was obtained following the procedure described for the preparation of **74**. The residue was purified by flash chromatography on silica gel chromatography (DCM/MeOH 50:1) to afford the title compound as a yellow solid in 67% yield. ^{1}H NMR (300 MHz, $CDCl_3$) δ: 7.19-6.91 (m, 2H), 6.82-6.68 (m, 1H), 6.30 (t, *J* = 2.2 Hz, 2H), 4.98 (s, 2H), 3.35 (s, 3H), 3.18 (t, *J* = 5.0 Hz, 4H), 2.64 (t, *J* = 5.0 Hz, 4H), 2.38 (s, 3H).

*1-(4-(Benzyloxy)-3-nitrophenyl)-N-methylpiperazine (**81**)*

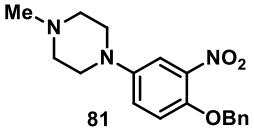

81

Starting from **73a**, compound **81** was obtained by following the procedure described for the preparation of **74**. The residue was purified by flash chromatography on silica gel chromatography (DCM/MeOH 50:1) to afford the title compound **81** as orange oil in 71% yield. ^{1}H NMR (300 MHz, $CDCl_3$) δ: 7.46-7.28 (m, 6H), 7.05-7.00 (m, 2H), 5.14 (s, 2H), 3.17-3.09 (m, 4H), 2.55 (t, *J* = 5.0 Hz, 4H), 2.34 (s, 3H).

*2-Amino-4-bromophenol (**82**)*

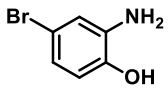

82

The compound **82** was synthesized from **72** by following the same protocol as described for the synthesis of **77** in 70% yield. ^{1}H NMR (300 MHz, $CDCl_3$) δ: 6.84 (s, 1H), 6.73 (d, *J* = 7.9 Hz, 1H), 6.57 (d, *J* = 8.1 Hz, 1H), 4.17 (s, 1H), 3.97-3.40 (m, 2H).

*4-Bromo-2-(1H-pyrrol-1-yl)phenol (**83**)*

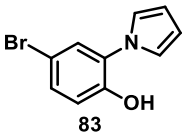

83

Compound **83** was synthesized in quantitative yield from **82** by following the same procedure as described for the synthesis of **54a**. ^{1}H NMR (300 MHz, $CDCl_3$) δ: 7.36 (dt, *J* = 8.5, 2.3 Hz, 2H), 6.96-6.87 (m, 1H), 6.83 (t, *J* = 2.1 Hz, 2H), 6.38 (t, *J* = 2.1 Hz, 2H).

*Ethyl 2-(4-bromo-2-(1H-pyrrol-1-yl)phenoxy)-2-(naphthalen-1-yl)acetate (**56g**)*

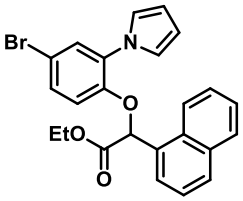

56g

Compound **56g** was synthesized from **83** and **58b** by following the same protocol as described for **56a**.The residue was purified on silica gel column chromatography (PE/EtOAc 20:1) in 60% yield. ^{1}H NMR (300 MHz, $CDCl_3$) δ: 7.59-7.48 (m, 4H), 7.50-7.36 (m, 5H), 7.36-7.26 (m, 2H), 7.13 (t, *J* = 7.7 Hz, 1H), 6.98 (d, *J* = 8.3 Hz, 1H), 6.18 (ddd, *J* = 13.4, 3.9, 1.4 Hz, 1H), 5.60 (s, 1H), 3.68 (dd, *J* = 4.0, 1.4 Hz, 2H), 1.57 (s, 3H).

*2-(4-Bromo-2-(1H-pyrrol-1-yl)phenoxy)-2-(quinolin-5-yl)acetic acid (**53i**)*

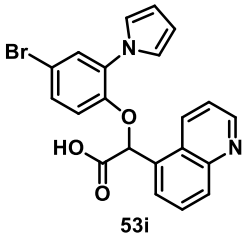

53i

Compound 53i was synthesized from **83** and **55a** by following the same procedure as described for the synthesis of **53a**, Method B. The residue was purified by a silica gel column chromatography (DCM/MeOH 20:1) in 60 % yield. ^{1}H NMR (300 MHz, $CDCl_3$) δ: 9.76 (s, 1H), 8.87 (d, *J* = 8.1 Hz, 2H), 8.73 (s, 1H), 7.92 (d, *J* = 7.5 Hz, 1H), 7.69 (s, 2H), 7.58-7.49 (m, 2H), 7.38 (s, 2H), 6.18 (s, 3H), 6.02 (s, 1H), 5.28 (s, 1H).

*2-Bromo-6-(quinolin-5-yl)benzo[b]pyrrolo[1,2-d][1,4]oxazepin-7(6H)-one (**52i**)*

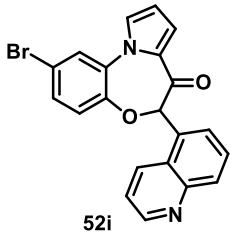

52i

Compound **52i** was synthesized from **53i** by following the same protocol as described for **52a**. The residue was purified by a silica gel column chromatography (PE/EtOAc 3:1) in 65% yield. ^{1}H NMR (300 MHz, $CDCl_3$) δ: 8.95 (dd, *J* = 4.1, 1.4 Hz, 1H), 8.49 (d, *J* = 8.5 Hz, 1H), 8.10 (d, *J* = 8.5 Hz, 1H), 7.61-7.38 (m, 4H), 7.39-7.21 (m, 2H), 7.10 (dd, *J* = 8.6, 2.0 Hz, 1H), 6.64 (d, *J* = 8.5 Hz, 1H), 6.56 (dt, *J* = 7.9, 3.9 Hz, 1H), 6.15 (s, 1H). 406.0 $[M+H]^+$.

*(2-chloroquinolin-3-yl)boronic acid (**85**)*

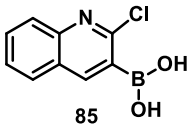

85

Diisopropylamine (430 µL, 3.058 mmol) was added to a solution of *n*-butyllithium (1.6 M in hexane, 1.9 mL, 3.058 mmol) in dry THF (8 mL) at -78 °C and stirred at the same temperature for 1 h. A solution of commercially available **84** (500 mg, 3.058 mmol) in dry THF (6 mL) was added to the reaction mixture while maintaining the temperature and stirred for another 2 h. Afterwards, a solution of trimethyl borate (340 µL, 3.058 mmol) in dry THF (4 mL) was added at -78 °C and stirred for another 2 h by maintaining the temperature. Water was added at -10 °C and the reaction mixture was allowed to reach the room temperature while stirring continously. The aqueous layer was extracted with Et_2O (2 x 10 mL). A solution of 6N HCl was added to the aqueous layer to adjust the pH = 4 and was extracted with Et_2O (1 x 10 mL). The combined organic layers was dried over

anhydrous Na_2SO_4, filtered, and concentrated under vacuum at 20 °C to obtain the product in 79% yield without any purification.^{1}H NMR (300 MHz, DMSO) δ: 8.60 (s, 2H), 8.42 (s, 1H), 8.01 (d, *J* = 8.4 Hz, 1H), 7.91 (d, *J* = 8.5 Hz, 1H), 7.78 (ddd, *J* = 8.4, 6.9, 1.5 Hz, 1H), 7.62 (ddd, *J* = 8.1, 6.9, 1.2 Hz, 1H).

*2-Chloroquinolin-3-ol (**86**)*

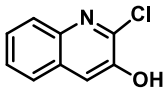

86

A solution of NH_4Cl (400 mg, 7.39 mmol) in water (6 mL) and 50% hydrogen peroxide (2.1 mL, 33.5 mmol) was added to the solution of **85** (828 mg, 3.99 mmol) in ethanol (6 mL) at room temperature and stirred for 16h. A white precipitate appeared. Solvent was removed completely and the crude was dissolved in diethyl ether. The organic layer was washed with water, dried over anhydrous sodium sulfate, filtered, and concentrated to afford the title compound in 90% yield. ^{1}H NMR (300 MHz, DMSO) δ: 11.09 (s, 1H), 7.88-7.76 (m, 2H), 7.66 (s, 1H), 7.61-7.44 (m, 2H).

*3-(Benzyloxy)-2-chloroquinoline (**87a**)*

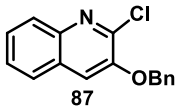

87

Compound **87a** was synthesized from **86** as described for the synthesis of **73a** in quantitative yield. ^{1}H NMR (300 MHz, $CDCl_3$) δ: 7.97 (t, *J* = 7.4 Hz, 1H), 7.64 (t, *J* = 10.9 Hz, 1H), 7.60-7.29 (m, 8H), 5.23 (d, *J* = 5.8 Hz, 2H).

*3-(Benzyloxy)-2-(1H-pyrrol-1-yl)quinoline (**80c**)*

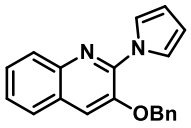

80c

Compound **80c** was synthesized from **87a** by following the same protocol as described for the synthesis of **74**. The residue was purified on an alumina gel column chromatography (PE/EtOAc, 5:1) in 58% yield.^{1}H NMR (300 MHz, $CDCl_3$) δ: 7.99 (d, *J* = 8.4 Hz, 1H),

7.91-7.83 (m, 2H), 7.70 (d, *J* = 8.0 Hz, 1H), 7.63-7.54 (m, 2H), 7.54-7.35 (m, 6H), 6.43-6.32 (m, 2H), 5.26 (s, 2H).

*2-(1H-Pyrrol-1-yl)quinolin-3-ol (**54e**)*

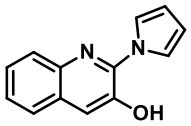

54e

Compound **54e** was synthesized from **80c** by following the same protocol as described for **76** in quantitative yield.

This compound was also synthesized from **80d**. BBr_3 (1.0 M solution in DCM, 13 µL, 0.134 mmol) was added slowly to a solution of **80d** (10 mg, 0.046 mmol) in dry DCM (1 mL) at 0 °C and the reaction mixture was stirred for 30 minutes by maintaining the temperature. After that the reaction mixture was stirred at room temperature for 12h. Reaction mixture was quenched with a saturated solution of $NaHCO_3$, extracted with DCM (3 x 10 mL). The combined organic layers was dried over anhydrous sodium sulfate, filtered, and concentrated. The residue was purified on silica gel column chromatography (PE/EtOAc, 5:1) to provide the compound **54e** as a yellow solid in 55% yield. ^{1}H NMR (300 MHz, $(CD_3)_2CO$) δ: 9.99 (s, 1H), 8.00-7.91 (m, 2H), 7.88 (d, *J* = 8.3 Hz, 1H), 7.82-7.70 (m, 2H), 7.55 (t, *J* = 7.6 Hz, 1H), 7.45 (t, *J* = 7.5 Hz, 1H), 6.33-6.22 (m, 2H).

*2-((2-(1H-Pyrrol-1-yl)quinolin-3-yl)oxy)-2-(naphthalen-1-yl)acetic acid (**53j**)*

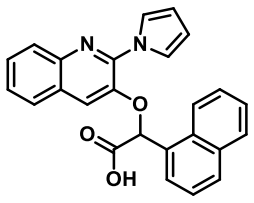

53j

Compound **53j** was synthesized from **54e** and **55b** by following the same procedure as **53a**, Method B in 56% yield after the purification on silica gel chromatography (DCM/MeOH 10:1). ^{1}H NMR (300 MHz, CD_3OD) δ: 8.51-8.39 (m, 1H), 7.96-7.67 (m, 8H), 7.60-7.35 (m, 5H), 6.53 (s, 1H), 6.25-6.14 (m, 2H).

*5-(Naphthalen-1-yl)quinolin[3,2-b]pyrrolo[1,2-d][1,4]oxazepin-4(5H)-one (**52j**)*

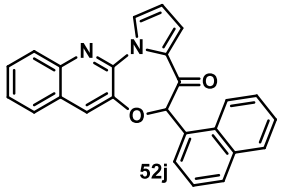

52j

Compound **52j** was synthesized from **53j** by following the same procedure as per the synthesis of **52b**. The residue was purified in alumina column chromatography (PE/EtOAc 5:1) in 75% yield. ^{1}H NMR (300 MHz, $CDCl_3$) δ: 8.39-8.26 (m, 2H), 7.94 (d, *J* = 8.5 Hz, 1H), 7.85 (d, *J* = 8.2 Hz, 1H), 7.79-7.52 (m, 5H), 7.49-7.32 (m, 3H), 7.20 (d, *J* = 4.7 Hz, 2H), 6.68-6.59 (m, 1H), 6.45 (s, 1H).

*5-(Naphthalen-1-yl)quinolin[3,2-b]pyrrolo[1,2-d][1,4]oxazepin-4-yl acetate (**47**)*

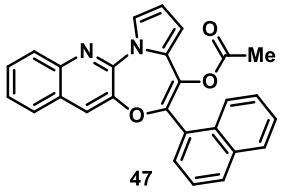

47

The compound **47** was synthesized from **52j** by following the same procedure as described for the synthesis of **29**. The residue was purified on silica gel column chromatography (*n*-hexane/EtOAc 20:1) to afford **47** in 72% yield. ^{1}H NMR (300 MHz, $CDCl_3$) δ: 8.21-7.81 (m, 5H), 7.64 (d, *J* = 8.1 Hz, 3H), 7.60-7.39 (m, 5H), 6.50 (s, 2H), 1.87 (s, 3H); ^{13}C NMR (75 MHz, $CDCl_3$) δ: 168.8, 145.1, 144.8, 144.3, 133.8, 131.2, 130.3, 129.9, 129.4, 128.4, 128.3, 128.1, 127.5, 127.3, 127.0, 126.6, 126.4, 126.3, 125.1, 123.2, 112.2, 111.2, 20.5.

5-(Naphthalen-1-yl)quinolin[3,2-b]pyrrolo[1,2-d][1,4]oxazepin-4-yl diethylcarbamate (48)

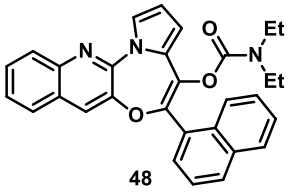

48

To a solution of **52j** (20 mg, 0.053 mmol) in dry THF (1 mL), sodium *bis*(trimethylsilyl)amide (1 M solution in THF, 133 mL, 0.13 mmol) was added at -78 °C and stirred for 30 min. A solution of phosgene (68 μL, 0.636 mmol) in 20% toluene was added at to the reaction mixture at -78 °C and stirred for another 10 min. After that,

diethylamine (77 µL, 0.742 mmol) and TEA (16 µL, 0.10 mmol) were added together into the reaction mixture at the same temperature and stirred for another 2 h. Water was added slowly to the reaction mixture at 0 °C and the solution was extracted rapidly with EtOAc (3 x 5 mL). The combined organic layers were dried over anhydrous sodium sulfate, filtered, and concentrated under reduced pressure at 20 °C and the residue was purified in (PE/EtOAc 7:1) to afford the compound **48** in 42% yield. ^{1}H NMR (300 MHz, $CDCl_3$) δ: 8.24-8.13 (m, 1H), 8.07-7.84 (m, 4H), 7.76-7.36 (m, 8H), 6.58-6.43 (m, 2H), 3.06 (t, *J* = 12.7 Hz, 2H), 2.96 (dd, *J* = 13.6, 6.6 Hz, 2H), 0.87 (t, *J* = 6.7 Hz, 3H), 0.69 (t, *J* = 6.9 Hz, 3H). ^{13}C NMR (75 MHz, $CDCl_3$) δ: 153.1, 145.4, 144.9, 144.3, 144.1, 134.4, 133.6, 131.4, 130.7, 129.6, 128.4 (2C), 128.1, 127.6, 127.4, 127.2, 126.4, 126.3, 126.1, 125.1, 122.9, 122.8, 112.1, 111.9, 111.3, 111.1, 42.1, 41.5, 13.7, 13.0.

*5-(Naphthalen-1-yl)quinolin[3,2-b]pyrrolo[1,2-d][1,4]oxazepin-4-yl-4-methylpiperazine-1-carboxylate (**49**)*

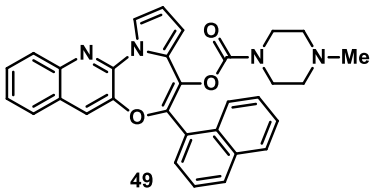

49

The compound **49** was synthesized from **52j** by following the same procedure as 48 in presence of N-methylpiperazine. The residue was purified on a silica gel column chromatography (DCM/ MeOH 60:1) to afford **49** in 65% yield. ^{1}H NMR (300 MHz, $CDCl_3$) δ: 8.13 (d, *J* = 7.9 Hz, 1H), 8.07-7.92 (m, 3H), 7.96-7.82 (m, 2H), 7.75-7.38 (m, 8H), 6.61-6.44 (m, 2H), 3.25 (d, *J* = 32.8 Hz, 4H), 2.14 (s, 5H), 1.75 (s, 2H). ^{13}C NMR (75 MHz, $CDCl_3$) δ: 152.5, 145.2, 144.9, 144.3, 143.7, 134.3, 133.7, 131.3, 130.7, 129.7, 129.4, 128.4, 128.3, 128.1, 127.8, 127.4, 127.3, 126.9, 126.9, 126.6, 126.4, 125.3, 123.2, 123.1, 112.4, 111.4, 67.9, 53.9, 45.5, 43.9.

*1-tert-Butyl 4-(5-(naphthalen-1-yl)quinolin[3,2-b]pyrrolo[1,2-d][1,4]oxazepin-4-yl) piperidine-1,4-dicarboxylate (**88**)*

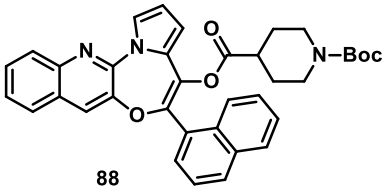

88

Compound **88** was synthesized from **52j** by following the same procedure as **36** in quantitative yield. ^{1}H NMR (300 MHz, $CDCl_3$) δ: 8.20-7.81 (m, 5H), 7.65 (d, *J* = 12.2 Hz, 3H), 7.48 (d, *J* = 9.2 Hz, 5H), 6.46 (d, *J* = 14.3 Hz, 2H), 3.65 (d, *J* = 11.1 Hz, 3H), 3.34 (s, 1H), 2.63 (s, 2H), 2.27 (s, 1H), 1.76 (d, *J* = 52.7 Hz, 2H), 1.40 (s, 9H).

*5-(Naphthalen-1-yl)quinolin[3,2-b]pyrrolo[1,2-d][1,4]oxazepin-4-yl piperidine-4-carboxylate (**50**)*

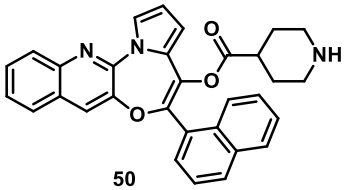

50

Compound **50** was synthesized from **52j** by following the same procedure as **37** in 79%. ^{1}H NMR (300 MHz, $CDCl_3$) δ: 8.11-7.81 (m, 5H), 7.75-7.58 (m, 3H), 7.59-7.36 (m, 5H), 6.47 (dd, *J* = 13.0, 9.7 Hz, 2H), 4.78 (s, 1H), 2.58 (s, 4H), 2.48-2.26 (m, 1H), 1.67 (s, 2H), 1.47 (d, *J* = 6.7 Hz, 2H). ^{13}C NMR (75 MHz, $CDCl_3$) δ: 171.0, 144.9, 144.8, 144.3, 143.9, 133.6, 133.4, 131.1, 130.2, 129.5, 128.4, 128.2, 127.6, 127.1, 126.8, 126.6, 125.9, 125.8, 125.2, 123.5, 123.4, 112.2, 112.1, 111.4, 111.2, 42.4, 37.8, 24.9.

*2-Chloro-3-methoxyquinoline (**87b**)*

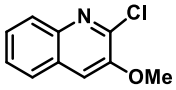

87b

The compound **87b** was synthesized from **86** by following the same procedure as described for **87a** in presence of methyl iodide without any purification as a light brown solid in quantitative yield. ^{1}H NMR (300 MHz, $CDCl_3$) δ: 7.94 (d, *J* = 8.1 Hz, 1H), 7.70 (dd, *J* = 7.9, 1.3 Hz, 1H), 7.52 (tdd, *J* = 14.7, 7.1, 1.4 Hz, 2H), 7.38 (s, 1H), 3.99 (s, 3H).

*3-Methoxy-2-(1H-pyrrol-1-yl)quinoline (**80d**)*

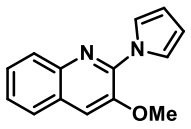

80d

The compound **80d** was synthesized from **87b** by following the same procedure as described for **80c**. The residue was purified by column chromatography on silica gel (PE/EtOAc, 5:1) to provide the title compound as a dark-yellow solid in 74% yield. ^{1}H NMR (300 MHz, $CDCl_3$) δ: 7.97 (d, *J* = 8.1 Hz, 1H), 7.82-7.76 (m, 2H), 7.72 (d, *J* = 8.0 Hz, 1H), 7.60-7.43 (m, 3H), 6.38 (t, *J* = 2.2 Hz, 2H), 4.02 (s, 3H). ESI-MS *m/z* 225.0 $[M+H]^+$.

*4-Nitro-2-(1H-pyrrol-1-yl)phenol (**90**)*

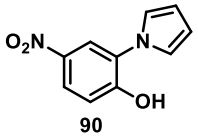

90

The compound **90** was synthesized from the commercially available **89** by following the same procedure as described for the synthesis of **54a** without any purification in quantitative yield. ^{1}H NMR (300 MHz, CD_3OD) δ: 8.14 (d, *J* = 2.8 Hz, 1H), 8.07 (dd, *J* = 9.0, 2.8 Hz, 1H), 7.14 – 7.06 (m, 3H), 6.30 – 6.23 (m, 2H). ESI-MS *m/z* 204.9 $[M+H]^+$.

*4-Amino-2-(1H-pyrrol-1-yl)phenol (**91**)*

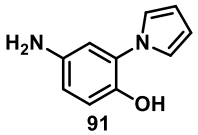

91

Compound **91** was synthesized from **90** by following the same procedure as described for **77** in 70% yield. ^{1}H NMR (300 MHz, CD_3OD) δ: 6.99 (t, *J* = 2.1 Hz, 2H), 6.76 (d, *J* = 8.5 Hz, 1H), 6.69 (d, *J* = 2.5 Hz, 1H), 6.57 (dd, *J* = 8.6, 2.4 Hz, 1H), 6.18 (t, *J* = 2.0 Hz, 2H). ESI-MS *m/z* 175.0 $[M+H]^+$.

*4-Methoxy-3-(1H-pyrrol-1-yl)aniline (**92**)*

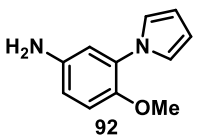

92

Compound **92** was synthesized from **91** in quantitative yield without any purification by following the same procedure as described for **87b**. ^{1}H NMR (300 MHz, $CDCl_3$) δ: 8.21-8.15 (m, 1H), 8.00 (s, 1H), 7.10-7.07 (m, 1H), 7.06-6.99 (m, 2H), 6.35 (t, J = 2.1 Hz, 2H), 3.95 (d, J = 15.4 Hz, 3H).

*5-(((4-Methoxy-3-(1H-pyrrol-1-yl)phenyl)amino)methylene)-2,2-dimethyl-1,3-dioxane-4,6-dione (**93**)*

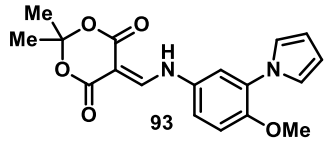

93

A solution of meldrum acid (90 mg, 0.631 mmol) in trimethoxymetahne (623 µL, 5.698 mmol) was refluxed at 105 °C for 1 h. A solution of **92** (100 mg, 0.571 mmol) in dry DMF (1 mL) was added to the reaction mixture and refluxed for another 1 h. Water was added to the cooled down reaction mixture and the precipitate was filtered off by washing with water and saturated solution of brine to obtain the product in 80% yield without any purification. ^{1}H NMR (300 MHz, CDCl3) δ: 8.48 (d, J = 14.3 Hz, 1H), 8.00 (s, 1H), 7.18-7.08 (m, 2H), 7.00 (d, J = 8.8 Hz, 1H), 6.96-6.88 (m, 2H), 6.24 (s, 2H), 4.60 (s, 1H), 3.82-3.75 (s, 3H), 1.72-1.61 (s, 6H).

*N-(4-(Benzyloxy)-3-(1H-pyrrol-1-yl)phenyl)cinnamamide (**94**)*

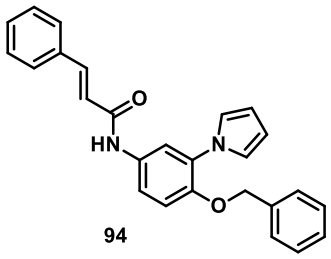

94

Intermediate **92** (100 mg, 0.378 mmol) and dry TEA (53 µL, 0.378 mmol) was added into a solution of cinnamoyl chloride (63 mg, 0.378 mmol) in dry DCM (2 mL) at room temperature and stirred for 2 h. A saturated solution of NH_4Cl was added dropwise to the reaction mixture and the aqueous layer was extracted with DCM (3 x 10mL). The combined organic layer was dried with anhydrous sodium sulfate, filtered, and concentrated under reduced pressure at 20 °C. The residue was purified on a silica gel column chromatography (PE/EtOAc 5:1) to obtain the product **94** in 80% yield. ^{1}H NMR (300 MHz, $CDCl_3$) δ: 8.58 (s, 1H), 7.74 (d, *J* = 15.5 Hz, 1H), 7.63 (s, 1H), 7.53 (t, *J* = 14.7

Hz, 1H), 7.40 (d, *J* = 6.7 Hz, 2H), 7.37-7.19 (m, 8H), 7.04 (s, 2H), 6.91 (d, *J* = 8.8 Hz, 1H), 6.67 (d, *J* = 15.6 Hz, 1H), 6.28 (s, 2H), 4.92 (s, 2H). ESI-MS *m/z* 395.0 $[M+H]^+$.

*5-Methoxy-2,4-dinitrobenzaldehyde (**96**)*

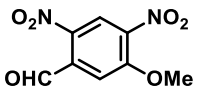

96

The commercially available **95** (500 mg, 3.7 mmol) was added to a solution of H_2SO_4 (0.8 mL) and HNO_3 (0.8 mL) at -10 °C and the reaction mixture was stirred for 1 h at the same temperature. A solid precipitate appeared. Water was added dropwise to the reaction mixture at the same temperature. Aqueous layer was extracted with EtOAc (5 x 3 mL) and the organic layer was washed with a saturated solution of brine, dried with anhydrous sodim sulfate, filtered, and concentrated. The residue was purified on a silica gel column chromatography (PE/EtOAC 5:1) to afford the title compound in 20% yield. ^{1}H NMR (300 MHz, CDCl3) δ: 10.55 (s, 1H), 8.71 (s, 1H), 7.57 (s, 1H), 4.17 (s, 3H).

*2,4-Diamino-5-methoxybenzaldehyde (**97**)*

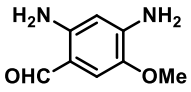

97

Compound **97** was synthesized from **96** in 48% yield by following the same procedure as the synthesis of **77** and a silica gel column chromatography (PE/EtOAc 5:1). ^{1}H NMR (300 MHz, $(CD_3)_2CO$) δ: 9.48 (s, 1H), 6.82 (s, 1H), 6.54 (s, 2H), 6.01 (s, 1H), 5.35 (s, 2H), 3.77 (s, 3H). ESI-MS *m/z* 167.1 $[M+H]^+$.

*(Z)-4-(((2,2-Dimethoxyethyl)imino)methyl)-2-nitrophenol (**99**)*

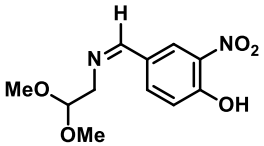

99

2,2-dimethoxyethylamine (94 mg, 0.897 mmol) was added into a suspension of **98** (100 mg, 0.598 mmol) in toluene (1 mL) at room temperature and then the reaction mixture was refluxed at 110 °C for 12 h. 5 mL of toluene was added to the cooled down reaction

mixture and the solvent was removed under reduced pressure. The crude was used for the next step without any further purification by considering a quantitative yielding step.[1]H NMR (300 MHz, $(CD_3)_2CO$) δ: 8.43 (d, *J* = 2.0 Hz, 1H), 8.34 (s, 1H), 8.08 (dd, *J* = 8.7, 2.0 Hz, 1H), 7.21 (t, *J* = 9.4 Hz, 1H), 4.54 (dd, *J* = 5.7, 5.0 Hz, 1H), 3.72 (d, *J* = 5.3 Hz, 2H), 3.34 (d, *J* = 0.9 Hz, 6H).

PART 1 ABBREVIATION

AIBN	Azobisisobutirronitrile
AMPK	*5*' Adenosine monophosphate-activated protein kinase
APC	Adenomatous polyposis coli
ATG	Autophagy related genes
BINAP	*2,2′-bis*(diphenylphosphino)-1,1′-binaphthyl
CCND1	Cyclin D1
CDI	*1,1*'-Carbonyldiimidazole
CDK1	Cyclin dependent kinase 1
CDKN2A	Cyclin dependent kinase inhibitor 2A
CLint	Intrinsic clearance
COX-2	Cyclooxygenase-2
CQ	Chloroquine
CRT	Chemoradiotherapy
CT	Chemotherapy
Cryo-EM	Cryogenic electron microscopy
CYP	Cytochrome P450
DCE	Dichloroethane
DCM	Dichloromethane
DIAD	Diisopropyl azodicarboxylate
DIPA	Diisopropylamine
DIPEA	*N*,*N*-Diisopropylethylamine
DMAP	4-Dimethylaminopyridine
DMF	*N*,*N*-Dimethylformamide
DNA	Deoxyribonucleic acid
DSC	Disuccinimidyl carbonate
EAC	Esophageal adenocarcinoma
EBSS	Earle's balanced salt solution
EGTA	Ethylene glycol tetraacetic acid
ESCC	Esophageal squamous cell carcinoma
ESI-MS	Electrospray ionization mass spectroscopy
GAB	Glycerol- ethylene glycol tetraacetic acid

GDP	Guanosine diphosphate
GFP-LC3	Green fluorescent protein-Light chain 3
GLOBOCAN	Global cancer incidence, mortality and prevalence
GTP	Guanosine triphosphate
HCQ	Hydroxychloroquine
HDR	high-dose-rate
HFIP	Hexafluoroisopropanol
HL	Human leukemia
HLM	Human liver microsome
HPLC	High pressure liquid chromatography
HPV	Human papilloma virus
HRESI-MS	High resolution electrospray ionization mass spectroscopy
HSV	Herpes simplex virus
Hz	Hertz
IaCh	Intra-arterial chemotherapy
ICT	Induction chemotherapy
LAMP	Lysosome-associated proteins
LDA	Lithium diisopropylamide
LC/MSD	Liquid chromatography/mass selective detector
MAPK	Mitogen-activated protein kinase
MDA	Microtubule destabilizing agents
MDM2	Mouse double minute 2 homolog
MDR	Multi-drug resistance
MHz	Megahertz
MOM	Methoxymethyl
MT	Microtubule
MTA	Microtubule targeting agents
mTORC	Mammalian/mechanistic target of rapamycin complex 1
MTT	3-(4,5-dimethylthiazol-2-yl)-2,5-diphenyltetrazolium bromide
RFP	red fluorescent protein
MSA	Microtubule stabilizing agents
NADPH-GS	Nicotinamide adenine dinucleotide phosphate generating system
NBS	*N*-Bromosuccinimide

NIS	*N*-Iodosuccinimide
NMR	Nuclear magnetic resonance
NRU	Neutral Red Uptake
OS	Overall survival
OSCC	Oral squamous cell carcinoma
PBOX	Pyrrolobenzoxazepines
PE	Phosphatidylethanolamine
PGP	Phosphoglycolate phosphatase
PI3K	Phosphoinositide 3-kinase
PNOX	Pyrrolonaphthooxazepines
PPOEL	Potentially premalignant oral epithelial lesions
RB	Retinoblastoma
RMSD	Root-mean-square deviation
RPMI	Roswell Park Memorial Institute
RT	Radiotherapy
SAR	Structure activity relationship
SEM	Scanning electron microscopy
TEA	Triethylamine
TFA	Trifluoroacetic acid
THF	Tetrahydrofuran
TLC	Thin layer chromatography
TMRM	Tetramethylrhodamine, methyl ester
UICC	Union for International Cancer Control
ULK1	Autophagy activating kinase 1 complex
UV-VIS	Ultra violet-visible
VPS34	Class III phosphoinositide 3-kinase

PART 1 REFERENCES

(1) Cheng, M. F.; Lin, S. R.; Tseng, F. J.; Huang, Y. C.; Tsai, M. J.; Fu, T. S.; Weng, C. F. The Autophagic Inhibition Oral Squamous Cell Carcinoma Cancer Growth of 16-Hydroxy-Cleroda-3,14-Dine-15,16-Olide. *Oncotarget* **2017**, *8* (45), 78379–78396.

(2) Joshi P, Dutta S, Chaturvedi P, N. S. Head and Neck Cancers in Developing Countries. *Rambam Maimonides Med. J.* **2014**, *5* (2), e0009. https://doi.org/10.5041/RMMJ.10143.

(3) Sinevici, N.; O'Sullivan, J. Oral Cancer: Deregulated Molecular Events and Their Use as Biomarkers. *Oral Oncol.* **2016**, *61*, 12–18. https://doi.org/10.1016/j.oraloncology.2016.07.013.

(4) Hema Shree, K.; Ramani, P.; Sherlin, H.; Sukumaran, G.; Jeyaraj, G.; Don, K. R.; Santhanam, A.; Ramasubramanian, A.; Sundar, R. Saliva as a Diagnostic Tool in Oral Squamous Cell Carcinoma – a Systematic Review with Meta Analysis. *Pathol. Oncol. Res.* **2019**, *25* (2), 447–453. https://doi.org/10.1007/s12253-019-00588-2.

(5) Soodan, K. S.; Priyadarshni, P.; Kumar, M.; Sharma, S. Systematic Review on Oral Cancer. *EC Dent. Sci.* **2018**, *3*, 116–119.

(6) Bray, F.; Ferlay, J.; Soerjomataram, I.; Siegel, R. L.; Torre, L. A.; Jemal, A. Global Cancer Statistics 2018: GLOBOCAN Estimates of Incidence and Mortality Worldwide for 36 Cancers in 185 Countries. *CA. Cancer J. Clin.* **2018**, *68* (6), 394–424. https://doi.org/10.3322/caac.21492.

(7) Robert, B. M.; Dakshinamoorthy, M.; Ganapathyagraharam Ramamoorthy, B.; Dhandapani, M.; Thangaiyan, R.; Muthusamy, G.; Nirmal, R. M.; Prasad, N. R. Predicting Tumor Sensitivity to Chemotherapeutic Drugs in Oral Squamous Cell Carcinoma Patients. *Sci. Rep.* **2018**, *8* (1), 1–10. https://doi.org/10.1038/s41598-018-33998-4.

(8) Malik, U. U.; Zarina, S.; Pennington, S. R. Oral Squamous Cell Carcinoma: Key Clinical Questions, Biomarker Discovery, and the Role of Proteomics. *Arch. Oral Biol.* **2016**, *63*, 53–65. https://doi.org/10.1016/j.archoralbio.2015.11.017.

(9) Feller, L.; Wood, N. H.; Khammissa, R. A. G. et al. Human Papillomavirus-Mediated Carcinogenesis and HPV-Associated Oral and Oropharyngeal Squamous Cell Carcinoma . Part 2 : Human Papillomavirus Associated Oral and Oropharyngeal Squamous Cell Carcinoma. *Head Face Med.* **2010**, *6:15* (1), 2–7.

(10) Noguti, J.; De Moura, C. F. G.; De Jesus, G. P. P.; Da Silva, V. H. P.; Hossaka, T. A.; Oshima, C. T. F.; Ribeiro, D. A. Metastasis from Oral Cancer: An Overview. *Cancer Genomics-Proteomics* **2012**, *9* (5), 329–335.

(11) Leemans, C. R.; Braakhuis, B. J. M.; Brakenhoff, R. H. The Molecular Biology of Head and Neck Cancer. *Nat. Rev. cancer* **2011**, *11* (1), 9.

(12) Rothenberg, S. M.; Ellisen, L. W. The Molecular Pathogenesis of Head and Neck Squamous Cell Carcinoma. *J. Clin. Invest.* **2012**, *122* (6), 1951–1957. https://doi.org/10.1172/JCI59889.

(13) Awan, K. H.; Patil, S. Association of Smokeless Tobacco with Oral Cancer–Evidence from the South Asian Studies: A Systematic Review. *J Coll Physicians Surg Pak* **2016**, *26* (9), 775–780.

(14) Sinha, D. N.; Abdulkader, R. S.; Gupta, P. C. Smokeless Tobacco- associated Cancers: A Systematic Review and Meta- analysis of Indian Studies. *Int. J. cancer* **2016**, *138* (6), 1368–1379.

(15) Warnakulasuriya, S.; Dietrich, T.; Bornstein, M. M.; Peidró, E. C.; Preshaw, P. M.; Walter, C.; Wennström, J. L.; Bergström, J. Oral Health Risks of Tobacco Use and Effects of Cessation. *Int. Dent. J.* **2010**, *60* (1), 7–30.

(16) Bosetti, C.; Gallus, S.; Peto, R.; Negri, E.; Talamini, R.; Tavani, A.; Franceschi, S.; La Vecchia, C. Tobacco Smoking, Smoking Cessation, and Cumulative Risk of Upper Aerodigestive Tract Cancers. *Am. J. Epidemiol.* **2008**, *167* (4), 468–473. https://doi.org/10.1093/aje/kwm318.

(17) Rosenquist, K. Risk Factors in Oral and Oropharyngeal Squamous Cell Carcinoma: A Population-Based Case-Control Study in Southern Sweden. *Swed. Dent. J. Suppl.* **2005**, No. 179, 1–66.

(18) Samatha, Y.; Sai Sankar, A. J.; Ganapathy, K. S.; Srinivas, K.; Ankineedu, D.; Subhashini Choudary, A. L. Clinicopathologic Evaluation of Lesions Associated with Tobacco Usage. *J. Contemp. Dent. Pract.* **2015**, *15* (4), 466–472. https://doi.org/10.5005/jp-journals-10024-1564.

(19) Al-Attas, S. A.; Ibrahim, S. S.; Amer, H. A.; Darwish, Z. E. S.; Hassan, M. H. Prevalence of Potentially Malignant Oral Mucosal Lesions among Tobacco Users in Jeddah, Saudi Arabia. *Asian Pacific J. Cancer Prev.* **2014**, *15* (2), 757–762. https://doi.org/10.7314/apjcp.2014.15.2.757.

(20) Chandra, P.; Govindraju, P. Prevalence of Oral Mucosal Lesions among Tobacco Users. *Oral Health Prev. Dent.* **2012**, *10* (2), 149–153.

(21) Vargas-Ferreira, F.; Nedel, F.; Etges, A.; Gomes, A.; Furuse, C.; Tarquinio, S. Etiologic Factors Associated with Oral Squamous Cell Carcinoma in Non-Smokers and Non-Alcoholic Drinkers: A Brief Approach. *Braz Dent J* **2012**, *23* (5), 586–590.

(22) Warnakulasuriya, K.; Ralhan, R. Clinical, Pathological, Cellular and Molecular Lesions Caused by Oral Smokeless Tobacco–a Review. *J. oral Pathol. Med.* **2007**, *36* (2), 63–77.

(23) Lubin, J. H.; Purdue, M.; Kelsey, K.; Zhang, Z.-F.; Winn, D.; Wei, Q.; Talamini, R.; Szeszenia-Dabrowska, N.; Sturgis, E. M.; Smith, E. Total Exposure and Exposure Rate Effects for Alcohol and Smoking and Risk of Head and Neck Cancer: A Pooled Analysis of Case-Control Studies. *Am. J. Epidemiol.* **2009**, *170* (8), 937–947.

(24) Johnson, N. Tobacco Use and Oral Cancer : A Global Perspective. *J. Dent. Educ.* **1991**, *65* (4), 328–339.

(25) Campisi, G.; Panzarella, V.; Giuliani, M.; Lajolo, C.; Di Fede, O.; Falaschini, S.; Di Liberto, C.; Scully, C.; Lo Muzio, L. Human Papillomavirus: Its Identikit and Controversial Role in Oral Oncogenesis, Premalignant and Malignant Lesions. *Int. J. Oncol.* **2007**, *30* (4), 813–823.

(26) Termine, N.; Panzarella, V.; Falaschini, S.; Russo, A.; Matranga, D.; Lo Muzio, L.; Campisi, G. HPV in Oral Squamous Cell Carcinoma vs Head and Neck Squamous Cell Carcinoma Biopsies: A Meta-Analysis (1988–2007). *Ann. Oncol.* **2008**, *19* (10), 1681–1690.

(27) Siebers, T. J. H.; Merkx, M. A. W.; Slootweg, P. J.; Melchers, W. J. G.; van Cleef, P.; Wilde, P. C. M. No High-Risk HPV Detected in SCC of the Oral Tongue in the Absolute Absence of Tobacco and Alcohol - A Case Study of Seven Patients. *Oral Maxillofac. Surg.* **2008**, *12* (4), 185–188.

(28) Ali, J.; Sabiha, B.; Jan, H. U.; Haider, S. A.; Khan, A. A.; Ali, S. S. Genetic Etiology of Oral Cancer. *Oral Oncol.* **2017**, *70*, 23–28. https://doi.org/10.1016/j.oraloncology.2017.05.004.

(29) Gupta, B.; Bray, F.; Kumar, N.; Johnson, N. W. Associations between Oral Hygiene Habits, Diet, Tobacco and Alcohol and Risk of Oral Cancer: A Case–Control Study from India. *Cancer Epidemiol.* **2017**, *51*, 7–14. https://doi.org/10.1016/j.canep.2017.09.003.

(30) Porter, S.; Gueiros, L. A.; Leão, J. C.; Fedele, S. Risk Factors and Etiopathogenesis of Potentially Premalignant Oral Epithelial Lesions. *Oral Surg. Oral Med. Oral Pathol. Oral Radiol.* **2018**, *125* (6), 603–611.

https://doi.org/10.1016/j.oooo.2018.03.008.

(31) Gharat, S. A.; Momin, M.; Bhavsar, C. Oral Squamous Cell Carcinoma: Current Treatment Strategies and Nanotechnology-Based Approaches for Prevention and Therapy. *Crit. Rev. Ther. Drug Carr. Syst.* **2016**, *33* (4), 363–400. https://doi.org/10.1615/CritRevTherDrugCarrierSyst.2016016272.

(32) Huang, S.-H.; O'Sullivan, B. Oral Cancer: Current Role of Radiotherapy and Chemotherapy. *Med. Oral Patol. Oral Cir. Bucal* **2013**, *18* (2), e233-40. https://doi.org/10.4317/medoral.18772.

(33) Pendleton, K. P.; Grandis, J. R. Cisplatin-Based Chemotherapy Options for Recurrent and/or Metastatic Squamous Cell Cancer of the Head and Neck. *Clin. Med. Insights Ther.* **2013**, *5*, 103–116. https://doi.org/10.4137/CMT.S10409.

(34) Freeman, K.; Connock, M.; Cummins, E.; Gurung, T.; Taylor-Phillips, S.; Court, R.; Saunders, M.; Clarke, A.; Sutcliffe, P. Fluorouracil Plasma Monitoring: Systematic Review and Economic Evaluation of the My5-FU Assay for Guiding Dose Adjustment in Patients Receiving Fluorouracil Chemotherapy by Continuous Infusion. *Health Technol. Assess.* **2015**, *19* (91), 1–321.

(35) Chakraborty, S.; Geetha, M.; Sujith, K. M.; Biji, M. S.; Sateeshan, B. Palliative Low Dose Fortnightly Methotrexate in Oral Cancers: Experience at a Rural Cancer Centre from India. *South Asian J. cancer* **2014**, *3* (3), 166–170.

(36) Ledwitch, K.; Ogburn, R.; Cox, J.; Graham, R.; Fritzsche, A.; Gosnell, D.; Manning, T. Taxol: Efficacy against Oral Squamous Cell Carcinoma. *Mini Rev. Med. Chem.* **2013**, *13* (4), 509–521.

(37) Caponigro, F.; Longo, F.; Perri, F.; Ionna, F. Docetaxel in the Management of Head and Neck Cancer. *Anticancer. Drugs* **2009**, *20* (8), 639–645.

(38) Lasrado, S.; Moras, K.; Pinto, G. J.; Bhat, M.; Hegde, S.; Sathian, B.; Luis, N. A. Role of Concomitant Chemoradiation in Locally Advanced Head and Neck Cancers. *Asian Pac J Cancer Prev* **2014**, *15* (10), 4147–4152.

(39) Eder-Czembirek, C.; Rechinger, S.; Kornek, G.; Selzer, E.; Seemann, R. Experience in Intra-Arterial Chemotherapy Using Two Protocols for the Treatment of OSCC over Two Decades at the University Hospital Vienna. *Clinics* **2018**, *73*, e433.

(40) Furusaka, T.; Asakawa, T.; Tanaka, A.; Matsuda, H.; Ikeda, M. Efficacy of Multidrug Superselective Intra-Arterial Chemotherapy (Docetaxel, Cisplatin, and 5-Fluorouracil) Using the Seldinger Technique for Tongue Cancer. *Acta Otolaryngol.* **2012**, *132* (10), 1108–1114.

(41) Miyake, M.; Ohbayashi, Y.; Iwasaki, A.; Sawai, F.; Toyama, Y.; Nishiyama, Y. Superselective Intra-Arterial Infusion Chemotherapy with Nedaplatin for Oral Cancer: A Pharmacological Study of the Dose Clearance. *J. Maxillofac. Oral Surg.* **2015**, *14* (3), 616–623. https://doi.org/10.1007/s12663-014-0730-9.

(42) Busch, C. J.; Tribius, S.; Schafhausen, P.; Knecht, R. The Current Role of Systemic Chemotherapy in the Primary Treatment of Head and Neck Cancer. *Cancer Treat. Rev.* **2015**, *41* (3), 217–221.

(43) Lau, A.; Li, K. Y.; Yang, W. F.; Su, Y. X. Induction Chemotherapy for Squamous Cell Carcinomas of the Oral Cavity: A Cumulative Meta-Analysis. *Oral Oncol.* **2016**, *61*, 104–114. https://doi.org/10.1016/j.oraloncology.2016.08.022.

(44) Ozaki, H.; Ishikawa, S.; Kitabatake, K.; Yusa, K.; Sakurai, H.; Iino, M. Functional and Aesthetic Rehabilitation with Maxillary Prosthesis Supported by Two Zygomatic Implants for Maxillary Defect Resulting from Cancer Ablative Surgery: A Case Report/Technique Article. *Odontology* **2016**, *104* (2), 233–238.

(45) Jacobson, A. S.; Alpert, E.; Persky, M.; Okay, D.; Buchbinder, D.; Lazarus, C. Transoral Mandibulectomy and Double Barrel Fibular Flap Reconstruction. *Laryngoscope* **2015**, *125* (9), 2119–2122.

(46) Lin, D. T.; Yarlagadda, B. B.; Sethi, R. K. V; Feng, A. L.; Shnayder, Y.; Ledgerwood, L. G.; Diaz, J. A.; Sinha, P.; Hanasono, M. M.; Yu, P. Long-Term Functional Outcomes of Total Glossectomy with or without Total Laryngectomy. *JAMA Otolaryngol. Neck Surg.* **2015**, *141* (9), 797–803.

(47) Ridha, H.; Garioch, J. J.; Tan, E. K.; Heaton, M. J.; Igali, L.; Moncrieff, M. D. Intraoperative Use of Mohs' Surgery for the Resection of Major Cutaneous Head and Neck Cancer under General Anaesthetic: Initial Experiences, Efficiency and Outcomes. *J. Plast. Reconstr. Aesthetic Surg.* **2015**, *68* (12), 1706–1712.

(48) Wang, X. J.; Yu, J.; Wong, S. H.; Cheng, A. S.; Chan, F. K.; Ng, S. S.; Cho, C. H.; Sung, J. J.; Wu, W. Kk. autophagy/Introduction/1-s2. .-S. pd. A Novel Crosstalk between Two Major Protein Degradation Systems. *Autophagy* **2013**, *9* (10), 1500–1508. https://doi.org/10.4161/auto.25573.

(49) Ding, W. X.; Yin, X. M. Mitophagy: Mechanisms, Pathophysiological Roles, and Analysis. *Biol. Chem.* **2012**, *393* (7), 547–564. https://doi.org/10.1515/hsz-2012-0119.

(50) Kaushik, S.; Cuervo, A. M. Chaperone-Mediated Autophagy: A Unique Way to Enter the Lysosome World. *Trends Cell Biol.* **2012**, *22* (8), 407–417.

https://doi.org/10.1016/j.tcb.2012.05.006.

(51) Effect of Cinacalcet on Cardiovascular Disease in Patients Undergoing Dialysis. *N. Engl. J. Med.* **2012**, *367* (26), 2482–2494. https://doi.org/10.1056/nejmoa1205624.

(52) Wong, P. M.; Feng, Y.; Wang, J.; Shi, R.; Jiang, X. Regulation of Autophagy by Coordinated Action of MTORC1 and Protein Phosphatase 2A. *Nat. Commun.* **2015**, *6*, 8048–8059. https://doi.org/10.1038/ncomms9048.

(53) Egan, D. F.; Shackelford, D. B.; Mihaylova, M. M.; Gelino, S.; Kohnz, R. A.; Mair, W.; Vasquez, D. S.; Joshi, A.; Gwinn, D. M.; Taylor, R.; et al. Phosphorylation of ULK1 (HATG1) by AMP-Activated Protein Kinase Connects Energy Sensing to Mitophagy. *Science (80-.).* **2011**, *331*, 456–461. https://doi.org/10.1126/science.1196371.

(54) Pattingre, S.; Tassa, A.; Qu, X.; Garuti, R.; Xiao, H. L.; Mizushima, N.; Packer, M.; Schneider, M. D.; Levine, B. Bcl-2 Antiapoptotic Proteins Inhibit Beclin 1-Dependent Autophagy. *Cell* **2005**, *122* (6), 927–939. https://doi.org/10.1016/j.cell.2005.07.002.

(55) Tai, W. T.; Shiau, C. W.; Chen, H. L.; Liu, C. Y.; Lin, C. S.; Cheng, A. L.; Chen, P. J.; Chen, K. F. Mcl-1-Dependent Activation of Beclin 1 Mediates Autophagic Cell Death Induced by Sorafenib and SC-59 in Hepatocellular Carcinoma Cells. *Cell Death Dis.* **2013**, *4* (2), e485. https://doi.org/10.1038/cddis.2013.18.

(56) Takahashi, Y.; Coppola, D.; Matsushita, N.; Cualing, H. D.; Sato, Y.; Liang, C.; Jung, J. U.; Cheng, J. Q.; Mulé, J. J.; Jack, W.; et al. Bif-1 Interacts with Beclin 1 through UVRAG and Regulates Autophagy and Tumorigenesis. *Nat. Cell Biol.* **2007**, *9* (10), 1142–1151.

(57) Strappazzon, F.; Vietri-Rudan, M.; Campello, S.; Nazio, F.; Florenzano, F.; Fimia, G. M.; Piacentini, M.; Levine, B.; Cecconi, F. Mitochondrial BCL-2 Inhibits AMBRA1-Induced Autophagy. *EMBO J.* **2011**, *30* (7), 1195–1208. https://doi.org/10.1038/emboj.2011.49.

(58) Molejon, M. I.; Ropolo, A.; Re, A. L.; Boggio, V.; Vaccaro, M. I. The VMP1-Beclin 1 Interaction Regulates Autophagy Induction. *Sci. Rep.* **2013**, *3*, srep01055. https://doi.org/10.1038/srep01055.

(59) Walczak, M.; Martens, S. Dissecting the Role of the Atg12-Atg5-Atg16 Complex during Autophagosome Formation. *Autophagy* **2013**, *9* (3), 424–425. https://doi.org/10.4161/auto.22931.

(60) Pankiv, S.; Clausen, T. H.; Lamark, T.; Brech, A.; Bruun, J. A.; Outzen, H.;

Øvervatn, A.; Bjørkøy, G.; Johansen, T. P62/SQSTM1 Binds Directly to Atg8/LC3 to Facilitate Degradation of Ubiquitinated Protein Aggregates by Autophagy. *J. Biol. Chem.* **2007**, *282* (33), 24131–24145. https://doi.org/10.1074/jbc.M702824200.

(61) Huynh, K. K.; Eskelinen, E. L.; Scott, C. C.; Malevanets, A.; Saftig, P.; Grinstein, S. LAMP Proteins Are Required for Fusion of Lysosomes with Phagosomes. *EMBO J.* **2007**, *26* (2), 313–324. https://doi.org/10.1038/sj.emboj.7601511.

(62) Folkerts, H.; Hilgendorf, S.; Vellenga, E.; Bremer, E.; Wiersma, V. R. The Multifaceted Role of Autophagy in Cancer and the Microenvironment. *Med. Res. Rev.* **2019**, *39* (2), 517–560. https://doi.org/10.1002/med.21531.

(63) Macintosh, R. L.; Ryan, K. M. Autophagy in Tumour Cell Death. *Semin. Cancer Biol.* **2013**, *23* (5), 344–351. https://doi.org/10.1016/j.semcancer.2013.05.006.

(64) Yun, C. W.; Lee, S. H. The Roles of Autophagy in Cancer. *Int. J. Mol. Sci.* **2018**, *19* (11), 1–18. https://doi.org/10.3390/ijms19113466.

(65) He, S.; Li, Q.; Jiang, X.; Lu, X.; Feng, F.; Qu, W.; Chen, Y.; Sun, H. Design of Small Molecule Autophagy Modulators: A Promising Druggable Strategy. *J. Med. Chem.* **2018**, *61* (11), 4656–4687. https://doi.org/10.1021/acs.jmedchem.7b01019.

(66) Galluzzi, L.; Baehrecke, E. H.; Ballabio, A.; Boya, P.; Bravo-San Pedro, J. M.; Cecconi, F.; Choi, A. M.; Chu, C. T.; Codogno, P.; Colombo, M. I.; et al. Molecular Definitions of Autophagy and Related Processes. *EMBO J.* **2017**, *36* (13), 1811–1836. https://doi.org/10.15252/embj.201796697.

(67) Liang, X. H.; Jackson, S.; Seaman, M.; Brown, K.; Kempkes, B.; Hibshoosh, H.; Levine, B. Induction of Autophagy and Inhibition of Tumorigenesis by Beclin 1 . *Nature* **1999**, *402* (6762), 672–676. https://doi.org/10.1038/45257.

(68) Guo, J. Y.; Chen, H.-Y.; Mathew, R.; Fan, J.; Strohecker, A. M.; Karsli-Uzunbas, G.; Kamphorst, J. J.; Chen, G.; Lemons, J. M. S.; Karantza, V.; et al. Activated Ras Requires Autophagy to Maintain Oxidative Metabolism and Tumorigenesis. *Genes Dev.* **2011**, *25* (5), 460–470. https://doi.org/10.1101/gad.2016311.

(69) Kubisch, J.; Türei, D.; Földvári-Nagy, L.; Dunai, Z. A.; Zsákai, L.; Varga, M.; Vellai, T.; Csermely, P.; Korcsmáros, T. Complex Regulation of Autophagy in Cancer – Integrated Approaches to Discover the Networks That Hold a Double-Edged Sword. *Semin. Cancer Biol.* **2013**, *23* (4), 252–261. https://doi.org/https://doi.org/10.1016/j.semcancer.2013.06.009.

(70) Meijer, A. J.; Codogno, P. Autophagy: Regulation and Role in Disease. *Crit. Rev.*

Clin. Lab. Sci. **2009**, *46* (4), 210–240. https://doi.org/10.1080/10408360903044068.

(71) Lorin, S.; Hamaï, A.; Mehrpour, M.; Codogno, P. Autophagy Regulation and Its Role in Cancer. *Semin. Cancer Biol.* **2013**, *23* (5), 361–379. https://doi.org/https://doi.org/10.1016/j.semcancer.2013.06.007.

(72) Yoshii, S. R.; Mizushima, N. Monitoring and Measuring Autophagy. *Int. J. Mol. Sci.* **2017**, *18*, 1865–1876. https://doi.org/10.3390/ijms18091865.

(73) Klionsky, D. J.; Abdelmohsen, K.; Abe, A.; Abedin, M. J.; Abeliovich, H.; Acevedo Arozena, A.; Adachi, H.; Adams, C. M.; Adams, P. D.; Adeli, K.; et al. Guidelines for the Use and Interpretation of Assays for Monitoring Autophagy (3rd Edition). *Autophagy* **2016**, *12* (1), 1–222. https://doi.org/10.1080/15548627.2015.1100356.

(74) Solitro, A. R.; Mackeigan, J. P. Leaving the Lysosome behind: Novel Developments in Autophagy Inhibition. *Future Med. Chem.* **2016**, *8* (1), 73–86. https://doi.org/10.4155/fmc.15.166.

(75) Sakagami, H.; Shimada, C.; Kanda, Y.; Amano, O.; Sugimoto, M.; Ota, S.; Soga, T.; Tomita, M.; Sato, A.; Tanuma, S. ichi; et al. Effects of 3-Styrylchromones on Metabolic Profiles and Cell Death in Oral Squamous Cell Carcinoma Cells. *Toxicol. Reports* **2015**, *2*, 1281–1290. https://doi.org/10.1016/j.toxrep.2015.09.009.

(76) Jordan, M. A.; Wilson, L. Microtubules as a Target for Anticancer Drugs. *Nat. Rev. Cancer* **2004**, *4* (4), 253–265. https://doi.org/10.1038/nrc1317.

(77) Sept, D. Microtubule Polymerization: One Step at a Time. *Curr. Biol.* **2007**, *17* (17), R764–R766. https://doi.org/https://doi.org/10.1016/j.cub.2007.07.002.

(78) Horio, T.; Murata, T. The Role of Dynamic Instability in Microtubule Organization . *Frontiers in Plant Science* . 2014, p 511.

(79) Alushin, G. M.; Lander, G. C.; Kellogg, E. H.; Zhang, R.; Baker, D.; Nogales, E. High-Resolution Microtubule Structures Reveal the Structural Transitions in Alphabeta-Tubulin upon GTP Hydrolysis. *Cell* **2014**, *157* (5), 1117–1129. https://doi.org/10.1016/j.cell.2014.03.053.

(80) Vale, R. D.; Coppin, C. M.; Malik, F.; Kull, F. J.; Milligan, R. A. Tubulin GTP Hydrolysis Influences the Structure, Mechanical Properties, and Kinesin-Driven Transport of Microtubules. *J. Biol. Chem.* **1994**, *269* (38), 23769–23775.

(81) Desai, A.; Mitchison, T. J. Microtubule Polymerization Dynamics. *Annu. Rev. Cell Dev. Biol.* **1997**, *13*, 83–117. https://doi.org/10.1146/annurev.cellbio.13.1.83.

(82) Wang, H.-W.; Nogales, E. Nucleotide-Dependent Bending Flexibility of Tubulin Regulates Microtubule Assembly. *Nature* **2005**, *435* (7044), 911–915.

https://doi.org/10.1038/nature03606.

(83) Ilan, Y. Microtubules: From Understanding Their Dynamics to Using Them as Potential Therapeutic Targets. *J. Cell. Physiol.* **2019**, *234* (6), 7923–7937. https://doi.org/10.1002/jcp.27978.

(84) Dominguez-Brauer, C.; Thu, K. L.; Mason, J. M.; Blaser, H.; Bray, M. R.; Mak, T. W. Targeting Mitosis in Cancer: Emerging Strategies. *Mol. Cell* **2015**, *60* (4), 524–536. https://doi.org/10.1016/j.molcel.2015.11.006.

(85) Ifuji, A.; Kuga, T.; Kaibori, Y.; Saito, Y.; Nakayama, Y. A Novel Immunofluorescence Method to Visualize Microtubules in the Antiparallel Overlaps of Microtubule-plus Ends in the Anaphase and Telophase Midzone. *Exp. Cell Res.* **2017**, *360* (2), 347–357. https://doi.org/10.1016/j.yexcr.2017.09.025.

(86) Schneider, I.; Lenart, P. Chromosome Segregation: Is the Spindle All About Microtubules? *Curr. Biol.* **2017**, *27* (21), R1168–R1170. https://doi.org/10.1016/j.cub.2017.09.022.

(87) Jordan, M. A.; Horwitz, S. B.; Lobert, S.; Correia, J. J. Exploring the Mechanisms of Action of the Novel Microtubule Inhibitor Vinflunine. *Semin. Oncol.* **2008**, *35* (3 Suppl 3), S6–S12. https://doi.org/10.1053/j.seminoncol.2008.01.009.

(88) Chen, W.; Zhang, D. Kinetochore Fibre Dynamics Outside the Context of the Spindle during Anaphase. *Nat. Cell Biol.* **2004**, *6* (3), 227–231. https://doi.org/10.1038/ncb1104.

(89) Hayden, J. H.; Bowser, S. S.; Rieder, C. L. Kinetochores Capture Astral Microtubules during Chromosome Attachment to the Mitotic Spindle: Direct Visualization in Live Newt Lung Cells. *J. Cell Biol.* **1990**, *111* (3), 1039–1045. https://doi.org/10.1083/jcb.111.3.1039.

(90) Jordan, M. A.; Wendell, K.; Gardiner, S.; Derry, W. B.; Copp, H.; Wilson, L. Mitotic Block Induced in HeLa Cells by Low Concentrations of Paclitaxel (Taxol) Results in Abnormal Mitotic Exit and Apoptotic Cell Death. *Cancer Res.* **1996**, *56* (4), 816–825.

(91) Arnst, K. E.; Banerjee, S.; Chen, H.; Deng, S.; Hwang, D.-J.; Li, W.; Miller, D. D. Current Advances of Tubulin Inhibitors as Dual Acting Small Molecules for Cancer Therapy. *Med. Res. Rev.* **2019**, *39* (4), 1398–1426. https://doi.org/10.1002/med.21568.

(92) Dumontet, C.; Jordan, M. A. Microtubule-Binding Agents: A Dynamic Field of Cancer Therapeutics. *Nat. Rev. Drug Discov.* **2010**, *9* (10), 790–803.

https://doi.org/10.1038/nrd3253.

(93) Fennell, B. J.; Naughton, J. A.; Barlow, J.; Brennan, G.; Fairweather, I.; Hoey, E.; McFerran, N.; Trudgett, A.; Bell, A. Microtubules as Antiparasitic Drug Targets. *Expert Opin. Drug Discov.* **2008**, *3* (5), 501–518. https://doi.org/10.1517/17460441.3.5.501.

(94) Chatterji, B. P.; Jindal, B.; Srivastava, S.; Panda, D. Microtubules as Antifungal and Antiparasitic Drug Targets. *Expert Opin. Ther. Pat.* **2011**, *21* (2), 167–186. https://doi.org/10.1517/13543776.2011.545349.

(95) Emmerson, B. T. The Management of Gout. *N. Engl. J. Med.* **1996**, *334* (7), 445–451. https://doi.org/10.1056/NEJM199602153340707.

(96) Cerquaglia, C.; Diaco, M.; Nucera, G.; La Regina, M.; Montalto, M.; Manna, R. Pharmacological and Clinical Basis of Treatment of Familial Mediterranean Fever (FMF) with Colchicine or Analogues: An Update. *Curr. Drug Targets. Inflamm. Allergy* **2005**, *4* (1), 117–124. https://doi.org/10.2174/1568010053622984.

(97) Varidaki, A.; Hong, Y.; Coffey, E. T. Repositioning Microtubule Stabilizing Drugs for Brain Disorders. *Front. Cell. Neurosci.* **2018**, *12*, 226. https://doi.org/10.3389/fncel.2018.00226.

(98) Perez, E. A. Microtubule Inhibitors: Differentiating Tubulin-Inhibiting Agents Based on Mechanisms of Action, Clinical Activity, and Resistance. *Mol. Cancer Ther.* **2009**, *8* (8), 2086–2095. https://doi.org/10.1158/1535-7163.MCT-09-0366.

(99) Steinmetz, M. O.; Prota, A. E. Microtubule-Targeting Agents: Strategies To Hijack the Cytoskeleton. *Trends Cell Biol.* **2018**, *28* (10), 776–792. https://doi.org/10.1016/j.tcb.2018.05.001.

(100) Nettles, J. H.; Li, H.; Cornett, B.; Krahn, J. M.; Snyder, J. P.; Downing, K. H. The Binding Mode of Epothilone A on α,ß-Tubulin by Electron Crystallography. *Science (80-.).* **2004**, *305* (5685), 866 LP – 869. https://doi.org/10.1126/science.1099190.

(101) Kellogg, E. H.; Hejab, N. M. A.; Howes, S.; Northcote, P.; Miller, J. H.; Díaz, J. F.; Downing, K. H.; Nogales, E. Insights into the Distinct Mechanisms of Action of Taxane and Non-Taxane Microtubule Stabilizers from Cryo-EM Structures. *J. Mol. Biol.* **2017**, *429* (5), 633–646. https://doi.org/https://doi.org/10.1016/j.jmb.2017.01.001.

(102) Prota, A. E.; Bargsten, K.; Redondo-Horcajo, M.; Smith III, A. B.; Yang, C.-P. H.; McDaid, H. M.; Paterson, I.; Horwitz, S. B.; Fernando Díaz, J.; Steinmetz, M. O. Structural Basis of Microtubule Stabilization by Discodermolide. *ChemBioChem*

2017, *18* (10), 905–909. https://doi.org/10.1002/cbic.201600696.

(103) Wang, Y.; Yu, Y.; Li, G.-B.; Li, S.-A.; Wu, C.; Gigant, B.; Qin, W.; Chen, H.; Wu, Y.; Chen, Q. Mechanism of Microtubule Stabilization by Taccalonolide AJ. *Nat. Commun.* **2017**, *8* (1), 1–8.

(104) Field, J. J.; Díaz, J. F.; Miller, J. H. The Binding Sites of Microtubule-Stabilizing Agents. *Chem. Biol.* **2013**, *20* (3), 301–315. https://doi.org/https://doi.org/10.1016/j.chembiol.2013.01.014.

(105) Ojima, I.; Lichtenthal, B.; Lee, S.; Wang, C.; Wang, X. Taxane Anticancer Agents: A Patent Perspective. *Expert Opin. Ther. Pat.* **2016**, *26* (1), 1–20. https://doi.org/10.1517/13543776.2016.1111872.

(106) Brogdon, C. F.; Lee, F. Y.; Canetta, R. M. Development of Other Microtubule-Stabilizer Families: The Epothilones and Their Derivatives. *Anticancer. Drugs* **2014**, *25* (5), 599–609. https://doi.org/10.1097/CAD.0000000000000071.

(107) Kanakkanthara, A.; Rowe, M. R.; Field, J. J.; Northcote, P. T.; Teesdale-Spittle, P. H.; Miller, J. H. BetaI-Tubulin Mutations in the Laulimalide/Peloruside Binding Site Mediate Drug Sensitivity by Altering Drug-Tubulin Interactions and Microtubule Stability. *Cancer Lett.* **2015**, *365* (2), 251–260. https://doi.org/10.1016/j.canlet.2015.06.001.

(108) Hamel, E.; Day, B. W.; Miller, J. H.; Jung, M. K.; Northcote, P. T.; Ghosh, A. K.; Curran, D. P.; Cushman, M.; Nicolaou, K. C.; Paterson, I.; et al. Synergistic Effects of Peloruside A and Laulimalide with Taxoid Site Drugs, but Not with Each Other, on Tubulin Assembly. *Mol. Pharmacol.* **2006**, *70* (5), 1555–1564. https://doi.org/10.1124/mol.106.027847.

(109) Prota, A. E.; Bargsten, K.; Northcote, P. T.; Marsh, M.; Altmann, K.-H.; Miller, J. H.; Diaz, J. F.; Steinmetz, M. O. Structural Basis of Microtubule Stabilization by Laulimalide and Peloruside A. *Angew. Chem. Int. Ed. Engl.* **2014**, *53* (6), 1621–1625. https://doi.org/10.1002/anie.201307749.

(110) Massarotti, A.; Coluccia, A.; Silvestri, R.; Sorba, G.; Brancale, A. The Tubulin Colchicine Domain: A Molecular Modeling Perspective. *ChemMedChem* **2012**, *7* (1), 33–42. https://doi.org/10.1002/cmdc.201100361.

(111) Dorléans, A.; Gigant, B.; Ravelli, R. B. G.; Mailliet, P.; Mikol, V.; Knossow, M. Variations in the Colchicine-Binding Domain Provide Insight into the Structural Switch of Tubulin. *Proc. Natl. Acad. Sci.* **2009**, *106* (33), 13775 LP – 13779. https://doi.org/10.1073/pnas.0904223106.

(112) Pérez-Pérez, M.-J.; Priego, E.-M.; Bueno, O.; Martins, M. S.; Canela, M.-D.; Liekens, S. Blocking Blood Flow to Solid Tumors by Destabilizing Tubulin: An Approach to Targeting Tumor Growth. *J. Med. Chem.* **2016**, *59* (19), 8685–8711. https://doi.org/10.1021/acs.jmedchem.6b00463.

(113) Ravelli, R. B. G.; Gigant, B.; Curmi, P. A.; Jourdain, I.; Lachkar, S.; Sobel, A.; Knossow, M. Insight into Tubulin Regulation from a Complex with Colchicine and a Stathmin-like Domain. *Nature* **2004**, *428* (6979), 198–202. https://doi.org/10.1038/nature02393.

(114) Akhmanova, A.; Steinmetz, M. O. Control of Microtubule Organization and Dynamics: Two Ends in the Limelight. *Nat. Rev. Mol. Cell Biol.* **2015**, *16* (12), 711–726. https://doi.org/10.1038/nrm4084.

(115) Wang, Z.; Chen, J.; Wang, J.; Ahn, S.; Li, C.-M.; Lu, Y.; Loveless, V. S.; Dalton, J. T.; Miller, D. D.; Li, W. Novel Tubulin Polymerization Inhibitors Overcome Multidrug Resistance and Reduce Melanoma Lung Metastasis. *Pharm. Res.* **2012**, *29* (11), 3040–3052. https://doi.org/10.1007/s11095-012-0726-4.

(116) Chen, J.; Ahn, S.; Wang, J.; Lu, Y.; Dalton, J. T.; Miller, D. D.; Li, W. Discovery of Novel 2-Aryl-4-Benzoyl-Imidazole (ABI-III) Analogues Targeting Tubulin Polymerization as Antiproliferative Agents. *J. Med. Chem.* **2012**, *55* (16), 7285–7289. https://doi.org/10.1021/jm300564b.

(117) Stengel, C.; Newman, S. P.; Leese, M. P.; Potter, B. V. L.; Reed, M. J.; Purohit, A. Class III Beta-Tubulin Expression and in Vitro Resistance to Microtubule Targeting Agents. *Br. J. Cancer* **2010**, *102* (2), 316–324. https://doi.org/10.1038/sj.bjc.6605489.

(118) Gan, P. P.; Pasquier, E.; Kavallaris, M. Class III Beta-Tubulin Mediates Sensitivity to Chemotherapeutic Drugs in Non Small Cell Lung Cancer. *Cancer Res.* **2007**, *67* (19), 9356–9363. https://doi.org/10.1158/0008-5472.CAN-07-0509.

(119) Bai, Z.; Gao, M.; Zhang, H.; Guan, Q.; Xu, J.; Li, Y.; Qi, H.; Li, Z.; Zuo, D.; Zhang, W.; et al. BZML, a Novel Colchicine Binding Site Inhibitor, Overcomes Multidrug Resistance in A549/Taxol Cells by Inhibiting P-Gp Function and Inducing Mitotic Catastrophe. *Cancer Lett.* **2017**, *402*, 81–92. https://doi.org/10.1016/j.canlet.2017.05.016.

(120) Kasibhatla, S.; Baichwal, V.; Cai, S. X.; Roth, B.; Skvortsova, I.; Skvortsov, S.; Lukas, P.; English, N. M.; Sirisoma, N.; Drewe, J.; et al. MPC-6827: A Small-Molecule Inhibitor of Microtubule Formation That Is Not a Substrate for Multidrug

Resistance Pumps. *Cancer Res.* **2007**, *67* (12), 5865–5871. https://doi.org/10.1158/0008-5472.CAN-07-0127.

(121) Mahal, K.; Resch, M.; Ficner, R.; Schobert, R.; Biersack, B.; Mueller, T. Effects of the Tumor-Vasculature-Disrupting Agent Verubulin and Two Heteroaryl Analogues on Cancer Cells, Endothelial Cells, and Blood Vessels. *ChemMedChem* **2014**, *9* (4), 847–854. https://doi.org/10.1002/cmdc.201300531.

(122) Wang, X.-F.; Guan, F.; Ohkoshi, E.; Guo, W.; Wang, L.; Zhu, D.-Q.; Wang, S.-B.; Wang, L.-T.; Hamel, E.; Yang, D.; et al. Optimization of 4-(N-Cycloamino)Phenylquinazolines as a Novel Class of Tubulin-Polymerization Inhibitors Targeting the Colchicine Site. *J. Med. Chem.* **2014**, *57* (4), 1390–1402. https://doi.org/10.1021/jm4016526.

(123) Leoni, L. M.; Hamel, E.; Genini, D.; Shih, H.; Carrera, C. J.; Cottam, H. B.; Carson, D. A. Indanocine, a Microtubule-Binding Indanone and a Selective Inducer of Apoptosis in Multidrug-Resistant Cancer Cells. *J. Natl. Cancer Inst.* **2000**, *92* (3), 217–224. https://doi.org/10.1093/jnci/92.3.217.

(124) Hwang, D.-J.; Wang, J.; Li, W.; Miller, D. D. Structural Optimization of Indole Derivatives Acting at Colchicine Binding Site as Potential Anticancer Agents. *ACS Med. Chem. Lett.* **2015**, *6* (9), 993–997. https://doi.org/10.1021/acsmedchemlett.5b00208.

(125) Arnst, K. E.; Wang, Y.; Hwang, D.-J.; Xue, Y.; Costello, T.; Hamilton, D.; Chen, Q.; Yang, J.; Park, F.; Dalton, J. T.; et al. A Potent, Metabolically Stable Tubulin Inhibitor Targets the Colchicine Binding Site and Overcomes Taxane Resistance. *Cancer Res.* **2018**, *78* (1), 265–277. https://doi.org/10.1158/0008-5472.CAN-17-0577.

(126) Zheng, Y.-B.; Gong, J.-H.; Liu, X.-J.; Wu, S.-Y.; Li, Y.; Xu, X.-D.; Shang, B.-Y.; Zhou, J.-M.; Zhu, Z.-L.; Si, S.-Y.; et al. A Novel Nitrobenzoate Microtubule Inhibitor That Overcomes Multidrug Resistance Exhibits Antitumor Activity. *Sci. Rep.* **2016**, *6*, 31472. https://doi.org/10.1038/srep31472.

(127) Siddiqui-Jain, A.; Hoj, J. P.; Cescon, D. W.; Hansen, M. D. Pharmacology and in Vivo Efficacy of Pyridine-Pyrimidine Amides That Inhibit Microtubule Polymerization. *Bioorg. Med. Chem. Lett.* **2018**, *28* (5), 934–941. https://doi.org/10.1016/j.bmcl.2018.01.053.

(128) Wang, J.; Chen, J.; Miller, D. D.; Li, W. Synergistic Combination of Novel Tubulin Inhibitor ABI-274 and Vemurafenib Overcome Vemurafenib Acquired Resistance

in BRAFV600E Melanoma. *Mol. Cancer Ther.* **2014**, *13* (1), 16–26. https://doi.org/10.1158/1535-7163.MCT-13-0212.

(129) JOHNSON, I. S.; ARMSTRONG, J. G.; GORMAN, M.; BURNETT, J. P. J. THE VINCA ALKALOIDS: A NEW CLASS OF ONCOLYTIC AGENTS. *Cancer Res.* **1963**, *23*, 1390–1427.

(130) Pettit, G. R. The Dolastatins BT - Fortschritte Der Chemie Organischer Naturstoffe Progress in the Chemistry of Organic Natural Products; Cavé, A., Cortes, D., Figadère, B., Laurens, A., Pettit, G. R., Herz, W., Kirby, G. W., Moore, R. E., Steglich, W., Tamm, C., Eds.; Springer Vienna: Vienna, 1997; pp 1–79. https://doi.org/10.1007/978-3-7091-6551-5_1.

(131) Crowley, P. J.; Lamberth, C.; Müller, U.; Wendeborn, S.; Nebel, K.; Williams, J.; Sageot, O.; Carter, N.; Mathie, T.; Kempf, H. Synthesis and Fungicidal Activity of Tubulin Polymerisation Promoters. Part 1: Pyrido [2, 3- b] Pyrazines. *Pest Manag. Sci. Former. Pestic. Sci.* **2010**, *66* (2), 178–185.

(132) Jordan, M. A.; Kamath, K.; Manna, T.; Okouneva, T.; Miller, H. P.; Davis, C.; Littlefield, B. A.; Wilson, L. The Primary Antimitotic Mechanism of Action of the Synthetic Halichondrin E7389 Is Suppression of Microtubule Growth. *Mol. Cancer Ther.* **2005**, *4* (7), 1086 LP – 1095. https://doi.org/10.1158/1535-7163.MCT-04-0345.

(133) Lindquist, N.; Fenical, W.; Van Duyne, G. D.; Clardy, J. Isolation and Structure Determination of Diazonamides A and B, Unusual Cytotoxic Metabolites from the Marine Ascidian Diazona Chinensis. *J. Am. Chem. Soc.* **1991**, *113* (6), 2303–2304. https://doi.org/10.1021/ja00006a060.

(134) Cormier, A.; Marchand, M.; Ravelli, R. B. G.; Knossow, M.; Gigant, B. Structural Insight into the Inhibition of Tubulin by Vinca Domain Peptide Ligands. *EMBO Rep.* **2008**, *9* (11), 1101–1106. https://doi.org/10.1038/embor.2008.171.

(135) Maderna, A.; Doroski, M.; Subramanyam, C.; Porte, A.; Leverett, C. A.; Vetelino, B. C.; Chen, Z.; Risley, H.; Parris, K.; Pandit, J.; et al. Discovery of Cytotoxic Dolastatin 10 Analogues with N-Terminal Modifications. *J. Med. Chem.* **2014**, *57* (24), 10527–10543. https://doi.org/10.1021/jm501649k.

(136) Ranaivoson, F. M.; Gigant, B.; Berritt, S.; Joullie, M.; Knossow, M. Structural Plasticity of Tubulin Assembly Probed by Vinca-Domain Ligands. *Acta Crystallogr. Sect. D* **2012**, *68* (8), 927–934.

(137) Gigant, B.; Wang, C.; Ravelli, R. B. G.; Roussi, F.; Steinmetz, M. O.; Curmi, P. A.;

Sobel, A.; Knossow, M. Structural Basis for the Regulation of Tubulin by Vinblastine. *Nature* **2005**, *435* (7041), 519–522. https://doi.org/10.1038/nature03566.

(138) Wieczorek, M.; Tcherkezian, J.; Bernier, C.; Prota, A. E.; Chaaban, S.; Rolland, Y.; Godbout, C.; Hancock, M. A.; Arezzo, J. C.; Ocal, O.; et al. The Synthetic Diazonamide DZ-2384 Has Distinct Effects on Microtubule Curvature and Dynamics without Neurotoxicity. *Sci. Transl. Med.* **2016**, *8* (365), 365ra159 LP-365ra159. https://doi.org/10.1126/scitranslmed.aag1093.

(139) Prota, A. E.; Bargsten, K.; Diaz, J. F.; Marsh, M.; Cuevas, C.; Liniger, M.; Neuhaus, C.; Andreu, J. M.; Altmann, K.-H.; Steinmetz, M. O. A New Tubulin-Binding Site and Pharmacophore for Microtubule-Destabilizing Anticancer Drugs. *Proc. Natl. Acad. Sci.* **2014**, *111* (38), 13817 LP – 13821. https://doi.org/10.1073/pnas.1408124111.

(140) Lambert, J. M.; Chari, R. V. J. Ado-Trastuzumab Emtansine (T-DM1): An Antibody–Drug Conjugate (ADC) for HER2-Positive Breast Cancer. *J. Med. Chem.* **2014**, *57* (16), 6949–6964. https://doi.org/10.1021/jm500766w.

(141) Menchon, G.; Prota, A. E.; Lucena-Agell, D.; Bucher, P.; Jansen, R.; Irschik, H.; Müller, R.; Paterson, I.; Díaz, J. F.; Altmann, K.-H.; et al. A Fluorescence Anisotropy Assay to Discover and Characterize Ligands Targeting the Maytansine Site of Tubulin. *Nat. Commun.* **2018**, *9* (1), 2106. https://doi.org/10.1038/s41467-018-04535-8.

(142) Kondoh, M.; Usui, T.; Kobayashi, S.; Tsuchiya, K.; Nishikawa, K.; Nishikiori, T.; Mayumi, T.; Osada, H. Cell Cycle Arrest and Antitumor Activity of Pironetin and Its Derivatives. *Cancer Lett.* **1998**, *126* (1), 29–32. https://doi.org/https://doi.org/10.1016/S0304-3835(97)00528-4.

(143) Watanabe, H.; Watanabe, H.; Usui, T.; Kondoh, M.; Osada, H.; Kitahara, T. Synthesis of Pironetin and Related Analogs: Studies on Structure-Activity Relationships as Tubulin Assembly Inhibitors. *J. Antibiot. (Tokyo).* **2000**, *53* (5), 540–545.

(144) Usui, T.; Watanabe, H.; Nakayama, H.; Tada, Y.; Kanoh, N.; Kondoh, M.; Asao, T.; Takio, K.; Watanabe, H.; Nishikawa, K.; et al. The Anticancer Natural Product Pironetin Selectively Targets Lys352 of α-Tubulin. *Chem. Biol.* **2004**, *11* (6), 799–806. https://doi.org/https://doi.org/10.1016/j.chembiol.2004.03.028.

(145) Bañuelos-Hernández, A. E.; Mendoza-Espinoza, J. A.; Pereda-Miranda, R.; Cerda-

García-Rojas, C. M. Studies of (−)-Pironetin Binding to α-Tubulin: Conformation, Docking, and Molecular Dynamics. *J. Org. Chem.* **2014**, *79* (9), 3752–3764. https://doi.org/10.1021/jo500420j.

(146) Yang, J.; Wang, Y.; Wang, T.; Jiang, J.; Botting, C. H.; Liu, H.; Chen, Q.; Yang, J.; Naismith, J. H.; Zhu, X.; et al. Pironetin Reacts Covalently with Cysteine-316 of α-Tubulin to Destabilize Microtubule. *Nat. Commun.* **2016**, *7* (1), 12103. https://doi.org/10.1038/ncomms12103.

(147) Prota, A. E.; Setter, J.; Waight, A. B.; Bargsten, K.; Murga, J.; Diaz, J. F.; Steinmetz, M. O. Pironetin Binds Covalently to ACys316 and Perturbs a Major Loop and Helix of α-Tubulin to Inhibit Microtubule Formation. *J. Mol. Biol.* **2016**, *428* (15), 2981–2988. https://doi.org/https://doi.org/10.1016/j.jmb.2016.06.023.

(148) Mc Gee, M. M.; Gemma, S.; Butini, S.; Ramunno, A.; Zisterer, D. M.; Fattorusso, C.; Catalanotti, B.; Kukreja, G.; Fiorini, I.; Pisano, C.; et al. Pyrrolo[1,5]Benzoxa(Thia)Zepines as a New Class of Potent Apoptotic Agents. Biological Studies and Identification of an Intracellular Location of Their Drug Target. *J. Med. Chem.* **2005**, *48* (13), 4367–4377. https://doi.org/10.1021/jm049402y.

(149) Campiani, G.; Nacci, V.; Fiorini, I.; De Filippis, M. P.; Garofalo, A.; Ciani, S. M.; Greco, G.; Novellino, E.; Williams, D. C.; Zisterer, D. M.; et al. Synthesis, Biological Activity, and SARs of Pyrrolobenzoxazepine Derivatives, a New Class of Specific "Peripheral-Type" Benzodiazepine Receptor Ligands. *J. Med. Chem.* **1996**, *39* (18), 3435–3450. https://doi.org/10.1021/jm960251b.

(150) Greene, L. M.; Butini, S.; Campiani, G.; Williams, D. C.; Zisterer, D. M. Pre-Clinical Evaluation of a Novel Class of Anti-Cancer Agents, the Pyrrolo-1, 5-Benzoxazepines. *J. Cancer* **2016**, *7* (15), 2367–2377. https://doi.org/10.7150/jca.16616.

(151) Zisterer, D. M.; Campiani, G.; Nacci, V.; Williams, D. C.; College, T.; Ireland, D. M. Z.; Farmaco, D.; Tecnologico, C.; Studi, U. D. Pyrrolo-1 , 5-Benzoxazepines Induce Apoptosis in HL-60 , Jurkat , and Hut-78 Cells : A New Class of Apoptotic Agents 1. **2000**, *293* (1), 48–59.

(152) Bright, S. A.; Greene, L. M.; Greene, T. F.; Campiani, G.; Butini, S.; Brindisi, M.; Lawler, M.; Meegan, M. J.; Williams, D. C.; Zisterer, D. M. The Novel Pyrrolo-1,5-Benzoxazepine, PBOX-21, Potentiates the Apoptotic Efficacy of STI571 (Imatinib Mesylate) in Human Chronic Myeloid Leukaemia Cells. *Biochem. Pharmacol.*

2009, *77* (3), 310–321. https://doi.org/10.1016/j.bcp.2008.10.008.

(153) Mulligan, J. M. Identification of Tubulin as the Molecular Target of Pro-Apoptotic Pyrrolo-1,5-Benzoxazepines. *Mol. Pharmacol.* **2006**, *70* (1), 60–70. https://doi.org/10.1124/mol.105.021204.

(154) O'Callaghan, K.; Palagano, E.; Butini, S.; Campiani, G.; Williams, D. C.; Zisterer, D. M.; O'Sullivan, J. Induction of Apoptosis in Oral Squamous Carcinoma Cells by Pyrrolo-1,5-Benzoxazepines. *Mol. Med. Rep.* **2015**, *12* (3), 3748–3754. https://doi.org/10.3892/mmr.2015.3832.

(155) Brindisi, M.; Ulivieri, C.; Alfano, G.; Gemma, S.; de Asis Balaguer, F.; Khan, T.; Grillo, A.; Chemi, G.; Menchon, G.; Prota, A. E.; et al. Structure-Activity Relationships, Biological Evaluation and Structural Studies of Novel Pyrrolonaphthoxazepines as Antitumor Agents. *Eur. J. Med. Chem.* **2019**, *162*, 290–320. https://doi.org/10.1016/j.ejmech.2018.11.004.

(156) Khan, T.; Relitti, N.; Brindisi, M.; Magnano, S.; Zisterer, D.; Gemma, S.; Butini, S.; Campiani, G. Autophagy Modulators for the Treatment of Oral and Esophageal Squamous Cell Carcinomas. *Med. Res. Rev.* **2019**.

(157) Greene, L. M.; Nolan, D. P.; Regan-Komito, D.; Campiani, G.; Williams, D. C.; Zisterer, D. M. Inhibition of Late-Stage Autophagy Synergistically Enhances Pyrrolo-1,5-Benzoxazepine-6-Induced Apoptotic Cell Death in Human Colon Cancer Cells. *Int. J. Oncol.* **2013**, *43* (3), 927–935. https://doi.org/10.3892/ijo.2013.1989.

(158) Federico, S.; Khan, T.; Relitti, N.; Chemi, G.; Brindisi, M.; Brogi, S.; Novellino, E.; Zisterer, D. M.; Campiani, G.; Gemma, S.; et al. A Jocic-Type Approach for a Practical and Scalable Synthesis of Pyrrolonaphthoxazepine (PNOX)-Based Potent Proapoptotic Agents. *Tetrahedron Lett.* **2018**, *59* (51), 4466–4470. https://doi.org/https://doi.org/10.1016/j.tetlet.2018.11.005.

(159) Ghosh, A. K.; Brindisi, M. Organic Carbamates in Drug Design and Medicinal Chemistry. *J. Med. Chem.* **2015**, *58* (7), 2895–2940. https://doi.org/10.1021/jm501371s.

(160) Heravi, M. M.; Kheilkordi, Z.; Zadsirjan, V.; Heydari, M.; Malmir, M. Buchwald-Hartwig Reaction: An Overview. *J. Organomet. Chem.* **2018**, *861*, 17–104. https://doi.org/https://doi.org/10.1016/j.jorganchem.2018.02.023.

(161) Ouarna, S.; K'tir, H.; Lakrout, S.; Ghorab, H.; Amira, A.; Aouf, Z.; Berredjem, M.; Aouf, N.-E. An Eco-Friendly and Highly Efficient Route for N-Acylation under

Catalyst-Free Conditions. *system* **2015**, *21*, 22.

(162) Kiso, Y.; Ukawa, K.; Akita, T. Efficient Removal of N-Benzyloxycarbonyl Group by a 'Push–Pull' Mechanism Using Thioanisole–Trifluoroacetic Acid, Exemplified by a Synthesis of Met-Enkephalin. *J. Chem. Soc. Chem. Commun.* **1980**, No. 3, 101–102. https://doi.org/10.1039/C39800000101.

(163) Chandrappa, S.; Vinaya, K.; Ramakrishnappa, T.; Rangappa, K. S. An Efficient Method for Aryl Nitro Reduction and Cleavage of Azo Compounds Using Iron Powder/Calcium Chloride. *Synlett* **2010**, *2010* (20), 3019–3022. https://doi.org/10.1055/s-0030-1259067.

(164) Artico, M.; Silvestri, R.; Massa, S.; Loi, A. G.; Corrias, S.; Piras, G.; La Colla, P. 2-Sulfonyl-4-Chloroanilino Moiety: A Potent Pharmacophore for the Anti-Human Immunodeficiency Virus Type 1 Activity of Pyrrolyl Aryl Sulfones. *J. Med. Chem.* **1996**, *39* (2), 522–530. https://doi.org/10.1021/jm950568w.

(165) Butini, S.; Gemma, S.; Brindisi, M.; Maramai, S.; Minetti, P.; Celona, D.; Napolitano, R.; Borsini, F.; Cabri, W.; Fezza, F.; et al. Identification of a Novel Arylpiperazine Scaffold for Fatty Acid Amide Hydrolase Inhibition with Improved Drug Disposition Properties. *Bioorg. Med. Chem. Lett.* **2013**, *23* (2), 492–495. https://doi.org/https://doi.org/10.1016/j.bmcl.2012.11.035.

(166) Urgaonkar, S.; Verkade, J. G. Palladium/Proazaphosphatrane-Catalyzed Amination of Aryl Halides Possessing a Phenol, Alcohol, Acetanilide, Amide or an Enolizable Ketone Functional Group: Efficacy of Lithium Bis(Trimethylsilyl)Amide as the Base. *Adv. Synth. Catal.* **2004**, *346* (6), 611–616. https://doi.org/10.1002/adsc.200404005.

(167) Vekariya, R. H.; Aubé, J. Hexafluoro-2-Propanol-Promoted Intermolecular Friedel-Crafts Acylation Reaction. *Org. Lett.* **2016**, *18* (15), 3534–3537. https://doi.org/10.1021/acs.orglett.6b01460.

(168) Chen, I. T.; Baitinger, I.; Schreyer, L.; Trauner, D. Total Synthesis of Sandresolide B and Amphilectolide. *Org. Lett.* **2014**, *16* (1), 166–169. https://doi.org/10.1021/ol403156r.

(169) Korenova, A., Netchitailo, P., & Decroix, B. Synthesis of 2,3-Dihydro-3-Hydroxy-2-(Pyrrol-1-Ylmethyl)-1H-Isoindol-1-One. An Intermediate for the Synthesis of Tetracyclic Systems. *J. Heterocycl. Chem.* **1998**, *35(1)*, 9–12.

(170) Brindisi, M.; Ulivieri, C.; Alfano, G.; Gemma, S.; de Asís Balaguer, F.; Khan, T.; Grillo, A.; Chemi, G.; Menchon, G.; Prota, A. E.; et al. Structure-Activity

Relationships, Biological Evaluation and Structural Studies of Novel Pyrrolonaphthoxazepines as Antitumor Agents. *Eur. J. Med. Chem.* **2019**, *162*, 290–320. https://doi.org/10.1016/j.ejmech.2018.11.004.

(171) Pak, K. C.; Lam, K. Y.; Law, S.; Tang, J. C. O. The Inhibitory Effect of Gleditsia Sinensis on Cyclooxygenase-2 Expression in Human Esophageal Squamous Cell Carcinoma. *Int. J. Mol. Med.* **2009**, *23* (1), 121–129.

(172) Sobolewski, C.; Cerella, C.; Dicato, M.; Ghibelli, L.; Diederich, M. The Role of Cyclooxygenase-2 in Cell Proliferation and Cell Death in Human Malignancies. *Int. J. Cell Biol.* **2010**, *2010*, 215158. https://doi.org/10.1155/2010/215158.

(173) Subbaramaiah, K.; Dannenberg, A. J. Cyclooxygenase 2: A Molecular Target for Cancer Prevention and Treatment. *Trends Pharmacol. Sci.* **2003**, *24* (2), 96–102. https://doi.org/10.1016/S0165-6147(02)00043-3.

(174) Dannenberg, A. J.; Altorki, N. K.; Boyle, J. O.; Dang, C.; Howe, L. R.; Weksler, B. B.; Subbaramaiah, K. Cyclo-Oxygenase 2: A Pharmacological Target for the Prevention of Cancer. *Lancet. Oncol.* **2001**, *2* (9), 544–551. https://doi.org/10.1016/S1470-2045(01)00488-0.

(175) Sui, H.; Zhou, S.; Wang, Y.; Liu, X.; Zhou, L.; Yin, P.; Fan, Z.; Li, Q. COX-2 Contributes to P-Glycoprotein-Mediated Multidrug Resistance via Phosphorylation of c-Jun at Ser63/73 in Colorectal Cancer. *Carcinogenesis* **2011**, *32* (5), 667–675. https://doi.org/10.1093/carcin/bgr016.

(176) Ratnasinghe, D.; Daschner, P. J.; Anver, M. R.; Kasprzak, B. H.; Taylor, P. R.; Yeh, G. C.; Tangrea, J. A. Cyclooxygenase-2, P-Glycoprotein-170 and Drug Resistance; Is Chemoprevention against Multidrug Resistance Possible? *Anticancer Res.* **2001**, *21* (3C), 2141–2147.

(177) Contino, G.; Eldridge, M. D.; Secrier, M.; Bower, L.; Fels Elliott, R.; Weaver, J.; Lynch, A. G.; Edwards, P. A. W.; Fitzgerald, R. C. Whole-Genome Sequencing of Nine Esophageal Adenocarcinoma Cell Lines. *F1000Research* **2016**, *5*, 1336. https://doi.org/10.12688/f1000research.7033.1.

(178) Gai, L.-X.; Wang, W.-Q.; Wu, X.; Su, X.-J.; Yang, F.-C. NIR Absorbing Reduced Graphene Oxide for Photothermal Radiotherapy for Treatment of Esophageal Cancer. *J. Photochem. Photobiol. B.* **2019**, *194*, 188–193. https://doi.org/10.1016/j.jphotobiol.2019.03.014.

(179) Garcia, E.; Hayden, A.; Birts, C.; Britton, E.; Rogerson, C.; Bleaney, C. W.; Cowie, A.; Pickard, K.; Mellone, M.; Choh, C.; et al. Author Correction: Authentication and

Characterisation of a New Oesophageal Adenocarcinoma Cell Line: MFD-1. *Scientific reports*. England January 2019, p 318. https://doi.org/10.1038/s41598-018-37591-7.

(180) He, S.; Li, Q.; Jiang, X.; Lu, X.; Feng, F.; Qu, W.; Chen, Y.; Sun, H. Design of Small Molecule Autophagy Modulators: A Promising Druggable Strategy. *J. Med. Chem.* **2018**, *61* (11), 4656–4687. https://doi.org/10.1021/acs.jmedchem.7b01019.

(181) Klionsky, D. J.; Abdelmohsen, K.; Abe, A.; Abedin, M. J.; Abeliovich, H.; Acevedo Arozena, A.; Adachi, H.; Adams, C. M.; Adams, P. D.; Adeli, K.; et al. Guidelines for the Use and Interpretation of Assays for Monitoring Autophagy (3rd Edition). *Autophagy* **2016**, *12* (1), 1–222. https://doi.org/10.1080/15548627.2015.1100356.

(182) Maurya, R.; Kumar, R.; Saran, S. AMPKα Promotes Basal Autophagy Induction in Dictyostelium Discoideum. *J. Cell. Physiol.* **2019**, *n/a* (n/a). https://doi.org/10.1002/jcp.29373.

(183) Yoshii, S. R.; Mizushima, N. Monitoring and Measuring Autophagy. *Int. J. Mol. Sci.* **2017**, *18*. https://doi.org/10.3390/ijms18091865.

(184) Iwatsubo, T.; Hirota, N.; Ooie, T.; Suzuki, H.; Shimada, N.; Chiba, K.; Ishizaki, T.; Green, C. E.; Tyson, C. A.; Sugiyama, Y. Prediction of in Vivo Drug Metabolism in the Human Liver from in Vitro Metabolism Data. *Pharmacol. Ther.* **1997**, *73* (2), 147–171. https://doi.org/10.1016/s0163-7258(96)00184-2.

Part 2

Development of novel β-lactam-based HDAC6 inhibitors as anticancer agents

PART 2 CHAPTER I

BACKGROUND

2.1.1 Introduction

Epigenetic modification regulates the heritability of gene expression through active post-translational modifications, including methylation, phosphorylation, acetylation, ribosylation, along with the post-translational modifications of the histone proteins and modification in the nucleosomal organization.[1,2] These modifications establish the 'epigenetic code', collectively identified as the 'epigenome' to modulate several developmental stages and diverse disease states.[3] Among all the post-translational modifications, there are many extensive studies focusing on histone acetylation and deacetylation.[4] The field of histone acetylation has rapidly developed over the past few decades. The dynamic status of histone acetylation is under the control of histone deacetylases (HDACs) and histone acetyltransferases (HATs), which play an important role in the regulation of gene expression. HATs mediate the acetylation of lysine residue associated with gene transcription, whereas HDACs show an opposite effect and the deacetylation leads to a more condensed chromatin structure; this fact leads to the repression in the gene transcription.[5] HDACs are frequently dysregulated and have been acknowledged as a crucial factor in numerous diseases, comprising cancer, neurodegenerative and inflammatory diseases.[6]

2.1.2 Classification of HDACs

There are four major classes of HDACs: three metal-containing classes and one NAD+-dependent class.[7,8] Based on their homology to yeast proteins , structure, function, and subcellular localization class I HDACs contain HDAC 1, 2, 3, and 8; class IIa HDACs are. HDAC4, 5, 7, and 9; class IIb HDACs are HDAC6 and 10; and HDAC11 is the only member of class IV HDAC. Class III deacetylases are seven sirtuins (SIRTs), SIRT1–7 that depend on NAD+ as a cofactor for their function.[9,10] The zinc-dependent amidohydrolases classes of HDACs, i.e., class I, II, and IV, are sensitive to hydroxamic acids that chelate Zn_2+. On the other hand, HDACs class III, which are resistant to cytosolic as well as hydroxamic acid-derived inhibitors, are inhibited by nicotinamide. A

common deacetylase as well as catalytic domain is shared by class I, II, and IV HDACs that catalyzes the deacetylation with the assistance of the histidine–aspartate charge transfer system.[11,12] A conserved deacetylase domain in the nucleus is possessed by class I HDACs. The class II HDACs govern the acetylation status of the non-histone substrates through shuttling between the nucleus and cytoplasm. Similarly, HDAC6 deacetylates the cellular proteins. Due to the lack of an intrinsic DNA-binding ability, the reinforcement of HDACs to DNA is facilitated via transcription factors and associated protein complexes. HDACs integrate with these transcription factors and protein complexes and reside there to obtain access to DNA. Sin3, mSin3A, N-CoR (nuclear receptor co-repressor), NuRD (nucleosome remodeling and deacetylation), Mi-2/NRD and PRC2, etc., provide shelter to HDAC1 and HDAC2, while SMRT complex performs this role for HDAC3.[8,11,13]

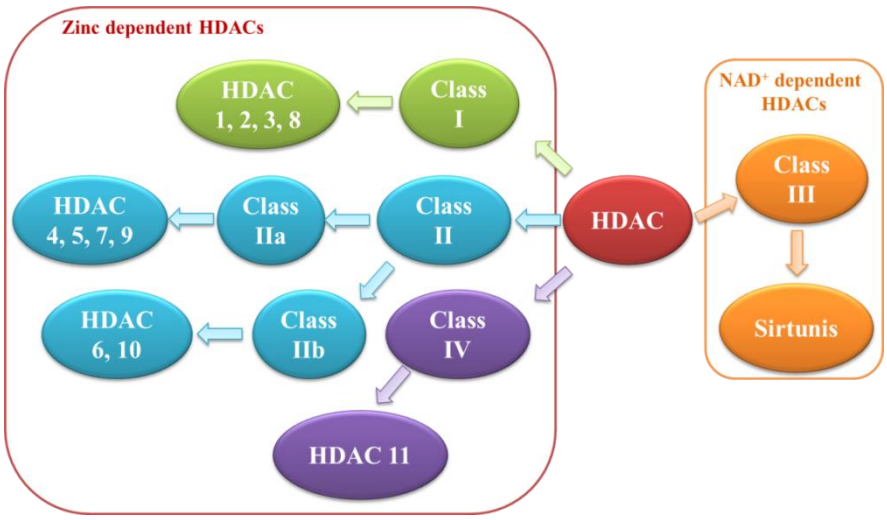

Figure 1. Classification of HDAC family

2.1.3 HDACs in cancer development

Cancer has conventionally been regarded as the commencement of multiple diseases driven by the accumulation of genetic mutation, along with the disruption of the epigenetic regulatory mechanism that leads to the occurrence of neoplasia.[5] Endogenous along with exogenous stimuli corrupt the canalization of cells through the reorganization of chromatin structure leading to the explicit of aberrant gene expression or repression, thereby conveying the cells to attain the features of cancer.[6] The disruption of epigenome and constitutional epimutations may lead to gene expression alteration and epigenetic abnormality, which promotes the malignant transformation of cells, cancer initiation and progression.[14] It is believed that epigenetic alteration and the genetic modifications such as

the loss or amplification of DNA and the loss of heterozygosity may be serving as the key initiating events in different forms of cancer.[15]

- **HDACs in cell cycle regulation**

HDAC inhibition has been demonstrated to have antiproliferative effects by inducing cell-cycle arrest in G1 phase via the up-regulation of cyclin-dependent kinase (CDK) inhibitors or by down-regulation of cyclins and CDKs.[16] Loss of HDAC1 and 2 induce expression of CDK inhibitors, leading to a cell-cycle block in G1. Knockdown of HDAC5 leads to a substantial up-regulation of p21 and down-regulation of cyclin D1 and CDK2/4/6, which leads in G1-phase cell-cycle arrest in human HCC cells.[17] HDAC inhibition might block the G1/S cellular transition by dephosphorylation and subsequently inhibiting E2F activities in the transcription of genes for the G1 progression. Besides to controlling the G1/S transition, HDAC1 knockdown in tumor cells impairs G2/M transition and inhibits the cell growth as evidenced by a reduction of mitotic cells and an increased percentage of apoptotic cells.[18] HDAC10 regulates the G2/M transition via the modulation of cyclin A2 expression. The effect of HDAC10 on the cyclin A2 transcription is dependent on let-7 and HMGA2.[19] Moreover, HDAC3 directly interacts with the cyclin A and regulates cyclin A stability by modulating its acetylation status. Given that cyclin A is vital for S phase progression and entry into mitosis, HDAC3 knockdown causes cell growth in S and G2/M phases.[20] Collectively, HDAC inhibition can stimulate the cell cycle arrest at either G1/S or G2/Mphase, suggesting HDACs as therapeutic targets for unusual cell growth and proliferation in cancer.

- **HDACs in apoptosis**

HDACs regulate apoptosis in several cancer cells through altering the expression of pro- and anti-apoptotic proteins. HDAC inhibition could prompt the intrinsic pathway by decreasing the expression of anti-apoptotic proteins and increasing the expression of pro-apoptotic proteins.[21] Inhibition of HDAC1, 2, and/or 3 is necessary for caspase-8 activation in non-small cell lung cancer.[22] Depletion of HDAC2 synergizes pancreatic cancer cells to TRAIL-induced apoptosis with an increased expression of TRAIL receptor DR5 (TRAIL-R2).[23] HDAC2 depletion results in activation of apoptosis via p53 and Bax activation and Bcl2 suppression in human lung cancer cells.[24] In gastric cancer cells, HDAC2 selectively knockdown the expression of pro-apoptotic factors Bax, AIF, and Apaf-1, and repressed

the expression of anti-apoptotic Bcl-2.[25] Inhibition of HDAC8 promoted BMF-mediated apoptosis in colon cancer cells.[26]

- **HDACs in autophagy**

Consistent with the double role of autophagy in cancer, many HDAC family members show both pro- and anti-autophagy activities.[27] Depletion or inhibition of HDAC1 is reported to stimulate autophagy by promoting accumulation of the autophagosomal marker LC3-II.[28] However, in mouse models, deletion of both the HDAC1 and HDAC2 in skeletal muscle blocks autophagy flux.[29] Recent research indicates that the oncogenic role of class IIa HDAC4 and HDAC5 in cancer cells would be derived at least partially via decreasing autophagic flux, but the detailed mechanism needs further investigation. In HDAC6 knockout mouse embryonic fibroblasts, HDAC6 appears to be important for ubiquitin-selective basal autophagy, but not in starvation-induced autophagy.[30] A similar mechanism is observed in mitophagy.[31] HDAC6-mediated deacetylation promotes autophagosome processing.[32] The acetylation level of LC3B-II is decreased upon serum deprivation and HDAC6 is at least partially responsible for deacetylating LC3-II. In neuroblastoma, depletion and inhibition of HDAC10 disables efficient autophagosome/lysosome fusion and interferes with the autophagic flux, resulting in an increase of sensitization to cytotoxic drug treatment. The deacetylation of Hsp70 protein families by HDAC10 might contribute to autophagy-mediated cell survival.[33] Overall, class IIb HDACs seem to mainly regulate autophagic flux at the level of autophagosome–autolysosome fusion via deacetylation of cytoplasmic proteins.[27] Sirt1 activity is essential for the induction of starvation-induced autophagy by directly deacetylating the critical regulators of the autophagy machinery, like Atg5, Atg7, Atg8, and LC3.[34] SIRT1 and the PI3K/Akt/mTOR pathway are found to be related to autophagy in prostate cancer cells.[35] Collectively, a better understanding of the context-dependent effects of individual HDACs enzymes on autophagic process will give us an advantage to treat cancers by exploiting this area in a specific targeted manner.

- **HDACs in metastasis of cancer**

Epithelial-to-mesenchymal transition (EMT) is a key process in cancer cell invasion and metastasis, and emerging studies have demonstrated the key role of HDACs in EMT regulation in several cancer contexts. It is characterized by the loss of epithelial cell markers, namely, epithelial-cadherin (CDH1), and several transcriptional repressors of

CDH1 have been identified. A mechanism of their action includes the recruitment of HDACs to the CDH1 promoter resulting in deacetylation of H3 and H4 histones. Treatment of cells with the HDAC inhibition induces CDH1 expression, and represses EMT and metastasis in triple-negative breast cancer. Deductions indicate the therapeutic potential of inhibition of class I HDACs in targeting EMT and metastasis of cancer cells.[36]

- **HDACs in angiogenesis**

Tumor growth and metastasis depend on angiogenesis. It is triggered by hypoxia or hypoxic microenvironment, and the cellular response to hypoxia is mainly regulated by transcription factor, hypoxia-inducible factors 1 a (HIF-1α). Many HDACs are associated with HIF-1α activity as cell treatment with HDAC inhibition causes HIF-1α degradation and functional repression. HDAC1 and 4 directly deacetylate HIF-1α and block degradation of the protein.[37,38] Instead of regulating HIF-1α acetylation, HDAC5 and 6 facilitate HIF-1α maturation and stabilization by deacetylating its chaperones, HSP70 and HSP90.[39] Inhibition of HDAC5 and 6 results in hyperacetylation of these chaperones, accumulation of the immature HIF-1α complex, and degradation of HIF-1α by the 20S proteasome. HDAC4, 5, and 7 increased transcriptional activity of HIF-1α by promoting its association with p300.[40,41] Taken together, HDACs play important roles in angiogenesis by modulating a multitude of pro- and anti-angiogenic factors, indicating that they are potential targets for anti-angiogenesis in cancer therapy.

2.1.4 Selective HDAC6 inhibitions in cancer

Overexpression of HDAC6 has been related to the invasive metastatic behavior of tumor cells. HDAC6 plays a role in regulation of microtubule dynamics by the acetylation of tubulin and microtubule-mediated processes, including cell migration and interactions.[42] The cell motility is regulated by tubulin function and actin network which is modulated by the actin remodeling protein.[43] HDAC6 can also regulate oncogenic Ras/MAPK signaling pathways, which are required for efficient tumor growth. Since the inhibition of HDAC6 stabilizes the MTs, other possible apoptotic pathways that inhibit oncogenic tumorigenesis need to be inspected. The overexpression of HDAC6 may be implicated in the malignant behavior of estrogen receptor positive breast cancer.[44] In addition, HDAC6 has been implicated in regulation of endothelial cell migration.[45] HDAC6 may contribute to the angiogenesis processes by modulating the stability of proangiogenic factors mediated by Hsp90, a substrate of HDAC6.[46,47] Since Hsp90 plays a role in the stabilization of some

transcription factors, loss of Hsp90 function by hyperacetylation may have an ‘‘indirect’’ effect on the regulation of gene expression.[48] Through its ubiquitin binding activity and interaction with other partner proteins, HDAC6 itself plays a role in degradation of misfolded proteins by binding polyubiquinated proteins and delivering to the dynein motor proteins for transport into aggresomes which are degraded by lysosomes. HDAC6 also participates in cell protection in response to environmental stress by interaction with stress granules.[49] Thus, the multiple functions of HDAC6, through deacetylase-dependent and-independent mechanisms, modulate many cellular pathways which are relevant to tumor cell biology and malignant behavior. On the basis of these functions, HDAC6 appears to be one of the most attractive targets among HDACs for cancer treatment.[50] HDAC6 should be considered as a target in cancer therapy due to its essential role in many signaling pathways that provide a benefit to malignant cells to survive and maintain its phenotype.

2.1.5 HDAC inhibitors in cancer

The usual structure of HDAC inhibitors (HDACi) is characterized by three primary domains, consisting of the zinc binding group (ZBG), the linker region, and the cap group.[51] Multiple studies have been reported to unveil the role of each domain in optimizing the drug-target interaction. The modification of the cap group appears the most promising strategy to generate isoform selectivity.[52] Most of the known inhibitors have a hydroxamic acid-based structure. HDAC inhibitors exhert inhibitory effect by their ability to chelate the zinc cofactor at the active site of the enzyme

Figure 2. Focused regions to develop HDAC inhibitors

A large number of HDAC inhibitors have been identified and numerous HDACis are nowadays at various stages of clinical trial development for the treatment of cancers.[53] Two inhibitors, vorinostat (SAHA, **1**) and romidepsin (depsipeptide, FK228, **2**) have been approved for the chemical treatment of cutaneous T-cell lymphoma. During a multidimensional chemical genetic screen with a cell based assay, Haggerty *et al.* identified tubacin, **3** within a set of 7392 small molecules as a selective inhibitor of HDAC6.[54,55] The large cap group is composed of six lipophilic rings and the

stereochemistry of the dioxane ring appears to confer selectivity allowing the cap group to interact with the protein surface. Tubacin inhibited the interaction of HDAC6 with the motor protein dynein and induced marked accumulation of ubiquitinated proteins. An interesting feature of tubacin was the lack of toxicity for normal haematological cells. Tubacin was used to validate HDAC6 as a drug target, but, as a consequence of its non-drug-like structure, high lipophilicity, and tedious synthesis, it is more useful as a research tool than as a drug.[56]

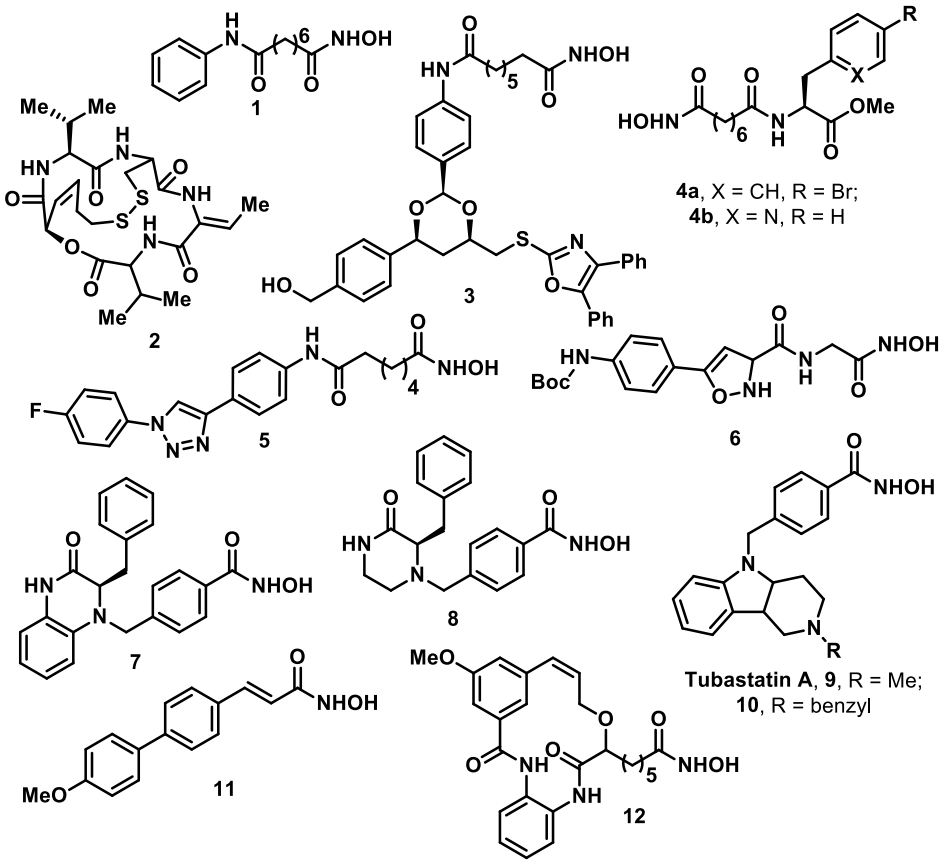

Figure 3. Available HDAC inhibitors from different class of biologically active compounds

In a series of biarylalanine-containing hydroxamic acids, the selectivity for HDAC6 was documented using immunoprecipitated HDAC1 and HDAC6.[57] The selectivity was confirmed by comparing histone and tubulin acetylation in treated cells. The most selective derivative was the synthetic intermediate with a bromophenylalanine structure and a suberic acid spacer. (**4a**). Taking the phenylalanine compounds as lead structures, a new series of analogues containing a pyridylalanine (**4b**) element was developed.[58]

The triazolylphenyl derivative **5** inhibited HDAC6 with a IC50 value of 1.9 nM. The same group described a series of hydroxamate-based HDAC inhibitors containing a

phenylisoxazole (**6**) as the cap group. Both the length of the linker chain and the amine-protecting group play a role in determining potency and selectivity.[59]

Amino acids were attached to a rigid aryl moiety to form 3,4-dihydroquinoxalin-2(1*H*)-one caps (**7**) or incorporated into less rigid piperazine-2,5-dione caps (**8**). The hydroxamate inhibitors showed selectivity up to 40-fold for HDAC6 over other class I/IIa HDACs. The selectivity and potency were found to be markedly dependent on the absolute configuration of the chiral moiety. The chiral structure-dependent selectivity was confirmed in cell-based assays. The majority of compounds effectively induced α-tubulin acetylation at a level comparable to that of **3**, with increased potency.[60]

A structure-based drug design combined with homology modeling techniques was used to develop a novel series of carbazole hydroxamic acids with alkyl and alkylaryl linker groups. Selectivity for HDAC6 was monitored by assays using purified human HDAC proteins. Optimization of the tricyclic group with the aim of reducing lipophilicity led to the synthesis of a tetrahydro-gcarboline analogue, **9** (tubastatin A), with 1000-fold selectivity over HDAC1. Substitutions in the carboline cap group were well-tolerated, with substitutions at position 2 of β-carbolines being optimal for HDAC6 activity and selectivity (**10**). Studies on Tubastatin A analogues revealed that a benzyl linker that occupies the hydrophobic channel of active site may be favorable for improving selectivity toward HDAC6.[61]

Recently, selected compounds of a novel series (ST3595, **11**) characterized by a cinnamic linker and a substituted phenyl group were found to be very effective induction of tubulin and p53 hyperacetylation. **11** inhibited class I and II HDAC with high preference for HDAC6 versus HDAC1.[62] This compound exhibited synergistic antitumor effects in combination with paclitaxel at well-tolerated doses.[63]

In particular, a relevant selectivity toward this isoform was detected within the group of diamide-based macrocycles (*R*)- and (*S*)-**12** (10–500-fold over the other HDACs). Further refinement of these novel non-natural macrocyclic templates could be promising for future development of more selective inhibitors of HDAC6.[64]

2.1.6 Our previous efforts to develop selective HDAC inhibitors

Our research group have reported a wide variety of chemical compounds as HDAC inhibitors in different diseases (**Figure 4**). A combined computational and medicinal chemistry efforts to rationally modulate HDAC isoform has been engaged to develop a

series of novel phenylpyrrole-based derivatives (**13**). *In vitro* evaluation on HDAC1 and HDAC6 enzyme isoforms was performed and selected compounds (**14a**,**b** and **15**)underwent western blot analysis on glioblastoma, neuroblastoma, and hematological tumor cell lines to verify their influence on tubulin and histone acetylation status in cell-based assays. The best compounds were assessed for their effects on cell cycle and apoptosis, showing a promising antitumor potential in hematological tumor cell lines and no toxicity on NIH3T3 cell.[65] In another attempt. a series of novel spiroindoline derivatives (**16**) capable of selective inhibition of the HDAC6 isoform has been reported. Computational studies and *in vitro* study of inhibitory potency for the developed compounds against HDAC6 and HDAC1 isoforms were converged by cell-based investigations on histone H3 and α-tubulin acetylation. The effects on cancer cell cycle and apoptosis of the best performing derivative **17** were assessed on cancer cell lines highlighting a promising antitumor potential. The compound was able to inhibit cell migration in neuroblastoma cells and did not show toxicity in NIH3T3 mouse fibroblasts.[66] Further attempts through virtual screening and phenotypical characterization of selected hits, we discovered two main classes of compounds characterized by the presence of a hydroxamate-based ZBG attached to a spiroindoline (**18a**,**b**) or tricyclic thieno[3,2-*b*]indole (**19a**,**b**,**c**) or indoline (**20**) core as cap groups. Some of the compounds were deeply studied and displayed to affect the viability of larval, juvenile, and adult schistosomes, to impact egg production *in vitro* and/or to induce morphological alterations of the adult schistosome reproductive systems. Of note, all of them inhibit the recombinant form of *Sm*HDAC8 enzyme *in vitro*.[67]

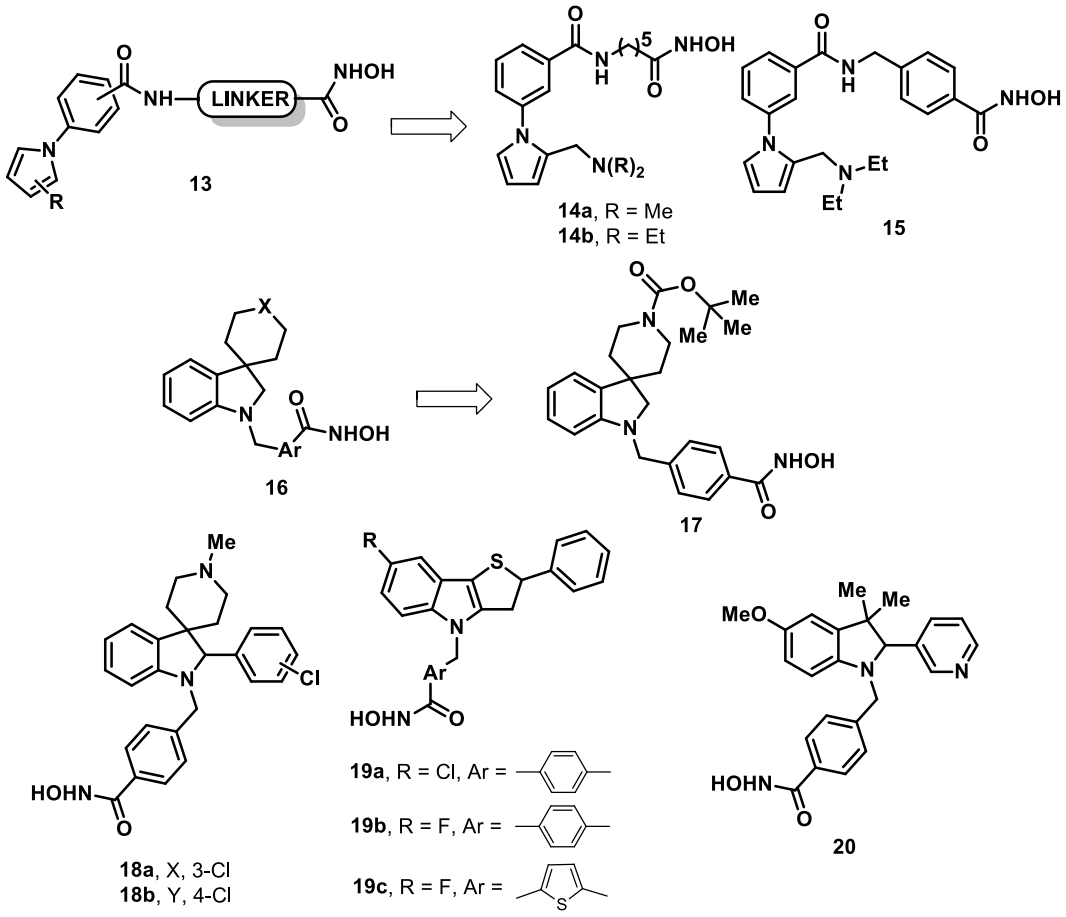

Figure 4. Previously explored compounds as selective HDAC inhibitors in cancer (**14**-**17**) and schistosomiasis (**18**-**20**)

2.1.7 β-lactams as anticancer agents

The family of beta-lactams have been used for many years to treat bacterial infections. Traditional betalactam antibiotics, such as penicillins (**21a**,**b**, **Figure 5**) and cephalosporins (**22**) contain a carboxyl group in close proximity to the lactam nitrogen, which is required for antimicrobial activity.[68] A potent β-lactam-based monoacylglycerol lipase (MGL) inhibitor (**23**) was characterized by Brindisi *et. al.*. Mode-of-action studies demonstrated the **23** by blocking MGL, increases 2-arachidonoylglycerol and behaves as a receptor. Administration of **23** in mice suffering from experimental autoimmune encephalitis ameliorates the severity of the clinical symptoms in a cannabinoid -dependent manner.[69]

The *N*-thiolated beta-lactams (**24a**,**b**), induce tumor cell apoptosis by introducing DNA damage in a potent, and more importantly, a tumor cell-specific manner with little or no effect on normal cells.[70] Cainelli *et al*., describe that 4-alkylidene-betalactams (**25** and **26**) inhibit matrix metalloproteinases-2, and -9, essential for the tumor induced neovascularization.[71] Banik *et al*., also show that beta-lactams with polyaromatic

substituents (**27**) induce tumor cell death in a variety of cancer cell lines, such as ovarian, prostate, breast, colon, and leukemic *in vitro* and demonstrated the inhibition of tumor cell growth in mice.[72]

In the context of HDAC inhibition, Reddy *et al.* synthesized β-lactam compounds (**28**) as dual inhibitor with cancer cell toxicity by restraining the NF-κB transcription factor mediated by HDAC inhibition.[73] *N*-thiomethyl-β-lactam (**29**-**32**) has also been reported as a ZBG in the design of new selective HDAC8 inhibitors.[74] Several lactam-based HDAC inhibitors have also been reported by numerous eorks.[75–77]

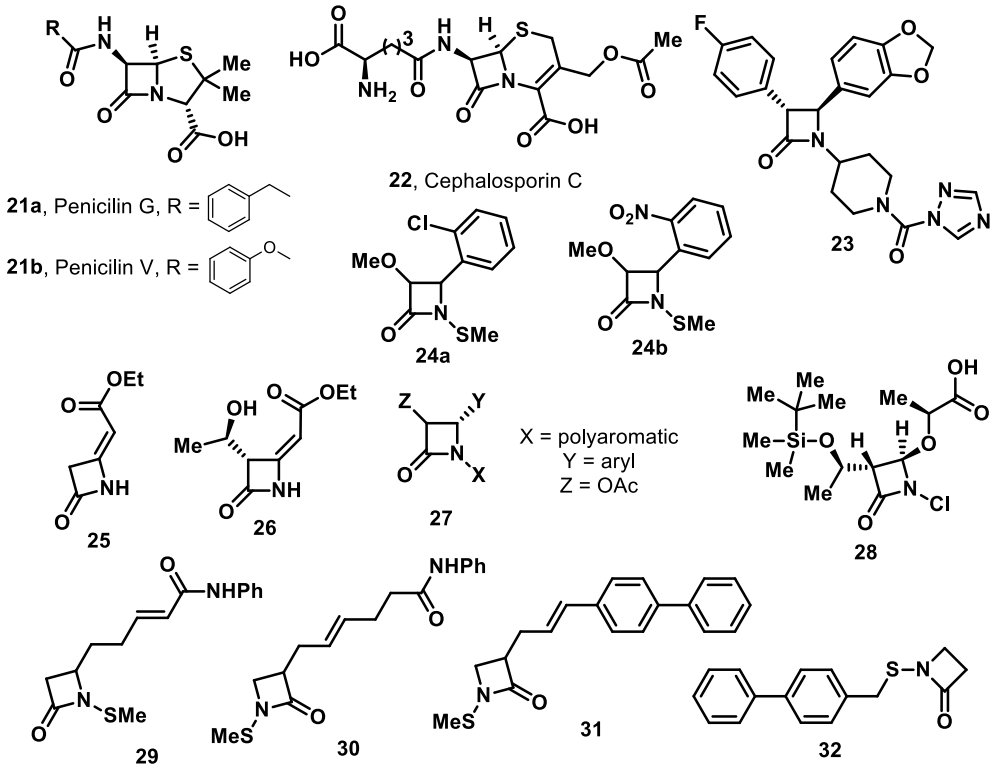

Figure 5. Available β-lactams as antibiotics (**21**-**22**), monoacylglycerol lipase inhibitor (**23**), anticancer agents (**24**-**28**), and HDAC inhibitor (**29**-**32**).

PART 2 CHAPTER II
AIM OF THE PROJECT

We concentrated on the development of HDAC6 selective inhibitors, bearing a β-lactam core structure. After performing a molecular modelling approach, we designed a series of compounds with different cap groups and linkers while retaining the hydroxamic acid as the common ZBG. This project was collectively developed by a direct and active involvement of many of our research group members. Beside my Marie-Curie TRACT project (Part1), I have synthesized four of the designed compounds (**Figure 6**).

The cap group is mainly represented by a β-lactam core with either a germinal *bis*(phenyl) (**33** and **34**) or vicinal *bis*(phenyl) (**35** and **36**) groups; offering a trans-isomeric form in the later. For the linker, either an *N*-benzylpiperidine-1-carboxamide (**33-35**) or *N*-tolylpiperidine-1-carboxamide (**36**) moiety was used.

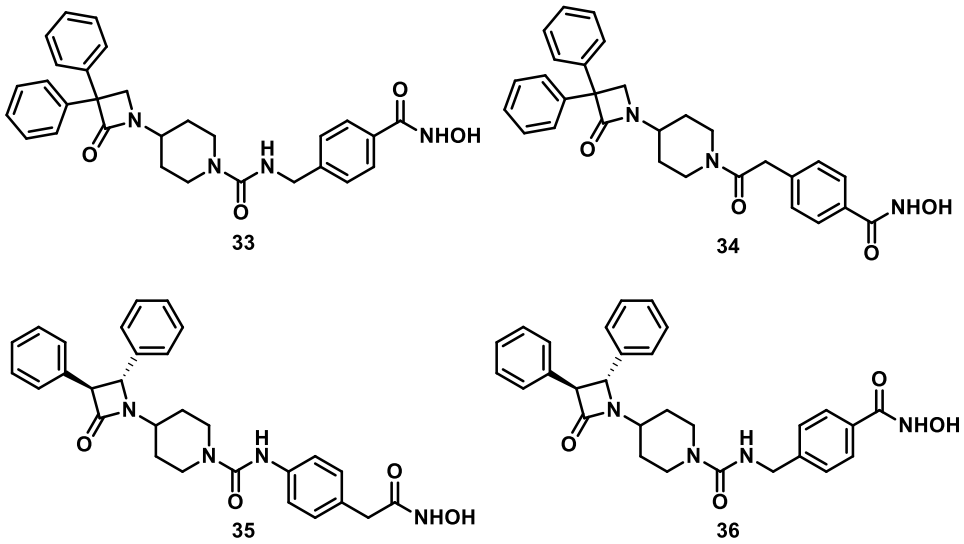

Figure 6. Designed HDAC6 selective inhibitors

PART 2 CHAPTER III

CHEMISTRY

A described in the **Scheme 1**, the synthesis of the intermediate **42** started from the commercially available 1-benzylpiperidin-4-amine, **37**, which was converted to a dimethylimidodithioate derivative **38** in presence of carbon disulfide and methyl iodide. **38** was then submitted to a non-photochemical [2+2] cycloaddition (also known as Staudinger ketene-imine cycloaddition or Staudinger synthesis) with 2,2-diphenylacetic acid (**39**, to produce the *in situ* ketene) and triphosgene to yield the β-lactam core **40**.[69,78] A selective reduction of *bis*(thiomethyl) group of **40** was achieved in presence of nickelchloride hexahydrate and sodium borohydride to produce the geminal *bis*(phenyl) derivative **41**, which after treatment with palladium in carbon under hydrogen pressure produced the key intermediate **42**.

Scheme 1. Synthesis of the intermediate **42**

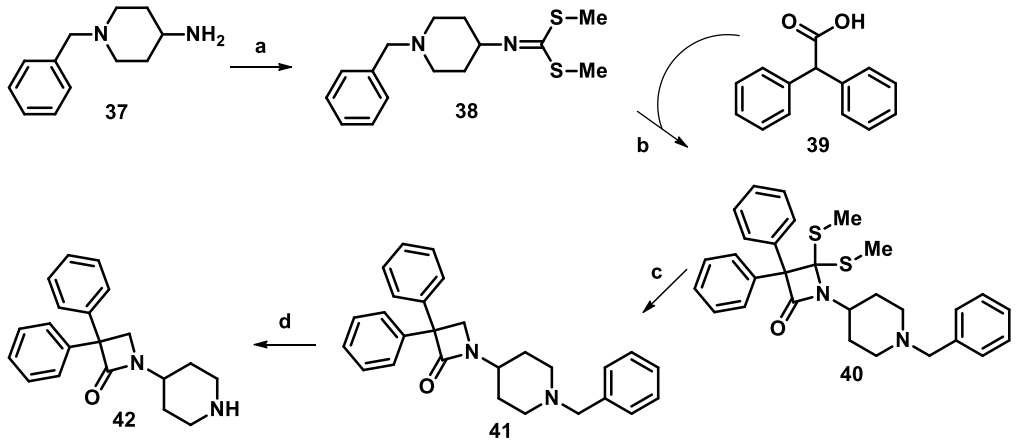

Reagents and Conditions: (a) i) CS_2, NaOH (20 M aqueous solution), toluene, 0 °C, 5 min; ii) MeI, TEBA, toluene, 20 °C, 30 min, quantitative; (b) triphosgene, TEA, dry DCM, 50 °C, 12 h, 52%; (c) $NiCl_2.6H_2O$, $NaBH_4$, MeOH, THF, 25 °C, 12 h, 20%; (d) Pd-C, H_2, MeOH, 12 h, quantitative.

Compound **44** was synthesized from our already developed β-lactam core compound **43** after the debenzylation on the piperidine moiety with 1-chloroethylchloroformate (**Scheme 2**).[69,79]

Scheme 2. Synthesis of intermediate **44**

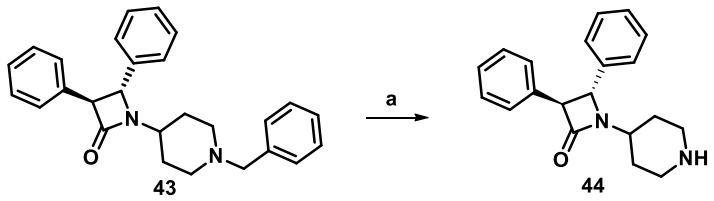

Reagents and Conditions: (a) i) 1-chloroethylchloroformate, dry DCM, 0 °C; ii) MeOH, 65 °C, 1 h, 50%.

Synthesis of the isocyanate intermediate **48** is described in **Scheme 3**. Commercially available methyl 4-(bromomethyl)benzoate, **45** was treated with sodium azide in dry DMF under reflux condition at 80 °C to produce the corresponding azide **46**. A Staudinger reaction on **46** in presence of triphenyl phosphine converted the azide group into the amine.[80] Compound **47** was treated with phosgene for the formation of isocyanate intermediate **48**, which was immediately used for the next step.

Scheme 3. Synthesis of the intermediate **48**

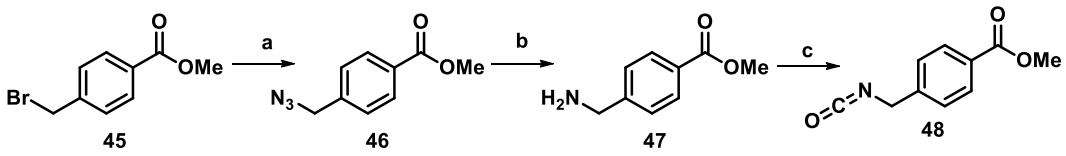

Reagents and Conditions: (a) NaN_3, dry DMF, 80 °C, 12 h, quantitative; (b) PPh_3, THF, H_2O, 25 °C, 12 h, 52%; (c) $COCl_2$ (20% in toluene), dry DCM, $NaHCO_3$ (s.s), 0 °C, 10 min, quantitative.

Scheme 4. Synthesis of **50** and **53**

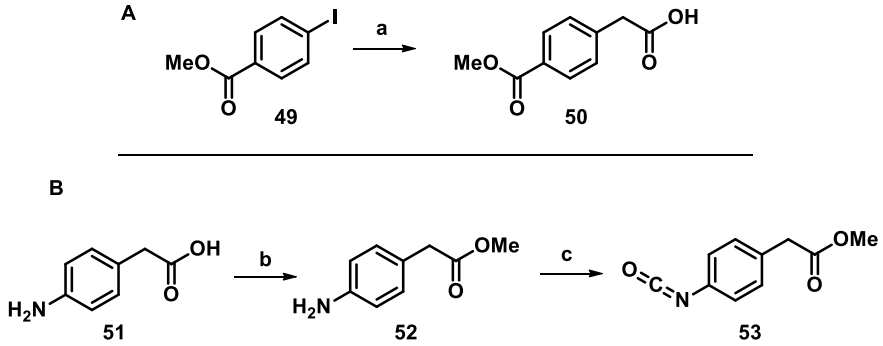

Reagents and Conditions: (a) $PdCl_2$, AgOAc, NaOAc, AcOH, 110 °C, 36 h, 20%; (b) $SOCl_2$, MeOH, 0 °C to 65 °C, 12 h, 92%; (c) $COCl_2$ (20% in toluene), dry DCM, $NaHCO_3$ (s.s), 0 °C, 10 min, quantitative.

As described in **Scheme 4**, intermediate **50** was synthesized directly from the commercially available methyl 4-iodobenzoate, **49** after refluxing it with silver and sodium

acetate with palladium chloride in acetic acid at 110 °C. Whereas, 2-(4-aminophenyl)acetic acid **51** was esterified to afford **52**, which underwent the used procedure in presence of phosgene for the preparation of **53**.

The synthesis of the final compounds **33** and **34** is described in the **Scheme 5**. The connecting urea bond in **54** was built up in the presence of the activated isocyanate **48**, the free piperidine containing compound **42**, and TEA operating at reflux condition in dry THF solution. Whereas, the amide containing compounds **55** was synthesized by reacting **42** and the phenylacetic acid compound **50** in the presences of EDCI, HOBt and DIPEA in dry DCM at room temperature. Both the compound **54** and **55** were converted into their hydroxamic acid derivatives **33** and **34**, respectively after treatment with hydroxyl amine and methanolic potassium hydroxide in DCM medium at room temperature.

Scheme 5. Synthesis of final compounds **33** and **34**

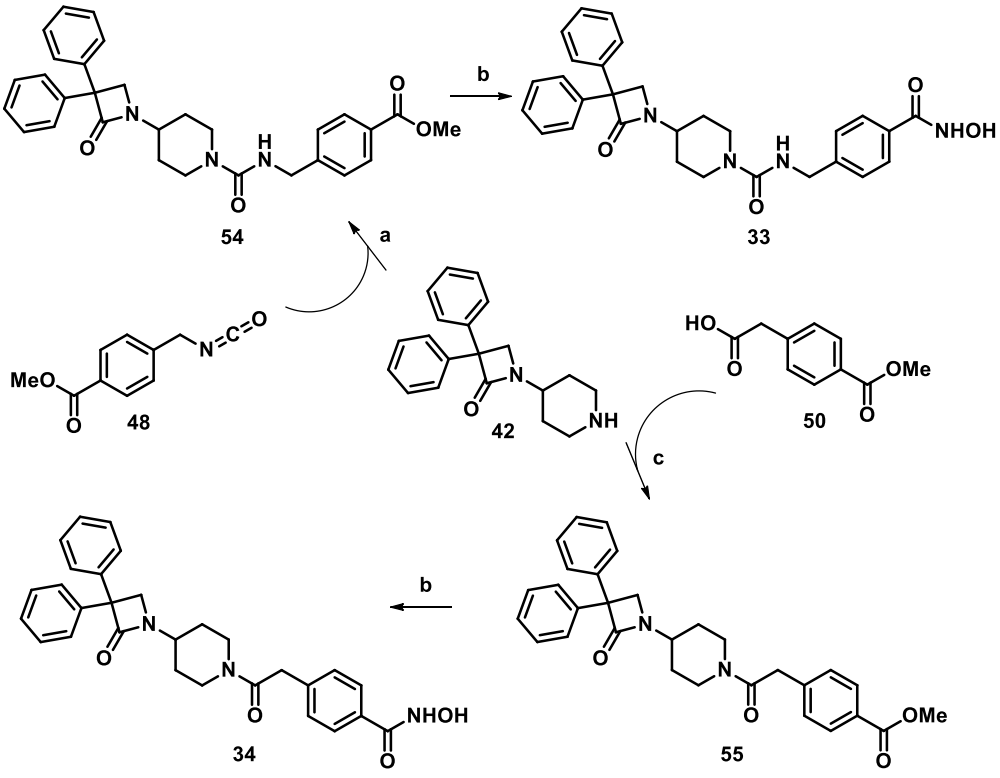

Reagents and conditions: (a) TEA, dry THF, 65 °C, 1.5 h, quantitative; (b) DCM, MeOH, NH_2OH, KOH (4 M in MeOH), quantitative; (c) DIPEA, EDCI, HOBt, dry DCM, 0 °C (15 min) to 25 °C (12 h), 60%.

The synthesis of final compounds **35** and **36** (**Scheme 6**) was accomplished from the intermediates **44**, **48**, and **53** by following the same approach as described for the synthesis of the urea compound **34**, described in **Scheme 5**.

Scheme 6. Synthesis of the final compounds **35** and **36**

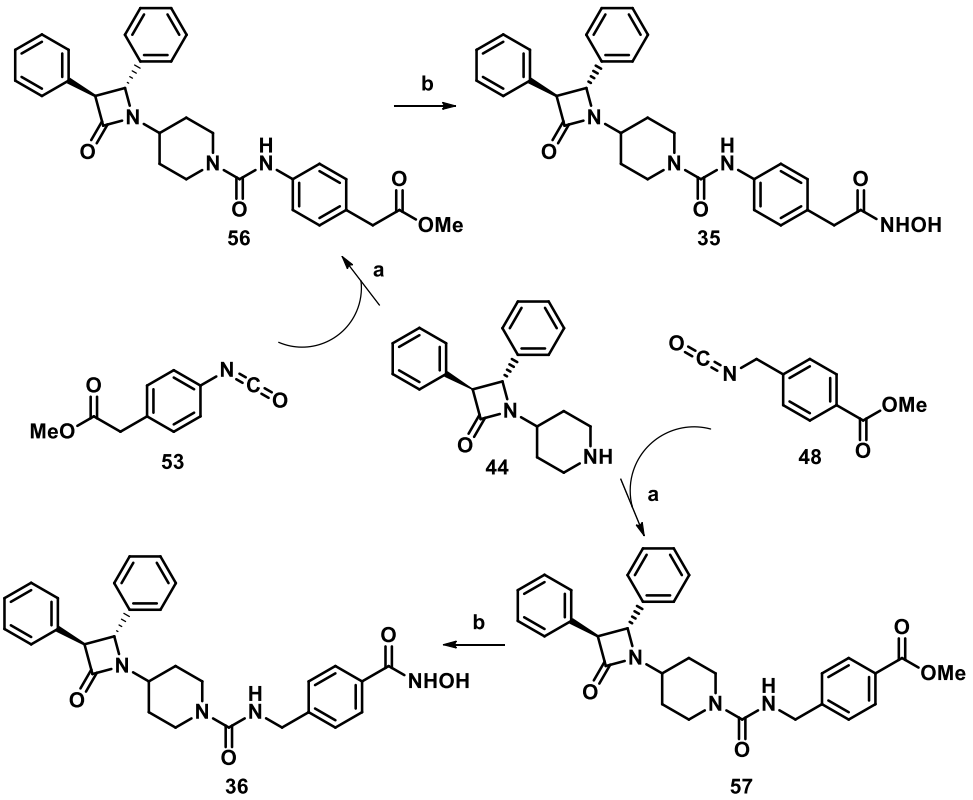

Reagents and conditions: (a) TEA, dry THF, 65 °C, 1.5 h, quantitative; (b) DCM, MeOH, NH_2OH, KOH (4 M in MeOH), quantitative.

PART 2 CHAPTER IV
RESULTS AND CONCLUSIONS

2.4.1. Results

All the synthesized compounds have been tested for their inhibitory effect on HDAC1 and HDAC6 isoforms (**Table 2**). Compound **33** proved to be 1265-fold selective for HDAC6 over HDAC1 with the IC_{50} value of 3.4 ± 0.8 nM. While compound **34** and **36** also selectively inhibited HDAC6 over HDAC1 with IC_{50} value of 91 ± 7 nM and 21 ± 1 nM, respectively. Compound **35** did not display any remarkable inhibition in these enzymatic studies.

Table 2. IC_{50} value assessment of the synthesized compounds on HDAC1 and HDAC6

Cpds	**HDAC1 IC_{50} µM (inhibition %, tested dose)**	**HDAC6 IC_{50} nM (inhibition %, tested dose)**	**Selectivity**
33	4.3 ± 0.3	3.4 ± 0.8	1265 fold
34	9.7 ± 3.9	91 ± 7	106 fold
36	4.2 ± 0.2	21 ± 1	200 fold
35	82.7% @ 50 µM 53.3% @ 10 µM 23.6%, @ 1 µM	102.6%, @ 50 µM 94.2%, @ 10 µM 60.2%, @ 1 µM	Not calculated

In addition, the X-ray crystallographic study of the best performing compounds **33** and **36** has been conducted with 1.8Å and 2.0Å value.

2.4.2 Conclusions

In conclusion, I have participated to the development of selective inhibitors of HDAC6 through the synthesis of a set of β-lactam cored compounds. The newly developed structures were inspired to the scaffold of a previously developed inhibitor identified by our research group. All the compounds have been tested for the individual inhibitory effect on both HDAC1 and HDAC6. The best compound **33** showed an IC_{50} value of 3.4 nM on HDAC6 with 1265-fold selectivity over the HDAC1 isoform. The two best performing compounds (**33** and **36**) have also been subjected to X-ray crystallographic studies. Further characterizations for ascertaining potential therapeutic applications are currently ongoing.

PART 2 CHAPTER V

EXPERIMENTAL SECTION

General Remarks

All chemicals and reagents were purchased from the commercial suppliers and used without further purification, unless and otherwise specified. Reaction progress was observed by thin-layer chromatography (TLC), carried out on silica (60 F254) or alumina (60 F254, basic) gel plates with detection by UV and the products were purified by means of either silica (60M, 0.040-0.063 μm) or alumina (90, standarized) column chromatography. ^{1}H and ^{13}C NMR spectra were documented in the indicated deuteriated solvent on a Varian 300 MHz or a Bruker 400 MHz spectrometer by using the residual signal of the deuterated solvent as internal standard. Splitting patterns are indicated by s (singlet), d (doublet), dd (doublet of doublets), t (triplet), q (quartet), m (multiplet), and br (broad); chemical shifts (δ) are defined in parts per million (ppm) and coupling constants (J) in Hertz (Hz). ESI-MS spectra were performed by an Agilent 1100 Series LC/MSD spectrometer. HRESIMS were carried out by a Thermo Finningan LCQ Deca XP Max ion-trap mass spectrometer equipped with Xcalibur software, operated in positive ion mode and conducted at the University of Naples, Italy. Yields denote to purified products. HPLC analysis were performed with a Shimadzu Prominence apparatus equipped with a scanning absorbance UV-VIS detector (Diode Array SPD-M20A) also equipped with a thermostatic chamber and Purospher®STAR, RP-18ε (5 μM) HPLC column. All moisture-sensitive reactions were executed under nitrogen atmosphere using oven-dried glassware and freshly distilled dry solvents.

*Dimethyl (1-benzylpiperidin-4-yl)carbonimidodithioate (**38**)*

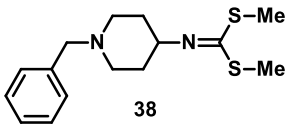

38

A solution of NaOH (10mL, 20 M aqueous) was added to the commercially available **37** (1000 mg, 5.26 mmol) at 0 °C and stirred for 5 min. A solution of carbon disulfide (400 mg, 5.26 mmol) in toluene (3 mL) was added to the reaction mixture, followed by a fast addition of methyl iodide (983 μL, 15.78 mmol) in toluene (3 mL) at room temperature and stirred for another 5 min. After that, benzyltriethylammonium chloride (120 mg, 0.526 mmol) was added to the reaction mixture and stirred for another 30 min. Toluene was

removed completely under reduced pressure. The crude was dissolved in Et_2O, washed with water, dried over anhydrous sodium sulfate, filtered, and concentrated to obtain the compound **38** in quantitative yield which was used in the next step without any further purification. ^{1}H NMR (300 MHz, $CDCl_3$) δ: 7.44-7.28 (m, 5H), 3.793.63 (m, 1H), 3.53 (d, *J* = 10.2 Hz, 2H), 2.91-2.78 (m, 2H), 2.55 (s, 3H), 2.37 (s, 3H), 2.30- 2.11 (m, 2H), 1.88-1.61 (m, 4H); ESI-MS *m/z* 294.8 $[M+H]^+$.

*1-(1-Benzylpiperidin-4-yl)-4,4-bis(methylthio)-3,3-diphenylazetidin-2-one (**40**)*

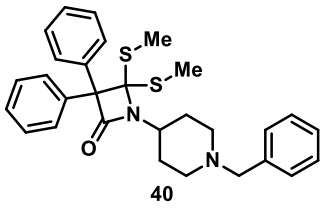

40

Triphosgene (227 mg, 0.765 mmol) was added to a solution of **39** (486 mg, 2.29 mmol) in dry DCM (9.3 mL) at room temperature and heated at 50 °C for 30 min. A solution of **38** (450 mg, 1.53 mmol) in dry DCM (9.3 mL) and TEA (640 µL, 4.59 mmol) was added to the reaction mixture and refluxed for 12 h. A saturated solution of $NaHCO_3$ was added slowly to the cooled down mixture at room temperature and the compound was extracted out with DCM (3 x 15 mL). The combined organic layers was dried over anhydrous sodium sulfate, filtered, and concentrated. The residue was purified with a silica gel column chromatography (DCM/Acetone 40:1) to obtain the product **40** in 52% yield. ^{1}H NMR (300 MHz, $CDCl_3$) δ: 7.73 (d, *J* = 7.0 Hz, 4H), 7.42-7.20 (m, 11H), 3.54 (s, 2H), 3.27 (dt, *J* = 19.8, 7.9 Hz, 1H), 3.00 (d, *J* = 11.7 Hz, 2H), 2.66-2.46 (m, 2H), 2.11-1.92 (m, 4H), 1.73 (s, 6H); ESI-MS *m/z* 488.9 $[M+H]^+$.

*1-(1-Benzylpiperidin-4-yl)-3,3-diphenylazetidin-2-one (**41**)*

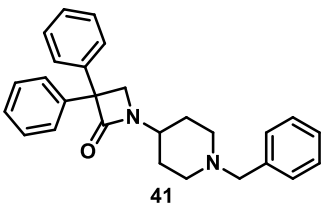

41

Nickel (II) chloride hexahydrate (730 mg, 3.069 mmol) and sodium borohydride (348 mg, 9.21 mmol) was added to a solution of **40** (300 mg, 0.614 mmol) in methanol (32 mL) and THF (8 mL) solution at room temperature and stirred for 2 h. After that, the reaction was quenched with a slow addition of water and extracted with EtOAc, dried over anhydrous

sodium sulfate, filtered, and concentrated. The residue was purified on a silica gel column chromatography (PE/EtOAc 1:1) to afford the compound **41** in 20% yield. ^{1}H NMR (300 MHz, $CDCl_3$) δ: 7.49-7.16 (m, 15H), 3.85 (s, 2H), 3.82-3.67 (m, 1H), 3.50 (s, 2H), 2.90 (d, *J* = 12.0 Hz, 2H), 2.07 (tt, *J* = 11.1, 5.5 Hz, 2H), 1.93-1.63 (m, 4H). ESI-MS *m/z* 396.9 $[M+H]^+$.

*3,3-Diphenyl-1-(piperidin-4-yl)azetidin-2-one (**42**)*

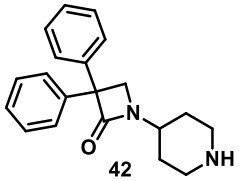

42

Catalytic amount of 10% Pd/C was added to a solution of **41** (250 mg, 0.631 mmol) in methanol (25 mL) at room temperature under nitrogen atmosphere. The mixture was stirred under hydrogen pressure for 12 h. Methanol was removed completely under reduced pressure; residue was diluted with EtOAc, filtered, and concentrated to obtain the compound **42** in quantitative yield. ^{1}H NMR (300 MHz, $CDCl_3$) δ: 7.49-7.16 (m, 15H), 3.85 (s, 2H), 3.82-3.67 (m, 1H), 3.50 (s, 2H), 2.90 (d, *J* = 12.0 Hz, 2H), 2.07 (tt, *J* = 11.1, 5.5 Hz, 2H), 1.93-1.63 (m, 4H). ESI-MS *m/z* 307.0 $[M+H]^+$.

*3,4-Diphenyl-1-(piperidin-4-yl)azetidin-2-one (**44**)*

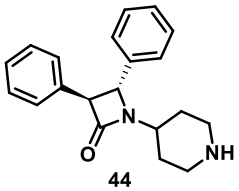

44

1-chloroethylchloroformate (30 μL, 0.271 mmol) was added to the solution of **43** (100 mg, 0.251 mmol) in dry DCM (2.5 mL) at 0 °C and stirred for 2 h at the same temperature. After that, solvent was evaporated completely at room temperature under reduced pressure and the crude was dissolved in methanol (5 mL) and refluxed at 65 °C for 1 h. Solvent was removed completely to afford the product in 50% yield. ^{1}H NMR (300 MHz, CD_3OD) δ: 7.49-7.17 (m, 10H), 4.65 (d, *J* = 2.2 Hz, 1H), 4.12 (t, *J* = 2.8 Hz, 1H), 3.94 (ddd, *J* = 19.3, 7.9, 3.6 Hz, 2H), 3.68 (tdd, *J* = 11.9, 8.0, 3.7 Hz, 1H), 2.92-2.70 (m, 2H), 1.87 (ddt, *J* = 42.0, 33.7, 16.1 Hz, 3H), 1.53-1.23 (m, 1H); ESI-MS *m/z* 307.0 $[M+H]^+$.

*Methyl 4-(azidomethyl)benzoate (**46**)*

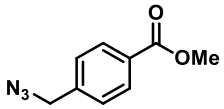

46

Sodium azide (283 mg, 4.355 mmol) was added to a solution of **45** (200 mg, 0.871 mmol) in dry DMF (1 mL) and refluxed at 90 °C for 12 h. Water was added at room temperature and the product was extracted out with EtOAc (3 x 10 mL). The combined organic layer was dried over anhydrous sodium sulfate, filtered, and concentrated to afford the title compound **46** in quantitative yield. ^{1}H NMR (300 MHz, ($(CD_3)_2CO$) δ: 8.08-7.97 (m, 2H), 7.54-7.44 (m, 2H), 4.54 (s, 2H), 3.90-3.83 (m, 3H).

*Methyl 4-(aminomethyl)benzoate (**47**)*

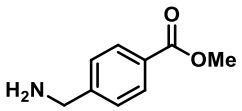

47

Triphenylphosphine (301 mg, 1.151 mmol) was added to a solution of **46** (200 mg, 1.046 mmol) in THF (4.5 mL) and water (0.7 mL) at room temperature and stirred for 12 h. Solution was diluted with water and then acidified to pH = 2 with a solution of 1(N) HCl. Aqueous solution was washed with Et_2O and then 1(M) NaOH was added to basify until pH = 9, extracted with DCM, dried over anhydrous sodium sulfate, filtered, and concentrated to afford the title compound in 52% yield. ^{1}H NMR (300 MHz, $CDCl_3$) δ: 8.02-7.88 (m, 2H), 7.34 (d, *J* = 8.1 Hz, 2H), 3.94-3.81 (m, 5H), 1.67 (s, 2H).

*Methyl 4-(isocyanatomethyl)benzoate (**48**)*

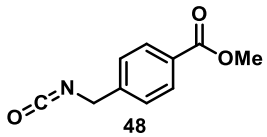

48

A saturated solution of $NaHCO_3$ (1.4 mL) was added to a solution of **47** (25 mg, 0.151 mmol) in dry DCM (1.4 mL) at 0 °C and stirred for 10 min. After that, the stirring was stopped completely and a solution of phosgene (37 μL, 0.303 mmol) in 20% toluene was added directly to the lower organic layer. Reaction mixture was stirred for another 15 min and extracted with DCM. The combined organic layer was dried over anhydrous sodium sulfate, filtered, and concentrated at room temperature. Toluene was removed completely form the crude of **48** under high vacuum and used for the next reaction immediately.

*2-(4-(Methoxycarbonyl)phenyl)acetic acid (**50**)*

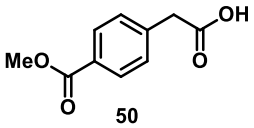

50

Sillver acetate (283 mg, 1.705 mmol), sodium acetate (468 mg, 5.707 mmol), and palladium chloride (20 mg, 0.113 mmol) was added to a suspension of **49** (300 mg, 1.141 mmol) in acetic acid (3 mL) and refluxed at 110 °C for 36 h. A saturated solution of NH_4Cl was added to the reaction mixture at room temperature and extracted with EtOAc (3 x 10 mL), dried over anhydrous sodium sulfate, filtered, and concentrated. The residue was purified with silica gel column chromatography (PE/EtOAc 1:1) to afford the compound **50** in 20% yield. ^{1}H NMR (300 MHz, $CDCl_3$) δ: 8.02-7.96 (m, 2H), 7.27-7.24 (m, 2H), 3.88 (d, *J* = 4.8 Hz, 3H), 3.76 (s, 2H).

*Methyl 2-(4-aminophenyl)acetate (**52**)*

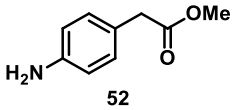

52

Thionyl chloride (0.3 mL, 4.000 mL) was added to a solution of **51** (200 mg, 1.321 mmol) in methanol (3 mL) at 0 °C and then was refluxed at 65 °C for 12 h. A saturated solution of $NaHCO_3$ was added to the reaction mixture at room temperature and methanol was removed completely under reduced pressure. Aqueous solution was extracted with DCM and the combined organic layer was dried over anhydrous sodium sulfate, filtered, and concentrated. The residue was purified on a silica gel column chromatography (DCM/MeOH 20:1) to afford the compound **52** in 92% yield. ^{1}H NMR (300 MHz, $CDCl_3$) δ: 7.05 (d, *J* = 8.3 Hz, 2H), 6.60 (t, *J* = 9.5 Hz, 2H), 3.65 (d, *J* = 12.6 Hz, 5H), 3.51 (s, 2H). ESI-MS *m/z* 166.1 $[M+H]^+$.

*Methyl 2-(4-isocyanatophenyl)acetate (**53**)*

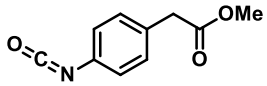

53

The compound **53** was synthesized from the amine **52** by following the same procedure as describe for the synthesis of **48**.

*Methyl 4-((4-(2-oxo-3,3-diphenylazetidin-1-yl)piperidine-1-carboxamido)methyl)benzoate (**54**)*

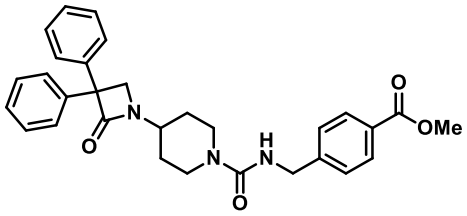

54

A solution of **48** (0.151 mmol) in dry THF (0.8 mL) was added to a solution of **42** (23 mg, 0.075 mmol) in dry THF (0.8 mL), followed by the addition of TEA (42 µL, 0.298 mmol). The reaction mixture was then refluxed at 65 °C for 1.5h. Solvent was removed completely under reduced pressure and the crude was purified on silica gel column chromatography (DCM/MeOH 10:1) to afford the compound **54** in quantitative yield. ^{1}H NMR (300 MHz, CD_3OD) δ: 7.93 (d, *J* = 8.0 Hz, 2H), 7.41-7.13 (m, 12H), 4.42-4.30 (m, 2H), 3.98 (t, *J* = 15.9 Hz, 2H), 3.92-3.83 (m, 5H), 3.83-3.69 (m, 1H), 2.96-2.81 (m, 2H), 1.94-1.50 (m, 4H). ESI-MS *m/z* 498.7 $[M+H]^+$.

*N-(4-(Hydroxycarbamoyl)benzyl)-4-(2-oxo-3,3-diphenylazetidin-1-yl)piperidine-1-carboxamide (**33**)*

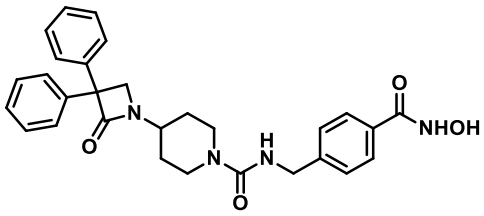

33

Hydroxyl amine (660 µL, 10.049 mmol) was added to a solution of **54** (50 mg, 0.100 mmol) in DCM (4 mL) and methanol (2 mL) at room temperature, followed by a dropwise addition of methanolic KOH (4M, 1.3 mL) solution and the reaction mixture was stirred for 3 h. After that, a solution of 1(N) HCl was added to the reaction mixture to reach the pH at 5-6. The solvent was removed completely under reduced pressure. The residue was purified on a silica gel flash column chromatography (DCM/MeOH/NH_4OH 10:1:0.1) to obtain the title compound in quantitative yield. ^{1}H NMR (300 MHz, DMSO) δ: 11.16-10.97 (m, 1H), 8.94 (s, 1H), 7.89 (s, 1H), 7.65 (d, *J* = 8.2 Hz, 2H), 7.43-7.17 (m, 10H), 7.11 (d, *J* = 5.7 Hz, 2H), 4.64-4.48 (m, 1H), 4.23 (d, *J* = 5.4 Hz, 2H), 4.00-3.82 (m, 3H), 3.78-3.59 (m, 4H), 2.78 (dd, *J* = 26.3, 15.2 Hz, 8H), 1.75 (d, *J* = 10.2 Hz, 6H), 1.51 (d, *J* =

11.5 Hz, 7H).^{13}C NMR (75 MHz, CD_3OD) δ: 169.9, 166.6, 158.3, 154.7, 144.4, 140.2, 130.5, 128.3, 127.0, 126.9, 126.8 (2C), 64.4, 52.3, 49.8, 43.6, 42.3, 29.1, 20.1, 13.4. ESI-MS *m/z* 496.2 $[M-H]^-$.

*Methyl 4-(2-oxo-2-(4-(2-oxo-3,3-diphenylazetidin-1-yl)piperidin-1-yl)ethyl)benzoate (**55**)*

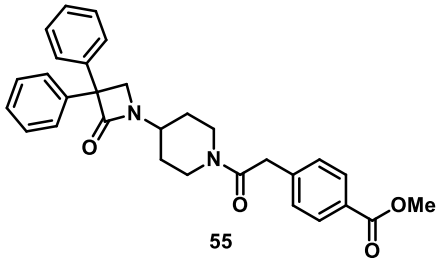

55

DIPEA (90 μL, 0.521 mmol), EDCI (31 mg, 0.162 mmol), and HOBt (27 mg, 0.201 mmol) were added sequentially into a solution of **50** (25 mg, 0.131 mmol) in dry DCM (2 mL) at 0 °C and stirred for 15 min. A solution of **42** (50 mg, 0.161 mmol) in dry DCM (2 mL) was added to the reaction mixture at the same temperature and then stirred at room temperature for 12 h. Reaction mixture was washed with a saturated solution of NH_4Cl, $NaHCO_3$, brine, dried over anhydrous sodium sulfate, filtered, and concentrated. The reaction crude was purified on a silica gel column chromatography (DCM/MeOH 50:1) to get the final compound **55** in 60% yield. ^{1}H NMR (300 MHz, $CDCl_3$) δ: 8.03-7.94 (m, 2H), 7.43-7.15 (m, 12H), 4.52 (d, *J* = 13.5 Hz, 1H), 3.95-3.86 (m, 3H), 3.86-3.79 (m, 2H), 3.79-3.70 (m, 3H), 3.16-2.99 (m, 1H), 2.94-2.69 (m, 1H), 1.85 (t, *J* = 14.4 Hz, 3H), 1.67-1.31 (m, 2H). ESI-MS *m/z* 482.8 $[M+H]^+$.

*N-Hydroxy-4-(2-oxo-2-(4-(2-oxo-3,3-diphenylazetidin-1-yl)piperidin-1-yl)ethyl)benzamide (**34**)*

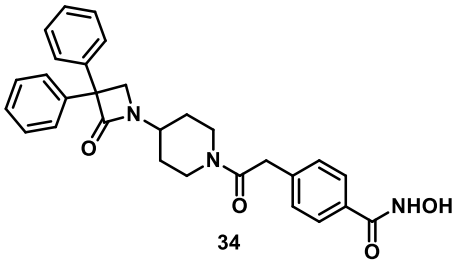

34

The title compound **34** was synthesized in quantitative yield from **55** by following the same procedure as described for **33**. ^{1}H NMR (300 MHz, DMSO) δ: 11.23-10.97 (m, 1H), 8.97 (s, 1H), 7.66 (d, *J* = 8.2 Hz, 2H), 7.39-7.09 (m, 12H), 4.24 (d, *J* = 12.4 Hz, 1H), 3.94-3.63 (m, 5H), 3.27 (dd, *J* = 1.1, 0.6 Hz, 1H), 3.17-2.99 (m, 1H), 2.78-2.61 (m, 1H), 1.74 (s,

2H), 1.48 (dd, *J* = 19.9, 11.4 Hz, 2H); ^{13}C NMR (75 MHz, CD_3OD) δ: 169.9, 158.3, 144.3, 140.2, 130.6, 128.3, 126.9, 126.9, 126.8, 64.5, 52.3, 49.8, 43.5, 42.3, 29.1. ESI-MS *m/z* 481.1 $[M-H]^-$.

*Methyl 2-(4-(4-(2-oxo-3,4-diphenylazetidin-1-yl)piperidine-1-carboxamido)phenyl)acetate (**56**)*

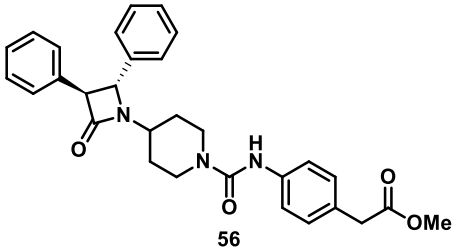

56

Compound **56** was synthesized from **44** and **53** by using the same procedure as described for **54** in quantitative yield. ^{1}H NMR (300 MHz, CD_3OD) δ: 7.97-7.87 (m, 2H), 7.48-7.20 (m, 10H), 7.13-6.99 (m, 2H), 4.69-4.61 (m, 1H), 4.37-4.31 (m, 2H), 4.14-4.08 (m, 1H), 4.07-3.96 (m, 1H), 3.91-3.82 (m, 4H), 2.83 (ddd, *J* = 18.6, 13.7, 2.7 Hz, 2H), 2.05-1.69 (m, 3H), 1.40 (ddd, *J* = 37.3, 20.6, 12.4 Hz, 2H). ESI-MS *m/z* 498.0 $[M+H]^+$.

*N-(4-(2-(Hydroxyamino)-2-oxoethyl)phenyl)-4-(2-oxo-3,4-diphenylazetidin-1-yl)piperidine-1-carboxamide (**35**)*

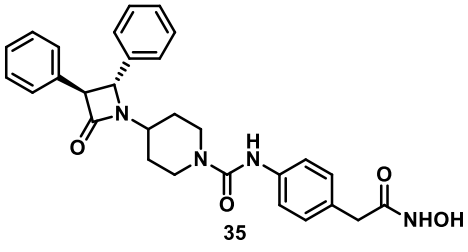

35

The title compound **35** was synthesized in quantitative yield from **56** by following the same procedure as described for **33**. ^{1}H NMR (300 MHz, CD_3OD) δ: 7.55-6.92 (m, 14H), 4.67 (d, *J* = 2.1 Hz, 1H), 4.15-3.88 (m, 3H), 3.78-3.57 (m, 1H), 3.32 (s, 2H), 2.90 (ddd, *J* = 17.2, 14.1, 7.2 Hz, 2H), 2.08-1.68 (m, 3H), 1.49 (ddd, *J* = 24.3, 11.9, 3.9 Hz, 1H); ^{13}C NMR (75 MHz, CD_3OD) δ: 169.6, 169.5, 156.2, 138.4, 138.3, 134.8, 129.5, 128.8, 128.7, 128.6, 128.5, 127.4, 127.1, 126.4, 120.8, 63.9, 63.2, 51.2, 42.8, 42.6, 38.6, 30.0, 29.6. ESI-MS *m/z* 481.1 $[M-H]^-$.

*Methyl 4-((4-(2-oxo-3,4-diphenylazetidin-1-yl)piperidine-1-carboxamido)methyl)benzoate (**57**)*

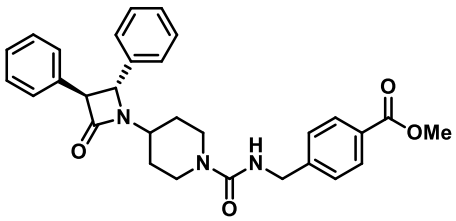

57

Compound **57** was synthesized from **44** by using the same procedure as described for **55** in quantitative yield. ^{1}H NMR (300 MHz, CD_3OD) δ: 7.99-7.86 (m, 2H), 7.49-7.20 (m, 12H), 4.64 (t, *J* = 4.9 Hz, 1H), 4.35 (s, 2H), 4.12 (t, *J* = 2.8 Hz, 1H), 4.08-3.85 (m, 5H), 3.68 (tdd, *J* = 11.9, 8.0, 3.7 Hz, 1H), 2.96-2.70 (m, 2H), 2.05-1.70 (m, 2H), 1.57-1.23 (m, 2H). ESI-MS *m/z* 498.0 $[M+H]^+$.

*N-(4-(Hydroxycarbamoyl)benzyl)-4-(2-oxo-3,4-diphenylazetidin-1-yl)piperidine-1-carboxamide (**36**)*

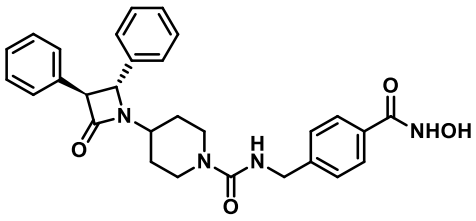

36

The title compound **36** was synthesized in quantitative yield from **57** by following the same procedure as described for **33**. ^{1}H NMR (300 MHz, DMSO) δ: 11.12 (s, 1H), 8.95 (s, 1H), 7.64 (d, *J* = 8.1 Hz, 2H), 7.51-7.16 (m, 10H), 7.12-6.98 (m, 2H), 4.71 (d, *J* = 2.0 Hz, 1H), 4.19 (d, *J* = 5.5 Hz, 2H), 4.11 (s, 1H), 3.87 (dd, *J* = 33.8, 13.3 Hz, 2H), 3.63-3.44 (m, 1H), 2.71 (dd, *J* = 25.3, 12.0 Hz, 2H), 1.96-1.55 (m, 4H); ^{13}C NMR (75 MHz, DMSO) δ: 168.1, 164.6, 157.4, 144.8, 139.5, 135.8, 131.4, 129.3, 129.2, 128.9, 127.9, 127.2, 63.9, 61.8, 51.0, 43.7, 42.8, 42.7, 30.5, 30.0. ESI-MS *m/z* 481.1 $[M-H]^-$.

PART 2 ABBREVIATIONS

AIF	Allograft inflammatory factor 1
Akt	Protein kinase B
Apaf-1	Apoptotic peptidase activating factor 1
ATG	Autophagy related genes
Bax	Bcl2 associated X
BMF	Bcl2 modifying factor
CDH1	Epithelial-cadherin
CDK	cyclin-dependent kinase
DCM	Dichloromethane
DIPEA	*N*,*N*-Diisopropylethylamine
DMF	*N*,*N*-Dimethylformamide
DNA	Deoxyribonucleic acid
DR5	Death receptor 5
EDCI	1-Ethyl-3-(3-dimethylaminopropyl)carbodiimide
EMT	Epithelial-to-mesenchymal transition
ESI-MS	Electrospray ionization mass spectroscopy
HATs	Histone acetyltransferases
HDACs	Histone deacetylases
HDACi	Histone deacetylase inhibitors
HIF-1α	Hypoxia-inducible factors 1 α
HMGA2	High Mobility Group AT-Hook 2
HOBt	Hydroxybenzotriazole
HPLC	High pressure liquid chromatography
HRESI-MS	High resolution electrospray ionization mass spectroscopy
Hsp70	Heat shock protein 70
IC_{50}	Half maximal inhibitory concentration
LC3-II	Light chain 3-II
LC/MSD	Liquid chromatography/mass selective detector
MAPK	mitogen-activated protein kinase
MGL	monoacylglycerol lipase

MHz	Megahertz
Mi-2/NRD	Nucleosome remodeling and deacetylation
mTOR	Mammalian/mechanistic target of rapamycin
NAD	Nicotinamide adenine dinucleotide
N-CoR	Nuclear receptor co-repressor
NF-κB	Nuclear factor kappa-light-chain-enhancer of activated B cells
PI3K	Phosphoinositide 3-kinase
PRC2	polycomb repressive complex 2
SIRTs	Sirtuins
*Sm*HDAC8	Schistosoma mansoni histone deacetylase 8
TEA	Triethylamine
TEBA	Benzyltriethylammonium chloride
THF	Tetrahydrofuran
TLC	Thin-layer chromatography
TRAIL	Tumor necrosis factor -related apoptosis-inducing ligand
UV-VIS	Ultraviolet-visible
ZBG	Zinc binding group

PART 2 REFERENCES

(1) Yang, X.-J.; Seto, E. HATs and HDACs: From Structure, Function and Regulation to Novel Strategies for Therapy and Prevention. *Oncogene* **2007**, *26* (37), 5310–5318. https://doi.org/10.1038/sj.onc.1210599.

(2) Oppermann, U. Why Is Epigenetics Important in Understanding the Pathogenesis of Inflammatory Musculoskeletal Diseases? *Arthritis Res. Ther.* **2013**, *15* (2), 209. https://doi.org/10.1186/ar4186.

(3) Oehme, I.; Deubzer, H. E.; Wegener, D.; Pickert, D.; Linke, J.-P.; Hero, B.; Kopp-Schneider, A.; Westermann, F.; Ulrich, S. M.; von Deimling, A.; et al. Histone Deacetylase 8 in Neuroblastoma Tumorigenesis. *Clin. Cancer Res.* **2009**, *15* (1), 91–99. https://doi.org/10.1158/1078-0432.CCR-08-0684.

(4) Xu, W. S.; Parmigiani, R. B.; Marks, P. A. Histone Deacetylase Inhibitors: Molecular Mechanisms of Action. *Oncogene* **2007**, *26* (37), 5541–5552. https://doi.org/10.1038/sj.onc.1210620.

(5) Nebbioso, A.; Tambaro, F. P.; Dell'Aversana, C.; Altucci, L. Cancer Epigenetics: Moving Forward. *PLoS Genet.* **2018**, *14* (6), e1007362. https://doi.org/10.1371/journal.pgen.1007362.

(6) Sharma, S.; Kelly, T. K.; Jones, P. A. Epigenetics in Cancer. *Carcinogenesis* **2010**, *31* (1), 27–36. https://doi.org/10.1093/carcin/bgp220.

(7) Parra, M.; Verdin, E. Regulatory Signal Transduction Pathways for Class IIa Histone Deacetylases. *Curr. Opin. Pharmacol.* **2010**, *10* (4), 454–460. https://doi.org/10.1016/j.coph.2010.04.004.

(8) Haberland, M.; Montgomery, R. L.; Olson, E. N. The Many Roles of Histone Deacetylases in Development and Physiology: Implications for Disease and Therapy. *Nat. Rev. Genet.* **2009**, *10* (1), 32–42. https://doi.org/10.1038/nrg2485.

(9) Yang, X.-J.; Seto, E. The Rpd3/Hda1 Family of Lysine Deacetylases: From Bacteria and Yeast to Mice and Men. *Nat. Rev. Mol. Cell Biol.* **2008**, *9* (3), 206–218. https://doi.org/10.1038/nrm2346.

(10) Barneda-Zahonero, B.; Parra, M. Histone Deacetylases and Cancer. *Mol. Oncol.* **2012**, *6* (6), 579–589. https://doi.org/10.1016/j.molonc.2012.07.003.

(11) Smith, B. C.; Denu, J. M. Chemical Mechanisms of Histone Lysine and Arginine Modifications. *Biochim. Biophys. Acta* **2009**, *1789* (1), 45–57. https://doi.org/10.1016/j.bbagrm.2008.06.005.

(12) Parbin, S.; Kar, S.; Shilpi, A.; Sengupta, D.; Deb, M.; Rath, S. K.; Patra, S. K. Histone Deacetylases: A Saga of Perturbed Acetylation Homeostasis in Cancer. *J. Histochem. Cytochem.* **2014**, *62* (1), 11–33. https://doi.org/10.1369/0022155413506582.

(13) Witt, O.; Deubzer, H. E.; Milde, T.; Oehme, I. HDAC Family: What Are the Cancer Relevant Targets? *Cancer Lett.* **2009**, *277* (1), 8–21. https://doi.org/10.1016/j.canlet.2008.08.016.

(14) Herceg, Z.; Ushijima, T. Introduction: Epigenetics and Cancer. *Advances in genetics*. United States 2010, pp 1–23. https://doi.org/10.1016/B978-0-12-380866-0.60001-0.

(15) Baxter, E.; Windloch, K.; Gannon, F.; Lee, J. S. Epigenetic Regulation in Cancer Progression. *Cell Biosci.* **2014**, *4* (1), 45. https://doi.org/10.1186/2045-3701-4-45.

(16) Chun, P. Histone Deacetylase Inhibitors in Hematological Malignancies and Solid Tumors. *Arch. Pharm. Res.* **2015**, *38* (6), 933–949. https://doi.org/10.1007/s12272-015-0571-1.

(17) Fan, J.; Lou, B.; Chen, W.; Zhang, J.; Lin, S.; Lv, F.; Chen, Y. Down-Regulation of HDAC5 Inhibits Growth of Human Hepatocellular Carcinoma by Induction of Apoptosis and Cell Cycle Arrest. *Tumour Biol.* **2014**, *35* (11), 11523–11532. https://doi.org/10.1007/s13277-014-2358-2.

(18) Senese, S.; Zaragoza, K.; Minardi, S.; Muradore, I.; Ronzoni, S.; Passafaro, A.; Bernard, L.; Draetta, G. F.; Alcalay, M.; Seiser, C.; et al. Role for Histone Deacetylase 1 in Human Tumor Cell Proliferation. *Mol. Cell. Biol.* **2007**, *27* (13), 4784–4795. https://doi.org/10.1128/MCB.00494-07.

(19) Li, Y.; Peng, L.; Seto, E. Histone Deacetylase 10 Regulates the Cell Cycle G2/M Phase Transition via a Novel Let-7-HMGA2-Cyclin A2 Pathway. *Mol. Cell. Biol.* **2015**, *35* (20), 3547–3565. https://doi.org/10.1128/MCB.00400-15.

(20) Vidal-Laliena, M.; Gallastegui, E.; Mateo, F.; Martinez-Balbas, M.; Pujol, M. J.; Bachs, O. Histone Deacetylase 3 Regulates Cyclin A Stability. *J. Biol. Chem.* **2013**, *288* (29), 21096–21104. https://doi.org/10.1074/jbc.M113.458323.

(21) Zhang, J.; Zhong, Q. Histone Deacetylase Inhibitors and Cell Death. *Cell. Mol. Life Sci.* **2014**, *71* (20), 3885–3901. https://doi.org/10.1007/s00018-014-1656-6.

(22) Riley, J. S.; Hutchinson, R.; McArt, D. G.; Crawford, N.; Holohan, C.; Paul, I.; Van Schaeybroeck, S.; Salto-Tellez, M.; Johnston, P. G.; Fennell, D. A.; et al. Prognostic and Therapeutic Relevance of FLIP and Procaspase-8 Overexpression in Non-Small

Cell Lung Cancer. *Cell Death Dis.* **2013**, *4* (12), e951–e951. https://doi.org/10.1038/cddis.2013.481.

(23) Schuler, S.; Fritsche, P.; Diersch, S.; Arlt, A.; Schmid, R. M.; Saur, D.; Schneider, G. HDAC2 Attenuates TRAIL-Induced Apoptosis of Pancreatic Cancer Cells. *Mol. Cancer* **2010**, *9*, 80. https://doi.org/10.1186/1476-4598-9-80.

(24) Jung, K. H.; Noh, J. H.; Kim, J. K.; Eun, J. W.; Bae, H. J.; Xie, H. J.; Chang, Y. G.; Kim, M. G.; Park, H.; Lee, J. Y.; et al. HDAC2 Overexpression Confers Oncogenic Potential to Human Lung Cancer Cells by Deregulating Expression of Apoptosis and Cell Cycle Proteins. *J. Cell. Biochem.* **2012**, *113* (6), 2167–2177. https://doi.org/10.1002/jcb.24090.

(25) Kim, J. K.; Noh, J. H.; Eun, J. W.; Jung, K. H.; Bae, H. J.; Shen, Q.; Kim, M. G.; Chang, Y. G.; Kim, S.-J.; Park, W. S.; et al. Targeted Inactivation of HDAC2 Restores P16INK4a Activity and Exerts Antitumor Effects on Human Gastric Cancer. *Mol. Cancer Res.* **2013**, *11* (1), 62–73. https://doi.org/10.1158/1541-7786.MCR-12-0332.

(26) Kang, Y.; Nian, H.; Rajendran, P.; Kim, E.; Dashwood, W. M.; Pinto, J. T.; Boardman, L. A.; Thibodeau, S. N.; Limburg, P. J.; Löhr, C. V; et al. HDAC8 and STAT3 Repress BMF Gene Activity in Colon Cancer Cells. *Cell Death Dis.* **2014**, *5* (10), e1476–e1476. https://doi.org/10.1038/cddis.2014.422.

(27) Koeneke, E.; Witt, O.; Oehme, I. HDAC Family Members Intertwined in the Regulation of Autophagy: A Druggable Vulnerability in Aggressive Tumor Entities. *Cells* **2015**, *4* (2), 135–168. https://doi.org/10.3390/cells4020135.

(28) Xie, H. J.; Noh, J. H.; Kim, J. K.; Jung, K. H.; Eun, J. W.; Bae, H. J.; Kim, M. G.; Chang, Y. G.; Lee, J. Y.; Park, H.; et al. HDAC1 Inactivation Induces Mitotic Defect and Caspase-Independent Autophagic Cell Death in Liver Cancer. *PLoS One* **2012**, *7* (4), e34265. https://doi.org/10.1371/journal.pone.0034265.

(29) Moresi, V.; Carrer, M.; Grueter, C. E.; Rifki, O. F.; Shelton, J. M.; Richardson, J. A.; Bassel-Duby, R.; Olson, E. N. Histone Deacetylases 1 and 2 Regulate Autophagy Flux and Skeletal Muscle Homeostasis in Mice. *Proc. Natl. Acad. Sci. U. S. A.* **2012**, *109* (5), 1649–1654. https://doi.org/10.1073/pnas.1121159109.

(30) Lee, J.-Y.; Koga, H.; Kawaguchi, Y.; Tang, W.; Wong, E.; Gao, Y.-S.; Pandey, U. B.; Kaushik, S.; Tresse, E.; Lu, J.; et al. HDAC6 Controls Autophagosome Maturation Essential for Ubiquitin-Selective Quality-Control Autophagy. *EMBO J.* **2010**, *29* (5), 969–980. https://doi.org/10.1038/emboj.2009.405.

(31) Lee, J.-Y.; Nagano, Y.; Taylor, J. P.; Lim, K. L.; Yao, T.-P. Disease-Causing Mutations in Parkin Impair Mitochondrial Ubiquitination, Aggregation, and HDAC6-Dependent Mitophagy. *J. Cell Biol.* **2010**, *189* (4), 671–679. https://doi.org/10.1083/jcb.201001039.

(32) Yang, F.-C.; Tan, B. C.-M.; Chen, W.-H.; Lin, Y.-H.; Huang, J.-Y.; Chang, H.-Y.; Sun, H.-Y.; Hsu, P.-H.; Liou, G.-G.; Shen, J.; et al. Reversible Acetylation Regulates Salt-Inducible Kinase (SIK2) and Its Function in Autophagy. *J. Biol. Chem.* **2013**, *288* (9), 6227–6237. https://doi.org/10.1074/jbc.M112.431239.

(33) Oehme, I.; Linke, J.-P.; Bock, B. C.; Milde, T.; Lodrini, M.; Hartenstein, B.; Wiegand, I.; Eckert, C.; Roth, W.; Kool, M.; et al. Histone Deacetylase 10 Promotes Autophagy-Mediated Cell Survival. *Proc. Natl. Acad. Sci. U. S. A.* **2013**, *110* (28), E2592-601. https://doi.org/10.1073/pnas.1300113110.

(34) Huang, R.; Xu, Y.; Wan, W.; Shou, X.; Qian, J.; You, Z.; Liu, B.; Chang, C.; Zhou, T.; Lippincott-Schwartz, J.; et al. Deacetylation of Nuclear LC3 Drives Autophagy Initiation under Starvation. *Mol. Cell* **2015**, *57* (3), 456–466. https://doi.org/10.1016/j.molcel.2014.12.013.

(35) Zhou, Z.-W.; Li, X.-X.; He, Z.-X.; Pan, S.-T.; Yang, Y.; Zhang, X.; Chow, K.; Yang, T.; Qiu, J.-X.; Zhou, Q.; et al. Induction of Apoptosis and Autophagy via Sirtuin1- and PI3K/Akt/MTOR-Mediated Pathways by Plumbagin in Human Prostate Cancer Cells. *Drug Des. Devel. Ther.* **2015**, *9*, 1511–1554. https://doi.org/10.2147/DDDT.S75976.

(36) Li, Y.; Seto, E. HDACs and HDAC Inhibitors in Cancer Development and Therapy. *Cold Spring Harb. Perspect. Med.* **2016**, *6* (10). https://doi.org/10.1101/cshperspect.a026831.

(37) Yoo, Y.-G.; Kong, G.; Lee, M.-O. Metastasis-Associated Protein 1 Enhances Stability of Hypoxia-Inducible Factor-1alpha Protein by Recruiting Histone Deacetylase 1. *EMBO J.* **2006**, *25* (6), 1231–1241. https://doi.org/10.1038/sj.emboj.7601025.

(38) Geng, H.; Harvey, C. T.; Pittsenbarger, J.; Liu, Q.; Beer, T. M.; Xue, C.; Qian, D. Z. HDAC4 Protein Regulates HIF1alpha Protein Lysine Acetylation and Cancer Cell Response to Hypoxia. *J. Biol. Chem.* **2011**, *286* (44), 38095–38102. https://doi.org/10.1074/jbc.M111.257055.

(39) Chen, I.-C.; Chiang, W.-F.; Huang, H.-H.; Chen, P.-F.; Shen, Y.-Y.; Chiang, H.-C. Role of SIRT1 in Regulation of Epithelial-to-Mesenchymal Transition in Oral

Squamous Cell Carcinoma Metastasis. *Mol. Cancer* **2014**, *13*, 254. https://doi.org/10.1186/1476-4598-13-254.

(40) Kato, H.; Tamamizu-Kato, S.; Shibasaki, F. Histone Deacetylase 7 Associates with Hypoxia-Inducible Factor 1alpha and Increases Transcriptional Activity. *J. Biol. Chem.* **2004**, *279* (40), 41966–41974. https://doi.org/10.1074/jbc.M406320200.

(41) Seo, H.-W.; Kim, E.-J.; Na, H.; Lee, M.-O. Transcriptional Activation of Hypoxia-Inducible Factor-1alpha by HDAC4 and HDAC5 Involves Differential Recruitment of P300 and FIH-1. *FEBS Lett.* **2009**, *583* (1), 55–60. https://doi.org/10.1016/j.febslet.2008.11.044.

(42) Aldana-Masangkay, G. I.; Sakamoto, K. M. The Role of HDAC6 in Cancer. *Biomed Res. Int.* **2010**, *2011*.

(43) Zhang, X.; Yuan, Z.; Zhang, Y.; Yong, S.; Salas-Burgos, A.; Koomen, J.; Olashaw, N.; Parsons, J. T.; Yang, X.-J.; Dent, S. R.; et al. HDAC6 Modulates Cell Motility by Altering the Acetylation Level of Cortactin. *Mol. Cell* **2007**, *27* (2), 197–213. https://doi.org/10.1016/j.molcel.2007.05.033.

(44) Saji, S.; Kawakami, M.; Hayashi, S.-I.; Yoshida, N.; Hirose, M.; Horiguchi, S.-I.; Itoh, A.; Funata, N.; Schreiber, S. L.; Yoshida, M.; et al. Significance of HDAC6 Regulation via Estrogen Signaling for Cell Motility and Prognosis in Estrogen Receptor-Positive Breast Cancer. *Oncogene* **2005**, *24* (28), 4531–4539. https://doi.org/10.1038/sj.onc.1208646.

(45) Kaluza, D.; Kroll, J.; Gesierich, S.; Yao, T.-P.; Boon, R. A.; Hergenreider, E.; Tjwa, M.; Rossig, L.; Seto, E.; Augustin, H. G.; et al. Class IIb HDAC6 Regulates Endothelial Cell Migration and Angiogenesis by Deacetylation of Cortactin. *EMBO J.* **2011**, *30* (20), 4142–4156. https://doi.org/10.1038/emboj.2011.298.

(46) Bolden, J. E.; Peart, M. J.; Johnstone, R. W. Anticancer Activities of Histone Deacetylase Inhibitors. *Nat. Rev. Drug Discov.* **2006**, *5* (9), 769–784. https://doi.org/10.1038/nrd2133.

(47) Spiegel, S.; Milstien, S.; Grant, S. Endogenous Modulators and Pharmacological Inhibitors of Histone Deacetylases in Cancer Therapy. *Oncogene* **2012**, *31* (5), 537–551. https://doi.org/10.1038/onc.2011.267.

(48) Ai, J.; Wang, Y.; Dar, J. A.; Liu, J.; Liu, L.; Nelson, J. B.; Wang, Z. HDAC6 Regulates Androgen Receptor Hypersensitivity and Nuclear Localization via Modulating Hsp90 Acetylation in Castration-Resistant Prostate Cancer. *Mol. Endocrinol.* **2009**, *23* (12), 1963–1972. https://doi.org/10.1210/me.2009-0188.

(49) Perego, P.; Cossa, G.; Zuco, V.; Zunino, F. Modulation of Cell Sensitivity to Antitumor Agents by Targeting Survival Pathways. *Biochem. Pharmacol.* **2010**, *80* (10), 1459–1465.

(50) Lee, J.-H.; Choy, M. L.; Ngo, L.; Foster, S. S.; Marks, P. A. Histone Deacetylase Inhibitor Induces DNA Damage, Which Normal but Not Transformed Cells Can Repair. *Proc. Natl. Acad. Sci.* **2010**, *107* (33), 14639–14644.

(51) Suzuki, T. Explorative Study on Isoform-Selective Histone Deacetylase Inhibitors. *Chem. Pharm. Bull. (Tokyo).* **2009**, *57* (9), 897–906. https://doi.org/10.1248/cpb.57.897.

(52) Butler, K. V; Kozikowski, A. P. Chemical Origins of Isoform Selectivity in Histone Deacetylase Inhibitors. *Curr. Pharm. Des.* **2008**, *14* (6), 505–528. https://doi.org/10.2174/138161208783885353.

(53) Robey, R. W.; Chakraborty, A. R.; Basseville, A.; Luchenko, V.; Bahr, J.; Zhan, Z.; Bates, S. E. Histone Deacetylase Inhibitors: Emerging Mechanisms of Resistance. *Mol. Pharm.* **2011**, *8* (6), 2021–2031. https://doi.org/10.1021/mp200329f.

(54) Haggarty, S. J.; Koeller, K. M.; Wong, J. C.; Grozinger, C. M.; Schreiber, S. L. Domain-Selective Small-Molecule Inhibitor of Histone Deacetylase 6 (HDAC6)-Mediated Tubulin Deacetylation. *Proc. Natl. Acad. Sci. U. S. A.* **2003**, *100* (8), 4389–4394. https://doi.org/10.1073/pnas.0430973100.

(55) Haggarty, S. J.; Koeller, K. M.; Wong, J. C.; Butcher, R. A.; Schreiber, S. L. Multidimensional Chemical Genetic Analysis of Diversity-Oriented Synthesis-Derived Deacetylase Inhibitors Using Cell-Based Assays. *Chem. Biol.* **2003**, *10* (5), 383–396. https://doi.org/10.1016/s1074-5521(03)00095-4.

(56) Hideshima, T.; Bradner, J. E.; Wong, J.; Chauhan, D.; Richardson, P.; Schreiber, S. L.; Anderson, K. C. Small-Molecule Inhibition of Proteasome and Aggresome Function Induces Synergistic Antitumor Activity in Multiple Myeloma. *Proc. Natl. Acad. Sci. U. S. A.* **2005**, *102* (24), 8567–8572. https://doi.org/10.1073/pnas.0503221102.

(57) Schäfer, S.; Saunders, L.; Eliseeva, E.; Velena, A.; Jung, M.; Schwienhorst, A.; Strasser, A.; Dickmanns, A.; Ficner, R.; Schlimme, S. Phenylalanine-Containing Hydroxamic Acids as Selective Inhibitors of Class IIb Histone Deacetylases (HDACs). *Bioorg. Med. Chem.* **2008**, *16* (4), 2011–2033.

(58) Schäfer, S.; Saunders, L.; Schlimme, S.; Valkov, V.; Wagner, J. M.; Kratz, F.; Sippl, W.; Verdin, E.; Jung, M. Pyridylalanine- containing Hydroxamic Acids as Selective

HDAC6 Inhibitors. *ChemMedChem Chem. Enabling Drug Discov.* **2009**, *4* (2), 283–290.

(59) Kozikowski, A. P.; Tapadar, S.; Luchini, D. N.; Kim, K. H.; Billadeau, D. D. Use of the Nitrile Oxide Cycloaddition (NOC) Reaction for Molecular Probe Generation: A New Class of Enzyme Selective Histone Deacetylase Inhibitors (HDACIs) Showing Picomolar Activity at HDAC6. *J. Med. Chem.* **2008**, *51* (15), 4370–4373.

(60) Smil, D. V; Manku, S.; Chantigny, Y. A.; Leit, S.; Wahhab, A.; Yan, T. P.; Fournel, M.; Maroun, C.; Li, Z.; Lemieux, A.-M. Novel HDAC6 Isoform Selective Chiral Small Molecule Histone Deacetylase Inhibitors. *Bioorg. Med. Chem. Lett.* **2009**, *19* (3), 688–692.

(61) Butler, K. V; Kalin, J.; Brochier, C.; Vistoli, G.; Langley, B.; Kozikowski, A. P. Rational Design and Simple Chemistry Yield a Superior, Neuroprotective HDAC6 Inhibitor, Tubastatin A. *J. Am. Chem. Soc.* **2010**, *132* (31), 10842–10846. https://doi.org/10.1021/ja102758v.

(62) Dallavalle, S.; Cincinelli, R.; Nannei, R.; Merlini, L.; Morini, G.; Penco, S.; Pisano, C.; Vesci, L.; Barbarino, M.; Zuco, V. Design, Synthesis, and Evaluation of Biphenyl-4-Yl-Acrylohydroxamic Acid Derivatives as Histone Deacetylase (HDAC) Inhibitors. *Eur. J. Med. Chem.* **2009**, *44* (5), 1900–1912.

(63) Zuco, V.; De Cesare, M.; Cincinelli, R.; Nannei, R.; Pisano, C.; Zaffaroni, N.; Zunino, F. Synergistic Antitumor Effects of Novel HDAC Inhibitors and Paclitaxel in Vitro and in Vivo. *PLoS One* **2011**, *6* (12).

(64) Auzzas, L.; Larsson, A.; Matera, R.; Baraldi, A.; Deschênes-Simard, B.; Giannini, G.; Cabri, W.; Battistuzzi, G.; Gallo, G.; Ciacci, A. Non-Natural Macrocyclic Inhibitors of Histone Deacetylases: Design, Synthesis, and Activity. *J. Med. Chem.* **2010**, *53* (23), 8387–8399.

(65) Brindisi, M.; Cavella, C.; Brogi, S.; Nebbioso, A.; Senger, J.; Maramai, S.; Ciotta, A.; Iside, C.; Butini, S.; Lamponi, S.; et al. Phenylpyrrole-Based HDAC Inhibitors: Synthesis, Molecular Modeling and Biological Studies. *Future Med. Chem.* **2016**, *8* (13), 1573–1587. https://doi.org/10.4155/fmc-2016-0068.

(66) Brindisi, M.; Senger, J.; Cavella, C.; Grillo, A.; Chemi, G.; Gemma, S.; Cucinella, D. M.; Lamponi, S.; Sarno, F.; Iside, C.; et al. Novel Spiroindoline HDAC Inhibitors: Synthesis, Molecular Modelling and Biological Studies. *Eur. J. Med. Chem.* **2018**, *157*, 127–138. https://doi.org/https://doi.org/10.1016/j.ejmech.2018.07.069.

(67) Saccoccia, F.; Brindisi, M.; Gimmelli, R.; Relitti, N.; Guidi, A.; Saraswati, A. P.; Cavella, C.; Brogi, S.; Chemi, G.; Butini, S. Screening and Phenotypical Characterization of Schistosoma Mansoni Histone Deacetylase 8 (Sm HDAC8) Inhibitors as Multistage Antischistosomal Agents. *ACS Infect. Dis.* **2019**.

(68) Kuhn, D.; Coates, C.; Daniel, K.; Chen, D.; Bhuiyan, M.; Kazi, A.; Turos, E.; Dou, Q. P. Beta-Lactams and Their Potential Use as Novel Anticancer Chemotherapeutics Drugs. *Front Biosci* **2004**, *9*, 2605–2617.

(69) Brindisi, M.; Maramai, S.; Gemma, S.; Brogi, S.; Grillo, A.; Di Cesare Mannelli, L.; Gabellieri, E.; Lamponi, S.; Saponara, S.; Gorelli, B. Development and Pharmacological Characterization of Selective Blockers of 2-Arachidonoyl Glycerol Degradation with Efficacy in Rodent Models of Multiple Sclerosis and Pain. *J. Med. Chem.* **2016**, *59* (6), 2612–2632.

(70) Kazi, A.; Hill, R.; Long, T. E.; Kuhn, D. J.; Turos, E.; Dou, Q. P. Novel N-Thiolated β-Lactam Antibiotics Selectively Induce Apoptosis in Human Tumor and Transformed, but Not Normal or Nontransformed, Cells. *Biochem. Pharmacol.* **2004**, *67* (2), 365–374.

(71) Cainelli, G.; Galletti, P.; Garbisa, S.; Giacomini, D.; Sartor, L.; Quintavalla, A. 4-Alkylidene-Azetidin-2-Ones: Novel Inhibitors of Leukocyte Elastase and Gelatinase. *Bioorg. Med. Chem.* **2003**, *11* (24), 5391–5399.

(72) Banik, I.; Becker, F. F.; Banik, B. K. Stereoselective Synthesis of β-Lactams with Polyaromatic Imines: Entry to New and Novel Anticancer Agents. *J. Med. Chem.* **2003**, *46* (1), 12–15.

(73) Reddy, C. B. R.; Reddy, S. R.; Suthindhiran, K.; Sivakumar, A. HDAC and NF-KB Mediated Cytotoxicity Induced by Novel N-Chloro β-Lactams and Benzisoxazole Derivatives. *Chem. Biol. Interact.* **2016**, *246*, 69–76.

(74) Galletti, P.; Quintavalla, A.; Ventrici, C.; Giannini, G.; Cabri, W.; Penco, S.; Gallo, G.; Vincenti, S.; Giacomini, D. Azetidinones as Zinc- Binding Groups to Design Selective HDAC8 Inhibitors. *ChemMedChem* **2009**, *4* (12), 1991–2001.

(75) Taddei, M.; Cini, E.; Giannotti, L.; Giannini, G.; Battistuzzi, G.; Vignola, D.; Vesci, L.; Cabri, W. Lactam Based 7-Amino Suberoylamide Hydroxamic Acids as Potent HDAC Inhibitors. *Bioorg. Med. Chem. Lett.* **2014**, *24* (1), 61–64. https://doi.org/https://doi.org/10.1016/j.bmcl.2013.11.072.

(76) Choi, E.; Lee, C.; Park, J. E.; Seo, J. J.; Cho, M.; Kang, J. S.; Kim, H. M.; Park, S.-K.; Lee, K.; Han, G. Structure and Property Based Design, Synthesis and Biological

Evaluation of γ-Lactam Based HDAC Inhibitors. *Bioorg. Med. Chem. Lett.* **2011**, *21* (4), 1218–1221. https://doi.org/https://doi.org/10.1016/j.bmcl.2010.12.079.

(77) Kim, H. M.; Lee, K.; Park, B. W.; Ryu, D. K.; Kim, K.; Lee, C. W.; Park, S.-K.; Han, J. W.; Lee, H. Y.; Lee, H. Y.; et al. Synthesis, Enzymatic Inhibition, and Cancer Cell Growth Inhibition of Novel δ-Lactam-Based Histone Deacetylase (HDAC) Inhibitors. *Bioorg. Med. Chem. Lett.* **2006**, *16* (15), 4068–4070. https://doi.org/https://doi.org/10.1016/j.bmcl.2006.04.091.

(78) Hart, D. J.; Ha, D. C. The Ester Enolate-Imine Condensation Route to. Beta.-Lactams. *Chem. Rev.* **1989**, *89* (7), 1447–1465.

(79) Badiola, K. A.; Quan, D. H.; Triccas, J. A.; Todd, M. H. Efficient Synthesis and Anti-Tubercular Activity of a Series of Spirocycles: An Exercise in Open Science. *PLoS One* **2014**, *9* (12).

(80) Lin, F. L.; Hoyt, H. M.; van Halbeek, H.; Bergman, R. G.; Bertozzi, C. R. Mechanistic Investigation of the Staudinger Ligation. *J. Am. Chem. Soc.* **2005**, *127* (8), 2686–2695. https://doi.org/10.1021/ja044461m.

Publications

1) Relitti, N.; Saraswati, A. P.; Federico, S.; **Khan, T**.; Brindisi M.; Zisterer, D.; Brogi, S.; Gemma S.; Butini, S.; Campiani, G. Telomerase-based cancer therapeutics: a review on their clinical trials. *Curr. Top. Med. Chem.* **2020**, *20*, 1-25.

2) **Khan, T**.; Relitti, N.; Brindisi M.; Magnano S.; Zisterer D.; Gemma S.; Butini S.; Campiani G. Autophagy modulators for the treatment of oral and esophageal squamous cell carcinomas. *Med. Res. Rev.* **2019**, 1-59.

3) Brindisi, M.; Ulivieri, C.; Alfano, G.; Gemma, S.; de Asís Balaguer, F.; **Khan, T**.; Grillo, A.; Chemi, G.; Menchon, G.; Prota, A. E.; Olieric, N.; Lucena-Agell, D.; Barasoain, I.; Diaz, J. F.; Nebbioso, A.; Conte, M.; Lopresti, L.; Magnano, S.; Amet, R.; Kinsella, P.; Zisterer, D. M.; Ibrahim, O.; O'Sullivan, J.; Morbidelli, L.; Spaccapelo, R.; Baldari, C.; Butini, S.; Novellino, E.; Campiani, G.; Altucci, L.; Steinmetz, M. O.; Brogi, S. Structure-Activity Relationships, Biological Evaluation and Structural Studies of Novel Pyrrolonaphthoxazepines as Antitumor Agents. *Eur. J. Med. Chem.* **2019**, *162*, 290–320.

4) Federico, S.; **Khan, T**.; Relitti, N.; Chemi, G.; Brindisi, M.; Brogi, S.; Novellino, E.; Zisterer, D. M.; Campiani, G.; Gemma, S.; Butini, S. A Jocic-Type Approach for a Practical and Scalable Synthesis of Pyrrolonaphthoxazepine (PNOX)-Based Potent Proapoptotic Agents. *Tetrahedron Lett.* **2018**, *59*, 4466–4470.

Presentations

1) "ESR8 - Development of Novel Autophagy Modulators to Improve the Sensitivity of OSCC to Chemotherapy," oral presentation at TRACT kick-off meeting (Trinity College Dublin, March 2017).
2) "ESR8 - Development of Novel Autophagy Modulators to Improve the Sensitivity of OSCC to Chemotherapy," poster presentation at TRACT kick-off meeting (Trinity College Dublin, March 2017).
3) "ESR8 - Development of Novel Autophagy Modulators to Improve the Sensitivity of OSCC to Chemotherapy," poster presentation on the Doctorate Day (University of Siena, December 2017).
4) "ESR8 - Development of Novel Autophagy Modulators to Improve the Sensitivity of OSCC to Chemotherapy," oral presentation at TRACT annual meeting (Queens University Belfast, April 2018)'
5) "ESR8 - Development of Novel Autophagy Modulators to Improve the Sensitivity of OSCC to Chemotherapy," poster presentation at TRACT annual meeting (Queens University Belfast, April 2018)'
6) "ESR8 - Development of Novel Autophagy Modulators to Improve the Sensitivity of OSCC to Chemotherapy," poster presentation at Emory@UNISI XV Edition (University of Siena, May 2018).
7) "Development of Novel Autophagy Modulators to Improve the Sensitivity of OSCC to Chemotherapy," poster presentation at European School of Medicinal Chemistry, ESMEC (University of Urbino, July 2018).
8) "Development of Novel Autophagy Modulators to Improve the Sensitivity of OSCC to Chemotherapy," poster presentation on the Doctorate Day (University of Siena, December 2018).
9) "Development of Novel Autophagy Modulators to Improve the Sensitivity of OSCC to Chemotherapy," poster presentation at TRACT annual meeting (Trinity College Dublin, January 2019).
10) "Development of Novel Autophagy Modulators to Improve the Sensitivity of OSCC to Chemotherapy," poster presentation at European School of Medicinal Chemistry, ESMEC (University of Urbino, July 2019).

11) "Development of Novel Autophagy Modulators to Improve the Sensitivity of OSCC to Chemotherapy," oral presentation at European School of Medicinal Chemistry, ESMEC (University of Urbino, July 2019).
12) "Development of Novel Autophagy Modulators to Improve the Sensitivity of OSCC to Chemotherapy," oral presentation on the Doctorate Day (University of Siena, December 2019).

Acknowledgements